Selected Technical Papers

STP 1566

ASTM INTERNATIONAL
Standards Worldwide

Geopolymer Binder Systems

Editors:
Leslie Struble
James K. Hicks

Selected Technical Papers STP1566
Geopolymer Binder Systems

Editors:
Leslie Struble
James K. Hicks

ASTM International
100 Barr Harbor Drive
PO Box C700
West Conshohocken, PA 19438-2959

Printed in the U.S.A.

ASTM Stock #: STP1566

Library of Congress Cataloging-in-Publication Data
Geopolymer Binder Systems / editors, Leslie Struble, James K. Hicks.
pages cm
"This compilation of Selected Technical Papers, STP1566 on Geopolymer Binder Systems, contains peer-reviewed papers that were presented at a symposium held June 26–27, 2012 in San Diego, CA ... sponsored by ASTM International Committee C01 on Cement, Subcommittee C01.10 on Hydraulic Cements for General Concrete Construction, and Committee C09 on Concrete and Concrete Aggregates"--Foreword.
Includes bibliographical references.
ISBN 978-0-8031-7554-9
1. Polymer-impregnated concrete--Congresses. 2. Cement--Congresses. 3. Binders (Materials)--Congresses. 4. Inorganic polymers--Congresses. 5. Aluminum silicates--Congresses. I. Struble, Leslie J. II. Hicks, James K. III. ASTM International Committee C01 on Cement. IV. ASTM International Committee C09 on Concrete and Concrete Aggregates.
TA443.P58G36 2013
620.1'36--dc23 2013021383

Photocopy Rights

Peer Review Policy

Each paper published in this volume was evaluated by two peer reviewers and at least one editor. The authors addressed all of the reviewers' comments to the satisfaction of both the technical editor(s) and the ASTM International Committee on Publications.

The quality of the papers in this publication reflects not only the obvious efforts of the authors and the technical editor(s), but also the work of the peer reviewers. In keeping with long-standing publication practices, ASTM International maintains the anonymity of the peer reviewers. The ASTM International Committee on Publications acknowledges with appreciation their dedication and contribution of time and effort on behalf of ASTM International.

Citation of Papers

When citing papers from this publication, the appropriate citation includes the paper authors, "paper title", STP title and volume, STP number, Paper doi, ASTM International, West Conshohocken, PA, Paper, year listed in the footnote of the paper. A citation is provided as a footnote on page one of each paper.

Printed in Bay Shore, NY
June, 2013

Foreword

THIS COMPILATION OF *Selected Technical Papers,* STP1566 on *Geopolymer Binder Systems*, contains peer-reviewed papers that were presented at a symposium held June 26-27, 2012 in San Diego, CA. The symposium was sponsored by ASTM International Committee C01 on Cement, Subcommittee C01.10 on Hydraulic Cements for General Concrete Construction, and Committee C09 on Concrete and Concrete Aggregates.

The Symposium Co-Chairpersons and STP Co-Editors are Leslie Struble, University of Illinois Urbana, Urbana, IL, USA and James K. Hicks, Ceratech Inc., Baltimore, MD, USA.

Contents

Overview vii

Overview of Geopolymer Cement
L. Struble, E. Kim, and L. Gómez-Zamorano 1

Assessment of the Glassy Phase Reactivity in Fly Ashes Used for Geopolymer Cements
K. L. Aughenbaugh, P. Stutzman, and M. C. G. Juenger 11

Microstructural Changes Responsible for Hardening of Fly Ash–Slag Geopolymers Studied through Infrared Spectroscopy
S. Puligilla and P. Mondal 21

Study on the Suitability of Volcanic Amorphous Aluminosilicate Rocks (Perlite) for the Synthesis of Geopolymer-Based Concrete
M. Taxiarchou, D. Panias, Ch. Panagiotopoulou, A. Karalis, and C. Dedeloudis 34

The Use of Aluminosilicates to Create Novel, High Performance and Sustainable Binders for Mortars, Plasters and Renders With Class Leading Low CO_2 Footprints
R. R. Gibson 54

Rheological Behavior of Fly-Ash-Based Geopolymers
C. Montes and E. N. Allouche 72

Evaluating the Use of Accelerated Test Methods for Chloride Transport in Alkali Activated Slag Concretes Using Electrical Impedance and Associated Models
N. Neithalath and D. Ravikumar 85

Activated Class C Fly Ash Cement
J. K. Hicks 108

Statistical-Based Approach for Predicting the Mechanical Properties of Geopolymer Concretes
E. I. Diaz-Loya, E. N. Allouche, and D. Cahoy 119

Selected Studies of the Durability of Fly-Ash-Based Geopolymer Concretes
K. Kupwade-Patil, E. N. Allouche, C. A. Watts, and Md. S. Badar 144

Performance-Based Specification for Geopolymer Cement Binders and Supporting Laboratory Data
R. W. Zubrod 165

Alkali-activated Binders and Concretes: The Path to Standardization
J. L. Provis 185

Development, Standardization, and Applications of Alkali-activated Concretes
J. S. J. van Deventer, D. G. Brice, S. A. Bernal, and J. L. Provis 196

Summary of Panel Discussion 213

Overview

Portland cement has been the primary binder in structural concrete since the early 1800s. With increasing awareness of the damaging effects of CO_2 emissions has come increasing pressure on the cement industry to develop more sustainable binders. One such binder system is geopolymers and related alkali-activated aluminosilicates. These materials are being increasingly and actively studied, are already being marketed as specialty products, and are being explored for use in structural concrete.

On June 26-27, 2012, an ASTM International symposium was held in San Diego, CA to address topics relating to geopolymer binder systems. The symposium was sponsored by ASTM International Committee C01 on Cement and Committee C09 on Concrete and Concrete Aggregates.

This special technical publication (STP) is a compilation of papers derived from presentations at this international symposium. The papers provide useful background understanding of geopolymer binders and their performance. Several papers addressed key technical issues important in the production, characterization, and use of these binders, including durability issues. It is hoped that these topics will be of interest to practitioners as well as to researchers.

When performance specifications for hydraulic cement (C1157 and C1600) were written, non-portland binders were uncommon and the specifications were not widely used. The symposium provided an opportunity to consider whether these existing standards provide, on the one hand, an effective framework for further exploration of new sustainable binders and, on the other hand, reliable protection for users of these materials. Standardization was discussed at the symposium and is addressed explicitly in several papers in this volume. This topic will be of interest to subcommittees in C01 and C09 as well as other organizations concerned with standards for engineering materials.

The editors wish to acknowledge all those who gave presentations at the symposium, those who attended the symposium and engaged in a useful and lively discussion of various technical issues, the many authors who contributed to this STP, and the many reviewers who provided important feedback to the authors prior to publication. The editors also wish to acknowledge ASTM International Committees C01 and C09 who sponsored the symposium and the

ASTM International staff who provided invaluable assistance in organization of the symposium and publication of this volume.

Leslie J. Struble
University of Illinois
Urbana, Illinois

James Hicks
Ceratech, Inc.
Baltimore, MD
Symposium Co-chairs and Co-editors

Geopolymer Binder Systems
STP 1566, 2013
Available online at www.astm.org
DOI:10.1520/STP156620120106

Leslie Struble,[1] *Eric Kim,*[1] *and Lauren Gómez-Zamorano*[2]

Overview of Geopolymer Cement

REFERENCE: Struble, Leslie, Kim, Eric, and Gómez-Zamorano, Lauren, "Overview of Geopolymer Cement," *Geopolymer Binder Systems*, STP 1566, Leslie Struble and James K. Hicks, Eds., pp. 1–10, doi:10.1520/STP156620120106, ASTM International, West Conshohocken, PA 2013.[3]

ABSTRACT: The chemistry and molecular structure of geopolymers and their engineering behavior are reviewed, in part by comparison to hydrated Portland cement. The geopolymers form by reaction between a solid aluminosilicate and an aqueous alkali hydroxide solution. The reaction involves gelation and the product is an aluminosilicate comprised of silica and alumina tetrahedra linked in three dimensions. Engineering behavior is similar to that of hydrated Portland cement. Set time and strength depend on the reaction chemistry. Durability is generally seen to be good.

KEYWORDS: cement, concrete, geopolymer, alkali-activated aluminosilicate

Introduction

Geopolymers, more formally called alkali-activated aluminosilicates, are made by reaction of solid precursor powder with an aqueous alkali hydroxide solution. Geopolymers are being actively studied for a number of applications, one of which is as the binding constituent in structural concrete, as a replacement for Portland cement. Geopolymers set (that is, become hard) and gain strength much as Portland cement does when mixed with water, though the geopolymer reaction chemistry is distinctly different from Portland cement hydration and the resulting microstructures are therefore quite different. The purpose of this

Manuscript received July 5, 2012; accepted for publication January 10, 2013; published online April 30, 2013.

[1]University of Illinois at Urbana-Champaign, Department of Civil and Environmental Engineering, Urbana, IL 61801, United States of America.

[2]Universidad Autónoma de Nuevo León, Department of Mechanical and Electrical Engineering, Nuevo León, Mexico.

[3]ASTM Symposium on *Geopolymer Binder Systems* on June 26–27, 2012 in San Diego, CA.

paper is to give an overview of the geopolymer reaction chemistry and how it controls engineering properties.

Geopolymers show considerable promise as an alternative binder to Portland cement in the manufacture of concrete. They have the important advantage of substantially reduced greenhouse gas emissions. Furthermore, they can be manufactured from waste materials. And their engineering properties are excellent, in some cases superior to those obtained with the Portland cement. The technology is receiving much attention worldwide but so far very little application.

The term "geopolymer" was coined in the 1970s by Davidovits [1,2]. Since the 1990s, much of the fundamental research on geopolymers was performed by a group in the Department of Chemical and Biomolecular Engineering at the University of Melbourne in Australia led by van Deventer and a group at the Eduardo Torroja Institute at the National Research Council (CSIC) in Spain led by Palomo. Both contributed much to a recent book on geopolymers [3]. This and other research has greatly extended our knowledge concerning this interesting system.

Reaction Chemistry

The geopolymer reaction occurs when an amorphous aluminosilicate precursor is mixed with an aqueous alkali hydroxide activator solution to produce a disordered alkali aluminosilicate gel [4]. The reaction involves dissolution, gelation, and polymerization (as shown schematically in Fig. 1). The reaction begins when dissolution of the precursor produces aluminate and silicate ions in the solution. With increasing concentration of alumina and silica, the species equilibrate, forming oligomers. At some point the alumina and silica oligomers link to form a three-dimensional aluminosilicate network, a gel. The gel structure continues to develop through polymerization.

The precursor is a solid aluminosilicate powder. It is usually amorphous, allowing fairly rapid dissolution. The best studied precursor is calcined clay (metakaolin), although waste materials (slag, fly ash, and others) are sometimes utilized. The activator solution contains alkali hydroxide (typically sodium or potassium) and water. It may also contain silica (often in the form of a hydrous alkali silicate such as waterglass); alkali hydroxide to speed up dissolution of the precursor and alkali silicate to allow manipulation of the silica/alumina ratio in the mixture. The rate of dissolution depends on concentration of the alkaline solution, the specific alkali cation used, and the structure and composition of the aluminosilicate precursor material.

Nanostructure

On the atomic scale, geopolymer gel is comprised of Si^{4+} and Al^{3+} cations tetrahedrally coordinated to O^{2-} anions. On the molecular scale, it is comprised

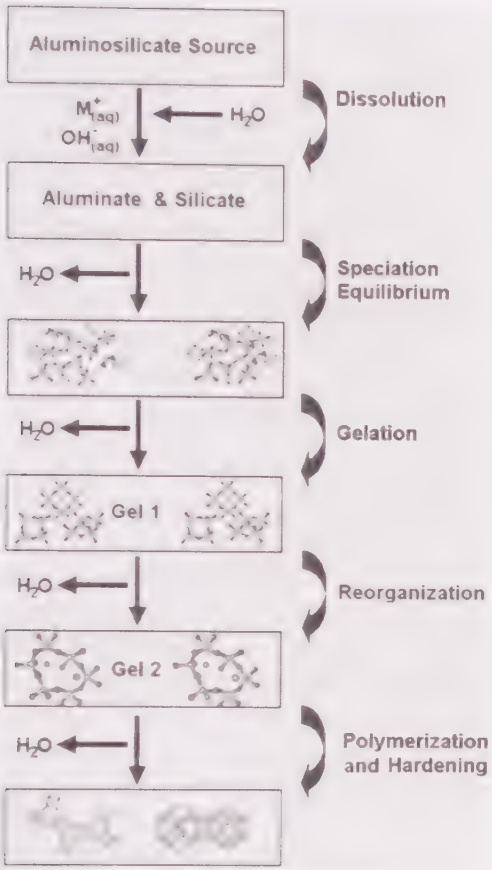

FIG. 1—*Conceptual model of geopolymerization [4].*

of SiO_4^{-4} and AlO_4^{-5} tetrahedra that link by sharing all four corners [5]. Although geopolymers are mainly x-ray amorphous, their structures are similar to those of zeolites and some form well-crystallized zeolite structures over time, depending on reaction conditions. Figure 2 displays a conceptual model of the amorphous molecular structure [6]. The aluminosilicate network has some negative charge, the value of which depends on silica/alumina, and therefore requires cations for charge balance. These cations are hydrated and are located in cavities in the aluminosilicate network, just as charge-balancing cations occur in zeolites. The molecular structure of the geopolymer gel depends on the Si/Al and the reaction conditions.

Initially, Davidovits postulated that geopolymers had a backbone structure similar to organic polymers and created a nomenclature to describe the connectivity of the three-dimensional framework structure of linked SiO_4 and $MAlO_4$ tetrahedra (where M is a monovalent cation, i.e., Na^+, K^+) [2]. The nomenclature uses three linear oligomeric building units called polysialates. Sialate is an

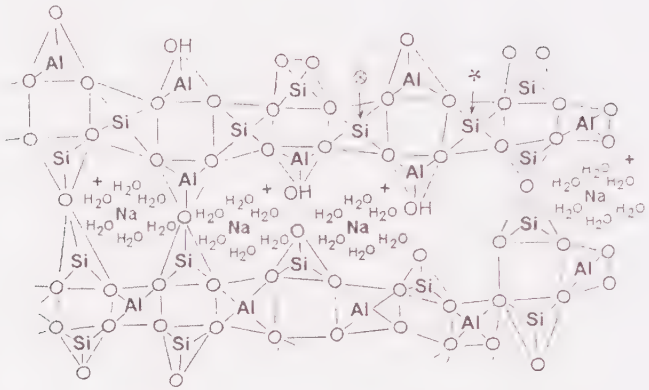

FIG. 2—*Schematic illustration of geopolymer structure [6].*

abbreviation for silicon-oxo-aluminate and is used to describe the bonding of silicon and aluminium by bridging oxygen. Polysialates are believed to have the general formula $M_p\{(SiO_2)_z AlO_2\}_p \times wH_2O$ where p is the degree of polycondensation, z is either 1, 2, or 3 and w describes water content of the composite (Fig. 3). The polysialate oligomers are described as chain and ring polymers with Si^{4+} and Al^{3+} in IV-fold coordination with oxygen and range from amorphous to semi-crystalline.

However, as noted by Duxson [7], this notation appears to contradict the three-dimensional network structure described previously, because the polysialate oligomers are two-dimensional. Thus, the model that Davidovits used to describe the geopolymer structure does not adequately describe the three-dimensional structure and fails to account for Al–O–Al linkage.

Research in aluminosilicates minerals and zeolites has produced an alternative notation for the "backbone of alkali aluminosilicate systems" [8]. The notation is $Q^n(m\text{Al})$, where n is the coordination number of the silicon centers and m is the number of Al neighbors surrounding the silicon connected through

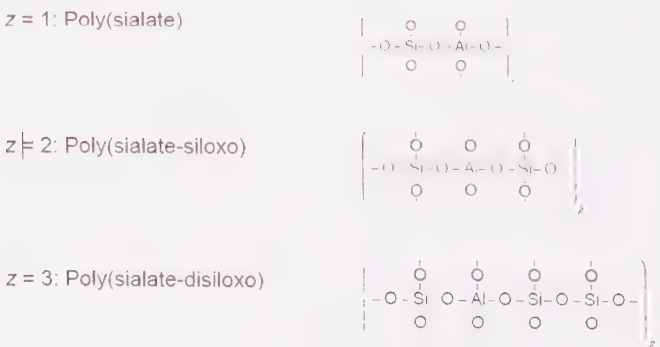

FIG. 3—*Polysialate units [7].*

bridging oxygen bonds (it should be noted that $0 \leq m \leq n \leq 4$). This notation has proven very useful in describing aluminosilicates regardless of their degree of long-range order.

Discussion of Reaction Chemistry and Structure

The reaction of aluminosilicate precursor with alkali hydroxide to produce a geopolymer is distinctly different from the reaction of Portland cement with water to produce CSH. As described above, the geopolymer reaction consists of dissolution, which produces alumina and silica oligomers, followed by gelation/polymerization of an aluminosilicate gel. Portland cement hydration, on the other hand, consists of initial dissolution, which produces calcium and silicate ions, followed by precipitation of a calcium silicate hydrate (CSH). The geopolymer gel has a three-dimensional network structure, whereas CSH has a two-dimensional structure formed by Ca–O octahedral sheets and silica tetrahedral chains [9]. In Portland cement hydration, water is essential both as the medium through which the reaction occurs and as an essential component of the product. In geopolymers, water is also the medium for the reaction but is not a component of the reaction product, rather the gelation releases water into the pores of the geopolymer. Thus, the two different reaction processes produce different reaction products.

Engineering Properties

As recently reviewed by Duxson et al. [4], the raw materials and processing conditions are critical in determining the setting behavior, workability, strength, and stiffness of the geopolymer. Depending on the raw materials and the processing conditions, geopolymers can exhibit a wide variety of engineering properties, including high compressive strength. The microstructure and the mechanical properties of geopolymers depend predominantly on their precursor materials and on their chemical composition.

Little has been written about setting of geopolymers. The setting appears to be associated with the gelation step and to be controlled in part by the kinetics of precursor dissolution. A recent study showed that geopolymer set times vary from minutes to hours and depend on gel composition, increasing when silica/alumina increases, and reducing when calcium is added to the mixture [10].

More is known about strength. The gelation and polymerization stages control the microstructure of final product and therefore its strength and stiffness. Quite high-strength values are reported, often in excess of 50 MPa, especially with early curing at an elevated temperature. An example is shown in Series 1 of Fig. 4 (a metakaolin geopolymer, SiO_2/Al_2O_3 by mole 3.9, H_2O/Na_2O by mole 10, water/solid by mass 0.51, cured in the laboratory at approximately 25°C for the first 2 h then at 60°C for 24 h, then in the laboratory for the

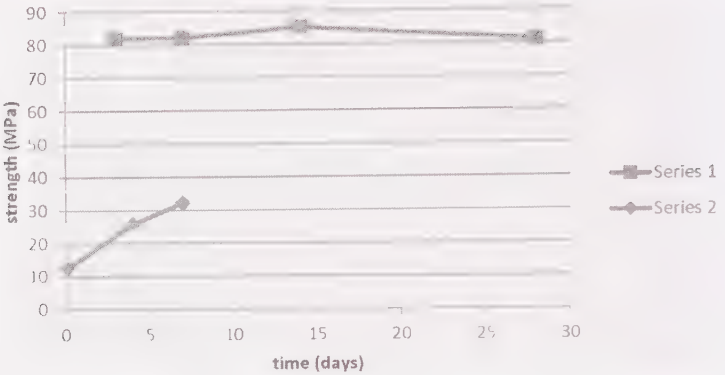

FIG. 4—*Compressive strength development for two geopolymer samples.*

remainder [11]). In addition, strength is generally seen to develop very quickly [12]. In our experience, the full compressive strength is typically reached within a few hours when initial curing takes place at a modestly elevated temperature [13]. Series 1 of Fig. 4 is an example of this rapid strength gain. Even when initial curing is at room temperature, strength development is quite rapid, as in the example Series 2 of Fig. 4 (a metakaolin geopolymer, SiO_2/Al_2O_3 by mole 2.8, H_2O/Na_2O by mole 10, water/solid by mass 0.55, cured at 100% RH and 21°C for the first 2 h then in the laboratory for the remainder).

It has been shown repeatedly that strength is related to composition and microstructure of the geopolymer gel. There is a direct correlation between mechanical strength and silica/alumina ratio, a correlation explained by the fact that the Si–O–Si bonds in the gel are stronger than Si–O–Al and Al–O–Al bonds [12]. However, it has also been seen that the optimum strength of geopolymers made using metakaolin occurs at an intermediate silica/alumina ratio [14,15], and the reduction in strength in high silica/alumina mixes has been attributed to unreacted material, which is weak and acts as a defect [16].

Several authors have pointed out that geopolymers are materials with very good resistance to chemical attack. For example, Palomo et al. [17] reported that mortars made with alkali-activated metakaolin were very stable when immersed in aggressive solutions of various types (deionized water, seawater, sodium sulfate solution, and sulfuric acid). But many studies have shown deterioration, mainly fly-ash-based, exposed to acetic, sulfuric, or nitric acid solution [18–23]. And Bakharev [24] reported strength loss of fly-ash-based geopolymers in solutions of sodium and magnesium sulfates. Several studies [24–27] showed that the performance of fly-ash-based geopolymers in aggressive environments depended on the intrinsic ordering of the components within the gel, with greater crystallinity providing more stability in environments such as sulfuric and acetic acid solutions.

A troublesome issue that needs to be controlled before geopolymers can be considered for use in structural concrete is the effect of reaction chemistry on

set time and strength, particularly set. As noted previously, set is strongly affected by the gel composition. The effect of silica/alumina in the gel can conveniently be controlled by manipulating the amount of soluble silica or alumina in the activator solution. This manipulation is complicated with precursors that dissolve slowly or incompletely, such as fly ash, for which it is necessary to measure the composition of the soluble (or reactive) portion of the precursor rather than the bulk precursor composition, but research is underway to solve this issue. But it is more difficult to control the effect of calcium, which is found in many potential precursor materials such as fly ash or slag. This calcium strongly reduces set time, the reason for this effect is not known, and at the moment no means of controlling it has been reported.

Another troublesome issue is shrinkage. Geopolymers are seen to resist shrinkage during drying [17]. But mass loss and shrinkage are seen as the gel undergoes structural changes on heating that produce densification [28] (and shrinkage during aging of gels is a well-documented behavior [29]). The shrinkage at higher temperature depends in part on the Si/Al of the gel [28]. Although we have not measured the shrinkage directly, our experience is that it is considerable, often leads to cracking, occurs in geopolymers not heated above room temperature, and clearly needs to be controlled to utilize geopolymers as a binder in structural concrete. Such shrinkage is undoubtedly reduced in concrete by aggregates and perhaps even by fillers.

Summary and Conclusions

Geopolymers show promise as a binder in place of Portland cement in structural concrete. Geopolymers form by reaction between an aluminosilicate precursor, usually amorphous, and an alkali hydroxide activator solution. The reaction proceeds by dissolution of precursor and gelation/polymerization to produce silica and alumina tetrahedra linked in three dimensions in a structure similar to that found in zeolites. Although the reaction chemistry and molecular structure of the product are quite different, geopolymers set and gain strength much as do Portland cement. Set time is seen to depend on precursor dissolution kinetics and the reaction chemistry, especially silica/alumina and calcium content. Strength is seen to depend on gel composition (more specifically on silica/alumina). Good durability is seen with metakaolin geopolymers but deterioration in some environments is reported for geopolymers made using fly ash. Control of reaction chemistry is needed to achieve targeted setting behavior and strength development. Shrinkage of the gel remains a key issue.

Acknowledgments

Preparation of this paper was supported in part by the National Science Foundation (DMR 1008102). Strength data were provided by Cesar Rojas, a student

at the University of Illinois. Figure 1 is reprinted from Ref 4 with kind permission from Springer Science and Business Media and Fig. 2 is reprinted from Ref 6 with permission from Elsevier.

References

[1] Davidovits, J., "Synthesis of New High Temperature Geo-Polymers for Reinforced Plastics/Composites," *Fourth Annual Pacific Technical Conference and Technical Displays*, Society of Plastic Engineers, 1979, pp. 151–154.

[2] Davidovits, J., "Geopolymers: Inorganic Polymeric New Materials," *J. Therm. Anal.*, Vol. 37, 1991, pp. 1633–1656.

[3] *Geopolymers*, J. Provis and J. van Deventer, Eds., CRC Press, Boca Raton, FL, 2009, 454 pp.

[4] Duxson, P., Fernández-Jiménez, A., Provis, J., Lukey, G., Palomo, A., and van Deventer, J., "Geopolymer Technology: The Current State of the Art," *J. Mater. Sci.*, Vol. 42, 2007, pp. 2917–2933.

[5] Ferndndez-Jiménez, A. and Palomo, A., "Nanostructure/Microstructure of Fly Ash Geopolymers," *Geopolymers*, J. Provis and J. van Deventer, Eds., CRC Press, Boca Raton, FL, Chap. 6, 2009.

[6] Barbosa, V., MacKenzie, K., and Thaumaturgo, C., "Synthesis and Characterization of Materials Based on Inorganic Polymers of Alumina and Silica: Sodium Polymers," *Int. J. Inorg. Mater.*, Vol. 2, 2000, pp. 309–317.

[7] Duxson, P., 2006, "The Structure of Thermal Evolution of Metakaolin Geopolymers," Ph.D. thesis, University of Melbourne, Melbourne.

[8] Engelhard, G., Lippma, E., and Magi, M., "Ordering of Silicon and Aluminum Ions in the Framework of NaX Zeolites—A Solid-State High-Resolution Si-29 NMR Study," *J. Chem. Soc., Chem. Commun.*, 1981, pp. 712–713, DOI: 10.1039/C39810000712.

[9] Taylor, H., *Cement Chemistry*, 2nd ed., Thomas Telford, London, England, 1997, Chap. 5.

[10] Suraneni, P., Puligila, S., Kim, E., Chen, X., Struble, L., and Mondal, P., "Monitoring Setting of Geopolymers," *ACI J. Mater* (to be published).

[11] Balandran, M., 2011, "Geopolymers Synthesized Using Two Types of Activators," M.S. thesis, FIME-UANL, San Nicolás de los Garza, Mexico.

[12] Duxson, P., Provis, J., Lukey, G., and van Deventer, J., "The Role of Inorganic Polymer Technology in the Development of 'Green Concrete,'" *Cement Concrete Res.*, Vol. 37, 2007, pp. 1590–1597.

[13] Vega-Cordero, E., Gómez-Zamorano, L. Y., and Escalante-García, J. I., "Synthesis of Metakaolin-Based Geopolymers and the Effect of the Incorporation of Geothermal Silica Waste," *Proceedings of the XIII ICCC International Congress on the Chemistry of Cement*, 2011, pp. 177.

[14] de Jong, B. and Brown, G., "Polymerization of Silicate and Aluminate Tetrahedra in Glasses, Melts, and Aqueous Solutions—I. Electronic Structure of $H_6Si_2O_7$, $H_6AlSiO_7^{-1}$, and $H_6Al_2O_7^{-2}$," *Geochim. Cosmochim. Acta*, Vol. 44, 1980, pp. 491–511.

[15] Rowles, M. and O'Connor, B., "Chemical Optimisation of the Compressive Strength of Aluminosilicate Geopolymers Synthesised by Sodium Silicate Activation of Metakaolinite," *J. Mater. Chem.*, Vol. 13, 2003, pp. 1161–1165.

[16] Duxson, P., Provis, J., Lukey, G., Mallicoat, S., Kriven, W., and van Deventer, J., "Understanding the Relationship Between Geopolymer Composition, Microstructure and Mechanical Properties," *Colloid Surface*, Vol. 269, 2005, pp. 47–58.

[17] Palomo, A., Blanco-Valera, M., Granizo, M., Puertas, F., Vázquez, T., and Grutzeck, M., "Chemical Stability of Cementitious Materials Based on Metakaolin," *Cement Concrete Res.*, Vol. 29, 1999, pp. 997–1004.

[18] Steenie, E., Hardjito, D., Sumajouw, M., and Vijaya, B., "Performance of Fly Ash-Based Geopolymer Concrete Under Sulfate and Acid Exposure," *Geopolymer, Green Chemistry and Sustainable Development Solutions*, J. Davidovits, Ed., Geopolymer Institute, Saint-Quentin France, 2005, p. 236.

[19] Song, X., Marosszeky, M., Brungs, M., and Chango, Z., "Response of Geopolymer Concrete to Sulphuric Acid Attack," *Geopolymer, Green Chemistry and Sustainable Development Solutions*, J. Davidovits, Ed., Geopolymer Institute, Saint-Quentin, France, 2005, p. 236.

[20] Song, X., Marosszeky, M., Brungs, M., and Munn, M., "Durability of Fly Ash Based Geopolymer Concrete Against Sulphuric Acid Attack," International Conference on Durability of Building Materials and Components, Lyon France, 2005.

[21] Bakharev, T., Sanajayan, J., and Cheng, Y., "Resistance of Alkali-Activated Slag Concrete to Acid Attack," *Cement Concrete Res.*, Vol. 33, 2003, pp. 1607–1611.

[22] Allahverdi, A. and Skvara, F., "Nitric Acid Attack on Hardened of Geopolymeric Cements. Part 1," *Ceram. Silikátay*, Vol. 45, 2001, pp. 81–88.

[23] Davidovits, J., Comrie, D., Paterson, J., and Ritcey, D., "Geopolymeric Concretes for Environmental Protection," *ACI Concrete Int.*, Vol. 12, 1990, pp. 30–40.

[24] Bakharev, T., "Durability of Geopolymer Materials in Sodium and Magnesium Sulfate Solutions," *Cement Concrete Res.*, Vol. 35, 2005, pp. 1233–1246.

[25] Bakharev, T., "Resistance of Geopolymer Materials to Acid Attack," *Cement Concrete Res.*, Vol. 25, 2005, pp. 658–670.

[26] van Jaarsveld, J., van Deventer, J., and Lorenzen, L., "Factors Affecting the Immobilization of Metals in Geopolymerized Fly Ash," *Metall. Mater. Trans. B*, Vol. 29, 1998, pp. 283–291.

[27] van Jaarsveld, J. and van Deventer, J., "Effect of the Alkali Metal Activator on the Properties of Fly Ash-Based Geopolymers," *Indust. Eng. Chem. Res.*, Vol. 38, 1999, pp. 3932–3941.

[28] Duxson, P., Lukey, G., and van Deventer, J., "Physical Evolution of Na-Geopolymer Derived from Metakaolin up to 1000°C," *J. Mater. Sci.*, Vol. 42, 2007, pp. 3044–3054.

[29] Brinker, C. and Scherer, G., *Sol-Gel Science*, Academic, Orlando, FL, 1990, Chap. 6.

Geopolymer Binder Systems
STP 1566, 2013
Available online at www.astm.org
DOI:10.1520/STP156620120105

Katherine L. Aughenbaugh,[1] *Paul Stutzman,*[2] *and Maria C. G. Juenger*[3]

Assessment of the Glassy Phase Reactivity in Fly Ashes Used for Geopolymer Cements

REFERENCE: Aughenbaugh, Katherine L., Stutzman, Paul, and Juenger, Maria C. G., "Assessment of the Glassy Phase Reactivity in Fly Ashes Used for Geopolymer Cements," *Geopolymer Binder Systems*, STP 1566, Leslie Struble and James K. Hicks, Eds., pp. 11–20, doi:10.1520/STP156620120105, ASTM International, West Conshohocken, PA 2013.[4]

ABSTRACT: Geopolymer cements have not found widespread use as a Portland cement replacement, in part because of the difficulty in proportioning mixtures in a reliable manner. Unlike Portland cements, which are manufactured materials with relatively consistent compositions, geopolymers are made from natural or waste aluminosilicate powders that come from a variety of sources and have highly variable compositions. These powders are mixed with caustic solutions, which must be selected carefully to optimize strength and durability. Geopolymer cement can be designed by tailoring caustic solution composition to the reactive phase composition of the solid component of the mixture; however, assessing which phases are reactive is challenging for complex and heterogeneous solids, such as fly ash. The work presented here focuses on applying a scanning electron microscopy and multispectral image analysis (SEM-MSIA) method to identify and quantify the reactive glassy phases in fly ash and to determine how these phases dissolve over time in a caustic activating solution. The fly ash was selected based upon its oxide contents and was analyzed for phase content using X-ray diffraction and Rietveld analysis (RQXRD) and SEM-MSIA, which identified multiple glassy phases in the fly ash. Next, the fly ash was suspended in 8 M NaOH, and tested at various time intervals with SEM-MSIA to track changes in the

Manuscript received June 30, 2012; accepted for publication October 3, 2012; published online April 23, 2013.

[1]The Univ. of Texas at Austin, Austin, TX 78712, United States of America, e-mail: katy.aughenbaugh@utexas.edu

[2]National Institute of Standards and Technology, Gaithersburg, MD 20899, United States of America.

[3]The Univ. of Texas at Austin, Austin, TX 78712, United States of America.

[4]ASTM Symposium on *Geopolymer Binder Systems* on June 26–27, 2012 in San Diego, CA.

amounts of each individual glassy phase initially identified in the fly ash. The results showed that an aluminosilicate glass (C-A-S) with a moderate amount of calcium appeared to be the most reactive between 0 and 28 days for a Class F fly ash. Other phases that were identified in the fly ash included a high-Ca C-A-S glass, two aluminosilicate glasses with different S/A ratios, two alkali-modified A-S phases, and an iron-containing glass.

KEYWORDS: fly ash, geopolymers, reactivity

Introduction

Geopolymers are aluminosilicate-based cementing materials that can be used instead of Portland cement as a binder for concrete. The material is formed by mixing an aluminosilicate powder with a caustic activating solution, commonly an alkali hydroxide and/or alkali silicate [1]. A large body of the research on geopolymer cements has been completed using metakaolin as the aluminosilicate source [2–4], which serves as a model geopolymer precursor because of its nearly pure aluminosilicate composition with little crystalline material. Fly ash can also be used as an aluminosilicate source for geopolymer formation because it contains a large proportion of reactive glassy aluminosilicates, and it has an added environmental benefit of being a recycled material.

A major challenge in using fly ash as the sole geopolymer precursor material for concrete is that it is difficult to determine whether a given fly ash will react sufficiently with the activating solution. One chemical method for testing reactivity is hydrofluoric acid dissolution, which measures the reactive silica content of the fly ash by comparing the weight of the treated material to the original sample weight [5,6]. However, the acid requires extreme care in handling, and it does not represent the highly caustic environment that the fly ash is subjected to in geopolymer formation. Analytical methods of fly ash characterization include x-ray diffraction (XRD) and scanning electron microscopy (SEM). There is some evidence that the vitreous alumina content of a fly ash may affect its reactivity as a geopolymer, which is calculated by subtracting the amount of crystalline alumina-bearing minerals obtained using XRD from the bulk oxide composition of fly ash [7]. It is also known that there are multiple glassy phases within a fly ash sample, and it is important to identify these glasses because they can react differently when exposed to caustic solutions [8]. Thus, how the silica and alumina are bound within the fly ash is also important. Several researchers [9–12] have used SEM x-ray point counting methods to ascertain the chemical composition of the various glasses within fly ash in an attempt to better understand its internal structure and potential for reactivity.

Combining the methods of fly ash dissolution and x-ray mapping analysis may be a promising option for testing the reactivity of fly ash. Because the reaction of fly ash to form a geopolymer is a dissolution-precipitation process [4], a dissolution method using a caustic solution instead of an acidic solution can be used to assess how much of the fly ash is available to react [8,13,14].

TABLE 1—*LEGS fly ash oxide composition from x-ray fluorescence spectroscopy, as reported from Headwaters Resources.*

Al_2O_3	SiO_2	CaO	Fe_2O_3	K_2O	MgO	Na_2O	SO_3	TiO_2	LOI
17.8	54.14	10.7	7.74	1.43	2.31	0.45	0.4	1.2	0.09

The reacted material can then be separated from the solution for analysis. The work presented in this paper examined a fly ash using x-ray mapping in its initial state and after 28 days exposure to 8 mol/L sodium hydroxide. These results were used to determine approximately how much of the fly ash was reacting in such conditions and to find out which of the phases that were identified in the original fly ash were the most reactive.

Materials and Methods

A Class F fly ash [15] from Limestone Electric Generating Station (LEGS) in Jewett, TX was selected for the study. The fly ash was chosen based on its oxide composition, which was similar to those of fly ashes that performed well in studies in Australia [16]. Table 1 lists the oxide analysis and loss-on-ignition (LOI) for the LEGS fly ash. The activating solution for the materials was 8 mol/L NaOH solution, like that used by Fernández-Jiménez et al. [7], which was made from 50 wt. % prepared NaOH solution (ACS reagent grade) diluted with ultrapure water (18.5 ± 0.5 mΩ-cm).

When cured at 23 C, geopolymer mortars made from LEGS fly ash and 8 mol/L NaOH had relatively low strength at 7 days and moderate strength at 28 days when compared to mortars made with nine other fly ashes that were mixed and cured under identical conditions (unpublished data). For the geopolymer mortar, low strength was defined as less than 1 MPa, moderate strength was defined as 1–14 MPa, and high strength was defined as greater than 14 MPa. These are relatively low strengths for cementitious materials but are expected values for geopolymers made using Class F fly ash and cured at 23 C. Most geopolymer studies use high temperature curing, which increases compressive strength [4,7]. The LEGS fly ash was selected for this study because of its moderate reactivity in terms of compressive strength.

Rietveld analysis of XRD data was used to calculate the amount of bulk glassy phase in the fly ash after subtracting the amounts of the identified crystalline phases. X-ray diffraction analysis was performed using a Siemens D500 X-ray diffractometer.[5] The X-ray source produced Cu Kα radiation and

[5]Certain commercial materials and equipment are identified to adequately specify experimental procedures. In no case does such identification imply recommendation or endorsement by the National Institute of Standards and Technology, nor does it imply that the items identified are necessarily the best available for the purpose.

operated at 40 kV and 30 mA. A long dwell time of 6 s per step was used to increase the x-ray counts at each step for better resolution of phases. The scans were run from 10°–70° 2*θ* with a step size of 0.02° 2*θ*. The crystalline phases were identified using files from the inorganic crystal structure database,[6] and Rietveld analysis was completed with TOPAS Academic version software (Coelho). Zinc oxide (ACS reagent grade) was used as an internal standard and interground with the fly ash at 10 % by mass using ethanol as a dispersant and an agate mortar and pestle.

SEM-MSIA includes x-ray mapping of selected elements on epoxy-mounted fly ash specimens. Full details on the preparation process were published by Chancey [10]. X-ray mapping was completed using a field emission SEM fitted with two energy dispersive spectroscopy (EDS) detectors, which collected approximately 60000–80000 counts/s. The microscope was operated at 15 kV accelerating voltage, and the EDS maps were collected very slowly with a 256 μs dwell time per pixel and a 1024 × 1024 map size. Each scan was run for approximately 1 h, which is 14 passes of the field of view. Multispectral image analysis has been described for minerals [17] and fly ash [10] and is only summarized briefly here. The raw x-ray maps were smoothed using ImageJ,[7] and they were then stacked digitally using Multispec.[8] Three maps were viewed simultaneously as red, green, and blue channels; by changing which elemental maps were turned on, the user gained familiarity with the composition of the fly ash. Groups of pixels were then selected in regions of varied composition (based on appearance of the three-channel RGB image) and were defined as the training field for various phases in the fly ash. The Multispec program then assigned every pixel in the image to one of the defined fields from which an area percentage of each phase was calculated. The volume of spherical fly ash particles was assumed equal to the area [18]; after converting to volume, published densities were used to calculate weight percentages of each phase present.

The specimens in this study consisted of fly ash in its original state and solid residue of the fly ash after selective dissolution using NaOH. The dissolution method was performed as follows: 2 g fly ash was mixed with 10 mL 8 mol/L NaOH solution. These were mixed in nonreactive plastic vials, sealed with a screw-cap lid, and placed on a laboratory rotisserie (LabQuake) in a room at 23 °C that rotated the samples end-over-end at approximately 10 rpm until the desired time had elapsed. At 28 days, the sample was removed from the rotisserie and the solid material was separated from the liquid under vacuum using a 2.7 μm filter paper on a Buchner funnel. The solid material

[6]FIZ/NIST Inorganic Crystal Structure Database (ICSD), http://www.nist.gov/srd/nist84.cfm
[7]ImageJ, http://rsbweb.nih.gov/ij/
[8]Multispec, https://engineering.purdue.edu/biehl/MultiSpec/

TABLE 2—*LEGS fly ash crystalline and bulk amorphous content.*

Phase	Crystalline phases (wt. %)	Phase	Amorphous phases (wt. %)
Quartz	12.54 ± 1.98	Bulk amorphous	72.44 ± 1.76
Mullite (2:1)	3.63 ± 0.52	Vitreous alumina	15.87 ± 0.40
Magnetite	0.92 ± 0.12	Vitreous silica	40.29 ± 1.86
Anhydrite	0.34 ± 0.08		
Periclase	0.12 ± 0.12		

was dried for approximately an hour in air, then scraped from the paper into a vial and placed in a vacuum desiccator for complete drying.

Results

Results from x-ray diffraction and Rietveld analyis from three independent replicate samples are shown in Table 2. From these data, the crystalline phases were subtracted to reveal the amount of each oxide in "vitreous" phases. It has been suggested in the literature [7] that the amount of vitreous alumina, in particular, affects the reactivity of the fly ash. Fernández-Jiménez et al. [7] tested two fly ashes, one with a vitreous alumina content of 20.45 wt. % and another with 14.11 wt. %, with the same vitreous silica content of 50 wt. %. Geopolymers made from the ash with higher vitreous alumina outperformed the ash with lower vitreous alumina content in terms of degree of reaction, as measured by hydrochloric acid dissolution of reaction products. The LEGS fly ash examined in this study had a vitreous alumina content of 15.87 ± 0.4 wt. % (Table 2). This implies that the fly ash should not perform well as a geopolymer, because its vitreous alumina content is closer to that of the poorly performing fly ash tested by Fernández-Jiménez et al. [7]. It should be noted that the vitreous silica content of the LEGS fly ash was 40.29 ± 1.89 wt. %, which was lower than the 50 wt. % vitreous silica content studied in both samples by Fernández-Jiménez et al. [7]. However, it should be noted that Fernández-Jiménez et al. [7] cured their specimens at 85 C, which was much hotter than the samples in this study and the reaction pathways are somewhat different at higher temperatures [4]. Therefore, more research is necessary on the relationship between vitreous alumina and silica content and geopolymer performance.

Nine phases were identified in the fly ash using SEM-MSIA[9]: quartz, A-S 1 (high aluminum), A-S 2, C-A-S 1 (high Ca), C-A-S 2 (moderate Ca), N-A-S, K-A-S, iron-rich, and voids. The intensity ratios from x-ray maps for each of the phases containing calcium, aluminum, and silicon are given in Table 3.

[9]Cement chemistry notation is used for defining the glasses: C = CaO, S = SiO_2, A = Al_2O_3, F = Fe_2O_3, f = FeO, S = SO_3, M = MgO, N = Na_2O, K = K_2O, and H = H_2O. Dashes are used to signify that the stoichiometry of the glass is not indicated in the name of the glass.

TABLE 3—*Phase intensity ratios for glass in a LEGS fly ash.*

Phase Designation	S/A	C/S/A
A-S 1 (high Al)	0.36	–
A-S 2	0.77	–
C-A-S 1 (high Ca)	1.10	4.74/1.74/1.0
C-A-S 2 (moderate Ca)	0.61	1.14/1.0/1.4
N-A-S	0.79	–
K-A-S	1.14	–

Note: 15-kV operating conditions.

Phase-assignment images for the unexposed LEGS fly ash and the 28-day exposed fly ash are shown in Fig. 1. The images were used to calculate mass percentages of each phase, shown in Fig. 2. No reaction product was noted in the specimen after 28 days exposure to NaOH. Because it was assumed that glassy phases would dissolve over time when exposed to the NaOH and that the quartz was nonreactive [19], it was expected that the relative amount of quartz in the solid material would increase with exposure time to the sodium hydroxide solution. This was observed in the raw data. Thus, the quartz was used as an internal standard, and the amount of quartz in the reacted specimen was set to the same value as that in the raw specimen with the remaining phases adjusted proportionally. This enabled calculation of the amount of fly ash that dissolved in the sodium hydroxide. The amount of quartz calculated in the original fly ash was 10.7 wt. % calculated using MSIA and 12.5 wt. % using Rietveld analysis. The quartz calculated using MSIA on the 28-day exposure sample was 15.3 wt. %, resulting in a scale factor of 0.7 for the remaining phases. The results showed that about 30 wt. % of the fly ash dissolved from the original sample.

As shown in Fig. 2, the A-S 2 phase (S/A = 0.77) decreased after 28 days of exposure to the NaOH. Similarly, the C-A-S 2 phase (S/A = 0.61) decreased greatly from 0 to 28 days. N-A-S phase (sodium aluminosilicate) (S/A = 0.79) entirely disappeared by 28 days. The C-A-S 1 phase (S/A = 1.10) did not

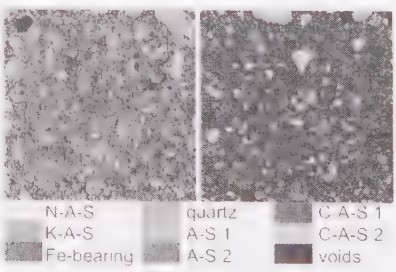

FIG. 1—*LEGS fly ash pixel assignments map (left) and after 28 days of NaOH exposure (right).*

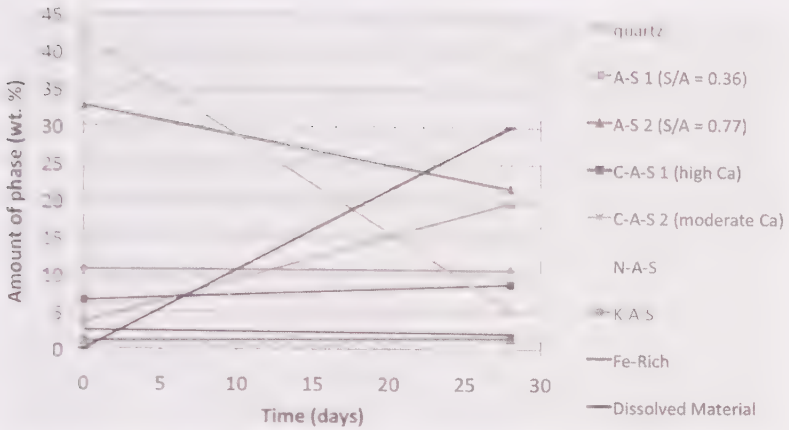

FIG. 2—*Changes in amount of each glassy phase in the LEGS fly ash at 0 days of exposure to 8 M NaOH and after 28 days of exposure to 8 M NaOH. The lines serve to guide the eye and do not predict trends between these two times.*

significantly change from 0 days to 28 days. Likewise, the K-A-S phase (potassium aluminosilicate) (S/A = 1.14) and the iron-containing phase stayed approximately even from 0 to 28 days. The A-S 1 (S/A = 0.32) phase increased from 0 to 28 days. As previously discussed, the quartz was set to equal its initial amount at 28 days, so its plot shows no change from 0 to 28 days

Discussion

Hemmings and Berry [19] wrote an excellent paper discussing the glass in coal fly ashes in which they described the ideal glass structure for silicon-based glasses as pure silica tetrahedra with short-range order; whereas aluminum can substitute with silicon nearly interchangeably, calcium, sodium, potassium, and magnesium serve as network-modifiers in the system. Both substitution and modification lead to increased disorder in the glass network, which causes the glass to be reactive under certain conditions [19]. These concepts are applied in the discussion of results from this dissolution study of LEGS fly ash.

Because of their assumed disordered nature, it was surprising that the K-A-S and high-Ca C-A-S 1 phases did not seem to have reacted at 28 days. However, the both the K and Ca are considered contaminants that change the reaction mechanism of the glass [4]. Based on the results the K-A-S and C-A-S 1 glasses present in the LEGS fly ash seem to be chemically bound in such a way as to prohibit reaction with the NaOH. The disordered N-A-S phase was fully dissolved and not detectable at 28 days, which was as expected. Similarly, the moderate Ca C-A-S 2 phase decreased greatly after exposure to NaOH, and thus may be the most reactive phase in the LEGS fly ash. The other phase that

dissolved in the presence of NaOH was the A-S 2 (S/A = 0.77) glass, which decreased somewhat at 28 days. Thus, the N-A-S, C-A-S 2, and A-S 2 phases show promise as phases to look for in potential raw materials for use in geopolymers. It is of interest that these three phases fall within a narrow range of S/A intensity ratios between approximately 0.6 and 0.8. The other phases detected in the fly ash have higher or lower S/A ratios than these three that reacted. Further studies of other ashes are necessary to prove the hypothesis that these particular glassy phases are desirable in ashes used for geopolymer cements activated with NaOH.

The results showed that the amount of iron-containing phases does not change with 28 days of exposure to concentrated NaOH. Iron is an important cation in geopolymer formation, but little is known about its exact effect on the reactions in geopolymer formation [4], which was not studied here. Thus, these phases may be nonreactive in geopolymer formation from LEGS fly ash, but further study is necessary.

The increase in the A-S 1 (S/A = 0.36) glass is difficult to explain. The intensity ratio shows that the aluminum is present in relatively large amounts in this phase, whereas the silicon is present in relatively low amounts. It is hypothesized that the relative proportions of the A-S 1 glass may inhibit dissolution. Additionally, it is possible that leaching of network-modifying ions from other phases occurred, which left behind material with similar composition to the A-S 1 phase. More detailed examination of the composition of this phase and the other phases over time is necessary to prove this hypothesis, as well as investigation of the reaction products and solution composition.

Conclusions

A fly ash that has been shown to make a moderate-strength geopolymer was exposed to NaOH in dilute proportions (6.4 solution-to-powder ratio) for 28 days in an attempt to determine its reactivity under the caustic conditions encountered in geopolymer production. Using RQXRD and SEM-MSIA, it was found that:

- The fly ash consisted of two aluminosilicate phases and two calcium-aluminosilicate phases, along with quartz, an iron-containing phase, and two alkali-modified aluminosilicates: potassium-modified and sodium-modified.
- The most reactive phase in the system appeared to be a moderate-calcium aluminosilicate glass (C-A-S 2, S/A = 0.61). The A-S 2 (S/A = 0.77) and N-A-S glassy phases also dissolved.
- It is unclear why the A-S 1 phase increased and the K-A-S phase did not react, but it is possible that high S/A ratio glasses (>1) are less soluble in the NaOH solution used.

The method described in this paper is proposed as a technique to assess the reactivity of phases in fly ash and determine the potential of the fly ash for geopolymeric reactivity. From these results, the presence of glasses such as C-A-S 2 and A-S 2 indicate promising starting materials for geopolymers. More work is necessary to characterize a variety of fly ashes using the same process and compare the results to a measure of reactivity, such as the amount of geopolymer formed or the compressive strength development.

References

[1] Davidovits, J., "Inorganic Polymeric New Material," *J. Therm. Anal.*, Vol. 37, 1991, pp. 1633–1656.

[2] Barbosa, V. F. F., MacKenzie, K. J. D., and Thaumaturgo, C., "Synthesis and Characterization of Materials Based on Inorganic Polymers of Alumina and Silica: Sodium Polysialate Polymers," *Int. J. Inorg. Mater.*, Vol. 2, 2000, pp. 309–317.

[3] Rowles, M. and O'Connor, B., "Chemical Optimization of the Compressive Strength of Aluminosilicate Geopolymers Synthesized by Sodium Silicate Activation of Metakaolinite," *J. Mater. Chem.*, Vol. 13, 2003, pp. 1161–1165.

[4] Duxson, P., Fernández-Jiménez, A., Provis, J., Lukey, G. C., Palomo, A., and van Deventer, J. S. J., "Geopolymer Technology: The Current State of the Art," *J. Mater. Sci.*, Vol. 42, 2007, pp. 2917–2933.

[5] Kilgour, K. and Diamond, S., "The Internal Structure of a Low-Calcium Fly Ash," *Mater. Res. Soc. Symp. Proc.*, Vol. 113, 1988, pp 65–74.

[6] Fernández-Jiménez, A., de la Torre, A. G., Palomo, A., Lopez-Olmo, G., Alonso, M. M., and Aranda, M. A. G., "Quantitative Determination of Phases in the Alkaline Activation of Fly Ash. Part I: Potential Ash Reactivity," *Fuel*, Vol. 85, 2006, pp. 625–634.

[7] Fernández-Jiménez, A., de la Torre, A. G., Palomo, A., López-Olmo, G., Alonso, M. M., and Aranda, M.A.G., "Quantitative Determination of Phases in the Alkaline Activation of Fly Ash. Part II: Degree of Reaction," *Fuel*, Vol. 85, 2006, pp. 1960–1969.

[8] Chancey, R., "Characterization of Crystalline and Amorphous Phases and Respective Reactivities in a Class F Fly Ash," Ph.D. dissertation, The University of Texas at Austin, 2008.

[9] Williams, P. J., Biernacki, J. J., Rawn, C. L., Walker, L., and Bai, J., "Microanalytical and Computational Analysis of Class F Fly Ash," *ACI Mater. J.*, Vol. 102, 2005, pp. 330–337.

[10] Chancey, R., Juenger, M. C. G., Stutzman, P., and Fowler, D. W., "Comprehensive Phase Characterization of Crystalline and Amorphous

Phases of a Class F Fly Ash," *Cement Concrete Res.*, Vol. 40, 2010, pp. 146–156.

[11] Dhole, R., "Sulfate Resistance of High Calcium Fly Ash Concrete," Ph.D. dissertation, The University of New Brunswick, 2010.

[12] Kruse, K. A., "Characterization of High-Calcium Fly Ash for Evaluating the Sulfate Resistance of Concrete," Thesis, The University of Texas at Austin, Austin, TX, 2012.

[13] Chen-Tan, N. W., van Riessen, A., Ly, C. V., and Southam, D. C., "Determining the Reactivity of a Fly Ash for Production of Geopolymer," *J. Am. Ceram. Soc.*, Vol. 92, No. 4, 2009, pp. 881–887.

[14] Pietersen, H. S., "Reactivity of Fly Ash and Slag in Cement," Ph.D. dissertation, Delft University of Technology, Delft, The Netherlands, 1993.

[15] ASTM C618: "Standard Specification for Coal Fly Ash and Raw or Calcined Natural Pozzolan for Use in Concrete," *Annual Book of ASTM Standards*, ASTM International, West Conshohocken, PA.

[16] Lloyd, R. R., "The Durability of Inorganic Polymer Cements," Ph.D. thesis, University of Melbourne, Melbourne, Australia, 2008.

[17] Lydon, J. W., "The Measurement of the Modal Mineralogy of Rocks from SEM Imagery: The Use of MultiSpec and ImageJ Freeware," Geological Survey of Canada, Open File 4941, 37 pp. 2005.

[18] Bentz, D. P. and Rémond, S., "Incorporation of Fly Ash into a 3-D Cement Hydration Microstructure Model," *Report No. NISTIR 6050*, National Institute of Standards and Technology, Gaithersburg, MD, 1997.

[19] Hemmings, R. T. and Berry, E. E., "On the Glass in Coal Fly Ashes: Recent Advances," *Mater. Res. Soc. Symp. Proc.*, Vol. 113, 1988, pp. 3–38.

Geopolymer Binder Systems
STP 1566, 2013
Available online at www.astm.org
DOI:10.1520/STP156620120084

Sravanthi Puligilla[1] *and Paramita Mondal*[2]

Microstructural Changes Responsible for Hardening of Fly Ash–Slag Geopolymers Studied through Infrared Spectroscopy

REFERENCE: Puligilla, Sravanthi and Mondal, Paramita, "Microstructural Changes Responsible for Hardening of Fly Ash–Slag Geopolymers Studied through Infrared Spectroscopy." *Geopolymer Binder Systems*, STP 1566, Leslie Struble and James K. Hicks, Eds., pp. 21–33, doi:10.1520/STP156620120084. ASTM International, West Conshohocken, PA 2013.[3]

ABSTRACT: Geopolymers are being studied extensively as a potential replacement for Portland cement. However, very few studies have focused on characterizing the setting and stiffening of geopolymers. The main objective of this research is to relate microstructural changes with the hardening of geopolymers, especially Class F fly ash–slag-based geopolymers. The raw materials were thoroughly mixed with potassium silicate and potassium hydroxide for activation. The hardening rate was studied using the Proctor penetration test (ASTM C430) and the shear wave ultrasonic wave reflection method. The microstructural changes responsible for hardening were studied by characterizing geopolymer solids using Fourier transform infrared spectroscopy (FTIR) and the x-ray diffraction method (XRD). It was observed that XRD could not detect the changes happening with time because the geopolymer product was amorphous. However, FTIR clearly showed a shift in the Si-O-*T* (*T* = Al, Si) asymmetric stretching band to lower wavenumbers, indicating the development of a geopolymer product with time. The main drawback of using FTIR was that Si-O-*T* vibrations from the initial ash, the geopolymer product, and calcium silicate hydrate yield an overlapping spectrum resulting in a broad hump that was

Manuscript received June 16, 2012; accepted for publication November 19, 2012; published online April 26, 2013.

[1]Graduate Research Assistant, Dept. of Civil and Environmental Engineering, 2145 Newmark Civil Engineering Laboratory, Univ. of Illinois, 205 N. Mathews Ave., Urbana, IL 61801-2352, United States of America.

[2]Assistant Professor, Dept. of Civil and Environmental Engineering, 2129 Newmark Civil Engineering Laboratory, Univ. of Illinois, 205 N. Mathews Ave., Urbana, IL 61801-2352, United States of America.

[3]ASTM Symposium on *Geopolymer Binder Systems* on June 26–27, 2012 in San Diego, CA.

difficult to interpret. In order to resolve this, FTIR was performed on the solid residue after selective dissolution of calcium silicate hydrate and geopolymer product by salicylic acid and hydrochloric acid, respectively. This revealed the presence of calcium silicate hydrate in the samples at an early age.

KEYWORDS: fly ash–slag geopolymer, hardening, FTIR, UWR, Proctor, C-S-H

Introduction

Metakaolin geopolymers made with high alkalinity and cured at high temperatures have been widely studied, and they exhibit uniform properties. The properties of geopolymers that use fly ash as a raw material (Class C and Class F) are variable and gaining much importance as a result of their abundance. Moreover, the composition of fly ash varies drastically and can change the setting time of fly ash geopolymers from a few minutes to a few days. For example, Class F fly ash geopolymers made with activators of low alkalinity and cured at ambient temperature take as long as 3 days or more to set. Previous studies have revealed that the addition of calcium in any soluble form accelerates the hardening process [1–3]. However, the reasons for this accelerated hardening are still being studied. Earlier studies found rapid hardening in the presence of calcium by measuring initial and final set times using Vicat (ASTM C191 [4]) [5]. The inability of Vicat to successfully monitor the hardening rate of pastes has prompted researchers to employ novel techniques such as shear wave ultrasonic wave reflection (S-wave UWR) and Proctor penetration methods (ASTM C403 [6]) to study the hardening rate and define the set times for geopolymers [2,3,7]. UWR is a continuous measurement technique and therefore offers an advantage over traditional penetration tests like Proctor and Vicat. Proctor and Vicat measure the resistance offered to a penetrating needle only at discrete intervals; thus there is the possibility of missing events between those discrete measurements. UWR has been widely used to understand the hardening behavior of cement pastes. A few studies have shown recently that it can be successfully employed to monitor the hardening rate of geopolymers [8,9]. However, because of the gelatinous nature of the geopolymer, it is recommended that S-wave UWR be used in conjunction with the Proctor resistance method [7]. Studies have successfully monitored the hardening of fly ash geopolymers in the presence of calcium by using both S-wave UWR and the Proctor penetration method [2,3,7].

In the presence of calcium, some studies have hypothesized that the early precipitation of calcium hydroxide or C-S-H creates nucleation sites,[4] promoting early geopolymerization and accelerated hardening [1]. The coexistence of C-S-H and geopolymeric gel already has been observed by several authors in later-age

[4]Cement chemist's notation: C-S-H is an abbreviation for calcium silicate hydrate of variable composition; C = CaO, S = SiO_2, and H = H_2O.

samples [10]. However, it is much more difficult to characterize the material at an early age in order to investigate for the presence of C-S-H and geopolymer because of the abundance of unreacted raw material and the amorphous nature of the products formed. Fourier transform infrared spectroscopy (FTIR) has been used as an important tool to characterize gels like geopolymers. The infrared (IR) spectra of geopolymers and precursors consist of the strongest vibrations found in all aluminosilicates. They are assigned to internal vibrations of Si–O–Si and Si–O–Al and are found at 950–1250 cm^{-1} and 420–500 cm^{-1}. However, attention should be given to the fact that the presence of Si–O–*T* (*T* = Al, Si) vibrations of different origins—namely, from the initial ash, geopolymer product, and calcium silicate hydrate—yields an overlapping spectrum band resulting in a broad hump whose correct interpretation is difficult.

In order to overcome this difficulty, the geopolymers can be subjected to various chemical attacks such as salicylic acid–methanol (SAM) extraction and HCl treatment. The SAM extraction separates calcium silicates from the unreacted fly ash, unreacted slag, and geopolymer. The HCl treatment dissolves geopolymers, zeolites, and unreacted slag grains and removes calcium ions from hydrated silicate and aluminate phases, leaving behind unreacted fly ash [11,12]. Dissolution techniques followed by FTIR and x-ray diffraction (XRD) studies can give more insightful information about this otherwise difficult problem. The present study employs UWR and the Proctor penetration method to define the hardening rate of fly ash–slag geopolymer and employ characterization techniques such as FTIR and XRD to understand the reasons for the hardening.

Experimental Procedures

The raw materials used in the study were Class F fly ash (supplied by Boral Technologies) and ground granulated blast furnace slag (supplied by the Lafarge corporation). The oxide compositions of fly ash and slag (provided by suppliers) are given in Table 1. Raw materials were activated using a mixture of reagent-grade potassium silicate and potassium hydroxide pellets supplied by Fisher Scientific. The water-to-solids ratio was 0.32, and the modulus of the activator SiO_2/K_2O was 1.25. The concentration of the activator solution was 2.3 M.

Potassium hydroxide crystals were dissolved in water and mixed with potassium silicate to achieve a desired modulus of 1.25. The activator solution was stored overnight before being mixed with dry powders. Geopolymer was synthesized by mixing 75 % of fly ash and 25 % of slag (by total weight of powders) with the activator solution. Dry powders were weighed and were mixed for 30 s in a KitchenAid mixer. The activator solution was added and mixed for the next 3.5 min at the same speed. The reaction was observed to be

TABLE 1—*Oxide composition of raw materials used in the study, wt. %.*

Composition	Fly Ash	Slag
SiO_2	60.17	35.7
Al_2O_3	21.91	11.21
CaO	1.81	39.4
Na_2O	0.81	0.26
K_2O	2.13	0.48
MgO	1.28	10.74
Fe_2O_3	7.57	0.42
SO_3	0.17	0.58

sensitive to temperature and shear rate. To maintain the uniformity across the different tests, all raw materials were stored at a constant temperature (22°C ± 2°C), and 500 g of material was mixed at constant shear unless otherwise mentioned.

A modified version of the standard procedure mentioned in ASTM C403 [6] was employed to determine the hardening rate of geopolymers using the Proctor method as described elsewhere [11]. The mixing procedure was the same as described earlier, except for the amount of the mix (2000 g instead of 500 g). After the sample was prepared, it was poured into a container 150 mm × 150 mm in size to a depth of 50 mm. The container was tapped against a table three times to level out the paste and then covered with a moist towel to prevent the evaporation of water. Six needles were used with respective cross-sections of 645 mm^2, 323 mm^2, 161 mm^2, 65 mm^2, 32 mm^2, and 16 mm^2. An Instron testing frame was programmed such that needles would penetrate to a depth of 25 mm in 10 ± 2 s as prescribed in the code. Measurements were made starting with the needle of the largest area, and needles were changed as needed to provide the required penetration (~25 mm in 10 ± 2 s) until the smallest needle was used. The measured load was divided by the area of the needle to calculate the penetration resistance and plotted against time.

The S-wave UWR test was performed according to the procedure developed by Chung et al. [8]. After mixing, paste was poured into a container with an approximate size of 50 mm × 60 mm × 50 mm. The container was made of a high-impact polystyrene 6.25 mm in thickness. A contact type 2.25 MHz S-wave transducer was attached to the bottom of the container, and the container acted as a buffer between the paste and the transducer. The transducer was connected to a pulser/receiver unit that was connected to a computer equipped with a digitizer.

When a normal wave is incident at a boundary between two different materials, a part of the energy is reflected and a part of it is transmitted. The amount of wave energy reflected depends on the relative acoustic impedances of the two materials and is governed by the reflection coefficient R.

$$R = \left| \frac{z_p - z_b}{z_p + z_b} \right| \quad (1)$$

where z_p and z_b are the acoustic impedances of the paste and the buffer, respectively. Shear waves can be transmitted through a solid, but not through a fluid. As the geopolymer paste transforms from liquid to solid, the amount of transmitted shear wave energy increases and the reflection coefficient decreases. Therefore, changes in paste as a function of time can be monitored using UWR when a buffer of constant acoustic impedance is used. The time domain signals of the reflected ultrasonic pulses are measured and analyzed to determine the normal incidence reflection coefficient of the interface between the buffer and the paste. More details of the signal processing of the method can be found elsewhere [8]. The behavior of mixes obtained from S-wave UWR was compared with the results from the Proctor penetration method. The rate of stiffening was monitored for 24 h or until complete debonding was seen. Debonding can be described as a phenomenon whereby paste loses contact with the buffer material, creating an air gap. The presence of the air gap reflects all the shear energy, which inhibits the measurement of any meaningful data thereafter.

Raw materials and geopolymer samples were analyzed using XRD. Representative samples were collected at various ages, treated with acetone to stop the reaction, and finely powdered. X-ray diffractograms were recorded on a Siemens-Bruker D 5000 using Cu K_γ radiation at a voltage of 40 kV and a current of 30 mA. Specimens were scanned from 5 –70 2θ at 0.02 2θ steps and stepped at a rate of 1° min^{-1}. A Thermo Nicolet Nexus 670 Fourier transform infrared spectrophotometer with an attenuated total reflectance accessory was used in absorption mode to acquire spectra in the frequency range of 2000–750 cm^{-1} at a resolution of 4 cm^{-1}. A small amount of powdered sample was placed on the detector in order to collect a spectrum.

The presence of C-S-H was predicted to cause rapid hardening in geopolymer samples. However, C-S-H is amorphous and hard to distinguish from other phases, such as geopolymer. Therefore, SAM extraction was performed on samples collected at various ages. For SAM extraction, 1 g of geopolymer sample was added to a solution containing 9 g of salicylic acid mixed in 35 ml of methanol [12]. The mixture was stirred for 2 h, and the suspension was vacuum filtered using a Buchner funnel and a no. 50 Whattman filter. Insoluble residue was washed with methanol and stored in a vacuum desiccator until analysis. XRD and FTIR were done on these specimens in order to observe changes after the treatment.

Geopolymer products were selectively dissolved via treatment of the hardened paste with HCl. As described elsewhere, the experimental procedure consists of adding 1 g of activated fly ash (fly ash and slag in this case) to a beaker containing 250 ml of (1:20) HCl [13]. The mixture was stirred for 3 h, and stirring

was followed by filtration. Insoluble residue was washed with de-ionized water several times to achieve a neutral *p*H. The insoluble residue was dried at 100°C and then stored in the vacuum desiccator until the FTIR analysis was done.

Results and Discussion

Hardening of Geopolymer Pastes

Figure 1 presents a plot of the S-wave reflection coefficient versus the time for fly ash–slag geopolymer, along with the penetration resistance as measured via the Proctor method. The S-wave reflection almost remains constant for the first 10 min, and this is followed by a rapid drop indicating rapid hardening. The slope of the curve decreases after 60 min, indicating a reduction in the hardening rate. Data collection after 160 min was not possible as a result of the complete debonding of the sample from the buffer material.

Figure 1 also presents the Proctor resistance plotted as a function of time. The paste shows a rapid increase in resistance starting 5 min after mixing and continues at the same rate until the 80 min mark. This corresponds to a rapid drop in the reflection coefficient as observed via UWR, indicating rapid hardening/strength development. The slope of the Proctor resistance curve decreases around 80 min, indicating that the rate of strength gain has slowed down and hardening is continuing at a decreased rate. The time at which the slope of the Proctor resistance curve changes correlates well with the slope change of the S-wave reflection coefficient curve from UWR.

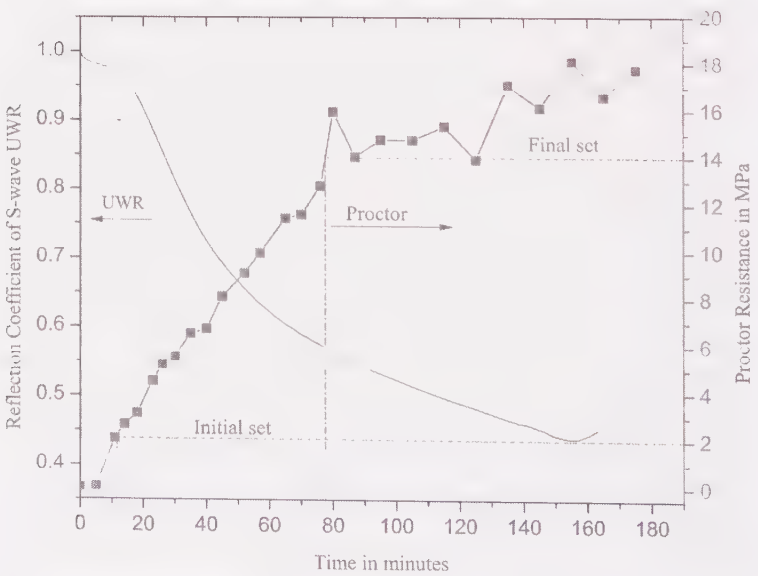

FIG. 1—*S-wave UWR and Proctor penetration tests on the fly ash–slag geopolymer.*

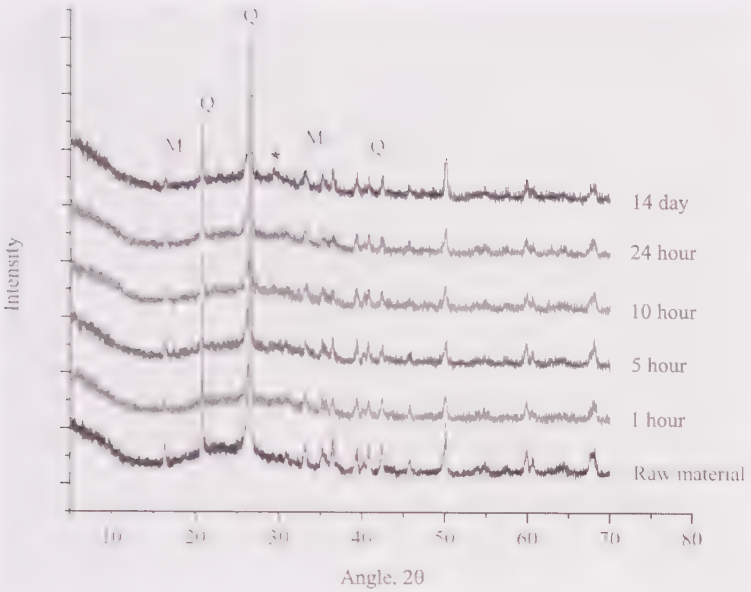

FIG. 2—*XRD patterns of fly ash-slag geopolymer at various ages. Q, quartz; M, mullite. There is a new peak designated by *.*

The penetration resistance values of cement paste corresponding to the values of initial and final setting of mortar extracted from concrete (according to ASTM C403 [6]) are defined as 2 MPa and 14 MPa, respectively [13]. Using this criterion, the initial set time of fly ash–slag geopolymer is determined to be 10 min, and the final set time is 80 min. These mixes are characterized as rapid hardening. These results agree with other studies showing that in the presence of soluble calcium ions, the setting of fly ash geopolymer is accelerated.

Characterization of Solid Geopolymer Product

The accelerated hardening (from UWR and Proctor) in the presence of soluble calcium ions is predicted based on the early precipitation of C-S-H [1–3]. Characterization techniques such as FTIR and XRD are used to characterize geopolymer solids and detect the presence of C-S-H at an early age. Samples of different ages, namely, 10 min, 60 min, 10 h, 24 h, and 14 days, were chosen (the first two are during the rapid hardening phase measured by UWR and Proctor) to characterize the evolution of products with time.

Figure 2 gives XRD patterns of fly ash-slag geopolymer at 60 min, 5 h, 10 h, 24 h, and 14 days, along with that of the raw material. The geopolymer samples collected at various ages were compared with the base raw material (fly ash + slag). Though significant hardening was observed at 60 min via both UWR and the Proctor method, the XRD pattern of fly ash–slag geopolymer at an age of 60 min did not differ from the XRD pattern of the raw material, and a

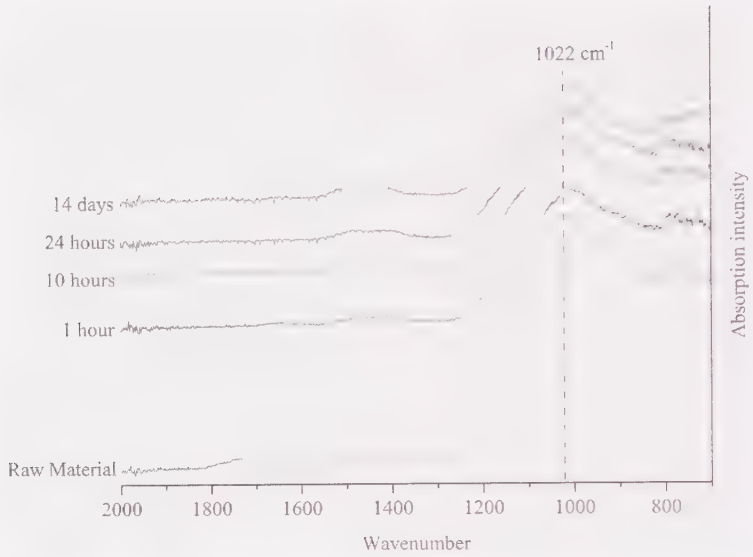

FIG. 3—*FTIR of the fly ash–slag geopolymer showing the shift in the position of the main band with time.*

similar observation was made with samples 5 h, 10 h, and 24 h old. XRD does not indicate the formation of new products because of their amorphous nature. The sample at 14 days shows a new peak at 29° 2*θ*, which can be attributed to either calcium carbonate or C-S-H. The samples were analyzed using FTIR to decipher the nature of amorphous products. Spectra were analyzed for the main asymmetric stretching vibration of Si–O–*T*, which lies in the range of 1100–900 cm^{-1}. The Si–O–*T* asymmetric stretching vibration band is referred to as the main band hereinafter. The changes in the FTIR spectra of fly ash–slag geopolymers with time are given in Fig. 3. The spectra for pure fly ash and pure slag are taken separately and added in the ratio to obtain the spectrum for raw material. The main Si–O–*T* asymmetric band of raw material (fly ash + slag) is at 1022 cm^{-1}. In Fig. 3, the band associated with the Si–O–*T* asymmetric stretching vibration shifts perceptibly to a lower frequency with time. The exact position of this band depends on the Al/Si ratio of the product and the Al atom content per unit of formula [14]. The band shifted to 990 cm^{-1} in 14 days, indicating the ongoing product formation.

The XRD pattern of the geopolymer at 60 min does not differ much from that of the base raw material, but Fig. 3 shows that the main asymmetric band shifts to a lower frequency within 60 min. This indicates the early formation of product, which explains the rapid hardening seen with UWR and the Proctor method. The presence of product is clear from the shift in the peak position, but the nature of the product cannot be deciphered. This is because of the overlapping spectra of Si–O–*T* vibrations from fly ash, geopolymer, and C-S-H.

Therefore, further analysis was done by treating the samples with SAM and HCl, and insoluble residues were analyzed using FTIR. The FTIR results of the sample at 60 min are given in Fig. 4.

Figure 4 shows that fly ash–slag geopolymer at 60 min has a main band with a peak centered at 1005 cm^{-1}, and after SAM extraction, the band shifts to 1038 cm^{-1}. The shift in the peak position indicates that some product has dissolved in SAM. Glasser et al. have studied the effect of various chemical treatments on cement–slag blends and concluded that there is partial dissolution of unreacted slag grains during SAM treatment [15]. It was recommended that the partial dissolution of slag be considered in the calculation of the degree of slag hydration. However, these treatments are still considered suitable for selectively dissolving certain phases that enrich the remaining phases, to use for other characterization methods such as nuclear magnetic resonance [16,17]. In the current study, FTIR characterization was performed on 100 % slag before and after the treatment with SAM. The FTIR spectrum was found to be essentially unchanged, even though a 12 % weight loss was observed. Therefore, the shift in the FTIR peak after SAM treatment can be considered as due only to the dissolution of calcium silicates, as SAM treatment does not affect fly ash and geopolymer. After the HCl treatment, the band moved to 1041 cm^{-1}, which is nothing but unreacted fly ash. This shift is greater than

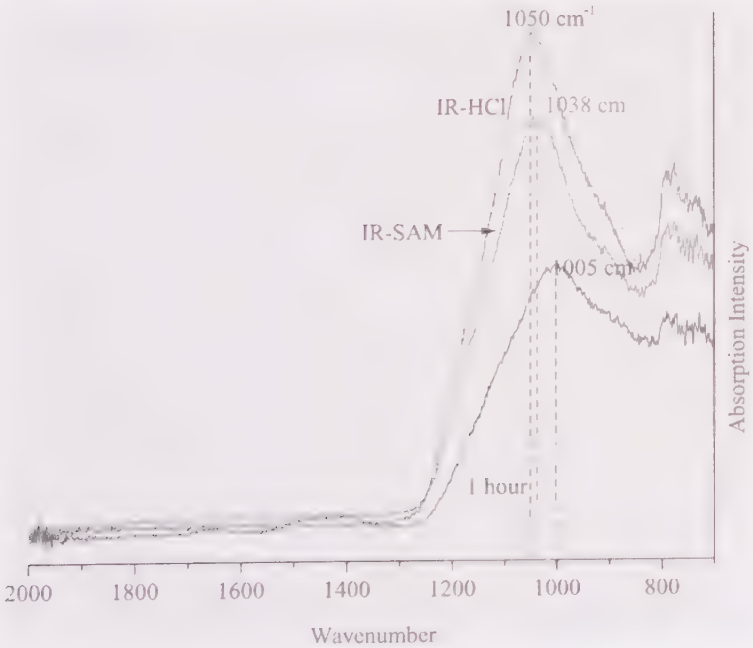

FIG. 4—*FTIR spectrum of 60-minute-old fly ash -slag sample. IR spectra of insoluble residue from SAM treatment (IR-SAM) and HCl treatment (IR-HCl) are also given.*

what has been observed after SAM treatment. In addition to dissolving geopolymer, HCl treatment also dissolves unreacted slag and depletes calcium silicate hydrates of calcium ions. The SAM treatment gives an indication of the presence of C-S-H, but the HCl treatment does not suggest the presence of geopolymer. However, energy dispersive spectroscopy (EDS) investigation of the sample at 60 min performed in a parallel study on a similar system indicates the presence of geopolymer [2]. The combined results of FTIR, FTIR on insoluble residue after chemical attacks, and EDS indicate the coexistence of C-S-H and geopolymer at 60 min. Yip et al. suggested that in the presence of soluble calcium, C-S-H precipitates and acts as nucleation sites [1]. This promotes the precipitation of geopolymer and results in accelerated hardening. The coexistence of C-S-H and geopolymer at an early age during the rapid hardening phase indicates that the precipitation of C-S-H could be the reason for the accelerated hardening.

The IR spectra of fly ash–slag geopolymer at ages of 10 h and 24 h also show a shift in the position of the main band after each successive treatment (similar to Fig. 4). XRD study of a 14-day-old sample indicated the presence of a new peak that could be either C-S-H or $CaCO_3$. So, FTIR was done on the sample at 14 days, and this was followed by various selective dissolution techniques in an attempt to understand the nature of product. Figure 5 shows that the sample at 14 days has a main band with a peak centered at 990 cm^{-1}, and after SAM extraction, the band shifted to 1026 cm^{-1}. After HCl treatment, the band moved to 1046 cm^{-1}, which is again very similar to the unreacted fly ash.

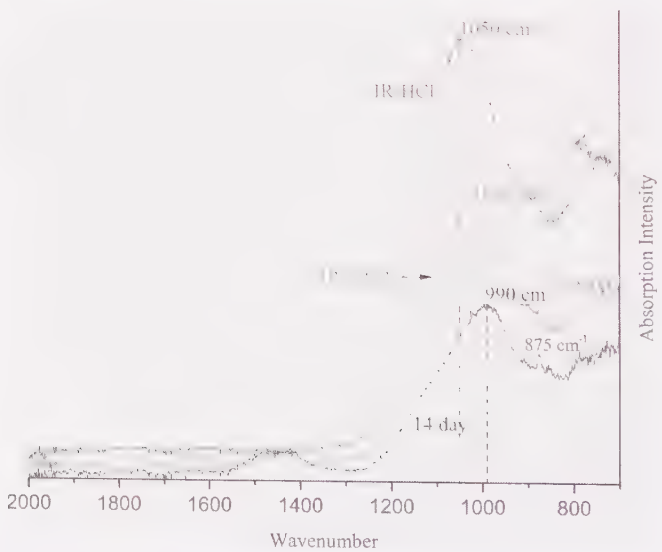

FIG. 5—*FTIR spectrum of 14-day-old fly ash–slag sample. IR spectra of insoluble residue from SAM (IR-SAM) and HCl (IR-HCl) treatments are also given. The absorption intensity is given on the y-axis.*

The change in the band position after selective dissolution treatments indicates the presence of C-S-H gel, and EDS data (as reported elsewhere) combined with FTIR indicate the presence of geopolymer gel in a 14-day-old sample [2]. The broad peak at 1450 cm^{-1} indicates a typical C–O stretching vibration and is attributed to $CaCO_3$. A smaller peak visible at 875 cm^{-1} in the original sample also indicates the presence of calcium carbonate, which explains a new peak visible via XRD. The presence of calcium carbonate is more prominent in older samples than in the early-age samples, indicating carbonation during the curing or storage of samples.

Conclusions

1. A combination of the Proctor penetration test and the shear wave ultrasonic wave reflection (S-wave UWR) method was successfully used to monitor the hardening of geopolymer. Fourier transform infrared spectroscopy (FTIR) and the x-ray diffraction method (XRD) were employed to relate microstructural changes to hardening.
2. FTIR was found to be sensitive enough to indicate product formation as early as 60 min, though overlapping Si–O–Si and Si–O–Al bands from unreacted fly ash, geopolymer, and calcium silicate hydrate made it difficult to determine the nature of the product formed.
3. FTIR performed on solid residues after selective dissolution using salicylic acid and hydrochloric acid, combined with EDS data from a different study, was successful in proving the coexistence of C-S-H and geopolymer in both early and later age samples.
4. The formation of C-S-H at an early age is predicted to be a reason for accelerated hardening as observed in the case of fly ash–slag geopolymers.

Acknowledgments

The writers thank Prof. Leslie J. Struble, Prof. John S. Popovics, and Prannoy Suraneni for their invaluable help with the use of UWR and Proctor instruments. X-ray diffraction analyses are carried out in part in the Frederick Seitz Materials Research Laboratory Central Facilities, University of Illinois, which are partially supported by the U.S. Department of Energy under Grant Nos. DE FG02 07 07ER46453 and DE FG02 07ER46471. The writers also thank Prof. Timothy Strathmann and Derek Vardon for their help with the FTIR instrument.

References

[1] Yip, C. K., Lukey, G. C., Provis, J. L., and van Deventer, J. S. J., "Effect of Calcium Silicate Sources on Geopolymerisation," *Cem. Concr. Res.*, Vol. 38(4), 2008, pp. 554–564.

[2] Puligilla, S. and Mondal, P., "Role of Slag in Microstructural Development and Hardening of Fly Ash-Slag Geopolymer," *Cem. Concr. Res.*, Vol. 43, 2013, pp. 70–80.

[3] Puligilla, S., 2011, "Understanding the Role of Slag on Geopolymer Hardening and Microstructural Development," M.S. thesis, University of Illinois at Urbana Champaign, IL, p. 72.

[4] ASTM C191-08: "Standard Test Methods for Time of Setting of Hydraulic Cement by Vicat Needle," *Annual Book of ASTM Standards*, ASTM International, West Conshohocken, PA.

[5] Kumar, S., Kumar, R., and Mehrotra, S. P., "Influence of Granulated Blast Furnace Slag on the Reaction, Structure and Properties of Fly Ash-based Geopolymer," *J. Mater. Sci.*, Vol. 45(3), 2010, pp. 607–615.

[6] ASTM C403/C403-08: "Standard Test Method for Time of Setting of Concrete Mixtures by Penetration Resistance," *Annual Book of ASTM Standards*, ASTM International, West Conshohocken, PA.

[7] Suraneni, P., Puligilla, S., Eric, K. H., Chen, X., Struble, L. J., and Mondal, P., "Monitoring Setting of Geopolymers," *ACI Mater. J.* (unpublished).

[8] Chul-Woo, C., 2010, "Ultrasonic Wave Reflection Measurements on Stiffening and Setting of Cement Paste," Ph.D. thesis, University of Illinois at Urbana Champaign, IL, p. 197.

[9] Suraneni, P., 2011, "Ultrasonic Wave Reflection Measurements on Self-compacting Cements and Concretes," M.S. thesis, University of Illinois at Urbana Champaign, IL, p. 119.

[10] Yip, C. K., Lukey, G. C., and van Deventer, J. S. J., "The Coexistence of Geopolymeric Gel and Calcium Silicate Hydrate at the Early Stage of Alkaline Activation," *Cem. Concr. Res.*, Vol. 35(9), 2005, pp. 1688–1697.

[11] Fernandez-Jimenez, A., de la Torre, G., Palomo, A., Lopez-Olmo, G., Alonso, M. M., and Aranda, A. G., "Quantitative Determination of Phases in the Alkaline Activation of Fly Ash. Part II: Degree of Reaction," *Fuel*, Vol. 85, 2006, pp. 1960–1969.

[12] Taylor, H. F. W., *Cement Chemistry*, Thomas Telford, London, 1997.

[13] Chul-Woo, C., Maciej, M., In-Young, P., and Struble, L. J., "On the Evaluation of Setting Time of Cement Paste Based on ASTM C403 Penetration Resistance Test," *J. Test. Eval.*, Vol. 38(5), 2010, pp. 527–533.

[14] Fernandez-Jimenez, A. and Palomo, A., "Mid-infrared Spectroscopic Studies of Alkali-activated Fly Ash Structure," *Microporous Mesoporous Mater.*, Vol. 86(1–3), 2005, pp. 207–214.

[15] Luke, K. and Glasser, F. P., "Selective Dissolution of Hydrated Blast Furnace Slag Cements," *Cem. Concr. Res.*, Vol. 17, 1987, pp. 273–282.

[16] Vanessa, K., Emmanuel, G., and Scrivener, K. L., "Methods for Determination of Degree of Reaction of Slag in Blended Cement Pastes," *Cem. Concr. Res.*, Vol. 42, 2012, pp. 511–525.

[17] Dyson, H. M., Richardson, I. G., and Brough, A. R., "A Combined 29 Si MAS NMR and Selective Dissolution Technique for the Quantitative Evaluation of Hydrated Blast Furnace Slag Cement Blends," *J. Am. Ceram. Soc.*, Vol. 2, 2007, pp. 598–602.

Geopolymer Binder Systems
STP 1566, 2013
Available online at www.astm.org
DOI:10.1520/STP156620120077

M. Taxiarchou,[1] *D. Panias,*[1] *Ch. Panagiotopoulou,*[1] *A. Karalis,*[2] *and C. Dedeloudis*[2]

Study on the Suitability of Volcanic Amorphous Aluminosilicate Rocks (Perlite) for the Synthesis of Geopolymer-Based Concrete

REFERENCE: Taxiarchou, M., Panias, D., Panagiotopoulou, Ch., Karalis, A., and Dedeloudis, C., "Study on the Suitability of Volcanic Amorphous Aluminosilicate Rocks (Perlite) for the Synthesis of Geopolymer-Based Concrete," *Geopolymer Binder Systems*, STP 1566, Leslie Struble and James K. Hicks, Eds., pp. 34–53, doi:10.1520/STP156620120077, ASTM International, West Conshohocken, PA 2013.[3]

ABSTRACT: Geopolymerization is a low-cost, low-energy-demanding, green technology that can transform a variety of silicate and aluminosilicate raw materials and industrial by-products into useful, high-added-value products. Because of their excellent mechanical properties, the use of geopolymeric materials for the replacement of traditional construction materials is gaining ground. The most commonly used raw materials for geopolymer synthesis include metakaolin, fly ash, ground granulated blast furnace slag, and their mixtures. In this work, an amorphous aluminosilicate rock (perlite) was selected as a raw material in order to determine its utility in the synthesis of new Portland cementless binders for concrete. The effect of the following synthesis parameters on the development of the mechanical properties of the geopolymeric formulations were studied: the curing conditions (t – 24, 48, 72 h; T = 50 C, 70 C, 90 C); the water/solid mass ratio (m_w/m_s – 0.28 to 0.37); the Si/Al molar ratio (5.6 to 6.5); and the alkali content and type of alkali ion (R/Al molar ratio – 0.65 to 1.05; R Na or K). The structural changes were identified by means of x-ray diffraction (XRD), Fourier transform

Manuscript received June 15, 2012; accepted for publication November 20, 2012; published online April 24, 2013.

[1]National Technical University of Athens, School of Mining and Metallurgical Engineering, Athens, Greece 15780.

[2]S&B Industrial Minerals S.A., Athens, Greece 14564.

[3]ASTM Symposium on *Geopolymer Binder Systems* on June 26–27, 2012 in San Diego, CA.

infrared spectroscopy (FTIR), and scanning electron microscopy (SEM), and the mechanical properties were evaluated through compressive strength measurements. The most promising formulations were used for the synthesis of mortars using standard silica sand, according to ASTM C109/109C. Also in this case, compressive strength measurements were carried out while the structure was observed using XRD, FTIR, and SEM. The present study shows that perlite is a promising raw material for geopolymer synthesis, resulting in geopolymeric pastes with compressive strengths greater than 30 MPa. In contrast to the other raw materials currently used for geopolymerization, the geopolymerization of perlite requires a prolonged curing time of a total duration of 5 days at 70°C.

KEYWORDS: geopolymer concrete, perlite, compressive strength

Introduction

Geopolymer technology is new, upcoming technology in the area of construction materials, producing materials with excellent mechanical and thermal properties [1]. Geopolymer synthesis is based on the activation of aluminosilicate materials by an alkali metal hydroxide and an alkali metal salt and their transformation into a three-dimensional inorganic amorphous structure [2].

There are a number of factors that are reported to affect geopolymerization, such as the Si/Al molar ratio [3–5], the water content [6], the alkali content [4,7], and the curing conditions [6,8]. Theoretically, any aluminosilicate material can serve as the raw material for geopolymerization under certain conditions. Other works have reported the formation of geopolymers from natural minerals [9–11], calcined clays [12,13], and industrial by-products [14–17]. The most commonly used raw materials for geopolymer synthesis include ground granulated blast furnace slag, fly ash, and metakaolin, as the geopolymers produced from these possess enhanced properties. In this work, the geopolymerization of an aluminosilicate rock, perlite, is studied.

Our main aim was to investigate the utilization of perlite as a raw material for the synthesis of new Portland-cementless binders for concrete. The ability to produce geopolymers with good mechanical properties from aluminosilicate rocks that are generally not preferred for the synthesis of compact geopolymers is another opportunity related to the raw material selection [9,18]. The main parameters that affect the geopolymerization of perlite were studied, and their effect on the compressive strength and the structure of the synthesized inorganic polymeric materials was determined.

Experimental

Raw Material

Perlite used in the present study was obtained from S&B Industrial Minerals S.A. and originates on the island of Milos, Greece. The chemical composition

TABLE 1—*Chemical composition of perlite, % w/w.*

SiO_2	Al_2O_3	Fe_2O_3	CaO	MgO	K_2O	Na_2O	SO_3	L.O.I.
73.45	10.98	1.12	0.95	0.44	5.93	3.77	—	3.16

Note: L.O.I. = Loss of Ignition.

of the perlite is presented in Table 1. Its mean particle size (d_{50}), measured in a Malvern laser particle analyzer, was equal to 42.88 μm. According to x-ray diffraction analysis, this material was mostly amorphous, and the main crystalline phases that could be detected were quartz, cristobalite, Na-feldspars, K-feldspars, biotite, and traces of impurities such as maghemite and hydroxysodalite that are attributed to its processing.

A leaching test was also performed on perlite in order to estimate its ability to release silicon and aluminum species in sodium solution. The test was performed by mixing 0.5 ($\pm$0.0001) g of solid with 20 ml of NaOH 10 M solution at ambient temperatures for 24 h with continuous stirring. After filtering, the clear liquid part was diluted to 250 ml and neutralized by the addition of concentrated HCl acid. Atomic absorption spectroscopy of the solution, performed in a Perkin Elmer 2100, was used in order to determine the Al and Si concentrations in the solution. The results of the leaching test are presented in Table 2.

Experimental Procedures

Apart from perlite, an alkaline aqueous silicate activation solution was used for the synthesis of geopolymeric formulations. This solution was prepared by dissolving anhydrous sodium or potassium hydroxide in pellets (Merck, 99 % purity) in deionized water and adding commercial silicon oxide, 50 % w/w in H_2O in colloidal dispersion. The activation solution was prepared with appropriate quantities of the reactants, calculated according to the requirements of each experiment, and stored for a minimum of 24 h prior to its use to allow it to attain equilibrium. Perlite and the activation solution were mechanically mixed to form a homogeneous slurry that was then transferred to 50 mm $\times$ 50 mm $\times$ 50 mm cubic molds and mildly vibrated. The molds were covered and placed in a laboratory oven for curing. The curing conditions (e.g., temperature and time) were studied in detail as the first parameter affecting the mechanical properties of the produced inorganic polymeric materials. After curing, the cubic samples were left at ambient temperature for 7 days before we measured

TABLE 2—*Percent dissolution of Si and Al from perlite after leaching for 24 h in 10M NaOH solution.*

Solution/Measured Concentration	Si, ppm	Si, %	Al, ppm	Al, %
NaOH 10M	59.3	**9.19**	12.8	**11.73**

the compressive strength and carried out the x-ray diffraction (XRD), Fourier transform infrared (FTIR), and scanning electron microscopy (SEM) analyses.

For the preparation of mortars, standard silica sand was utilized with a grain distribution in line with ASTM C33-03 [19]. The perlite and sand quantities were in accordance with ASTM C109-109 M [20]. The mixing procedure was typical of geopolymer synthesis, with the geopolymer paste prepared first and the sand added at the end.

Analysis and Tests

The mineralogy and structure of the produced geopolymeric materials were studied by means of XRD on a SIEMENS D 5000 diffractometer, SEM on a JEOL JMS-5600, and FTIR using a Perkin Elmer Spectrum 100. The uniaxial compressive strength was measured using Advantest 9 and Sercomp 7.

Results and Discussion

Curing Conditions

The aim of the first set of experiments was to evaluate the effect of the curing conditions on the development of perlite-based geopolymers' compressive strength and define the optimal conditions in which the geopolymer reaction is favored. A series of geopolymer samples was synthesized with the following composition: Si/Al = 6.0, Na/Al = 0.75, s/w = 3.1. The samples were then allowed to cure under varying conditions (time = 24, 48, 72 h; intermediate phase duration = 0 to 6 days; temperature = 50 C, 70 C, 90 C).

The curing of geopolymers usually takes place in a single stage at a temperature of 50 C to 70 C for 24 to 72 h [21,22]. However, after curing at 70 C for 48 h, the perlite-based geopolymers did not possess any mechanical properties. The demolding revealed wet, plastic, and friable specimens. As a result, a second curing phase was introduced for the demolded specimens, after an intermediate stay of the specimens at ambient conditions. Figure 1 presents the compressive strength of geopolymer samples after the end of the second curing phase (at 70 C for 72 h) and varying durations of the intermediate stage. As can be seen, the presence of an intermediate stage between the two curing phases had practically no effect on the development of compressive strength. In all cases, the specimens reached almost the maximum of the specific synthesis compressive strength capacity (about 30 MPa), with slightly better results acquired with the omission of the intermediate stage (0 days).

In Fig. 2, the effect of the duration of the second curing phase on the compressive strength of geopolymers can be seen. Curing for 24 h resulted in specimens with reduced compressive strength, indicating incomplete geopolymerization, and their interior was still moist. Curing for 72 h led to an increase

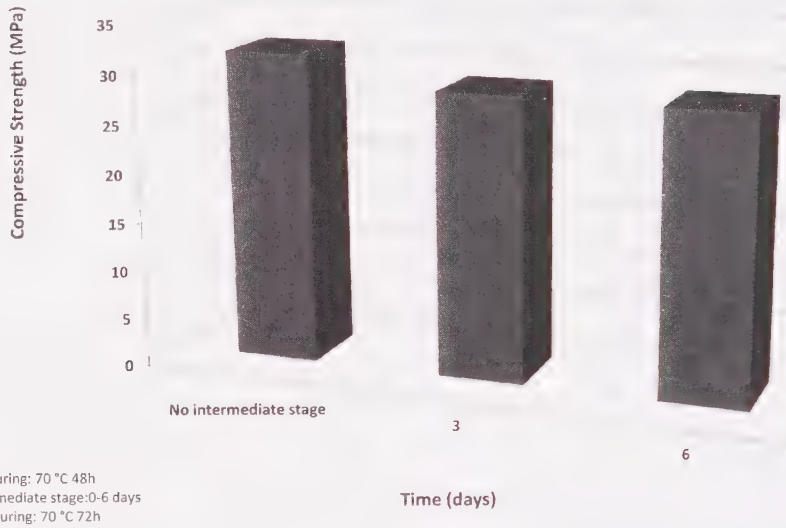

FIG. 1—*The effect of an intermediate curing stage on the compressive strength of perlite-based geopolymers (first curing: 70°C/48 h; intermediate stage: 0 to 6 days; second curing: 70°C/72 h).*

of the compressive strength and, possibly, a more complete reaction of the raw material.

The effect of the applied temperature in the second curing phase was also studied. The compressive strengths of the produced materials at different

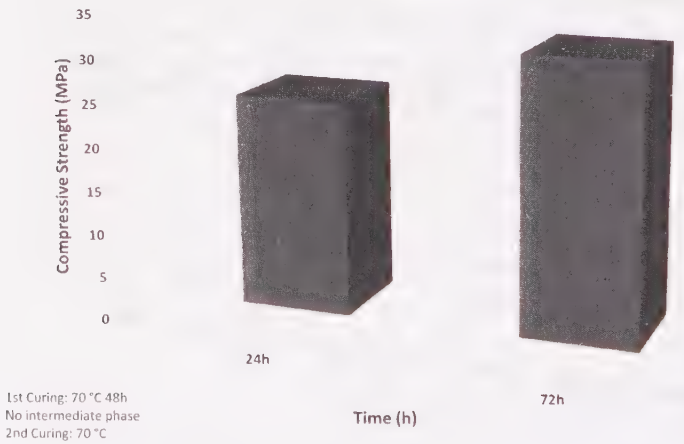

FIG. 2—*The effect of B curing phase duration on the compressive strength of perlite-based geopolymers (first curing: 70°C/48 h; no intermediate stage; second curing: 70°C).*

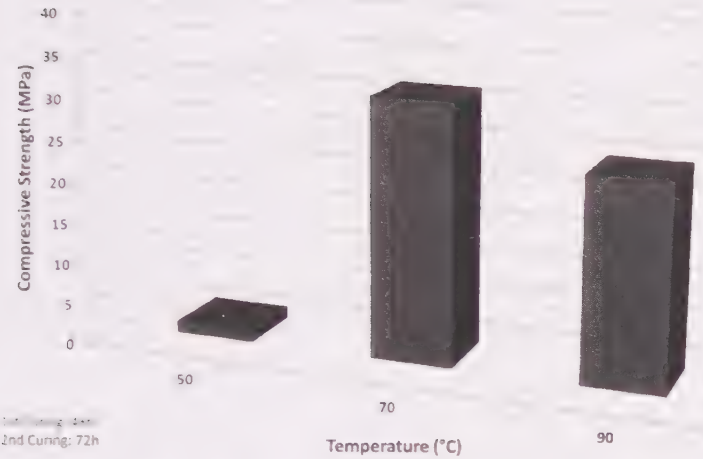

FIG. 3—*The effect of curing temperature on the compressive strength of perlite-based geopolymers (first curing: 48 h; no intermediate stage; second curing: 72 h).*

temperatures are given in Fig. 3. The optimum compressive strength was achieved after curing at 70 C. At 50 C, even with prolonged curing, the specimens remained moist and retained some plasticity, and their compressive strength was extremely low. The reduced mechanical properties can be attributed to the presence of water within the pores of the material, which can inhibit the completion of the reaction by moving reactants away from the reaction sites. After curing at 90 C, the samples did not contain any humidity and presented adequate compressive strength. Nevertheless, small cracks could be detected on their surface, which can be attributed to the abrupt evaporation of water due to the elevated temperature; this can lead to the collapse of the matrix during compressive strength testing.

The results from the study of the curing conditions indicate that the application of heat can accelerate the geopolymerization process but does not actually affect the given formulation capacity.

Effect of Water Content

Water is necessary for geopolymer synthesis in order to facilitate the mixing procedure, and it provides the means of transportation of the reactive species to the reaction sites. The effect of the water content was studied over a range of water-to-solid mass ratios from 0.28 to 0.37 g/g. The other parameters of the system were kept constant at molar ratios of Si/Al 6.0 and Na/Al 0.75 (initial concentrations of NaOH and SiO_2 in the aqueous phase were 5.4 M and 3.7 M, respectively). The compressive strengths of the synthesized geopolymers at the studied water-to-solid ratios (m_w/m_s) are presented in Fig. 4.

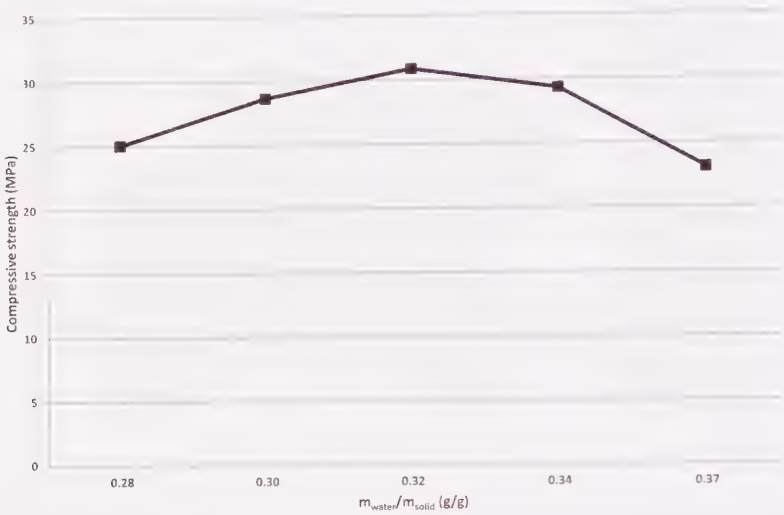

FIG. 4—*Compressive strength of perlite-based geopolymers in relation to the* m_w/m_s *ratio (Si/Al = 6.0, Na/Al = 0.75).*

The maximum compressive strength (around 30 MPa) was reached at m_w/m_s 0.32. There is a range of m_w/m_s values around this optimum value in which the compressive strength remains practically constant. At higher and lower ratios, the compressive strength decreases, although the XRD and FTIR patterns do not reveal any significant differences in the structure of the produced geopolymeric materials.

In the case of reduced water content, the compressive strength decrease can be attributed to the difficulties in the mixing procedure and the limited wetting of raw material, which can result in reduced participation of the available Si and Al and, therefore, reduced development of the geopolymeric network. Furthermore, the unreacted perlite, as a result of the limited wetting, can act as a defect of the geopolymeric matrix.

The increased presence of water possibly decreases the Si and Al species saturation level and reduces the rate of the polycondensation of their oligomers. Also, it has been suggested by other authors that an increased water content can promote the leaching of the most soluble reactants and their removal from the reaction sites [6]. Additionally, the excess water, which evaporates during the curing procedure, possibly leaves more pores, and this can have a negative effect on the mechanical properties.

Effect of the Initial SiO_2 Concentration in the Activation Solution

The Si/Al molar ratio is one of the most important parameters in geopolymer synthesis, because it can differentiate geopolymers' microstructures and, consequently, their properties [21,23,24]. Because the exact Si/Al ratios of the gel

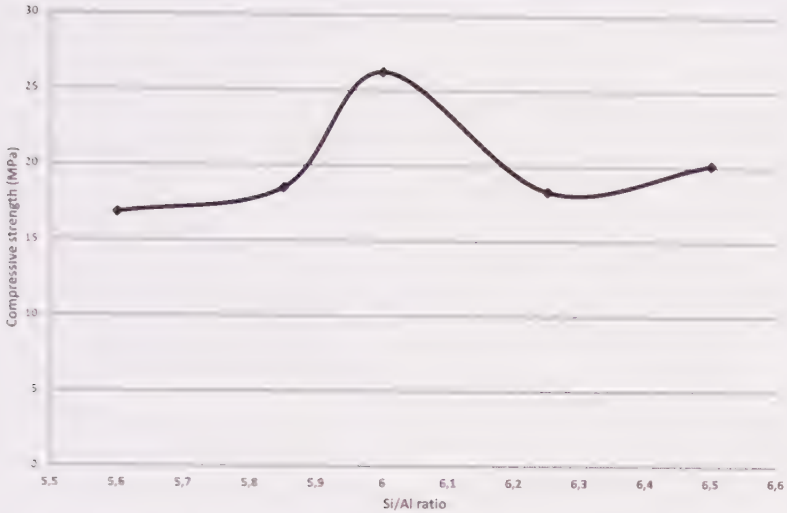

FIG. 5—*Compressive strength of perlite-based geopolymers in relation to the Si/Al molar ratio ($m_w/m_s = 0.32$, Na/Al = 0.75).*

formed during the reaction and of the final products cannot be defined because of the nature of geopolymerization, this ratio involves the initial Si and Al contents of the raw material and the activation solution. Therefore, it is an apparent ratio that cannot be used for comparisons between different raw materials, but it is a valuable tool for understanding the geopolymerization behavior of a specific raw material.

The effect of the initial silica concentration in the aqueous phase on the geopolymer compressive strength was investigated in the range of Si/Al molar ratios from 5.6 to 6.5. In all experiments of this series, the water content was kept constant and equal to $m_w/m_s = 0.32$, which is the optimum value obtained in the previous series of experiments, and the NaOH concentration in the aqueous solution was 5.7 M (Na/Al molar ratio = 0.75).

Figure 5 presents the compressive strength of the synthesized geopolymers in relation to the different Si/Al ratios. An Si/Al ratio of 5.6 refers to a geopolymer prepared without the addition of soluble silica, and, as can be seen, this geopolymer possesses relatively low compressive strength. The addition of soluble silica to the activation solution favors the development of geopolymers' compressive strength, which reached a value of 27 MPa at an Si/Al ratio of 6.0. Any further increase of the amount of soluble silica (higher Si/Al ratios) results in geopolymers with reduced mechanical properties.

In Figs. 6 and 7, the XRD and FTIR patterns of the geopolymers synthesized with different Si/Al ratios are presented and compared to that of perlite. As can be seen in Fig. 6, relative to the perlite XRD pattern, the XRD patterns of all geopolymer samples demonstrate a slight shift of the hump between 20 and 30 2θ, which is ascribed to the amorphous aluminosilicates. This shift is

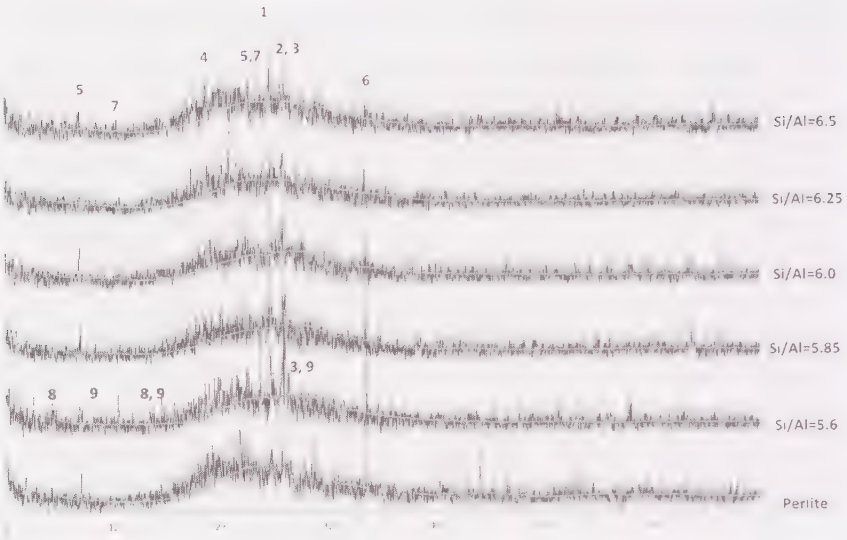

FIG. 6—*XRD of perlite and geopolymers synthesized with different Si/Al ratios. 1, quartz; 2, Na-feldspars; 3, K-feldspars; 4, cristoballite; 5, biotite; 6, maghemite; 7, hydroxysodalite; 8, Na-faujasite; 9, phillipsite.*

indicative of changes in the aluminosilicate network and can be attributed to geopolymerization [21]. Furthermore, in all geopolymer patterns, almost all crystalline phases (with the exception of hydroxysodalite) contained in the raw material can be detected, namely, quartz ($d_{100} = 3.35$ Å), cristobalite ($d_{999} = 4.05$ Å), Na-feldspars ($d_{100} = 3.2$ Å), K-feldspars ($d_{100} = 3.32$ Å), biotite ($d_{999} = 10.06$ Å), and maghemite ($d_{999} = 2.51$ Å). In the geopolymer sample synthesized without the addition of soluble silica (Si/Al – 5.6), new crystalline phases attributed to zeolites (Na-faujasite, $d_{100} = 14.28$ Å; Phillipsite, $d_{100} = 3.19$ Å, $d_{80} = 7.2$ Å) can be identified, and the characteristic peaks of hydroxysodalite ($d_{100} = 3.63$ Å, $d_{80} = 6.28$ Å) seem to be enhanced. The geopolymers with Si/Al ratios = 5.85 to 6.25 do not present any significant differences except for the disappearance of the hydroxysodalite peaks. Nevertheless, at Si/Al – 6.5, hydroxysodalite can be detected once again, indicating reduced participation of the raw material in the geopolymerization process.

Figure 7 shows the FTIR spectra of perlite and the synthesized geopolymers in relation to the Si/Al ratio. The spectrum of perlite is broad and relatively featureless because of the glassy nature of this material. The main aluminosilicate phases in perlite (both crystalline and amorphous) have overlapping peaks in the region of 800–1300 cm^{-1}. This broad hump is the main feature in both the perlite and the geopolymer spectra and is associated with the Si–O–*T* (*T* = tetrahedral Si or Al) asymmetric stretching vibrations. The maximum of this hump, in the case of perlite, is around 1043 cm^{-1}, whereas in the case of geopolymers this band changes shape and shifts to lower

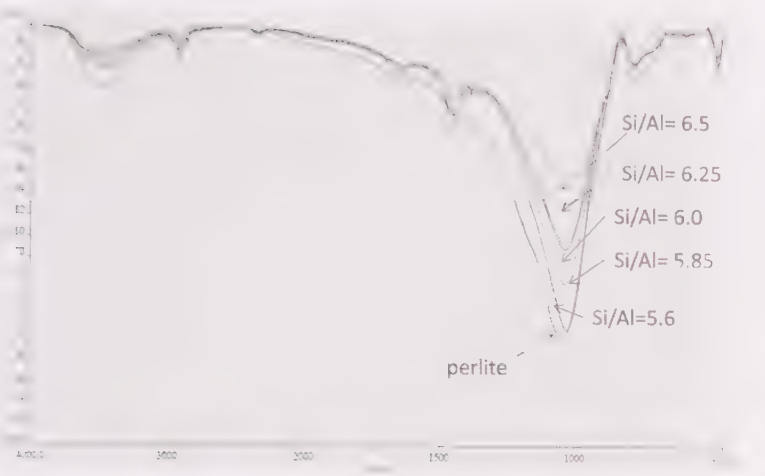

FIG. 7—*FTIR spectra of perlite and geopolymers synthesized with different Si/Al ratios.*

wavenumbers (1030 cm^{-1}). The position of this band gives an indication of the length and angle of the bonds in the silicate network. For amorphous silica, this peak occurs at approximately 1100 cm^{-1}. The shift of this band to lower wavenumbers, in the case of geopolymers, indicates an increase in the substitution of tetrahedral Al in the geopolymeric network. These values are in agreement with the relevant literature [25,26].

Figures 8 and 9 present SEM photographs of two different geopolymer samples with Si/Al ratios of 5.6 and 6.0, respectively. As can be seen in Fig. 8, the matrix of geopolymers synthesized with Si/Al = 5.6 presents a spongelike morphology with increased porosity. Within this matrix, unreacted crystalline phases (quartz, feldspars) are incorporated. The matrix of the geopolymer with Si/Al = 6.0, in Fig. 9, has a totally different morphology: that of a compact, homogeneous material with decreased porosity.

Taking into account all the presented data, geopolymers synthesized with different Si/Al ratios present significant differences regarding their mineralogy and microstructure, which could explain the differences in their compressive strength.

In the geopolymer sample with Si/Al = 5.6, along with the geopolymeric material, the formation of zeolites was observed. Taking into account the similarities between zeolitic and geopolymeric synthesis, this co-existence is not surprising and has also been reported by other authors [16,23]. The synthesis of crystalline phases is thermodynamically more favorable than that of amorphous phases, so in order to lead the reaction to the amorphous products, the system must be kinetically restrained. In the case of geopolymers, this can be achieved by reducing the water content, but such a state is induced mainly by the rapid polycondensation of Si oligomers. In the absence of soluble Si, the formation

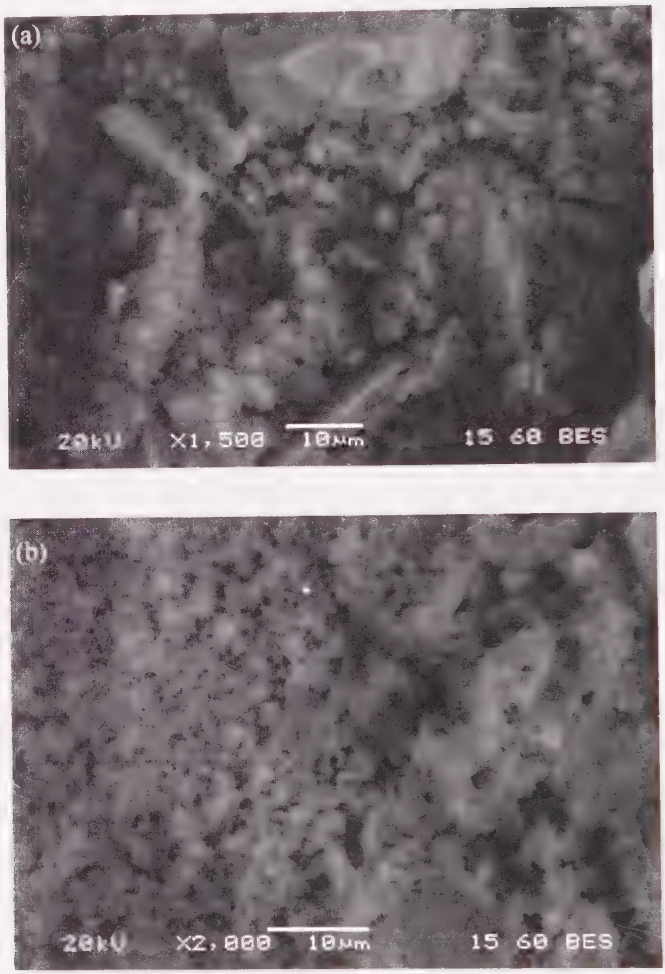

FIG. 8—*SEM photographs of the geopolymer matrix of the sample with Si/Al = 5.6.*

and polycondesation is delayed, favoring (locally) zeolitic synthesis. Furthermore, the formation of the zeolitic network requires the same species of Si and Al that are required for geopolymerization, rendering the two reactions competitive. The detection of zeolites within the geopolymer matrix indicates that some of the available Si and Al was consumed during the zeolitic synthesis, leaving the geopolymer structure stripped of nutrients, causing the formation of poor networks with little coherence and, consequently, low compressive strength.

At Si/Al ratios greater than 5.85, no newly formed zeolites could be detected that would explain the changes in compressive strength, possibly as a result of the increased content in soluble silicon, which can restrict significantly

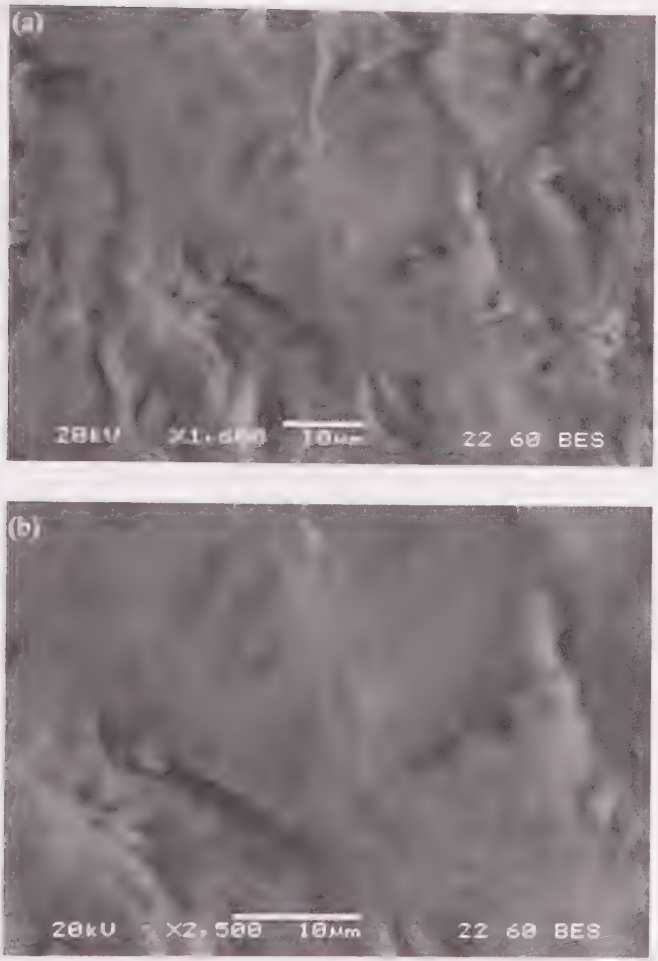

FIG. 9—*SEM photographs of the geopolymer matrix of the sample with Si/Al = 6.0.*

the mobility of the ionic species. In the literature, it is reported that during the first stages of raw material dissolution, there is a selective dissolution of Al, forming a loose, Al-rich gel, and the next stage includes the synchronized dissolution of Si and Al from the raw material sites that display Al deficiency [15,27]. It is possible that when the activation solution contains soluble silicon, the Si species from the solution react instantly with the Al species of the raw material, leading to the formation of oligomers, followed by their condensation. This results in the removal of Si and Al from the gel and, consequently, enhances the raw material dissolution reaction, explaining the compressive strength increase in the case of the geopolymer with Si/Al = 6.0. Nevertheless, a further increase of the soluble silicon in the initial solution (Si/Al > 6.0) results in almost saturated solutions that can inhibit the raw material

dissolution. Moreover, an increased concentration of Si can reduce the mobility of ionic species, inhibiting the access of alkalis to the reaction sites and, consequently, the participation of the raw material. In this case, the Si and Al species that participate in the formation of the geopolymeric structure are limited, making the network less dense and coherent and resulting in poor mechanical properties. The limited participation of the raw material in the geopolymerization when the soluble silicon content is increased is also made apparent by the reappearance of hydroxysodalite (crystalline phase present at the raw material) for Si/Al = 6.5, after its disappearance in geopolymers with Si/Al ratios greater than 5.85. The unreacted material can also act as a defect of the geopolymeric matrix.

Effect of Initial Alkali Concentration in the Activation Solution

Alkalis play a significant role during geopolymerization, because they affect the Si and Al dissolution from the raw material, they orientate the already dissolved species to lead to polycondensation, and they participate in the final structure by neutralizing the Al negative charge [4,28].

The compressive strengths of geopolymers in relation to the initial sodium concentration in the activation solution, expressed as the Na/Al molar ratio, are presented in Fig. 10. In this experimental series, the studied Na/Al molar ratios varied between 0.65 and 1.05, the m_w/m_s mass ratio was equal to 0.32, and the

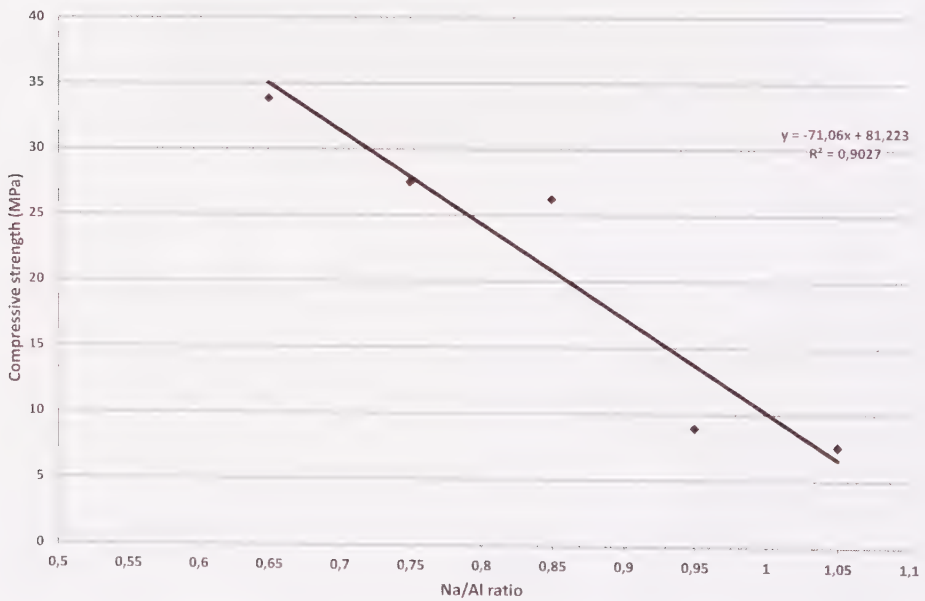

FIG. 10—*Compressive strength of perlite-based geopolymers in relation to the Na/Al molar ratio (Si/Al 6.0, m_w/m_s 0.32).*

Si/Al molar ratio was 6.0. The formulation with the lower sodium concentration had the greater compressive strength (about 35 MPa). The alkali content increase results in a slight decrease of the compressive strength, until the Na/Al ratio reaches 0.85. Further increase of the Na/Al ratio causes a sharp reduction of the compressive strength of the synthesized geopolymers (less than 10 MPa).

The XRD patterns of the synthesized geopolymers can be observed in Fig. 11. All geopolymer patterns contain the unreacted crystalline phases: quartz, cristobalite, Na-feldspars, K-feldspars, biotite, and maghemite. The characteristic peaks of hydroxysodalite that are present in the XRD pattern of perlite disappear in the case of geopolymers with Na/Al ratios lower than 0.95. They reappear in the patterns of geopolymers with Na/Al = 0.95 and 1.05, indicating reduced participation of the raw material in geopolymerization. Furthermore, in geopolymers with Na/Al = 1.05, the characteristic peaks of natrite ($d_{100} = 2.95$ Å) can be identified, indicating increased carbonation of the specimens.

The main feature of the FTIR patterns of the geopolymers (Fig. 12) involves the region between 800 and 1300 cm^{-1} attributed to the Si–O–Si and Si–O–Al asymmetric stretching vibrations. In all cases, the band at 800 and 1200 cm^{-1} shifts to lower wavenumbers in the geopolymeric materials, relative to the same band in the perlite spectrum, indicating the participation of Si and Al species in the geopolymeric network. Nevertheless, in the geopolymeric materials, this band is less intense with increasing Na/Al ratios, indicating reduced presence of the geopolymeric network. All samples, except perlite,

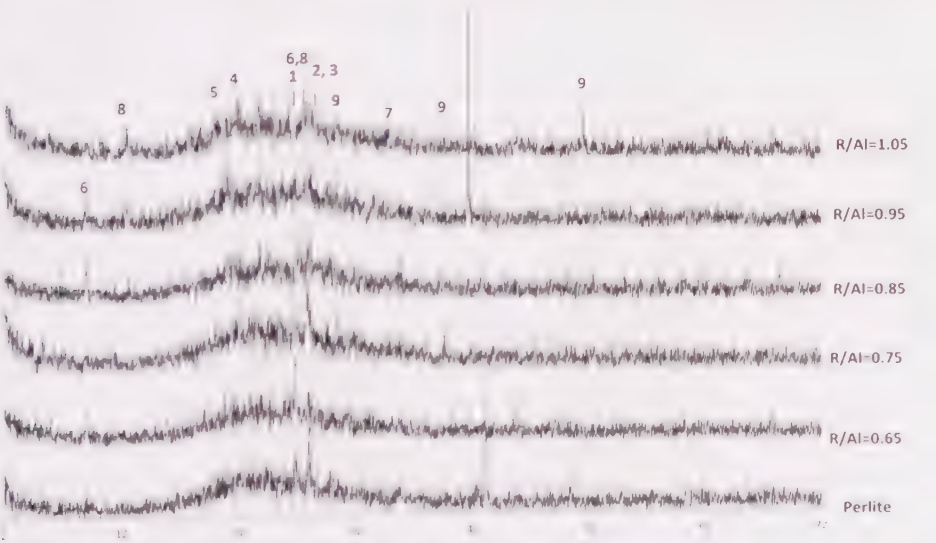

FIG. 11—*XRD of perlite and geopolymers synthesized with different Na/Al ratios. 1, quartz; 2, Na-feldspars; 3, K-feldspars; 4, cristoballite; 5, biotite; 6, maghemite; 7, hydroxysodalite; 8, natrite.*

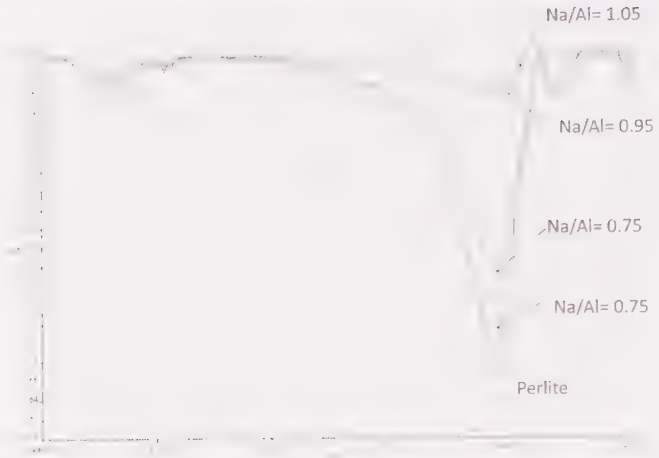

FIG. 12—*FTIR spectra of perlite and geopolymers synthesized with different Na/Al ratios.*

contain carbonate species, as pointed out by the presence of a band around 1450 cm^{-1}, related to anti-symmetric vibrations of CO_3^{2-} ions.

As can be seen from the presented data, the alkali content has a significant effect on the compressive strength of geopolymers, as well as on their structure. It is possible that for Na/Al = 0.65, the quantity of alkalis induces adequate perlite dissolution, the dissolved Si and Al species form a good geopolymeric network, and the majority of present Na participates in the network as a neutralizing agent. As indicated by the presence of carbonate species in the FTIR spectrum, not all the available sodium is bound in the network; a small quantity remains free and reacts with atmospheric CO_2. Despite the traces of matrix carbonation, the formed geopolymeric network results in a compact structure with increased compressive strength (34 MPa).

An increase in the alkali concentration results in a decrease in the compressive strength. In the case of a small increase in the alkali content (Na/Al = 0.75, 0.85), it is possible that the corresponding increase of the dissolution will be so limited that the presence of alkalis will be excessive. These free alkalis can either terminate the geopolymerization reaction by substituting one or more active sites of Si or remain unbound and carbonate. In both cases, the geopolymeric matrix is downgraded, explaining the slightly reduced compressive strength of the synthesized geopolymers. Further alkali increases induce severe degradation of the geopolymeric matrix, as the number of free alkalis is so great that they not only inhibit the raw material reaction, but also participate in the formation of a considerable amount of carbonates, detectable by XRD. The presence of carbonates within the geopolymer matrix can cause a significant decrease of the compressive strength, as has been indicated by other authors [28].

The type of alkali ion is thought to affect the geopolymerization; according to the literature, the presence of Na^+ favors the dissolution reaction, whereas K^+ leads to increased polycondensation [7,24]. Figure 13 presents the compressive strengths of geopolymers synthesized using the same formulation (Si/Al = 6.0, *R*/Al = 0.75 [*R* = Na or K], $m_w/m_s = 0.32$) and potassium hydroxide as an alkali activator. As can be seen, the compressive strength of the Na-geopolymer is almost double the compressive strength of the K-geopolymer. This can be attributed to the different behavior of the two alkalis during geopolymerization, but further investigation is required.

Synthesis of Geopolymer Mortars

As the aim of the present work was to assess whether perlite-based geopolymeric materials can be used as binder in concrete, one of the most promising formulations ([Si] 3.2 M, $m_w/m_s = 0.32$, Na/Al = 0.75) was used for the synthesis of mortars using standard silica sand according to ASTM C109/109 M [20]. Three samples were prepared with different water-to-solid ratios (w/s) (0.32, 0.34, and 0.37).

Figure 14 presents the compressive strengths of a geopolymer paste and the corresponding mortars. As was expected, the compressive strength of the mortars is less than that of the paste and reaches 18 MPa in the case of w/s = 0.37. The reduced compressive strength of the mortar can be attributed to the replacement of part of the binding material that is responsible for the high compressive strength by aggregates that possess inferior mechanical

FIG. 13—*Compressive strength of Na-geopolymers and K-geopolymers for the same formulation (Si/Al = 6.0, R/Al = 0.75 [R = Na or K], $m_w/m_s = 0.32$).*

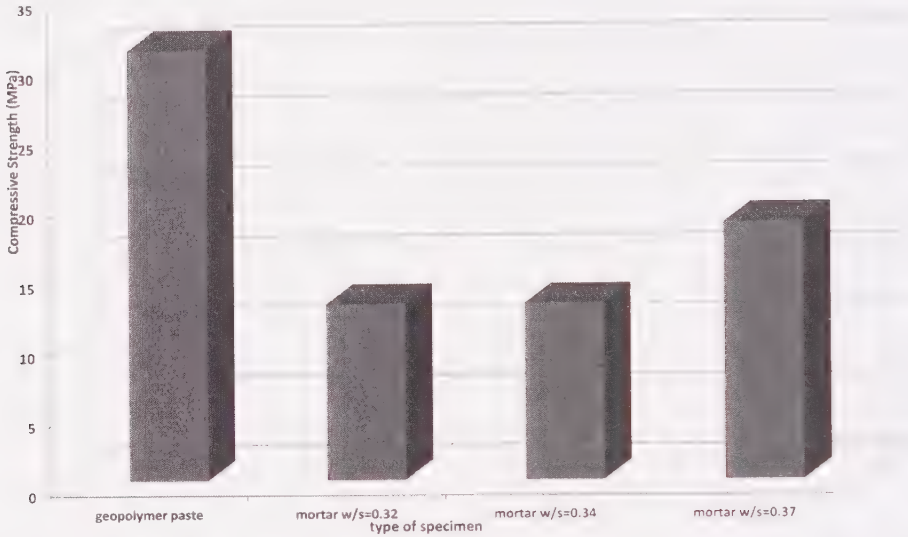

FIG. 14—*Compressive strength of geopolymer pastes and mortars, using the same synthesis parameters and different w/s ratios.*

properties. Furthermore, it is possible that the adhesion of the binder and the aggregates is not very good, so the interface between the geopolymer paste and the aggregates constitutes weak sites of the matrix that can lead to its collapse. However, these were preliminary experiments, and further research is required for system optimization.

Conclusions

In the present work, the main synthesis parameters affecting the compressive strength and structure of perlite-based geopolymeric materials were investigated. The study has proved that perlite is a promising raw material for geopolymer synthesis. The geopolymers obtained in the present study achieved a compressive strength of 34 MPa.

Relative to the geopolymerization of raw materials that have a previous thermal history, the geopolymerization of perlite requires the implementation of additional energy; the final products were obtained after two consecutive curing stages at 70°C amounting to a total duration of 5 days. The capability of aluminosilicate rocks to produce, under the proper conditions, geopolymers with enhanced compressive strength suggests that a distinction of the raw materials according to their mineralogical and thermal origin as "more reactive" and "less reactive" should be considered. Based on this separation, a different approach to the reaction conditions could be implemented, with the more

reactive raw materials such as fly ash and slag receiving one-stage curing and the less reactive raw materials receiving a prolonged, two-stage curing.

The water content affects the compressive strength of perlite-based geopolymers. Limited water content was found to be unfavorable for the development of compressive strength, possibly because of the reduced wetting of the raw material and the inhibition of the reactants' movement from and to the reaction sites. Excess water also resulted in decreased compressive strength, possibly as a result of the increased porosity that occurs when water abandons the matrix and the removal of the reactive species from the reaction sites. The optimum compressive strength was achieved with $m_w/m_s = 0.32$.

The Si/Al molar ratio seems to have a great effect on the development of geopolymers' compressive strength, as well as their mineralogical characteristics. Geopolymers synthesized without any soluble silica addition have reduced compressive strength, and newly formed zeolitic phases can be detected in the geopolymeric matrix. The maximum compressive strength of 28 MPa was achieved with a medium soluble silica addition (Si/Al = 6.0). Further increase of the Si/Al ratio results in decreased compressive strength.

The compressive strength of the synthesized geopolymers was greatly affected by the initial NaOH concentration in the activation solution. The less alkaline the activation solution is, the better the compressive strength of the geopolymers. Furthermore, with increased alkaline contents, traces of carbonates, such as natrite, can be detected within the geopolymer matrix.

All the synthesized mortars possessed compressive strength inferior to that of the paste. The best result achieved was 18 MPa. Further investigation is required.

Acknowledgments

The writers gratefully acknowledge the financial support of the European Commission within the frame of the Seventh Framework Programme (Project Contract No. 285463, Sustainable, innovative and energy sufficient concrete, based on integration of all-waste materials, SUS-CON).

References

[1] Davidovits, J., "Geopolymers: Inorganic Polymeric New Materials," *J. Mater. Educ.*, Vol. 16, 1994, p. 91.

[2] Davidovits, J., "Geopolymers: Inorganic Polymeric New Materials," *J. Therm. Anal. Calorim.*, Vol. 37, 1991, pp. 1633–1656.

[3] Davidovits, J., "Chemistry and Geopolymeric Systems Terminology," *Proceedings of Geopolymer '99*, Institute Geopolymere, Saint Quentin, France, 1999, pp. 9–40.

[4] Davidovits, J., "Geopolymers on the First Generation: SILIFACE Process," *Proceedings of Geopolymer '88*, Universite de Technologie de Compiegne, Compiegne, France, 1988, pp. 49–68.

[5] Xu, H. and van Deventer, J. S. J., "Effect of Source Materials on Geopolymerisation," *Ind. Eng. Chem. Res.*, Vol. 42, 2003, pp. 1698–1706.

[6] Barbosa, V. F. F., MacKenzie, K. J. D., and Thaumaturgo, C. D., "Synthesis and Characterization of Sodium Polysialate Inorganic Polymer Based on Alumina and Silica," *Proceedings of Geopolymer '99*, Institute Geopolymere, Saint Quentin, France, 1999, pp. 65–78.

[7] Provis, J. L. and van Deventer, J. S. J., "Geopolymerisation Kinetics. 1. In Situ Energy- dispersive X-ray Diffractometry," *Chem. Eng. Sci.*, Vol. 62, 2007, pp. 2309–2317.

[8] Davidovits, J., "Structural Characterisation of Geopolymeric Materials With X-ray Diffractometry and MAS-NMR Spectrometry," *Proceedings of Geopolymer '88*, Universite de Technologie de Compiegne, Compiegne, France, 1988, pp. 149–166.

[9] Xu, H. and van Deventer, J. S. J., "The Geopolymerisation of Aluminosilicate Materials," *Int. J. Min. Process.*, Vol. 59, 2000, pp. 247–258.

[10] Xu, H. and van Deventer, J. S. J., "The Effect of Alkali Metals on the Formation of Polymeric Gels From Alkali Feldspars," *Colloids Surf., A*, Vol. 216, 2003, pp. 27–44.

[11] Xu, H., van Deventer, J. S. J., and Lukey, G. C., "Effect of Alkali Metals on the Preferential Geopolymerisation of Stilbite/Kaolinite Mixtures," *Ind. Eng. Chem. Res.*, Vol. 40, 2001, pp. 3749–3756.

[12] Rowles, M. and O'Connor, B., "Chemical Optimization of the Compressive Strength of Aluminosilicate Geopolymers Synthesized by Sodium Silicate Activation of Metakaolinite," *J. Mater. Chem.*, Vol. 13(5), 2003, pp. 1161–1165.

[13] Schmucker, M. and Mackenzie, K. J. D., "Microstructure of Sodium Polysialate Siloxo Geopolymer," *Ceram. Int.*, Vol. 31, 2005, pp. 433–437.

[14] Phair, J. W. and van Deventer, J. S. J., "Characterisaton of Fly Ash Based Geopolymeric Binders Activated With Sodium Aluminate," *Ind. Eng. Chem. Res.*, Vol. 41, 2002, pp. 4242–4251.

[15] Fernandez-Jimenez, A. M., Palomo, A., and Criado, M., "Microstructure Development of Alkali Activated Fly Ash Cement: A Descriptive Model," *Cem. Concr. Res.*, Vol. 35, 2005, pp. 1204–1209.

[16] Backarev, T., "Geopolymeric Material Prepared by Using Class F Fly Ash and Elevated Temperature Curing," *Cem. Concr. Res.*, Vol. 35, 2005, pp. 1224–1232.

[17] Lee, W. K. W., van Deventer, J. S. J., and Lukey, G. C., "Effect of Anions on the Formation of Aluminosilicate Gel in Geopolymers," *Ind. Eng. Chem. Res.*, Vol. 41, 2002, pp. 4550–4558.

[18] Vaou, V. and Panias, D., "Thermal Insulating Foamy Geopolymers From Perlite," *Min. Eng.*, Vol. 23, 2010, pp. 1146–1151.

[19] ASTM C33-03: "Standard Specification for Concrete Aggregates," *Annual Book of ASTM Standards*, ASTM International, West Conshohocken, PA.

[20] ASTM C109-109M: "Standard Method for Compressive Strength of Hydraulic Cement Mortars," *Annual Book of ASTM Standards*, ASTM International, West Conshohocken, PA.

[21] Davidovits, J., *Geopolymer. Chemistry and Applications*, Institut Geopolymere, Saint Quentin, France, 2008.

[22] Palomo, A., Grutzeck, M. W., and Blanco, M. T., "Alkali Activated Fly Ashes: A Cement for the Future," *Cem. Concr. Res.*, Vol. 29, 1999, pp. 1323–1329.

[23] Duxson, P., Provis, J. L., Luckey, G. C., Mallicoat, S. W., Kriven, W. M., and van Deventer, J. S. J., "Understanding the Relationship between Geopolymer Composition, Microstructure and Mechanical Properties," *Colloids Surf., A*, Vol. 269(1–3), 2005, pp. 47–58.

[24] Duxson, P., Mallicoat, S. W., Lukey, G. C., Kriven, W. M., and van Deventer, J. S. J., "The Effect of Alkali and Si/Al Ratio on the Development of Mechanical Properties of Metakaolin-based Geopolymers," *Colloids Surf., A*, Vol. 292(1), 2006, pp. 8–20.

[25] Rees, C. A., Provis, J. L., Lukey, G. C., and van Deventer, J. S. J., "Attenuated Total Reflectance Fourier Transform Infrared Analysis of Fly Ash Geopolymer Gel Aging," *Langmuir*, Vol. 23, 2007, pp. 8170–8179.

[26] Rees, C. A., Provis, J. L., Lukey, G. C., and van Deventer, J. S. J., "In Situ ATR-FTIR Study of the Early Stages of Fly Ash Geopolymer Gel Formation," *Langmuir*, Vol. 23, 2007, pp. 9076–9082.

[27] Rees, C. A., Provis, J. L., Lukey, G. C., and van Deventer, J. S. J., "The Mechanism of Geopolymer Gel Formation Investigated through Seeded Nucleation," *Colloids Surf., A*, Vol. 318(1–3), 2008, pp. 97–105.

[28] Criado, M., Palomo, A., and Fernandez-Jimenez, A., "Alkali Activation of Fly Ashes. Part 1: Effect of Curing Conditions on the Carbonation of the Reaction Products," *Fuel*, Vol. 84, 2005, pp. 2048–2054.

Geopolymer Binder Systems
STP 1566, 2013
Available online at www.astm.org
DOI:10.1520/STP156620120076

Robin R. Gibson[1]

The Use of Aluminosilicates to Create Novel, High Performance and Sustainable Binders for Mortars, Plasters and Renders With Class Leading Low CO_2 Footprints

REFERENCE: Gibson, Robin R., "The Use of Aluminosilicates to Create Novel, High Performance and Sustainable Binders for Mortars, Plasters and Renders With Class Leading Low CO_2 Footprints," *Geopolymer Binder Systems*, STP 1566, Leslie Struble and James K. Hicks, Eds., pp. 54–71, doi:10.1520/STP156620120076, ASTM International, West Conshohocken, PA 2013.[2]

ABSTRACT: Development of sustainable, high performance mortars that are robust and easy-to-use is an important target for the construction industry. Since the 1940 s, use of lime mortars for construction has almost vanished as they are slow to cure and more difficult to use compared to cement products. Natural hydraulic limes remain as alternative binders to cement however their slow rate of set and unpredictable, low strengths prove problematic for specifiers and construction companies. Despite its popularity, cement mortars fail to meet most criteria for sustainability due to CO_2 emissions from cement manufacture and inability to recycle the material for reuse as binder. Further negative characteristics of cement mortars include excessive strength, inherent brittleness under load and lack of vapour permeability. Our research has explored the development of synthetic or pozzolanic hydraulic lime (PHL) technology to exploit its potentially more attractive sustainable credentials and physical characteristics. Work has focused on potentially highly active and novel additives to improve both the rate of set and overall final strength of mortars. We present preliminary data regarding the use of amorphous synthetic aluminosilicate materials (Al:Si ~ 1:5) to prepare synthetic hydraulic limes. In contrast to binder reactions which contain either only fly ash or metakaolins, the presence of high ratio synthetic aluminosilicate uniquely increases the rate of set, giving mortars with economically

Manuscript received June 14, 2012; accepted for publication November 20, 2012; published online April 24, 2013.

[1]Doctor, Limeco Limited, County Durham, DL12 9PF, UK.

[2]ASTM Symposium on *Geopolymer Binder Systems* on June 26–27, 2012 in San Diego, CA.

useful compressive and flexural strengths. Their reactive efficiency also retains high levels of free calcium hydroxide within a mortar which adsorb significant amounts of CO_2 on carbonation giving binders with class leading low CO_2 footprints in-use. It is postulated that the presence of dilute sialate species within the alkaline aqueous calcium hydroxide solution may be responsible for the increased reaction rate, producing discrete oligo-sialite species that give rise to long range 3D calcium disilicate/orthosialate species, similar to geopolymer structures. We speculate that such structures are responsible for rate of set and increased strength observed.

Introduction

Lime Use in Masonry Construction

Lime has been used as binder for mortars, plasters, and renders (hereafter referred to solely as mortar) for thousands of years in masonry construction. Historic mortars are generally blends of calcium hydroxide and local aggregate where calcium hydroxide was prepared by rough calcination of local limestone at temperatures >900 C to give calcium oxide (quicklime). Additions of equimolar or excess water in a process called "slaking" give powdered calcium hydroxide or lime putty respectively. Mortars prepared with calcium hydroxide alone are called air limes and cure in a two stage process consisting of water evaporation followed by carbonation. Some initial strength is given by water evaporation however long term strength, up to 2 N/mm^2, is driven by carbonation, a process which takes months to complete. Air limes cannot cure in the absence of air/CO_2 (i.e., underwater).

Porous sedimentary limestone with discrete particulate argillaceous (or siliceous) impurities can be used to prepare powdered calcium hydroxide binders for mortar called natural hydraulic limes (NHL). NHLs set more quickly than air-limes giving stronger mortars however, more importantly, such mortars can also set in the absence of air/CO_2 hence the use of the term "hydraulic." During processing, the impurities undergo significant changes during the limestone calcination at temperatures up to 1350 C [1] to give highly dehydrated calcium silicate/aluminosilicate and "siloxo-sialate" species that are intimate with the bulk calcium oxide product. Subsequent hydration or slaking produces a powdered NHL product, containing up to 40 % silicate/aluminosilicate species, 40 % free lime and unburnt $CaCO_3$, which is used as a binder directly. However the setting and strength performance of commercial NHLs still render them impractical for modern construction as setting and cure is frequently measured in weeks or months and final strength is unpredictable as NHLs need to be kept damp during the set period to achieve full strength which can be typically as 2 to 4 N/mm^2 in a minimum of 91 days.

It is clear that the highly dehydrated silicate species are responsible for the hydraulic action of NHL over air limes. It is interesting to note that rate of hydration of calcium oxide during slaking must be faster than that of the

hydration of dehydrated silicates to allow these silicate species to survive contact with water without set. Some commercial literature states that NHLs contain mostly cementicious belitic species [2,3] (C_2S) which react in the presence of water to give long range cementicious C-S-H or analogous aluminosilicate species which cause set. Some other aluminosilicate (C_3A) and perhaps very minor amounts of siloxo-sialate species may be present also. However while extensive cement research can demonstrate that it is the reaction of these intimate and homogenous belitic species created at temperatures in excess of 600°C that give cement improved setting and strength characteristics over hydraulic limes, it is postulated that the mechanism of cure for dilute systems such as synthetic hydraulic lime is not the same as for cementicious or NHL materials.

Delineating the Natural Hydraulic Lime and Pozzolanic Lime Set Mechanisms

The argillaceous impurities in limestone are generally accepted to be derived from skeletal fragments or terrestrial detritus that exist as discrete particulates within the sedimentary structure. During the processing of argillaceous limestone to manufacture NHL materials, manufactures claim that materials are calcined at temperatures up to 1350°C following by hydration (slaking) and light milling to give powdered binders. Examination of standard cement eutectic data would suggest that these temperatures are insufficient to give a C_3S/C_2S liquid phase during processing thereby it can be concluded that the discrete particles of argillaceous material will undergo significant dehydration and reaction to form C_2S particles, perhaps with a sialate core, which remain discrete in the final NHL product. Furthermore it can be suggested that the temperatures experienced during calcination cause the silicates/aluminosilicate particulates to undergo a rapid process of Ostwald ripening [4] creating "dead burnt" or very highly dehydrated species of low surface area whose surface consists largely of siloxane groups or calcium derivatives. Ostwald ripening is an entropy-driven process in which particle morphology changes over time to give lowest surface energy and where adjacent particles coalesce to increase overall average particle size. It is speculated that it is for this reason that mortars made with NHLs must be kept damp during cure and take an appreciable time to set and gain strength as the process of alkaline dissolution of the dead burnt silicate/aluminosilicate in the calcium hydroxide, water and aggregate mix is comparatively slow and therefore rate determining. Furthermore, should such discrete siloxo-sialate particles with C_2S shell be created during the preparation and cure of NHL materials, it can be speculated that set, cure and strength gain may in part due to further species of inorganic polymers forming within the matrix, such as products of the alkali-silicate reaction (ASR), rather than hydration of any C_2S species, as the discrete C_2S/siloxo-sialate particles react overtime in the alkaline medium. The potential ASR occurrence in highly

porous lime-rich mortar systems should not induce deleterious expansion effects as observed with dense cementicious materials.

Attempts have been made to prepare synthetic hydraulic limes to either prepare a product with improved performance over NHL or to remove the reliance on the very limited global source of commercial NHL material. Such materials are pozzolanic hydraulic limes (PHL), or synthetic hydraulic limes, and are prepared by blending standard calcium hydroxide powder and various known pozzolans such as fly ash, ground granulated blast furnace slag (ggbs), pumice dust, silica fume (a by-product of the silicon/ferrosilicon industry), fumed silica (prepared from silicon tetrachloride oxidized in a carbon arc) and metakaolin (kaolin calcined at up to 1000 C); however there is no independent evidence that they offer improved performance over NHL products. (This statement is supported by our work described in this paper). Moreover, the known pozzolans offer potentially worse environmental footprints due to necessary high temperature processing/CO_2 emissions or negative safety profile due to heavy metal and/or crystalline silica contents [5].

While NHL argillaceous impurities and common powdered pozzolans, such as fly ash and metakaolin, share a common chemistry, NHL materials are different as they are processed in excess $CaO/Ca(OH)_2$ delivering a mix of C_2S and perhaps dehydrated siloxo-sialite and C_3S species. Common pozzolans are all prepared during the essential high temperature processing of their precursors (e.g. coal) which contained heterogeneous clay-like impurities. The processing temperatures, typically exceeding 1000 C, drive off water giving stable, anhydrous species which are potentially highly reactive in the presence of aqueous alkaline species. Such pozzolans can be broadly described as $Na_xCa_yAl_z(SiO_4)_v$ depending on the exact composition of the precursor. As suggested previously, high temperature manufacturing processes create unreactive and low surface area potentially pozzolanic siloxo-sialate species which can be seen in Fig. 1.

Despite the modest performance, apparently dry powdered mixtures of hydrate lime and pozzolanic material are not observed to "go off" immediately on contact. Such mixes will contain appreciable levels of chemisorbed and physisorbed water, however the lack of reactivity of dry mixes is speculated to be due to consumption of such water by the hydration of dead-burnt species in the pozzolan. However on addition of excess water and aggregate to the $Ca(OH)_2$/pozzolan mix, a hydraulic set can undoubtedly occur. It is speculated that the mechanism of set and strength gain is more closely related to geopolymer chemistry than C_2S or C_3S hydration observed in cements. However it is unclear whether the mechanism is a simple alkaline dissolution of the pozzolan and precipitation as per a "sol-gel" reaction or whether a more complex inorganic condensation terpolymerisation is occurring which involves $Ca(OH)_2$ as a bidentate monomer and other complex sialate species. Few, if any, significant reports cover the preparation of geopolymers in divalent metal ion systems.

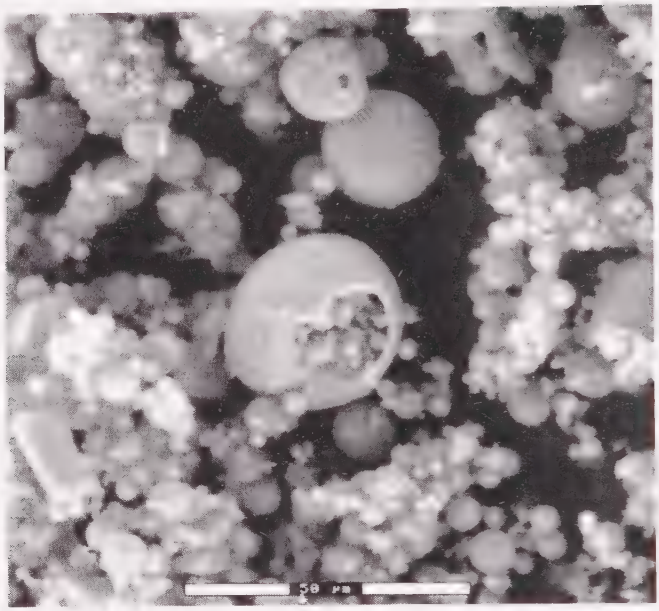

FIG. 1—*Mortar structure for 1:3 NHL 3.5 containing fly ash. [6].*

Qualitative studies have reported that geopolymers incorporating Ca^{2+} from ASTM type C fly ash produce geopolymer cements which cure more slowly and are weaker than their Na^{+} counterpart [7].

Geopolymer systems, a termed coined by Professor Davidovits [8], are described as copolymers of silicate and aluminosilicate species synthesised when dehydrated silicate and aluminosilicate species are dispersed in a monovalent MOH aqueous system, where M is typically Na. The ratio of Si to Al determines the physical characteristics of the final polymer where low ratios (1 Si: < 3Al) deliver a 3D, rigid, ordered systems and high ratios (1 Si: > 15 Al) deliver more 2D systems with less rigidity and more amorphous nature. Such inorganic copolymers whose Si:Al ratios are between 1:3 and 1:15 have an interim spectrum of characteristics in between the examples given. In geopolymers, despite the increased polyvalency of silicon over aluminium, it is aluminium that provides the cross-linking or branching functionality due to its increased reactivity. The polymerisation is driven by the presence of strong monovalent alkaline species, typically NaOH, which initiates polymerisation of the silicate/alumina species by nucleophilic attack driving regional dissolution of the silicate/aluminosilicate raw material and subsequent polymerisation accompanied by consumption of the alkaline initiator by the aluminosilicate species formed.

It is however intriguing to explore the reactivity of the aluminium species further as it remains unclear whether the Al^{3+} species in the bulk anhydrous

silicate/aluminsilicate assists dissolution within the alkaline aqueous phase or whether the kinetics of Al^{3+} drive polymerisation and silicate consumption thereby assisting dissolution of anhydrous silicate/aluminosilicate through modification of the silicate species in solution.

Many academic and several commercial examples of this chemistry are available with most commercial geopolymers being synthesised using fly ash raw materials, a co-product of the coal powdered electricity generating industry. A typical lignite or sub-bituminous coal offers 28 to 32 GJ/tonne of energy and typically contains between 6 % and 19 % ash content. Therefore 1 tonne of coal delivers ~30 GJ energy, 2.9 t of CO_2 [9] and approximately 0.12 t of fly ash. On a global basis, approximately 1750 M tonnes of coal are consumed in power generation producing some 250 M tonnes of fly ash [10]. Coal fired power station furnaces typically run between 1650 and 2000°C giving fly ash product as fine powdered glassy spheres whose average particle size is approximately 10 microns (see Fig. 1). Based on the processing temperature, it is postulated that the silicate/aluminosilicate species are essentially deactivated towards pozzolanic reaction or polymerisation without extended contact with highly alkaline aqueous conditions. Calcined clays, *metakaolin*, are also used for geopolymer synthesis. Metakaolins are prepared by high temperature calcination of kaolinitic material in rotary kiln at temperatures between 500 and 900° C to give high reactivity metakaolin or HRM. Care must be taken to avoid over burning the kaolin, a process which creates a non-reactive species; for example mullite. Unlike fly ash which is manufactured at temperatures to give dead-burnt aluminosilicates, HRM has the potential to exhibit greater activity however it is also speculated that highly dehydrated silicate/aluminosilicate species found in HRM are deactivated towards geopolymerisation as a result of the dehydroxylation of silica species that must occur at processing temperatures [11].

Delivering Improved Synthetic Hydraulic Lime Performance

However despite slow cure and modest strength, mortars made with existing air-limes, NHLs or PHLs have several attractive features such as their ability to accept modest movement (e.g. thermal expansion) that occurs in all construction, without causing instability, along with their autogenic (self-healing) and vapor permeable properties that make them attractive from a construction design perspective, often eliminating costly interventions such as expansion joints. Moreover mortars prepared with PHLs, NHLs or air limes have potential to absorb significant CO_2 during cure which, when combined with the ubiquitous and vast deposits of limestone across the globe and their proven durability in use, indicates a potential for this class of material as a fully sustainable binder. However to realise the economic and sustainable potential offered by synthetic pozzolanic hydraulic lime technology, it is essential to improve

physical performance (e.g. rate of set, strength) and CO_2 absorbing ability for which it is necessary to examine the chemistry and improve the efficiency of the pozzolanic reaction.

It is therefore postulated, based on the foregoing, that it is necessary to improve the availability of soluble silicate and aluminosilicate species within a PHL mortar to improve both the rate of set and strength. Furthermore, improvement in the availability of the silicate and aluminosilicate species may require the addition of less pozzolanic additive or impurity than typically found in existing pozzolanic materials or perhaps NHL materials where a significant dead-burnt silicate/aluminosilicate content may not react at all.

It is therefore speculated that it is necessary to avoid high temperature processing of silicate and aluminosilicate materials for use as effective pozzolans to ensure that they have not been subjected to significant dehydroxylation [11] prior to use. The use of a highly soluble and efficient pozzolanic material in a PHL mortar at lower levels could therefore increase the amount of free calcium hydroxide within the structure thus improving its CO_2 absorbing potential.

Synthetic silicas and aluminosilicates are prepared by precipitation from concentrated aqueous solutions of sodium silicate generally using an inorganic protic acid, such as sulphuric acid, or a Lewis acid, such as aluminium sulphate in the case of aluminosilicates. Sodium silicate is generally prepared by alkaline dissolution of freely available high silica sands. Such "sol-gel" precipitation or gelation processes give high surface area powdered structures of pure silica or aluminosilicate that are produced at low temperatures, typically below 300°C, giving silica structures that are rich in free, geranial or associated silanols (Si-OH) group but with minimal siloxane content. Such materials are totally amorphous containing few impurities. In the case of amorphous aluminosilicates, also called sodium aluminosilicates, the aluminium content is comparatively low with a Si:Al ratio of higher than 1:7. It is postulated that these materials are highly soluble and highly reactive when used as a pozzolanic additive to prepare PHLs.

Maximising CO_2 Uptake of PHLs

The production of calcium oxide, *quicklime*, from limestone produces significant quantities of CO_2 of between 1 and 2 metric tonnes of CO_2 per tonne of quicklime. The subsequent slaking of high calcium quicklime is an exothermic process that does not contribute significantly to the overall CO_2 emissions. Therefore around 0.75 metric tonnes plus water are required to make 1 metric tonne of calcium hydroxide. The CO_2 emissions are derived from a combination of decomposition products and fuel consumption. In high calcium limestone, the CO_2 contribution from decomposition is a constant at 0.785

TABLE 1—*Comparison of CO_2 emissions from processing various limestones with typical commercial kilns. Tonnes are* metric.

Kiln Type	Lime Product	Process CO_2 (t CO_2/t CaO)	Fuel	Combustion CO_2 (t CO_2/t CaO)	Total CO_2 Emission (t CO_2/t CaO)	CO_2 Emission per tonne of $Ca(OH)_2$
Long Rotary	High Calcium	0.785	Gas	0.53–0.58	1.31–1.37	~1.01
		0.785	Petcoke	0.80–0.90	1.58–1.68	~1.23
	Light burnt Dolomitic	0.913	Gas	0.58–0.63	1.50–1.54	~1.15
		0.913	Petcoke	0.90–1.10	1.81–1.91	~1.40
	Dear burnt Dolomitic	0.913	Petcoke	1.00–1.10	1.91–2.01	~1.48
Preheater Rotary	High Calcium	0.785	Gas	0.30–0.35	1.09–1.14	~0.84
	Light burnt	0.913	Gas	0.41–0.47	1.33–1.38	~1.02
	Dolomitic	0.913	Petcoke	0.67–0.75	1.58–1.66	~1.22
Mixed Feed	High Calcium	0.785	Gas	0.49–0.65	1.28–1.43	~1.02
Parallel flow Regenerative	High Calcium	0.785	Gas	0.21–0.25	1.00–1.04	~0.77
Other Shaft	High Calcium	0.785	Gas	0.28–0.30	1.06–1.09	~0.82

tonnes of CO_2 per tonne CaO. However there is considerable variation in the fuel efficiency of the various kiln types; see Table 1 [12].

To maximise CO_2 emission efficiency for quicklime production, it is therefore necessary to employ the most efficient shaft or vertical kilns, such as the parallel flow regenerative shaft kilns or PFR, utilising high calcium or high purity limestone. The calcination of dense or impure limestone in vertical kilns is not possible due to a process of decrepitation whereby differential thermal characteristics within the limestone causes sintering and generates solid fines which block the upwards flow of fuel, heat and escaping CO_2. It is for this reason that most limestone with significant levels of impurity, such as argillaceous limestone, are generally only processed in horizontal rotary kilns [13].

When a pure calcium hydroxide, derived from high calcium limestone manufactured in a PFR kiln, is used to prepare an air lime mortar, the $Ca(OH)_2$ starts to react with atmospheric CO_2 to produce $CaCO_3$ in situ. Aside from surface reaction with aggregate, all of the $Ca(OH)_2$ or free lime in the mortar is theoretically available to react with CO_2 during cure. 1 metric tonne of $Ca(OH)_2$ could hypothetically absorb up to 595 kg of CO_2 thereby reducing the embodied CO_2 footprint of masonry $Ca(OH)_2$ to 190 kg CO_2 within a year [14] which would compare favourably to the global average of 960 kg CO_2 per tonne for Portland cement [15]. While it is clear that some CO_2 is absorbed by cementicious materials, the amount absorbed is very modest and the time to complete the process is very lengthy [16] and often undesirable in many instances. Reaction of CO_2 with cements can remove the *p*H protective effect of Portlandite in the structure for key elements such as rebars.

However air-limes alone do not have the performance to meet economic imperatives for construction. While NHLs do have improved performance over air-limes, high levels of essential argillaceous impurities in the raw material combined with high temperature rotary kiln processing reduces the CO_2 absorption potential significantly. In an example where limestone contains 40 % argillaceous material, it requires around 1165 kg of raw material to prepare 856 kg of quicklime/argillaceous material in a rotary kiln, producing 1163 kg CO_2. 856 kg quicklime hydrates to 1000 kg of NHL containing 466 kg of argillaceous material. The remaining 534 kg of $Ca(OH)_2$ can theoretically absorb up to 317 kg CO_2. Overall therefore, the CO_2 footprint of 1 metric tonne of NHL in this example is 846 kg. Processing of such material in a vertical kiln would reduce the CO_2 footprint further.

In this quantitative and theoretical example, no account is made for the consumption of the $Ca(OH)_2$ through reaction with aggregate and argillaceous material and assumes that all $Ca(OH)_2$ is available for carbonation. The examples do however serve the purpose of directing research towards the development of an efficient pozzolanic material which can be combined in a low weight percentage with pure PFR kiln manufactured calcium hydroxide.

Our work has therefore centered on the preliminary examination of the use of synthetic amorphous silicas and aluminosilicates as a pozzolanic additive for pure calcium hydroxide powder for use as a binder to replace cement and gypsum in masonry construction.

Experimental

We prepared a range of PHL materials by combining commercially available synthetic amorphous silicas, synthetic amorphous aluminosilicates, HRMs or other potentially pozzolanic materials with a commercial powder calcium hydroxide conforming to BS EN459-1:2010 [17] to allow a performance comparison on a weight basis. Performance comparisons were made on 28 day 60 % RH cured samples as per BS EN 459-2:2010 [17]. Other standard testing such as available lime was completed in accordance with BS EN459-2:2010.

Preparation of "PHL 2" Sample

A PHL sample was prepared by blending of a powdered calcium hydroxide (Hydralime [18]) and commercial precipitated silica (Neosyl FC [19]) referred to hereafter as "PHL 2," where the silica forms 12 % of the total mass.

Preparation of "PHL 3.5" Sample

A PHL sample was prepared by blending of a powdered calcium hydroxide (Hydralime) and commercial precipitated aluminosilicate (Tixosil 38A [20])

referred to hereafter as "PHL 3.5," where the silica forms 12 % of the total mass. Tixosil 38A contains around 5 % Al on an as received basis. The bulk density of PHL 3.5 was measured at 540 g/L.

Preparation of "PHL2/Al(OH)$_3$" Sample

Commercially available "SH-20" Al(OH)$_3$ [21] was added to an aliquot of PHL 2 to give a PHL material containing 1 % Al and 11.8 % silica.

Preparation of "PHL/HRM #1" Sample

Commercial available HRM, Metamax [22], was combined with Hydralime to give a material in which the HRM forms 12 % of the total mass.

Preparation of "PHL/HRM #2" Sample

Commercial available HRM, Metastar 501 [23], was combined with Hydralime to give a material in which the HRM forms 12 % of the total mass.

Preparation of Mortar Samples

To ensure a level comparison, a standard mortar was prepared using PHL 3.5 in a 1:3 volumetric blend with a dried commercial sharp sand [24]. The bulk density of the sand was determined to be 1420 g/L. Therefore 2000 g of sharp sand were blended with 253 g of PHL sample and premixed for 5 min using a Hobart AE120 mixer with standard beater attachment. Subsequently, 175 g of deionised water were added to the premix and allowed to mix for a further 5 min. On completion of the mix, the mortar was transferred to rectilinear wooden moulds with dimensions of 160 mm (l) × 40 mm (w) × 40 mm (d) and tamped manually to achieve a compacted mortar prism. Any excess mortar was struck off the mould using a steel straight edge. The combined mould and mortar were then wrapped in PVC film, secured with elastic bands and stored in an oven at 20 C for 24 h prior to demoulding. The samples were then stored in an oven at 20 C and cured on open shelves for 7 or 28 days prior to compression or flexural testing as per BS EN 459-2:2010 using both hydraulic (>90 % RH) and formulated lime (~60 % RH) conditions. All PHL mortar samples were prepared in this way.

Two control mortars were prepared. A standard air lime was prepared using 2000 g sharp sand, 253 g of calcium hydroxide (Hydralime) and 175 g water. A commercial NHL3.5 [25] was used to prepare a comparison with 2000 g sharp sand, 253 g of NHL3.5, and 175 g water.

Method for Measurement of Bulk Density of a PHL

Prior to the test, the PHL sample is stored in a sealed container or bag without any agitation for at least 1 h to allow full settling. To test its bulk density, a

sample of PHL is taken from its container using a 1 L polyester scoop or similar and sprinkled into a 1 litre polypropylene container of known mass with ~11 cm open diameter and ~10.5 cm internal height. This process is repeated without delay between scoops until the PHL flows over the top of the plastic container. Using a metal straight edge, the excess PHL is struck from the top of the container leaving the container filled to its upper level. The mass of the PHL in the container is noted. Subsequently the container plus PHL contents held upright and introduced bottom-first into a vertical metal tube of internal diameter 14 cm and internal height 100 cm. At a convenient moment, the PHL/container is allowed to drop upright down the tube onto solid surface. This may result in the loss of some contents. The PHL/container is then weighed to calculate the mass of PHL remaining. Using a soft-bristled brush, the surface of the PHL powder is leveled off and its upper level within the container marked using indelible marker. The PHL powder is then discarded and the empty container refilled with water to the mark made previously. The container is then weighed once more to determine the mass hence volume of water. The bulk density is determined by dividing the mass of the PHL remaining in the container after dropping by the volume of water used to fill the container to the PHL fill mark after the drop. The result is recorded as g/L.

Measurement of Carbon Dioxide Absorption by Mortar on Cure

Standard mortar prisms were prepared and cured under conditions according to the method for the preparation of mortar. The mass of the prism were noted at 28 day interval and water content of the cured mortar determined on samples of the prism at 28, 91, 182, and 365 days. On deducting the water content, any increase in mass of the prism was attributed to the reaction of $Ca(OH)_2$ in the mortar with atmospheric CO_2 to give $Ca(CO)_3$.

Determination of Water Content of Cured Mortar

Fifty grams (±1 g) of cured mortar were weighed in a tared, aluminium foil dish. The dish and sample were introduced into an oven at 200°C for 1 h after which the sample and dish were reweighed. Any difference in mass before and after heating are attributed to free water loss and therefore water content of the mortar.

Results

Rate of Set and Compressive Strength

The rate of cure of mortars prepared with the PHL samples and therefore reactivity of the pozzolanic additives can be determined by examination of the

7 and 28 day compressive strengths whether cured under typical ambient relative humidity as might be found on a construction site as shown in Fig. 2 (i.e.~60 % at 20 C) or under artificially wet conditions where mortars are kept as wet as possible as shown in Fig. 3 (i.e. > 90 % RH at 20 C). Except for the commercial NHL 3.5 material which contains ~20 % silicate/aluminosilicate and 25 % free lime [26], the remaining PHLs contain almost identical elemental composition. The HRM pozzolans are typically contain 55 % SiO_2 and 40 % Al_2O_3 following ignition at 1000 C while PHL 2 pozzolan contains 100 % SiO_2 and PHL 3.5 pozzolan contains 89 % SiO_2 and 11 % Al_2O_3 following ignition at 1000 C. In the case of PHL2/$Al(OH)_3$, the blended pozzolan composition is 89 % SiO_2 and 11 % Al_2O_3.

Curing of an air lime [control mortar using $Ca(OH)_2$] alone under ~60 % RH gives interesting results as the strength build over 28 days to 1.3 N/mm^2 must be attributed to a combination of capillary action drawing $Ca(OH)_2$ particles together into the interstices between grains of aggregate and Van Der Waals forces emanating from the polar –OH groups of the lime. Qualitative phenolphthalein analysis of the test prism shows the calcium hydroxide to be almost entirely non-carbonated after 28 days. The poor strength displayed by

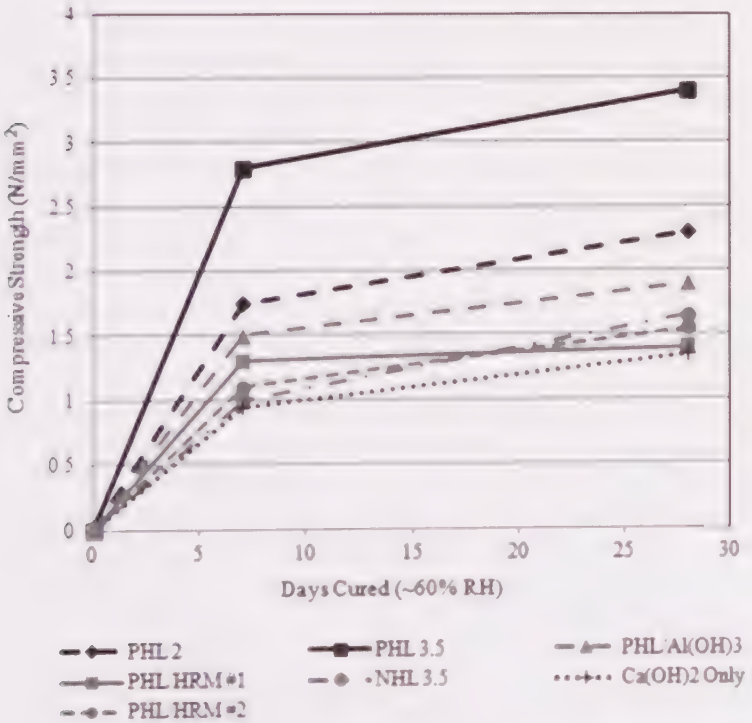

FIG. 2—*Compressive strengths of various PHL samples cured at 20 C under ~60 % RH to mimic ambient RH found on construction sites.*

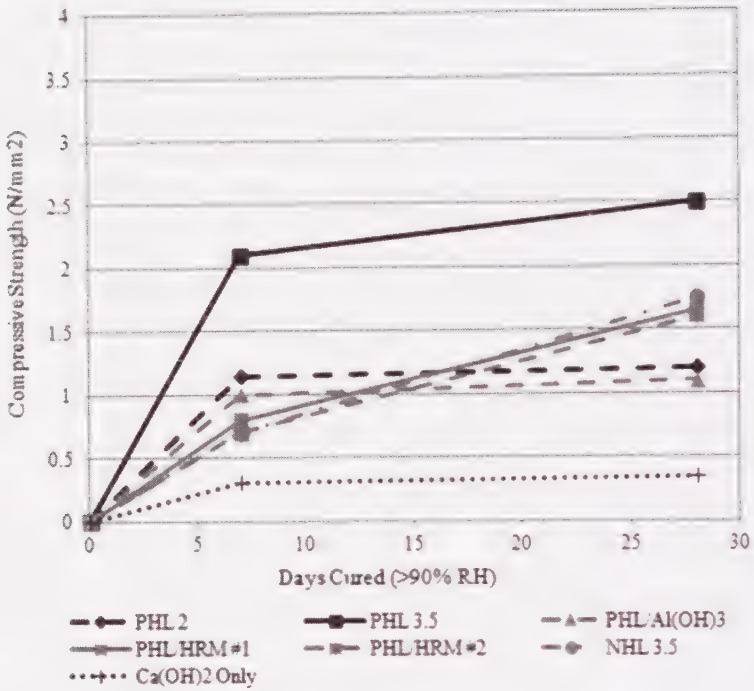

FIG. 3—*Compressive strengths of various PHL samples cured at 20°C at >90 % RH to simulate constant wet conditions.*

the same mortar cured under >90 % RH conditions is as expected as there is no mechanism available for cure over the time period.

The performance of the mortars prepared with control NHL 3.5 and PHLs + HRM are almost identical under both drying conditions. Under >90 % RH conditions, compressive strength continues to increase over and beyond 28 days. By comparison with the significant decrease in rate of strength gain for PHL2 and PHL3.5 samples between 1 to 7 and 8 to 28 days as shown in Fig. 3, suggesting exhaustion of the pozzolan component, the decrease in rate of compressive strength gain for NHL and PHL/HRM materials over the same periods is less marked. By comparison, the same mortar cured under 60 % RH conditions, show only a modest increase in compressive strength over $Ca(OH)_2$ alone which lends credibility to the hypothesis that water must be present in sufficient quantity to effect the pozzolanic reaction in NHL or PHLs containing HRM. These finding are supported by NHL product use recommendations from the manufacturers who suggest keeping mortars damp for at least the first seven days after application.

The rate of strength gain of the PHL 2 and PHL 3.5 is higher than NHL 3.5 or PHL/HRM blends at both 60 % and >90 % RH. The 28 day strength for both PHL 2 and PHL 3.5 when cured at 60 % RH is also higher and

significantly so for PHL3.5. Under ~90 % RH conditions, the gradient of compressive strength development for PHL 3.5 and, especially, PHL 2 tends towards zero as time approaches 28 days indicating an exhaustion of the active pozzolan species. There is a significant difference between both 7 and 28 day strengths of PHL 2 and PHL 3.5 prisms cured at 60 % and >90 % RH. It is speculated that the pozzolanic reaction for PHL 2 and 3.5 samples continues during capillary action caused by evaporation of water from the mortars cured at 60 %, forming bonds between the aggregate grains that are much stronger than when $Ca(OH)_2$ is used alone. While the same capillary action must be present during the 60 % RH cure of NHL 3.5, PHL/HRM #1 and PHL/HRM #2, the comparatively low strength must be attributable to either low reactivity of the pozzolan and/or loss of water from the matrix or a combination of both. This would suggest that PHL 2 and PHL 3.5 materials are able to retain a greater level of moisture within the drying and curing matrix at 60 % RH compared to NHL or HRM containing materials. The lower strength observed for PHL 2 and PHL 3.5 mortars cured at >90 % RH may be explained by simple dilution effect upon the lime binder throughout all voids in the aggregate, not just the interstices between grains.

The silica additive to PHL 2 has not been calcined in the presence of CaO or $Ca(OH)_2$ to give a C_2S structure so the mechanism of cure may be subtly different from that attributed to cementicious materials. Work in our laboratory has shown that PHL 2 (and PHL 3.5) materials are stable over many months and exhibit identical performance whether a mortar is prepared with them either immediately following the preparation of the PHL or many months afterward during which the PHLs are stored in dry containers. This suggests that the silica (or aluminosilicate) only reacts with the $Ca(OH)_2$ in the presence of excess water as typically found in a mortar. Water is present both in the silica and $Ca(OH)_2$ raw materials at 10 % and 2 % respectively when the PHLs exist as dry powders. It is therefore proposed that the reaction with PHL 2 on addition of excess water is either a simple sol-gel reaction consuming and redepositing silica species in the interstices forming a CSH variant between aggregate or more speculatively, a heteropolymerisation between $(SiO^{-}{}_{2})_4$ species and $Ca(OH)_2$ which concatenate linearly, forming intertwined chains that are either chemically or physically attached to the aggregate grains thereby providing set and strength. This position is analogous the polymer approach proposed by Davidovits for geopolymers. It is however most interesting to explore the difference in performance between the PHL 2 and PHL 3.5. Notionally they contain the same level of pozzolanic material at ~12 % but the PHL 3.5 displays significantly greater rate of strength gain and compressive strength. Attempts to recreate the performance of PHL 3.5 through blending of $Al(OH)_3$ and PHL 2 failed. Moreover the strength data suggests that $Al(OH)_3$ simply behaved as an inert diluent in the silica reaction. The aluminosilicate used to prepare PHL 3.5 was prepared by destabilising sodium silicate with an

appropriate aluminium containing lewis acid followed by an aqueous washing programme to remove salt by-products. The precipitated aluminosilicate product contains around 5 % Al which must exist in a different electronic environment to the $Al(OH)_3$ for PHL2/$Al(OH)_3$ at a molar ratio of approximately Al:Si of 1:7. It is postulated that the aluminium and silicon exist as orthosialate species within a silicate matrix which effects a radically different activity compared to silicate alone. It remains unclear however whether the presence of Al^{3+} within the PHL 3.5 matrix simply increases the rate and efficiency of dissolution of the silicate allowing more silicate into the bulk $Ca(OH)_2$ matrix at a greater rate to effect both quick cure and higher strength or whether, as is the postulated position for Geopolymers, the Al^{3+} species acts as cross-linking agent for the proposed [–Si-O-Ca-O-] type species which affords greater strength through an increase in 3D structure over the use of silica alone as observed in PHL 2. This position is analogous to terpolymerisation observed with 3 component multivalent organic monomer systems.

CO_2 Absorption of PHL 2 and PHL 3.5 Systems

PHL 2 and PHL 3.5 were assessed for their available lime content using BS EN459-2:2010, which determines the level of free $Ca(OH)_2$, showing 83 % and 86 % respectively. Such data is critical to mechanistic analysis as it suggests that the reaction between $Ca(OH)_2$ and silica species does not commence until excess water is added during mortar preparation as the data were obtained on PHL 2 and PHL 3.5 samples between 1 month and 1 year old. Furthermore, it is free lime that is responsible for subsequent reaction with atmospheric CO_2 so a high free lime content is desirable.

In an initial and simple experiment, prisms of PHL 2 and PHL 3.5 mortar (1:3 v/v) were prepared as described here and allowed to cure at 60 % RH, 20°C for 1 year. The masses of the prisms were noted periodically and samples of the prisms assessed for free water content. The data showed the loss of almost all water added to prepare the mortars by day 28 followed by an increase in prism mass over subsequent months as the $Ca(OH)_2$ content of the mortar was converted to $CaCO_3$ as is shown in Fig. 4. These preliminary data suggest that the PHL 2 and PHL 3.5 mortars were fully carbonated approximately 9 months after preparation which is supported by simple phenolphthalein analyses of the broken prism. As the silica additive forms 12 % of the PHL and the Hydralime $Ca(OH)_2$ was manufactured using PFR kilns, 1 metric tonne of PHL 2 or PHL 3.5 contains approximately 85 % free lime which when fully carbonated after 9 months gives a binder for mortar whose CO_2 footprint is approximately 233.6 kg CO_2 per tonne plus contribution from the silica additives. The CO_2 footprints of the silica additives are not available publicly. As the PHLs are used at around 11 % of a mortar formulation, this figure translates to approximately 26 kg of CO_2 per tonne of dry mortar plus

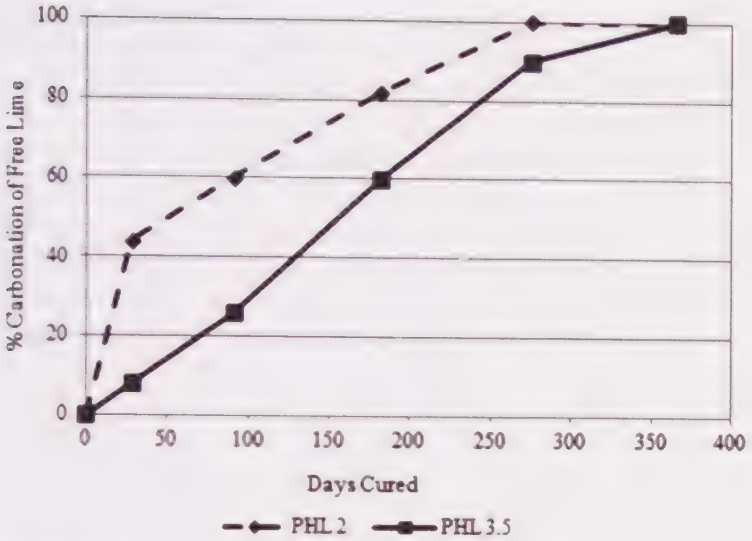

FIG. 4—*Preliminary data showing the carbonation rate of free lime in PHL 2 and PHL 3.5 samples.*

contribution from silica additives. As typical 1:1:6 cement mortars contain around 15 % Portland cement and 5 % hydrated lime by mass, the comparative mortar CO_2 footprint is 150 kg.

Summary

This preliminary data is presented to stimulate further exploration of efficient PHL materials with robust physical and sustainability claims. While civil engineering projects still demand monolithic cementicious or geopolymer materials, masonry still represents around 10 % of global construction methods and high performance materials with low embodied CO_2 are demanded for the preparation of mortars, plasters and renders. False perceptions exist within the construction industry that mortars must have a minimum strength of around 4 N/mm^2 to ensure integrity of buildings however most masonry construction from pre-1945 utilised lime products of low strength, typically from 1 to 2 N/mm^2 as exemplified by the use of $Ca(OH)_2$ alone in the preparation of mortar for this paper.

To accelerate research in this arena, it is necessary to explore further the nature of set, cure and strength and compare cements, geopolymers and other materials. While a huge body of work exists to support the cementicious set mechanism of the hydration of C_3S and C_2S species to give non-specific CSH structures for materials that are prepared using appropriate raw material at elevated temperatures, we speculate that the mechanism of set and cure for

PHL materials may proceed via different chemical species which may be closer to geopolymer systems than Portland cement. The process however remains unclear given the nature of raw material and processing methods.

It is proposed however that the general use of the term pozzolan is nebulous and thus obfuscates the mechanism underlying the cure and set of PHL materials.

We speculate that the set, strength and carbonation of mortars made with PHL materials is a three stage process where (i) siloxo-sialates react with divalent $Ca(OH)_2$ in the aqueous phase to form an initial heteropolymeric framework within the mortar (set), (ii) the process of (i) continues to consolidate until silicate and aluminosilicate species are either consumed or rendered inactive by loss of water (reaction medium) and iii) carbonation of the remaining $Ca(OH)_2$ to give $CaCO_3$ whose fine crystal structure followed by Ostwald ripening consolidate the mortar for long term strength. It remains to be understood whether the process in (i) and (ii) above is a simple sol-gel reaction, perhaps giving a CSH variant, or a more novel polymerisation actively incorporating Ca^{2-}.

Finally it has been shown that a new class of PHLs containing silicate/aluminosilicate species prepared at low temperature can be used as efficient binders for the preparation of mortar, plasters and renders. The efficiency of this silicate/aluminosilicate allows commercial binder materials that contain very high levels of free calcium hydroxide for subsequent CO_2 sequestration on cure. As the raw materials for all components are available in abundant supply across the globe, the sustainability claims can be substantiated.

References

[1] Hassibi M., "Factors Affecting the Quality of Quicklime," Chemco Systems L.P., Revision,1 March 17 2009, www.chemcosystems.net (Last accessed 12 June 2012).

[2] http://www.stastier.co.uk/nhl/info/pdfs/Hydraulicity_and_Properties_of_NHL.pdf, Setra Marketing 2006 [Last accessed 10 Oct. 2012 (see also www.c-e-s-a.fr)].

[3] Allen G., Allen, J., Elton, N., Farey, M., Holmes, S., Livesey, P., and Radonjic, M., *Hydraulic Lime Mortar*, Donhead, Shaftsbury, 2003a, p. 3.

[4] Ratke, L., Vorhees, P. W., *Growth and Coarsening: Ostwald Ripening in Materials Processing*, Springer-Verlag, Berlin, 2002.

[5] Hall, R. M. and Gwin, K. K., "Evaluation of Dust Exposures at LeHigh Portland Cement Company," National Institute for Occupational Health and Safety (NIOSH, USA), 2000, see http://www.cdc.gov/niosh/hhe/reports/pdfs/2000-0309-2857.pdf (Last accessed 10 Oct. 2012).

[6] Allen, G., Allen, J., Elton, N., Farey, M., Holmes, S., Livesey, P., and Radonjic, M., *Hydraulic Lime Mortar*, Donhead, Shaftsbury, 2003b, p. 84.

[7] Kristiawan, S. A., "Towards Environmentally Friendly Construction Materials With Class C Fly Ash Based Geopolymer." International Seminar on Climate Change, Environmental Insight for Climate Change Mitigation, Solo, 4-5 March 2011.

[8] Davidovits, J. J., "Geopolymers: Inorganic Polymeric New Materials," *Therm. Anal.*, Vol. 37(8), 1991, pp. 1633–56.

[9] Herold A., "Comparison of CO2 Emission Factors for Fuels Used in Greenhouse Gas Inventories and Consequences for Monitoring and Reporting Under the EC Emissions Trading Scheme," ETC/ACC Technical Paper 2003/10, July 2003.

[10] World Coal Association, "Coal Matters" factsheet, www.worldcoal.org, May 2012. World Coal Association, "Coal Conversion Facts" factsheet, www.worldcoal.org, Aug. 2007.

[11] McDaniel M. P., US4308172, Philips Petroleum Company.

[12] Entec UK Limited, "EU Emissions Trading Scheme Phase II. Review of New Entrants' Benchmark -Lime," Report for UK Government Dept. of Trade and Industry, Report Version 2, Aug. 2006.

[13] Oates, J. A. H., *Lime and Limestone*, Wiley-VCH Verlag GmbH, Weinheim, 1998, p. 98. See also www.britishlime.org/edu_dolo01.php (Last accessed 11 June 2012).

[14] Lawrence, R. M. H., "A Study of Carbonation in Non-hydraulic Lime Mortars," Ph.D. thesis, Univ. of Bath, UK, Oct. 2006.

[15] *Contribution of Working Group III to the fourth Assessment Report of the Intergovernmental Panel on Climate Change (IPCC), 2007*, B. Metz, O. R. Davidson, P. R. Bosch, R. Dave, and L. A. Meyer, Eds., Cambridge University Press, Cambridge, UK.

[16] Kjellsen K. O., Guimaraes, M., and Nilsson, A., "The CO_2 Balance of Concrete in a Life Cycle Perspective," Nordic Innovation Centre, Dec. 2006.

[17] BS EN459-1:2010 and BS EN459-2:2010, "Building Lime: Test Methods," BSI Group, UK.

[18] Lafarge, Buxton, UK (Hydralime product datasheet, Dec 2010).

[19] PQ Corporation, Warrington, UK (INEOS Silicas, "Keep it Flowing", Issue 1,Sept. 2002).

[20] Rhodia, Lyon, France (Product Datasheet, undated).

[21] Dadco (Suisse) SA, www.dadcoalumina.com.

[22] BASF Catalysts, NJ, USA.

[23] Imerys Materials Ltd, Par, UK.

[24] "Washed Sharp Sand," Chas. Long & Son Ltd, Richmond, UK.

[25] NHL3.5, CESA, St Astier, France.

[26] St. Astier Natural Hydraulic Limes, "Mineralogy and Chemistry of Raw Materials and Products," Setra Marketing 2006, see also www.c-e-s-a.fr.

Geopolymer Binder Systems
STP 1566, 2013
Available online at www.astm.org
DOI:10.1520/STP156620120094

Carlos Montes[1] *and Erez N. Allouche*[2]

Rheological Behavior of Fly-Ash-Based Geopolymers

REFERENCE: Montes, Carlos and Allouche, Erez N., "Rheological Behavior of Fly-Ash-Based Geopolymers," *Geopolymer Binder Systems*, STP 1566, Leslie Struble and James K. Hicks, Eds., pp. 72–84, doi:10.1520/STP156620120094, ASTM International, West Conshohocken, PA 2013.[3]

ABSTRACT: Geopolymers, a class of novel cementitious binders, have been gaining growing acceptance in commercial applications. One of the most important aspects for the commercialization of these products is their behavior in a plastic state. The workability of fresh geopolymer paste can be measured with several common tests, such as flow and slump; however, a more in-depth characterization of their rheology is essential to understand basic setting mechanisms. In this article, special consideration is given to the rheological behavior of geopolymer paste under the action of a surface tension-reducing agent (STRA). STRAs of two different types were utilized and their effect on compressive strength, viscosity, and flow evaluated. The degree of surface tension reduction for these agents was also investigated. Implications related to industrial applications of these materials were also discussed.

KEYWORDS: geopolymer, rheology, surface tension, workability, viscosity, coatings

Introduction

Geopolymers consist of a network of silicon-aluminum oxides [1]. Geopolymers are known for their excellent corrosion resistance to sulfuric acid and other agents commonly found in wastewater collection and storage systems

Manuscript received June 22, 2012; accepted for publication November 20, 2012; published online April 29, 2013.

[1]Post Doctoral Fellow, Alternative Binder Research Laboratory, Louisiana Tech Univ., Ruston, LA 71272, United States of America.

[2]Associate Professor of Civil Engineering and Research Director, Alternative Binder Research Laboratory, Louisiana Tech Univ., Ruston, LA 71272, United States of America.

[3]ASTM Symposium on *Geopolymer Binder Systems* on June 26–27, 2012 in San Diego, CA.

[2,3]. Geopolymers can be prepared out of different precursors, out of which fly ash is one with exceptional commercial possibilities [4]. Fly ash in North America is classified under two broad categories: Class C and Class F. Class C ash, in general, contains a larger amount of calcium oxide; Class F contains a larger sum of silicon and aluminum oxides, and therefore, a smaller content of calcium oxide [5]. Work has been conducted on both types of ash, and results have reported the benefits of the use of low calcium Class F ash, both in terms of corrosion resistance and setting time [6], although geopolymer produced from Class C ash generally yields a product of a higher strength [7]. It was demonstrated that because of these properties, low calcium geopolymer could be an excellent candidate for the replacement of Portland cement coatings for buried infrastructures subjected to ongoing biogenic corrosion [8].

However, geopolymers are known to show poor workability [9]. To date, limited work has been conducted to address geopolymer rheology, although reports show that geopolymers, like Portland cement, behave as a Bingham fluid and have a history-dependant rheological profile, i.e., geopolymers may be kept in a fluid form if subjected to constant shearing for a certain amount of time before initial setting starts [10]. Recent findings [11] confirm these observations and report the thixotropic behavior of geopolymers to depend on the molar concentration of the silicate and the ratio of silicate to hydroxide solutions. Other studies [12,13] reported similar findings in terms of the use of the Bingham model.

An important area where cementitious materials are used with less than satisfactory results in terms of long-term durability is the rehabilitation of sewer pipes and other components of wastewater conveyance and storage systems. These structures are exposed to degradation in which the main deteriorating agent is biogenic sulfuric acid [14]. Some of the most aggressive conditions have been reported in the Gulf Coast of the United States [15]. One way to rehabilitate aging concrete pipes is to apply a cementitious coating, which extends their service life for an additional 10 to 20 years [16]. However, under highly aggressive conditions, sewer structures made of ordinary Portland cement require frequent repairs, as often as every 6 months.

One of the most common ways to apply a cementitious coating to a substrate, such as a manhole wall or the inner wall of a pipe, is by spraying. In the case of a pipe's inner wall, spraying is achieved by means of a rotating centrifugal head, which receives the pumped mortar mix through a feed line. Good flow, workability, and adequate setting time are required characteristics to spray cement mortar using this technique.

The superior chemical resistance of geopolymers under the action of sulfuric acid makes them an excellent candidate for the replacement of Portland cement in this application [8]. However, geopolymers tend to exhibit poor workability compared to Portland cement. Their high viscosity and surface tension prevent them from being used in many industrial applications, because of challenges in the application and finishing processes.

Although the workability of geopolymers can be modified by means of modifying its basic formulation, the high surface tension of these materials is a major drawback when attempting to apply these materials utilizing current spraying equipment.

In addition to sprayability, one of the most important features of a mortar coating is its ability to bind to the substrate. A reduction in surface tension of the mortar is also essential to assure good adhesion between the parent surface and the coating because this property controls the ability of a material to wet a surface [17]. Geopolymers exhibit a very low affinity for substrates. Therefore, it is desirable to reduce geopolymer's surface tension, not only to improve their sprayability, but also to wet the substrate, hence improving adhesion.

Surface tension is caused by the attraction among the liquid's molecules by various intermolecular forces. In the bulk of the liquid, each molecule is pulled equally in all directions by the neighboring liquid molecules resulting in a net zero force. At the surface of the liquid, the molecules are pulled inward by other molecules deeper inside the liquid, and are not attracted so intensely by the molecules in the neighboring medium (air, vacuum, or another liquid), resulting in a net force, i.e., surface tension. Surface tension of a liquid is an important factor because of two reasons: sprayability and wetting of a surface. If surface tension is low, the formation of droplets will be improved, and therefore it will be easier to spray. In terms of adhesion, a critical surface energy needs to be obtained to achieve proper wetting of a solid body, thereby assuring adhesion. According to this same theory, the surface of a solid body is wetted by every fluid whose surface energy is less than the critical surface energy of the solid body.

One type of surfactant commonly used in the construction industry is an air entrainer. Although its main purpose is stabilizing air bubbles inside the concrete matrix to protect it from freeze-thaw by preventing concrete fatigue, it also produces a change in workability and a reduction of surface tension [18]. Air entrained concrete is often more workable and easier to pour; however, these characteristics have been poorly researched or taken advantage of in the concrete industry. These properties of surfactants are of great interest if they can improve geopolymer's workability. Therefore, it is interesting to investigate if surfactants would be useful to overcome the sprayability limitations of geopolymers to develop an effective coating system.

The increase in workability brought about by air-entrainment is usually described as some sort of "ball bearing" action of the air bubbles. These bubbles, which are usually several million per $in.^3$ of concrete, allow for easier deformation where the concrete is worked, resulting in an increase of workability [19].

Experimental Procedures

Class F fly ash from a thermo power plant in Miami Fort, FL was used in this study. Sodium silicate with a SiO_2/Na_2O ratio of 3.22 in a 37.2 wt. % solution

TABLE 1—*Chemical composition of fly-ash stockpile.*

Oxide	Class F Fly Ash, wt. %
SiO_2	50.25
Al_2O_3	22.56
Fe_2O_3	20.0
CaO	2.1
MgO	0.00
SO_3	0.50
LOI	2.48
Na_2O	0.00
Total	**97.89**
SiO_2/Al_2O_3	2.23
$SiO_2 + Al_2O_3$	72.81

in water and a viscosity of 180 centipoises was used as part of the activator solution for geopolymer. Sodium hydroxide (Na_2O) 99 wt. % was dissolved in water and used as the second part of the solution. The sand utilized met specifications set by ASTM C778 [20]. The chemical composition and particle size distribution of the fly ash are given in Table 1 and Fig. 1, respectively. Mineralogical composition of the fly ash is given in Table 2. All sodium hydroxide molar solutions were prepared in the lab and allowed to cool for 1 day prior to mixing. To enhance the sprayability of geopolymer, it was decided to explore the incorporation of a surface tension-reducing agent (STRA). Two types of STRAs at four additional levels and concentrations were utilized in the testing program. The design of experiments can be seen in Table 3.

A total of three mortar cubes were tested for compressive strength for each combination. Also, each measurement of flow and viscosity consists in three repetitions.

To prepare the geopolymer paste, a 12.5 M NaOH solution was mixed with the respective sodium silicate to prepare the alkaline solution. To perform the

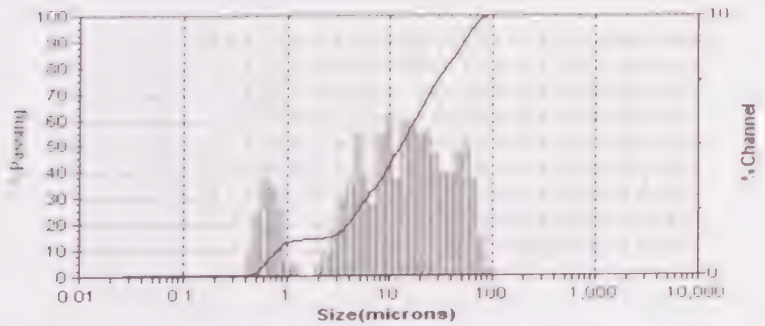

FIG. 1—*Particle size distribution of the fly ash used in this study.*

TABLE 2—*Mineralogical composition of fly ash utilized in this study.*

Minerals	Wt. %
Quartz	10.33
Mullite	25.27
Amorphous	64.4

compressive strength and flow tests, the precursor (fly ash) and sand were mixed in a 1:1 ratio, before being added to the activator solution. The desired surfactant amount was mixed with water until a uniform suspension was obtained. It was then immediately added to the sodium silicate to achieve surface tension reduction. The fresh mortar was cast into $2 \times 2 \times 2$ in ($50 \times 50 \times 50$ mm) cubical molds in two layers following ASTM C109 [21]. Compressive strength was measured after a 24 h curing period, following ASTM C109. Flow was evaluated for the fresh mortar immediately after mixing as per ASTM C1437 [22].

A separate mix of fly ash and solutions without sand was prepared to perform viscosity measurements. No sand was used to avoid abrasion of the rheometer spindles. The viscosity in paste was measured 30 min after the paste was prepared.

The equipment used was a DV-III Ultra rheometer from Brookfield, which is a controlled rate rheometer with capabilities to measure viscosities, yield stress, and other rheological characteristics. The equipment includes the necessary spindles and software to perform the measurements. In this case, it was required to create a curve of viscosity versus time, so a time of 30 min was selected together with a SV-27 spindle and a speed of 5 rpm.

The paste was poured into the cylindrical mold and the needle was inserted. The cylindrical mold containing the sample was then inserted in the sample holder. The cylindrical spindle was inserted with care as not to disturb

TABLE 3—*Research variables for the surfactant design of experiments.*

Research Variables	Levels
Surfactant type	Natural STRA; synthetic STRA
Addition level	0.25, 0.75, 1.25, 1.75 %
Concentration	10, 20, 30 %
Response Variables	**Methods**
Compressive strength	ASTM C109 [21]
Flow	ASTM C1437 [22]
Viscosity	Rheometer

the sample. After the procedure began, the rheometer created a viscosity curve with the points selected on the program. The data was then exported to Excel and analyzed. The data was to be used to construct viscosity versus time curves and served as an input for the software MINITAB, which was used to perform the design of the experiment's analysis.

Experimental Results and Discussion

Compressive Strength

Figure 2 shows the compressive strength for three different concentrations with respect to the total addition (as % of the fly-ash powder) of natural and synthetic STRA. It can be seen that both concentration and the level of addition have a negative effect on the compressive strength of the resulting geopolymer, mainly because of the inclusion of air and the reduction in density of the final product. The same tendency can be observed in the natural STRA, but the effect is less significant. One important observation in this regard is that the specimens made with synthetic STRA exhibited expansion. The reason for this may be the larger size of the molecules of the synthetic STRA compared with the natural STRA and therefore, the lower thermal stability of this type of STRA, which may also have had an effect on the strength as well.

Flow

In terms of flow, Fig. 3 shows that neither the addition level nor the concentration of the STRA had a significant effect on increasing or decreasing the flow for either STRA. Some authors point out that perhaps the flow table test is more appropriate for use with Portland cement and not with alkali-activated fly ash [13]. However, in this study, we could find that the presence of synthetic

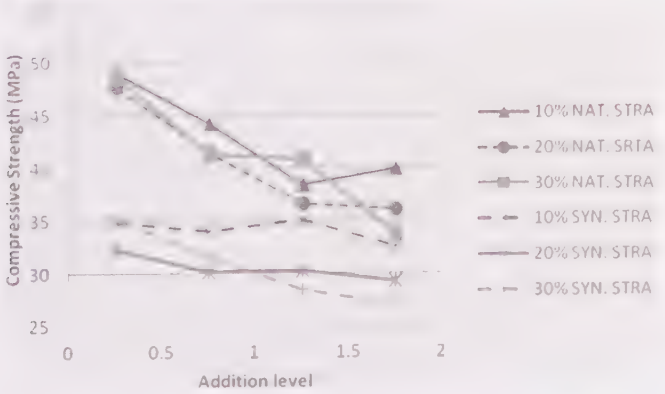

FIG. 2—*Compressive strength of natural and synthetic STRA geopolymer.*

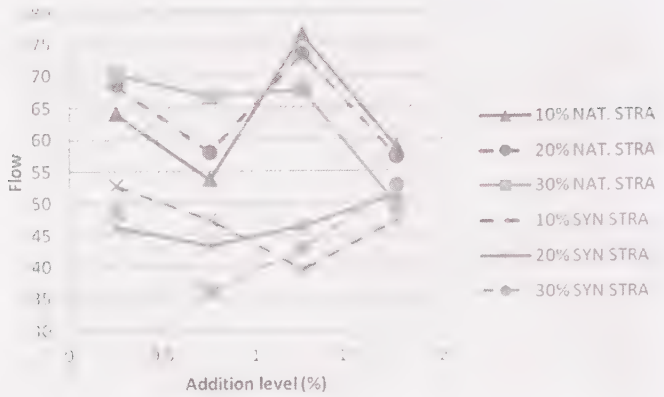

FIG. 3—*Flow for natural and synthetic STRA geopolymer.*

STRAs resulted in greater reduction in flow compared to the natural STRA, even if the level of addition within these two groups did not show a significant effect. Viscosity tests, however, provide more meaningful results.

Viscosity

From Fig. 4, it can be seen that the STRA type plays a significant role. Synthetic STRAs produced higher viscosities compared to natural STRAs and, therefore, resulted in mortars with poorer workability. The higher the level of addition, the lower the viscosity of the resulting mortars; however, the increase in concentration had an opposite effect, so the reduction in viscosity associated with the level of addition can be attributed to the increase in the volume of water and not of the STRA.

All of the samples examined in the previous section showed thixotropy. An example of this can be seen in Fig. 5. This thixotropic behavior is similar to

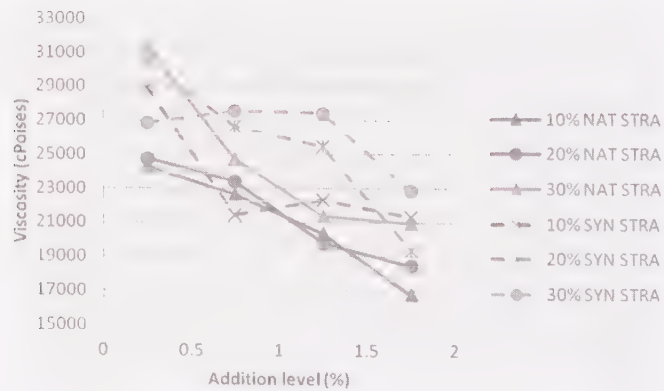

FIG. 4—*Viscosity for natural and synthetic STRA geopolymer.*

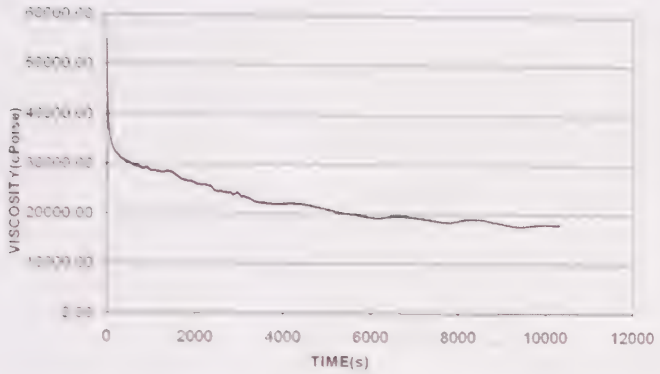

FIG. 5—*Thixotropic behavior of the geopolymer paste after 3 h of shearing.*

that reported in Ref [11]. Figure 6 shows how the reduced viscosity of the geopolymer paste following shearing is maintained after reducing the shear rate, an effect that could have important industrial applications.

The shear strain versus shear stress for a geopolymer paste after five different rest periods can be seen in Fig. 7. The Bingham model reported by Palomo et al., was found to be appropriate to describe the viscoplastic behavior of this geopolymer paste [10]. Palacios et al. suggested that as long as there is no CSH formation because of a high calcium content in the fly ash, the same Bingham model can be used to describe the geopolymer paste; otherwise a different model, such as Herschel-Bulkley should be used [12]. From the curve, it can be observed that the yield stress of the paste increases with the rest period, e.g., a longer rest period causes the paste to regain its rigidity. It is, therefore, beneficial to keep the geopolymer under continuous mixing before pouring industrial applications. The slope of the curve, which is the viscosity, also increases for different rest periods.

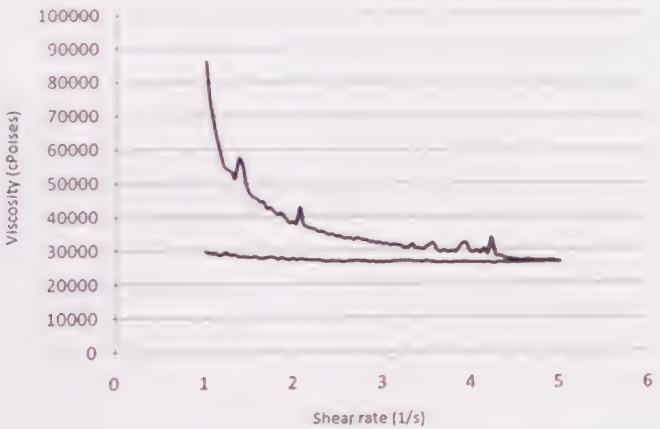

FIG. 6—*Shearing curve for thixotropic geopolymer.*

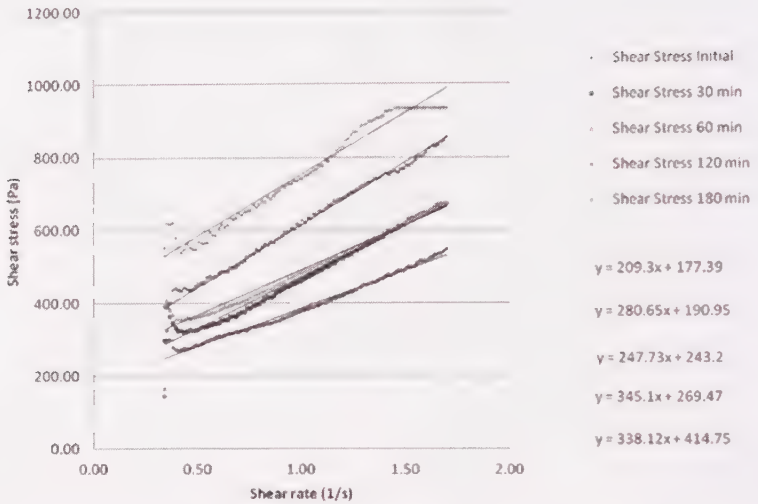

FIG. 7—*Shear stress and yield stress for the geopolymer sample after different rest periods.*

Surface Tension

Surface tension tests were performed using a Fisher surface tension meter, which considers droplet form to evaluate surface tension. Because the presence of synthetic STRA had a significant negative effect on the compressive strength of the geopolymer mortar, it was not considered in phase II of the analysis. Therefore, the surface tension tests were conducted only for the natural STRA. The same design of experiments for the variables of level of addition and concentration was performed for this type of STRA. The results from these tests are displayed in Fig. 8.

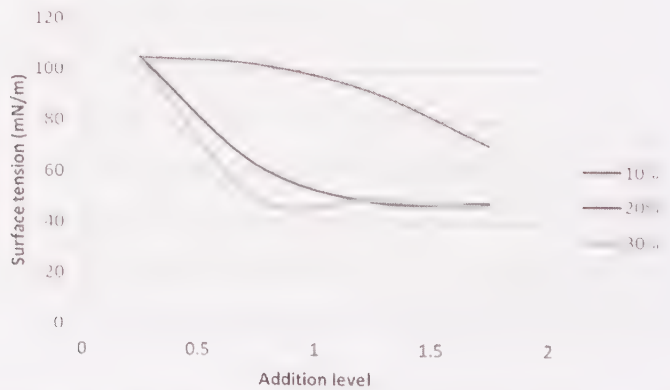

FIG. 8—*Surface tension reduction in the geopolymer using different levels of surfactants.*

FIG. 9—*Mixing and spraying during a sprayable geopolymer field test.*

An increased reduction in surface tension can be observed for increased addition levels and increased concentrations, demonstrating the effect of these admixtures on the geopolymer paste.

Field Tests

Three full-scale field tests were conducted for this geopolymer mix. Two of the tests were performed by the authors using "spray-buddy," a commercial

FIG. 10—*Spraying and finishing the geopolymer coating.*

air-assist spray system. The third test was performed by a contractor using a large commercial rig retrofitted for lining of manholes. The full-scale field tests provided significant insight into the performance of the formulation in terms of pumpability, sprayability, adherence to the concrete substrate, ability to "buildup" a new geopolymer coat on a vertical concrete surface, and finishability. The tests proved that the geopolymer mix could be sprayed with commercial equipment used by contractors for applying cementitious lining products (Figs. 9 and 10).

Conclusions

Results show that the use of STRAs could significantly improve the workability of these materials, both by modifying their viscosity and, more importantly, by reducing surface tension of the paste, enabling them to be sprayed and troweled. Based on the results of the field tests, additional refinements are underway aiming at simplifying field installations and enhancing productivity. The rheology of the geopolymer paste is an essential characteristic that must be considered in any commercial application developed for the construction industry.

Acknowledgments

The writers wish to express their gratitude and sincere appreciation to the Department of Energy and Cleco Power for financing this research work and also several ongoing research projects related to the durability of fly-ash-based geopolymer binders.

References

[1] Davidovits, J., "Properties of Geopolymer Cements," *Proceedings of the First International Conference on Alkaline Cements and Concretes*, Kiev, Ukraine, October 11–14, 1994, Geopolymer Institute, Saint-Quentin, France.

[2] Miranda, J. M., Fernández-Jiménez, A., González, J. A., and Palomo, A., "Corrosion Resistance in Activated Fly Ash Mortars," *Cement Concrete Res.*, Vol. 35, 2005, pp. 1210–1217.

[3] Song, X.-J., "Response of Geopolymer Concrete to Sulfuric Acid Attack," Proceedings of the World Congress Geopolymer, ACCI, School of Civil and Environmental Engineering, UNSW, Sydney, Australia, 2005.

[4] Ingram, C. and Crookes, B., "Inorganic Polymer Technology: Technical Overview and Market Study of Key Raw Materials," *Technical Report*, Department of Chemical and Biomolecular Engineering, The University of Melbourne, Melbourne, Australia, 2005, 157 pp.

[5] ASTM C618, 2008, "Standard Specification for Coal Fly Ash and Raw or Calcined Natural Pozzolan for Use in Concrete," *Annual Book of ASTM Standards*, ASTM International, West Conshohocken, PA.

[6] Wallah, S. E. and Rangan, B. V., "Low Calcium Fly Ash Based Geopolymer Concrete: Long-Term Properties," *Research Report GC2*, Faculty of Engineering, Curtin University of Technology, Perth, Australia, 2003.

[7] Keyte, L. M., Lukey, G. C., and van Deventer, J. S. J., "The Effect of Coal Ash Glasses Chemistry in the Tailored Design of Waste-Based Geopolymer Products," *Proceedings of the First International Conference on Engineering for Waste Treatment (WasteEng)* (on CD), Albi, France, May 17–19, 2005.

[8] Montes, C. and Allouche, E., "Evaluation of the Potential of Geopolymer Mortar in the Rehabilitation of Buried Infrastructure," *Struct. Infrastruct. Eng.*, Vol. 8, No. 1, 2012, pp. 89–98.

[9] Chindaprasirt, P., Chareerat, T., and Sirivivatnanon, V., "Workability and Strength of Coarse High Calcium Fly Ash Geopolymer," *Cement Concrete Comp.*, Vol. 29, No. 3, 2007, pp. 224–229.

[10] Palomo, A., Banfill, P. F. G., Fernández-Jiménez, A., and Swift, D. S., "Properties of Alkali-Activated Fly Ashes Determined from Rheological Measurements," *Adv. Cement Res.*, Vol. 17, 2005, pp. 143–151.

[11] Laskar, A. I. and Bhattacharjee, R., "Rheology of Fly-Ash Based Geopolymer Concrete," *ACI Mater. J.*, Vol. 108, No. 5, 2011, pp. 536–542.

[12] Palacios, M., Banfill, P. F. G., and Puertas, F., "Rheology and Setting of Alkali Activated Slag Pastes and Mortars: Effect of Organic Admixtures," *ACI Mater. J.*, Vol. 105, No. 2, 2008, pp. 120–148.

[13] Criado, M., Palomo, A., and Fernandez-Jimenez, A., "Alkali Activated Fly Ash: Effect of Admixtures on Paste Rheology," *Rheol. Acta*, Vol. 48, 2009, pp. 447–455.

[14] Hewayde, E., 2005, "Degradation of Concrete Sewer Pipes by Sulfuric Acid," Ph.D. thesis, University of Western Ontario, Canada.

[15] Environmental Protection Agency, "Hydrogen Sulfide Corrosion in Wastewater Collection and Treatment Systems," *Report No. EPA/09-91-010*, U.S. Environmental Protection Agency, Office of Water, Washington, D.C., 1991.

[16] Stein, D., *Rehabilitation and Maintenance of Drains and Sewers*, Ernst and Sohn, Berlin, Germany, 2001, Chap. 5, pp. 395–397.

[17] Zisman, W. A., *Contact Angle, Wettability and Adhesion Advances in Chemistry Series*, Vol. 43, F. M. Fowkes, Ed., American Chemical Society, Washington, DC, 1964.

[18] Dolch, W. L., "Air-Entraining Admixtures," *Concrete Admixtures Handbook. Properties, Science, and Technology*, 2nd ed., V. S. Ramachandran, Ed., William Andrew/Noyes, Portland, Maine, 1995.

[19] Edmeades, R., Hewlett, M., and Peter, C., "Cement Admixtures," *Lea's Chemistry of Cement and Concrete. Chemistry of Concrete and Cement*, Butterworth-Heinemann, Burlington, MA, 1998, pp. 843–848.

[20] ASTM C778: "Standard Specification for Standard Sand," *Annual Book of ASTM Standards*, ASTM International, West Conshohocken, PA.

[21] ASTM C109/C109M: "Standard Test Method for Compressive Strength of Hydraulic Cement Mortars (Using 2-in. or [50-mm] Cube Specimens)," *Annual Book of ASTM Standards*, ASTM International, West Conshohocken, PA.

[22] ASTM C1437: "Standard Test Method for Flow of Hydraulic Cement Mortar," *Annual Book of ASTM Standards*, ASTM International, West Conshohocken, PA.

Geopolymer Binder Systems
STP 1566, 2013
Available online at www.astm.org
DOI:10.1520/STP156620120104

Narayanan Neithalath[1] *and Deepak Ravikumar*[1]

Evaluating the Use of Accelerated Test Methods for Chloride Transport in Alkali Activated Slag Concretes Using Electrical Impedance and Associated Models

REFERENCE: Neithalath, Narayanan and Ravikumar, Deepak, "Evaluating the Use of Accelerated Test Methods for Chloride Transport in Alkali Activated Slag Concretes Using Electrical Impedance and Associated Models," *Geopolymer Binder Systems*, STP 1566, Leslie Struble and James K. Hicks, Eds., pp. 85–107, doi:10.1520/STP156620120104, ASTM International, West Conshohocken, PA 2013.[2]

ABSTRACT: The applicability of accelerated chloride transport test methods, viz., the rapid chloride permeability (RCP) and non-steady state migration (NSSM) tests, commonly used for conventional concretes, for alkali activated slag concrete systems is evaluated in this paper. Both powder and liquid sodium silicate activators are used to activate slag. The effects of changing the total Na_2O content and the activator modulus of both the powder and liquid activators on the RCP and NSSM values are reported. RCP values of activated slag concretes show that these concretes perform better than conventional concretes. However, NSSM tests provide values that are comparable to conventional concretes either with or without high performance cement replacement materials such as silica fume. Pore structural studies show that the waterglass activated concretes have lower porosities than the powder sodium silicate activated mixtures, but their critical pore sizes are larger, resulting in reduced transport resistance. Electrical circuit models are implemented on the impedance spectroscopic response of alkali activated and conventional concretes. The modeled circuit model parameters are similar for the alkali activated and conventional concretes. Moreover, the changes to these parameters induced by the NSSM test are similar in trends and magnitudes for both alkali activated and conventional

Manuscript received June 29, 2012; accepted for publication November 20, 2012; published online April 30, 2013.

[1]Arizona State University, Tempe, AZ.

[2]ASTM Symposium on *Geopolymer Binder Systems* on June 26–27, 2012 in San Diego, CA.

concretes, demonstrating the adequacy of the test method for alkali activated binders.

KEYWORDS: alkali activation, slag, electrical impedance, chloride transport, microstructure

Introduction

Rapid pace of infrastructural development has resulted in significant concerns relating to the emission of greenhouse gases to the atmosphere, massive consumption of dwindling natural resources, and utilization of energy at an unprecedented scale. Portland cement production contributes to all three of the above concerns, thereby necessitating the need to develop alternate binding materials that have lower energy footprint and environmental impact. Over the past few years, several options ranging from increased use of recycled and by-product cement replacement materials in ordinary Portland cement (OPC) concrete to complete replacement of OPC in concrete have been attempted. The latter category of binders is produced by the activation of waste or by-product aluminosilicates such as fly ash or slag by alkaline hydroxides or silicates [1–4]. These binders have been reported to exhibit mechanical and durability characteristics similar to or superior than those of ordinary Portland cement binders [5–9]. Ground granulated blast furnace slag is one of the most common materials employed to produce alkali activated binder systems because of the fairly rigorous existing understanding of slag as a cementitious material. In addition, alkali activation of slag also produces C-S-H gel as the reaction product.

Alkali activation of slag has been studied extensively [5,7,9–12]. The activating agent typically is a sodium silicate-based solution ($Na_2SiO_3.xH_2O$ + NaOH). Several parameters relating to the physical and chemical characteristics of slag and the activator influence the reaction kinetics [13] as well as the mechanical and durability properties of the final product [4,7,12,14–16]. A majority of the studies on alkali activated slags have been carried out using waterglass solutions as the activator. This presents issues with handling because of the caustic nature of the alkalis. Hence, in this study, powder activator, based on powder sodium silicate and sodium hydroxide pellets are also used as activating agents. While the strength of such binder systems is generally lower than those activated by waterglass solutions, by proper proportioning procedures, compressive strengths in the range of 30–35 MPa can be achieved [17], which is sufficient for most general purpose applications.

Resistance to ionic transport is one of the important durability criteria for concretes. Though a few studies have reported results on chloride ion transport through alkali activated slag concretes, a comprehensive treatment of the subject is lacking. This paper investigates chloride transport through powder and liquid sodium silicate activated slag concretes using well-accepted accelerated test methods such as rapid chloride permeability (RCP) and non-steady state

migration (NSSM) tests, and compares the transport parameters to those of plain and modified (using fly ash or silica fume) conventional concretes. Furthermore, electrical circuit models based on impedance spectroscopic responses are used to understand the effect of accelerated chloride transport on the material microstructure. A combination of experimentally measured chloride transport parameters and circuit models for material microstructure provides insights into the response of these concretes vis-à-vis those of conventional concretes as far as RCP or NSSM tests are concerned.

Experimental Program

Materials and Mixture Proportions

Alkali Activated Mixtures—The alkali activated concrete mixtures were prepared using ground granulated blast furnace slag (type 100, conforming to ASTM C989 [18]) as the binding material. The chemical composition of slag is shown in Table 1. The activating agents used are powder or liquid sodium silicate and NaOH in the form of pellets. The powder sodium silicate has a silica modulus (M_s, defined as the SiO_2-to-Na_2O ratio by mass) of 1.95. Note that the mass-based and molar M_s values are very comparable since the ratio of molecular masses of SiO_2 and Na_2O is 0.97. The liquid sodium silicate (waterglass) has an M_s of 3.26 and a solids content of 40 %. Addition of reagent-grade NaOH facilitated the changes in the M_s of the sodium silicate activator. In this paper, solid (or powder) sodium silicate activator implies that the activator is a combination of powder sodium silicate of M_s 1.95 and requisite amounts of NaOH required to bring the M_s of the activator to desired levels (between 0.6 and 1.5), and liquid sodium silicate (or waterglass) implies that the activator is a combination of waterglass of M_s 3.26 and NaOH solution required to bring the activator M_s to the desired levels (1.0, 1.5, or 2.0). For the powder activated mixtures, the M_s values had to be reduced to these lower levels in order to

TABLE 1—*Chemical composition of slag, OPC, fly ash, and silica fume.*

Composition (% by mass)	Slag	Cement	Silica Fume	Fly Ash
Silica (SiO_2)	36.0	20.2	93.4	50.24
Alumina (Al_2O_3)	10.5	4.7	0.42	28.78
Iron oxide (Fe_2O_3)	0.67	3.0	0.52	5.72
Calcium oxide (CaO)	39.8	61.9	1.91	5.86
Magnesium oxide (MgO)	7.93	2.6	–	1.74
Sodium oxide (Na_2O)	0.27	0.19	0.25	0.20
Potassium oxide (K_2O)	0.80	0.82	0.79	0.84
Sulfur trioxide (SO_3)	2.1	3.9	0.34	0.51
Loss on ignition	3.0	1.9	2.3	2.8

obtain 28 day compressive strengths in the range of 20–30 MPa, while for the waterglass activated mixtures M_s values in between 1.0 and 2.0 produced much higher 28 day compressive strengths [17,19]. The n values (Na_2O-to-slag ratio) used were 0.05 and 0.15 for the powder sodium silicate activated mixtures and 0.05 for the waterglass activated mixtures.

The slag content for the alkali activated concrete mixtures was 400 kg/m^3 and the liquid-to-powder ratio was maintained at 0.40. The powder consists of the slag, powder sodium silicate and NaOH for the mixtures activated using powder sodium silicate. The liquid consists of the added water and the amount of water in the sodium silicate solution when waterglass is used as the activator. River sand was used as the fine aggregate and pea gravel with a nominal maximum size of 9.5 mm was used as the coarse aggregate. The concrete specimens were cast in cylinders (100 mm diameter and 200 mm height) and moist cured until the testing time. Activated slag pastes were prepared for pore structural characterization studies.

Conventional Concrete Mixtures—Type I ordinary Portland cement conforming to ASTM C150 [20] was used to prepare the conventional concrete mixtures evaluated in this study. A Class F fly ash (FA) conforming to ASTM C618 [21], or a dry densified silica fume (SF) corresponding to ASTM C1240 [22] were used as partial cement replacement materials. The chemical composition of these materials is also shown in Table 1. Concrete mixtures were proportioned by replacing either 10 % or 20 % of cement with fly ash (indicated as FA 10 or FA 20 respectively in the tables and graphs), or 6 % or 9 % of cement with silica fume (indicated as SF 6 or SF 9), by mass. The water-to-cementing materials ratio (w/cm) for all the concretes was maintained at 0.40. The cementing materials content (cement + replacement materials) of the mixtures was fixed at approximately 400 kg/m^3. Cylindrical specimens (100 mm diameter × 200 mm height) were cast and demolded after a day of casting and cured at 23 ± 2°C and 98 % RH until the desired age of testing.

Test Methods

Chloride Transport Test Methods—Rapid chloride permeability (RCP, ASTM C 1202) and Non-steady state migration (NSSM, NT Build 492 [23]) tests were carried out on 50 mm thick discs cut from 200 mm long cylindrical specimens cured for 28, 56, or 90 days. For the RCP test, the specimens were conditioned by vacuum saturation, and enclosed in a cell flanked by reservoirs that contain 0.3 N NaOH solution on one side and 3 % NaCl solution on the other. A 60 V potential difference was applied between the electrodes placed on both faces of the specimen, for a duration of 6 h. The total charge passed (in coulombs) at the end of 6 h of testing is reported as the RCP value. This test is well-accepted for conventional concretes (even though a number of drawbacks

have been reported), and has been used recently for alkali activated concrete systems also [7]. For the NSSM test, the specimens were preconditioned by vacuum saturation with calcium hydroxide solution. The catholyte and anolyte solutions used were 2 N NaCl and 0.3 N NaOH, respectively. An initial voltage of 30 V was applied, and initial current recorded. The applied voltage and test duration were chosen based on the initial current. The test duration was maintained at 24 h and the voltage at 30 V for all the cases. After the test duration, the specimens were axially split and sprayed with a 0.1 M silver nitrate solution. The depth of chloride penetration was measured based on the precipitation of white silver chloride. The non-steady state migration coefficient (D_{nssm}) in m^2/s is given as

$$D_{nssm} = \frac{RT}{zFE}\frac{x_d - \alpha\sqrt{x_d}}{t} \tag{1}$$

$$\alpha = 2\sqrt{\frac{RT}{zFE}}\text{erf}^{-1}\left(1 - \frac{2c_d}{c_0}\right) \tag{2}$$

$E = (U\text{-}2)/L$,

where:

U = absolute voltage (V),

L = specimen thickness in m,

z = valence of the chloride ion,

F = Faraday constant,

R = molar gas constant,

T = average value of initial and final temperatures in K,

x_d = average value of the penetration depth in m,

t = test duration in seconds,

c_d = chloride concentration at which silver nitrate changes to silver chloride (0.07 N), and

c_0 = chloride concentration of the catholyte solution (2 N).

The value of c_d chosen is the one generally used for ordinary Portland cement concretes. However, the calculations for the migration coefficients were repeated with c_d values of 0.05 and 0.1, but this resulted in insignificant changes to the D_{nssm} value. Hence a c_d value of 0.07 itself is used in this study.

Pore Structure Characterization Using MIP—Mercury intrusion porosimetry (MIP) was carried out on small samples of oven dried alkali activated pastes using a porosimeter that can generate a maximum pressure of 414 MPa (60 000 psi) and evaluate a minimum pore diameter of 0.003 μm. The test was performed in two steps—the low pressure step evacuates the gases, fills the sample holder with mercury, and carries out the test up to 345 kPa (50 psi), and

the high pressure step reaches pressures of up to 414 MPa. A contact angle of 130° and a surface tension of 485 dynes/cm were used in the analysis.

Electrical Impedance Spectroscopy—Electrical impedance spectroscopy (EIS) was carried out on the concrete specimens prior to and after the chloride transport tests. The test configuration for EIS was the same as that used for the chloride transport tests. Similar arrangements have been reported in [24,25]. The EIS measurements after the test were carried out when the cell temperature reached near ambient levels so that the measured conductivity is not influenced significantly by the temperature change. EIS spectra were obtained using a Solartron 1260 gain-phase analyzer operating at a frequency range of 1 Hz to 10 MHz. A 250 mV AC signal was employed and 10 measurements per decade of frequency were recorded. The meeting point of the bulk and electrode arcs in a Nyquist plot (plot of real versus imaginary impedance) is denoted as the bulk resistance (R_b). The effective conductivity of the specimen (σ_{eff}) was calculated as

$$\sigma_{eff} = \frac{L}{R_b A} \tag{3}$$

where:

L = length (50 mm), and

A = cross sectional area (7854 mm^2), respectively of the specimen

Results and Discussions

Chloride Transport Parameters

The common accelerated test methods that are used to evaluate the chloride transport resistance of concretes include the rapid chloride permeability (RCP) test as per ASTM C 1202, and the non-steady state migration test as per NT BUILD 492. These tests are not without drawbacks as have been reported in several publications [26,27], but their ease of use and the reasonable ability to distinguish between the performances of different concretes have made them widely acceptable.

Rapid Chloride Permeability Values—Figure 1 depicts the RCP values of both the powder and liquid activated slag concretes as a function of the activator modulus (M_s). The n values used are 0.05 and 0.15 for the powder sodium silicate activated concretes whereas only an n value of 0.05 is used for the liquid activated concretes, the reasons for which were described in the experimental program section. It can be noticed from this figure that the concretes activated using powder sodium silicate have much lower RCP values as compared to those activated using the liquid activator. The charge passed for the powder sodium silicate activated slag concretes vary between 1000 and

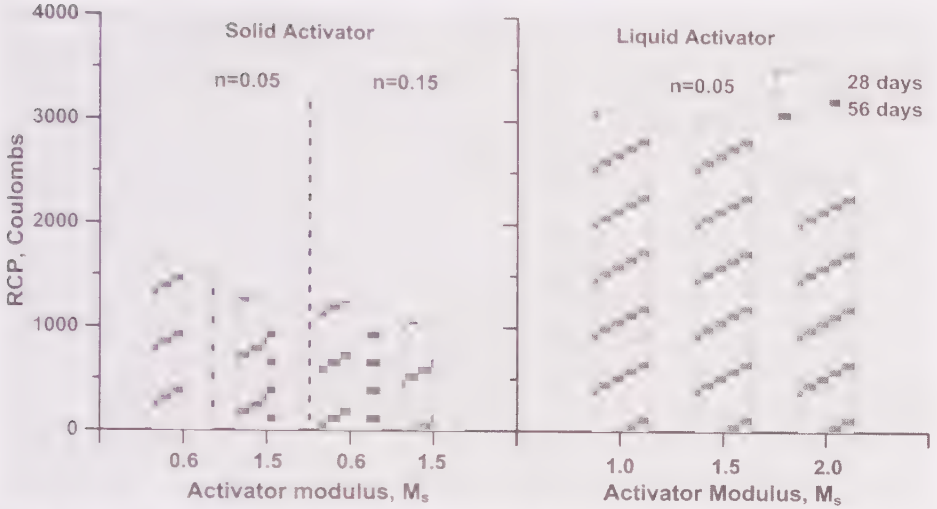

FIG. 1—*RCP values of powder and liquid sodium silicate activated slag concretes.*

1600 Cs, whereas the waterglass activated slag concretes show typically higher values, in the range of 2400 to 3000 Cs. Lower RCP values are observed for the powder sodium silicate activated mixtures when the *n* value is higher. The RCP values of the waterglass activated concretes are slightly higher than those reported earlier [7], but this can be attributed to an *n* value of 0.10 used in those studies as opposed to the value of 0.05 used in the present study. For both the powder and liquid activated concretes, the RCP values show a slight reduction with increase in the activator modulus.

In order to compare the RCP values of alkali activated and conventional concretes, the RCP values of conventional concretes (plain as well as fly ash and silica fume modified concretes) are shown in Fig. 2. Silica fume modified concretes show lower RCP values, attributable to pore structure densification and a lowering of the pore solution conductivity [28]. The pore structure refinement in fly ash modified concretes results in lower RCP values at later ages. When the RCP values of the alkali activated and conventional concretes are compared, the powder sodium silicate activated slag concretes are seen to have RCP values similar to those of silica fume modified concretes after 28 days whereas the waterglass activated slag concretes demonstrate RCP values similar to those of 56-day cured conventional concretes or 20 % fly ash modified concretes. The microstructural reasons for the lower RCP values of powder sodium silicate activated slag concretes are explained in a forthcoming section.

Non-Steady State Migration Coefficients—The non-steady state migration (NSSM) coefficients (D_{nssm}) of powder and liquid sodium silicate activated

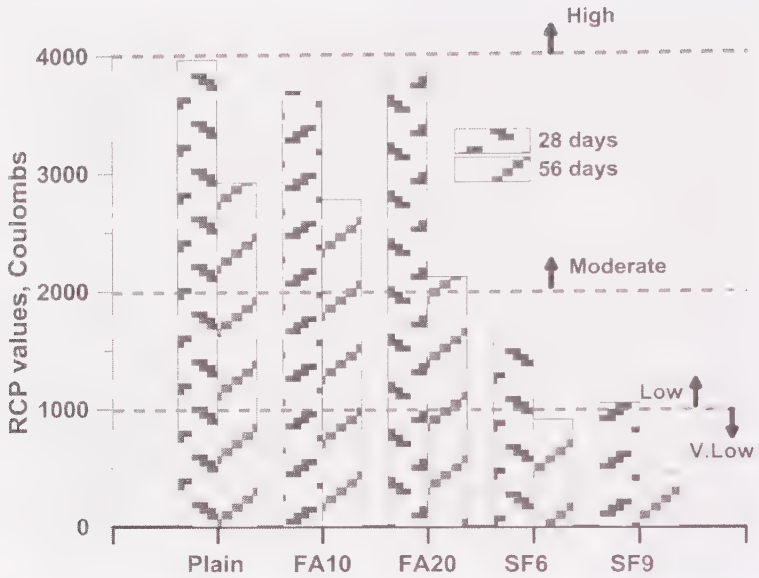

FIG. 2—*RCP values of plain and modified concretes for comparison.*

slag concretes are shown in Fig. 3. It can be observed that the D_{nssm} values are significantly reduced when the n value of the powder sodium silicate activated mixture is increased from 0.05 to 0.15. While the RCP values of the powder sodium silicate activated concretes were found to be significantly lower than

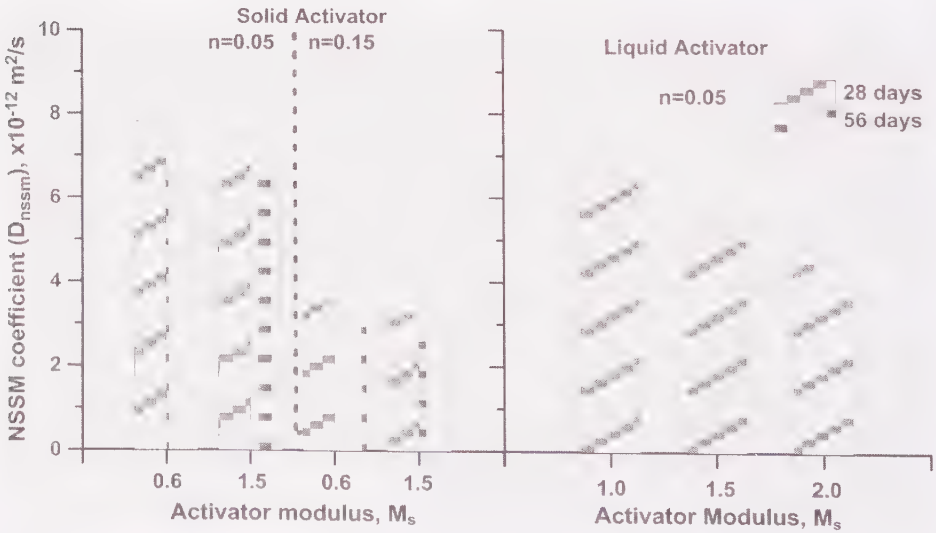

FIG. 3—*NSSM coefficients of powder and liquid sodium silicate activated slag concretes.*

those of liquid activated concretes, such a sharp distinction is not observed in the case of NSSM coefficients. This is partly attributed to the dependence of RCP values on pore solution conductivity—the solubility limits of the solid activator [13,19], results in reduced pore solution conductivity. The waterglass activated slag concrete having an n value of 0.05 and a lower activator M_s (of 1.0) demonstrates a D_{nssm} value similar to that of the powder activated mixtures of lower n value. For the powder sodium silicate activated concretes, the microstructural changes occurring with time are minimal as observed from the insignificant change in D_{nssm} values between 28 and 56 days.

The NSSM coefficients of conventional concretes are presented in Fig. 4. All the D_{nssm} values of the waterglass activated slag concretes are comparable to or lower than those of corresponding ordinary Portland cement concretes. The D_{nssm} values of the solid sodium silicate activated slag concretes are comparable to: (i) those of conventional concretes cured for 56 days when the n value is 0.05, and (ii) those of silica fume modified concretes when the n value is increased to 0.15.

The above discussions reveal that it is possible to proportion both powder and liquid activated slag concretes (having slag contents comparable to that of cementing materials content in a conventional concrete mixture) with chloride transport properties comparable to or better than those of conventional concretes. Along with the provision to obtain adequate mechanical properties, proportioning for adequate transport properties enables widespread use of this sustainable material.

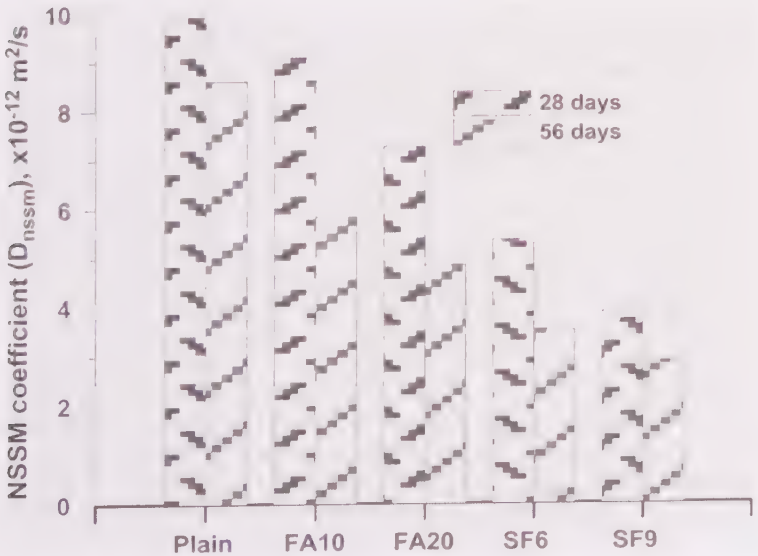

FIG. 4—*NSSM coefficients of plain and modified concretes for comparison.*

Dependence of Chloride Transport Parameters on Pore Structure—The dependence of pore structure on moisture and ionic transport in cementitious materials is well established. Based on the RCP and NSSM test results presented earlier, it is instructive to examine the influence of pore structure on the chloride ion transport resistance of these materials. In this study, mercury intrusion porosimetry (MIP) is used to describe the pore structure features of alkali activated concretes. There are not many published papers on the use of MIP for alkali activated concretes, mainly because of the several questions about the applicability of MIP to cementititous systems. The authors believe that the use of MIP as an indicator of the total pore volume, and as a relative measure of the pore sizes of different cementitious or alkali activated specimens, is justified. The drawbacks of MIP test such as the misrepresentation of the pore sizes due to the ink-bottle effect and collapse of pores under high pressure gain prominence when absolute values of pore sizes are sought. The pore sizes reported in this study are only used as comparative tools.

Figure 5(*a*) shows the cumulative pore volume intruded by mercury as a function of the pore sizes (subject to the simplifications used in the MIP analysis) for representative powder and liquid sodium silicate activated slag concretes. Results on an elaborate matrix of mixtures are presented in Ref [29]. It is observed that the cumulative pore volume intruded by mercury is about the same for solid sodium silicate activated pastes, irrespective of the n values used (in the range examined in this study). Hence, increasing the activator alkalinity through an increase in n value does not reduce the pore volume, even though this has been observed to increase the compressive strength [17,29] and reduce the chloride ion transport coefficients as described in the previous sections. The cumulative pore volume intruded is much lower for the liquid

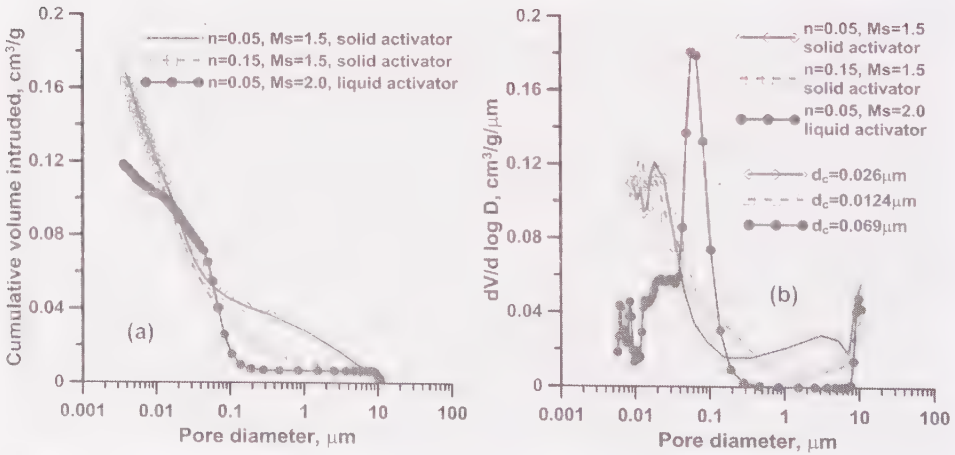

FIG. 5—*(a) Cumulative pore volume intruded, and (b) differential pore volume, for powder and liquid sodium silicate activated slag pastes.*

sodium silicate activated slag concrete. This has direct implications on the compressive strength, with the waterglass activated mixtures showing much higher compressive strengths than the powder sodium silicate activated concretes [13,19,29].

The differential pore volume ($dV/d\log D$), which can be used to deduce the critical (percolating) pore size for the activated pastes, is presented in Fig. 5(*b*). Contrary to the total pore volume that does not change with n value, the critical pore size is found to be much lower for the higher n value paste activated using powder solid sodium silicate. The reduction in both RCP and D_{nssm} values between mixtures made with $n = 0.05$ and $n = 0.15$ shown in Figs. 1 and 3 can therefore be attributed in part to the reduction in pore sizes. A comparison of RCP and NSSM coefficients shown in Figs. 1 and 3 shows that an increase in n value of the powder sodium silicate activator does not impact the RCP values appreciably but the NSSM coefficients are considerably reduced. Even when the pore sizes are reduced for the higher n value mixtures, as can be noticed from Fig. 5(*b*), the lack of a significant change in the RCP values can be ascribed to an increased pore solution conductivity in this case that compensates for the effect of refined pore structure. The use of powder sodium silicate also results in changes in reaction product composition [17] and morphology; thus changing the tortuosity or connectivity of the pore channels. This also contributes to the lower NSSM coefficients of the higher n value mixtures. For the waterglass activated concretes, even though the cumulative pore volume intruded is lower, the critical pore sizes are much higher as can be seen from Fig. 5(*b*). Figures 1 and 3 also show that the chloride transport parameters are higher for the waterglass activated slag mixtures, suggesting that the critical pore sizes are more influential than the reduced porosity in dictating transport. A detailed analysis proving this concept, both experimentally and using electrical circuit models for microstructure, has been provided in an earlier publication [24].

Bulk Resistance and Transport Parameters

The bulk resistances (R_b) of the specimens measured using EIS before the accelerated chloride transport tests are related to the chloride transport parameters, viz., the RCP value and the NSSM coefficient, in Figs. 6(*a*) and 6(*b*). The data corresponding to the mixtures activated using both the solid and liquid activators are shown here. From Fig. 6(*a*), it is seen that there is a good relationship between the bulk resistance of the sample and the RCP values. A very good linear relationship between conductivity of the specimens and the RCP values has been reported for conventional concrete specimens [24]. Note that resistance is directly used in this paper instead of conductivity and hence a power relationship between R_b and RCP values as shown in the figure results. The resistance-RCP value relationship for the alkali activated mixtures is not

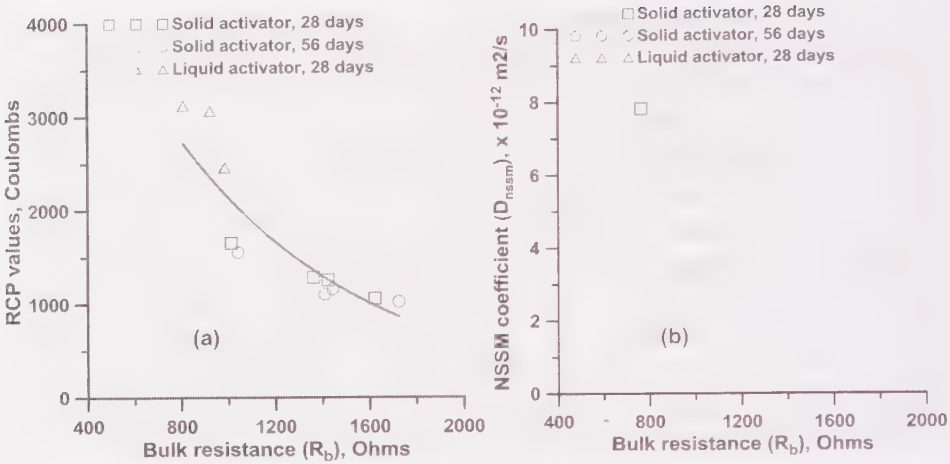

FIG. 6—*Relationship between bulk resistance measured before the transport tests and: (a) RCP values, and (b) NSSM coefficients.*

found to be as strong as those for conventional concretes. A number of reasons, including differences in the pore structure (pore sizes and tortuosity) [24,30], and changes in reaction product formation [17,19] can be attributed to this observation. In addition, the conductivity (or resistivity) of the solid phases in alkali activated systems could significantly vary based on the activator alkalinity and the method of incorporation of alkalis into the reaction products. This is in contrast to conventional cementitious systems where the solid phase can be estimated to have reasonably similar conductivities—in the range of 0.001–0.005 S/m [31]. Figure 6(*b*) depicts the relationship between the bulk resistances before the NSSM test and the NSSM coefficients. The scatter in the data is much larger as compared to the R_b-RCP relationship shown in Fig. 6(*a*). The major reason is that the RCP test is essentially a conductivity/resistivity test [24,26]. On the contrary, the NSSM coefficient is extracted through considerations of ionic movement under an external applied electrical field (predominantly migration, especially at voltages more than 10–15 V when the diffusive component can be neglected). The Nernst-Plank equation takes into account several parameters that are not considered in the determination of total charge passed and thus the lack of a direct relationship between R_b and NSSM coefficients is not surprising.

Figure 7(*a*) shows the changes in bulk resistances of the alkali activated concretes as a result of the RCP test. The bulk resistance decreases after the test, attributable to the penetration of chloride ions into the concrete, which reduces the overall electrical resistance of the material. The increase in the temperature of the specimens due to the higher applied potential might also result in lower resistances after the test, but the fact that the resistances were

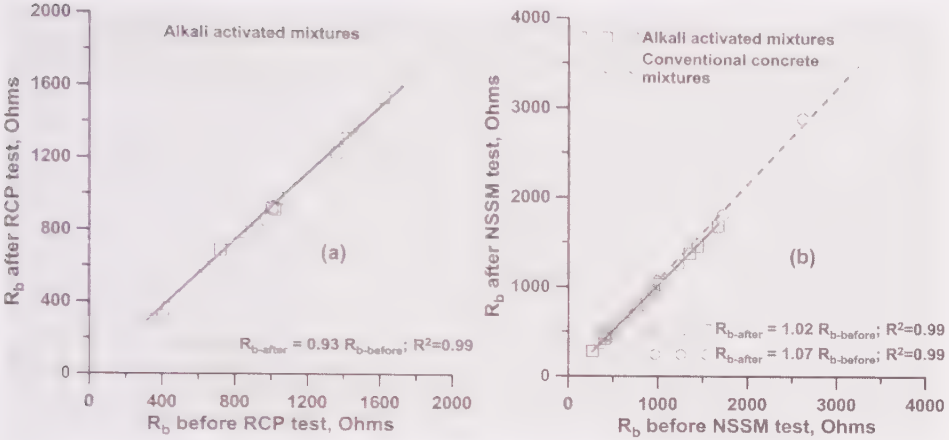

FIG. 7—*Bulk resistances of specimens before and after: (a) RCP test (for alkali activated concretes), and (b) NSSM tests (for both alkali activated and conventional concretes).*

measured after the specimens returned to the ambient temperature makes this less likely. Figure 7(*b*) shows the changes in R_b of the alkali activated and conventional concretes as a result of non-steady state migration. It is observed from this figure that the relationships between the bulk resistances before and after the NSSM test are very similar for the alkali activated and conventional concretes. Barring the two data points that belong to silica fume modified concretes (of very high resistances), there is almost nothing to choose between the R_b values of both these types of concretes. If it can be considered that the pore solution in alkali activated concretes is less resistive than those in conventional concretes, then the pore structure in those concretes need to be more refined so as to render the bulk resistance values quite similar. The adequacy of NSSM test for alkali activated concretes can be gleaned from this comparison with conventional concretes. The bulk resistances are found to be slightly higher after the migration test. The increase in resistance could be the result of the formation of new solid products either within the pores or as electrochemical double layer along the pore walls [30,32].

Electrical Circuit Models for Microstructure and the Influence of Transport on Model Parameters

In this section, effort is placed on understanding the influence of accelerated chloride transport tests on the material microstructure of both conventional and alkali activated concretes. One means of evaluating this influence is through the combined used of electrical impedance spectra of concretes before and after the transport tests, and associated circuit models that relate to the material microstructure. The Nyquist plots obtained from EIS contains several features

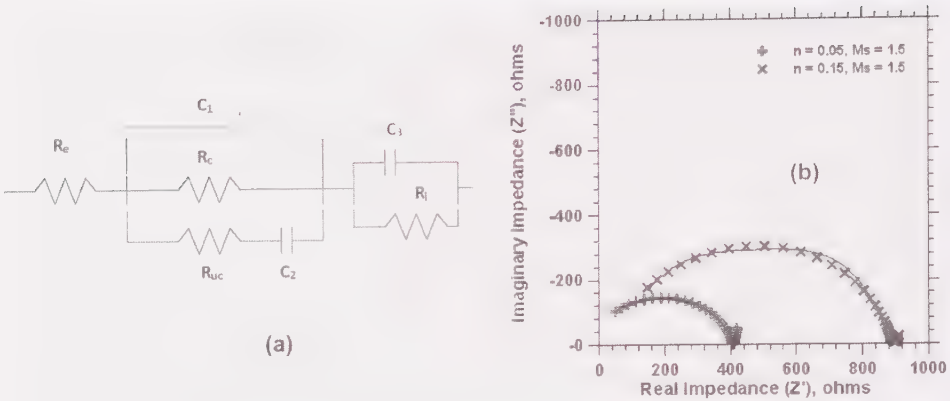

FIG. 8—*(a) Equivalent electrical circuit model for concrete microstructure, and (b) representative Nyquist plot and modeled curve for alkali activated slag concretes.*

of the microstructure that are otherwise not easily extractable such as the pore connectivity or tortuosity. Therefore EIS is ideal to understand the subtle changes that are introduced in the concrete specimen due to the chloride transport tests.

Different types of equivalent electrical circuit models have been used to represent the Nyquist plots of cementitious materials. These equivalent circuits are a combination of resistors, capacitors, and constant-phase elements, which when assembled in certain configurations, provide reliable representations of the pore structure. Several equivalent electrical circuits are used in the study of cement-based materials, and the one shown in Fig. 8(*a*) has been shown to adequately capture the material structure [33] and the accelerated chloride transport test configuration [24,30], and hence is used in this study. The resistance R_e in the circuit denotes the resistance of electrolyte between the electrodes and the concrete sample in the accelerated chloride transport test setup. The resistances R_c is associated with the ionic motion in the percolating or connected pores in the material and R_{uc} with the ionic motion in the unconnected or isolated pores in the material structure. C_1 is the dielectric capacitance related to the solid fraction (paste and the aggregates in concrete, or the paste phase alone in cement pastes), and C_2 is the capacitance associated with the double layer present between the pore walls and the pore solution. R_i and C_3 represent the resistance and capacitance of the specimen-electrode interface.

The total frequency dependent impedance $Z(\omega)$ of the system can be represented as

$$Z(\omega) = R_e + \frac{Z_1 Z_2}{Z_1 + Z_2} + Z_3 \tag{4}$$

Z_1, Z_2, and Z_3 = impedances of the element groups in the circuit.

The impedances Z_1 and Z_2, belong to the R_c-C_1 and R_{uc}-C_2 combinations respectively (bulk part of the system), and are denoted as

$$Z_1 = \frac{R_c}{1 + (j\omega R_c C_1)^{\alpha}} \tag{5a}$$

$$Z_2 = R_{uc}\left[1 + (j\omega R_{uc} C_2)^{-\beta}\right] \tag{5b}$$

α and β = dispersion factors and are obtained from the fits.

The equivalent circuit model parameters were extracted from the impedance spectra using ZView software. Figure 8(*b*) shows the EIS spectra and representative fits obtained from the equivalent electrical circuit for the bulk arc for two selected activated slag concretes. The fits are in good agreement with the measured impedance spectra as seen in the figure.

Significance of the Model Parameters—In this paper, only the impedance of the specimen, represented by the middle term in Eq 4, is considered. The resistance of the electrolyte between the specimen and the electrodes (R_e) and the impedance of the specimen-electrode interface (R_i and C_3) are not analyzed further because the focus is devoted towards a better understanding of the material before and after the test, and ascertaining how alkali activated systems respond vis-à-vis conventional concrete systems with respect to chloride transport. The foregoing sections have concentrated on the absolute values of transport parameters of both these types of concretes while the remainder of the paper will evaluate the changes in model parameters (which represent the microstructure) as a result of the transport tests.

The resistance associated with the ionic motion in the percolating pores (R_t) is one of the most important modeled electrical circuit parameters because transport is dominated by the connected pores in the material structure. It has been shown that tracking the changes in R_t can provide reliable indicators of the changes in material microstructure induced by the NSSM test [30]. Figures 9(*a*) and 9(*b*) depict the relationships between the bulk resistances (R_b) and R_t before the RCP and NSSM tests for alkali activated concretes and conventional concretes respectively. The R_b-R_t relationships are very similar for the alkali activated and conventional concretes, suggesting that the resistance (or conductivity) contributed by the connecting pores to the total resistance (or conductivity) of the system is similar in both the cases. The resistance of the connected pores is lower than the bulk resistances by about 10 % for both the alkali activated and conventional concretes.

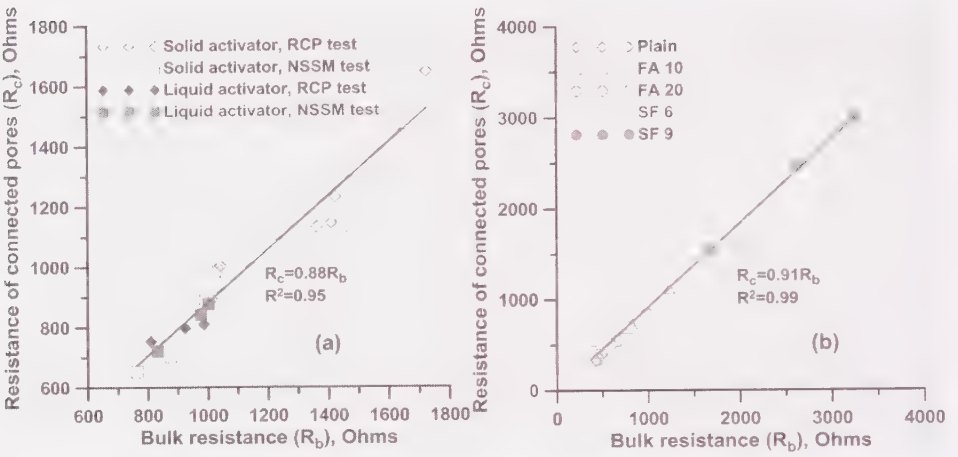

FIG. 9—*Relationship between bulk resistance and the resistance of connected pores for: (a) alkali activated concretes, and (b) conventional concretes.*

Equivalent Electrical Circuit Model Parameters Before and After NSSM Test—The equivalent circuit model parameters can also provide indications of the microstructural changes occurring in these specimens as a result of accelerated chloride transport tests. In an earlier section, the relationship between the bulk resistances of the specimens before and after the tests was shown. Here, the entire specimen response is broken down into equivalent electrical circuit elements and their responses before and after the transport tests are studied to gather information on the changes in material structure.

Figure 10(*a*) depicts the relationship between the resistances of the connected pores before and after the RCP test for the alkali activated concretes. The R_c values are generally lower after the RCP test for these concretes, which is in line with the observations on R_b shown in Fig. 7(*a*). The same reasons hold good in this case also. For the liquid activated mixtures, the relationship is not along expected lines, but this can very well be a result of the inadequate number of specimens evaluated. The relationship between the R_c values before and after the NSSM test for both alkali activated and conventional concretes are presented in Fig. 10(*b*). The trend is identical to that shown in Fig. 7(*b*) for the R_b values. It can be noticed that the alkali activated and conventional concretes conform to very similar trends with respect to the resistance of the connected pores before and after the NSSM test. This is an indication of the similarity in their material microstructures and in their response to electromigration. The increase in resistance of the connected pores can be attributed to either or both of: (i) formation of new products during the duration of the NSSM test, and (ii) reduction in the pore solution conductivity because of the replacement of highly conductive OH^- ions by the less conductive Cl^- ions.

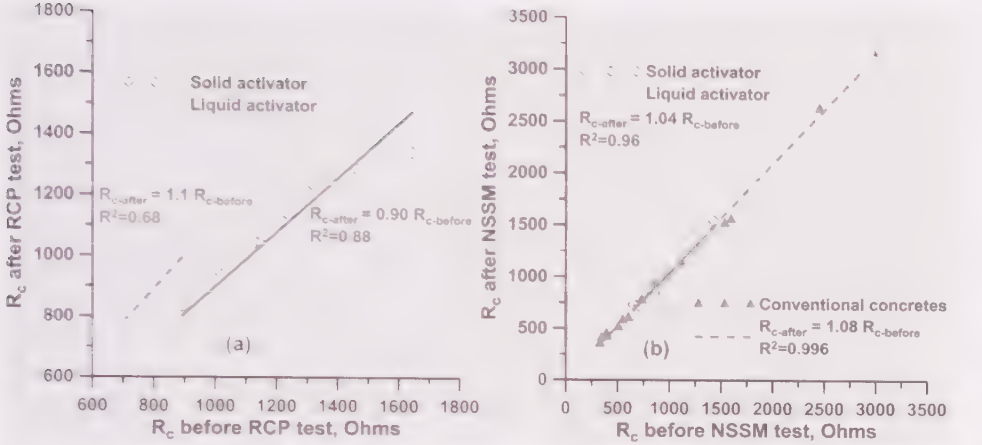

FIG. 10—*Relationship between resistances of the connected pores before and after: (a) RCP test, and (b) NSSM test.*

However, in the non-steady state test time interval, it is less likely that the OH^- ions are removed from the specimen [34,35]. Hence the increase in bulk resistances after the NSSM test could be more likely a result of the formation of new solid products either within the pores or as electrochemical double layers along the pore walls [32]. For conventional concretes, studies have shown that, under high external chloride ion concentrations (>1 M), the amount of bound chlorides was similar in non-steady state migration and natural diffusion experiments [36]. However, for alkali activated mixtures, one also needs to be cognizant of the fact that higher Na^+ and OH^- ion concentrations in the pore solution (from the alkaline activator) have been reported to reduce the formation of chloride binding products in the C-S-H gel [37]. This is an avenue that needs further microstructural investigation.

Figures 11(*a*) and 11(*b*) show the resistances of the unconnected pores before and after the RCP and NSSM tests respectively. In both the cases, R_{uc} values are seen to reduce after the test. For the RCP test, as can be observed from Figs. 10(*a*) and 11(*a*), both R_c and R_{uc} values decrease after the test, effectively reducing the bulk resistance (since R_b can be thought of as a complex combination of R_c and R_{uc}) as was observed from Fig. 7(*a*). For the NSSM test, even though the R_{uc} values reduce after the test, the R_c values are higher after the test, essentially resulting in slightly increased R_b values after the NSSM test as shown in Fig. 7(*b*). That is, an increase in R_c is accompanied by a decrease in R_{uc} in this case. When R_c increases, i.e., when the number and connectivity of the connected pores decreases, it is essential that the number and connectivity of the unconnected pores increases since some of the connected pores get converted into unconnected pores through the formation of solid products during the course of the NSSM test.

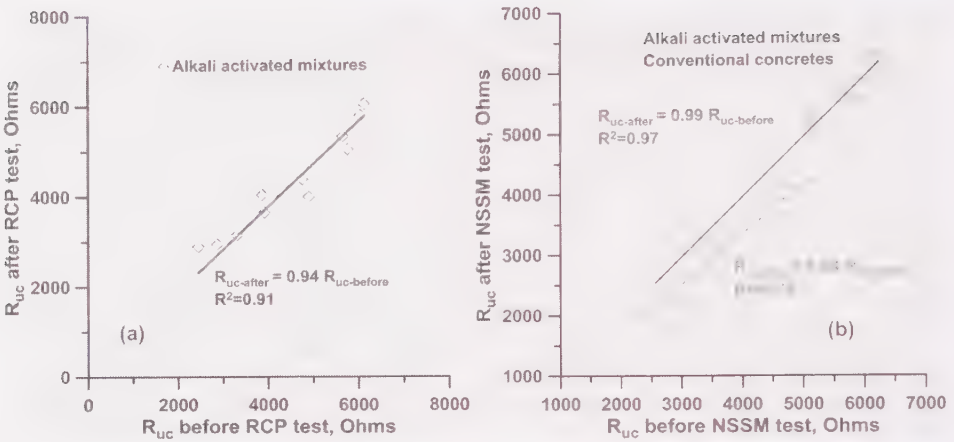

FIG. 11—*Relationship between resistances of the unconnected pores before and after: (a) RCP test, and (b) NSSM test.*

Another potent measure of the changes in material microstructure is the modeled capacitances in the equivalent electrical circuit. An increase in the capacitance associated with the solid fraction (C_1) reveals an increase in the amount of solid reaction products whereas an increase in the double layer capacitance (C_2) denotes the formation of reaction products along the pore walls. Figure 12(*a*) shows the values of the capacitances C_1 and C_2 before and after the NSSM tests for the alkali activated concretes, whereas Fig. 12(*b*) demonstrates the same for conventional concretes. The behavior is quite similar for both the concretes, with a 7 %–15 % increase in the capacitance of the solid

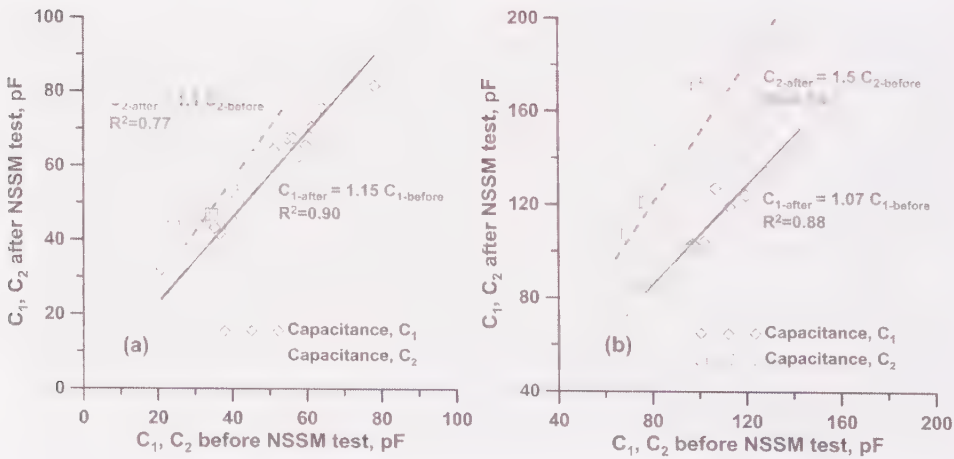

FIG. 12—*Relationship between the modeled capacitances before and after the NSSM test: (a) alkali activated concretes, and (b) conventional concretes.*

phase (C_1) after the NSSM test and a much drastic increase of 40 %–50 % in the pore wall-pore solution interfacial capacitance (C_2). The increases in both the R_1 and C_1 values, which correspond to the bulk of the specimen, indicate the formation of new products as a result of non-steady state electromigration. This potentially results in a reduced porosity, thereby increasing the bulk resistance slightly after the NSSM test as shown in Fig. 7(*b*). However, the much larger increase in C_2 values after the test indicates microstructural changes predominantly at the pore walls, resulting in an increase in the surface area of the pores [33,38] and thereby influencing the transport lengths. Thus, pore connectivity (or tortuosity) is the parameter that changes significantly as a result of the NSSM test. The changes in resistances R_b and R_c, and the capacitances C_1 and C_2 as a result of electromigration of chloride ions, which are similar in trends and magnitudes for both the alkali activated and conventional concretes, demonstrate the adequacy of the NSSM test to alkali silicate powder and liquid activated concretes.

Conclusions

This study has provided results of accelerated chloride transport tests on alkali silicate powder and liquid activated slag concretes, and compared them to those of plain and modified OPC concretes. In addition, electrical impedance spectra and associated models are used to discern the influence of accelerated chloride transport on the material microstructure. The salient conclusions of this study are provided here.

(i) Sodium silicate powder and liquid activated slag concretes (of varying n and M_s values) demonstrated RCP values and NSSM coefficients that are comparable to or lower than those of conventional concretes. The powder sodium silicate activated slag concretes had RCP values similar to those of 28-day cured silica fume modified concretes and the waterglass activated slag concretes showed RCP values similar to those of 56-day cured conventional concretes or 20 % fly ash modified concretes.

(ii) The NSSM coefficients of the solid sodium silicate activated slag concretes were comparable to those of conventional concretes cured for 56 days when the n value is 0.05, and to those of silica fume modified concretes when the n value was increased to 0.15. The powder sodium silicate activated concretes showed significantly lower RCP values than the waterglass activated concretes, but such a distinct change was not observed in the case of NSSM coefficients. This demonstrates the dependence of RCP values on pore solution conductivity. The pore structural features (total pore volume and pore sizes) resulting in reduced transport coefficients

for the powder sodium silicate activated concretes, even when they show lower strengths than waterglass activated mixtures, have been quantified.

(iii) The bulk resistances of the alkali activated slag concrete specimens were adequately related to the RCP values, similar to those for conventional concretes. The scatter in the R_b-NSSM coefficient relationship was much larger. The relationship between the R_b values before and after the NSSM test was identical for the alkali activated and conventional concretes, pointing to the adequacy of NSSM test for alkali activated concretes also.

(iv) Equivalent circuit models for electrical impedance spectra before and after the chloride transport tests revealed similarities in responses between alkali activated and conventional concretes. The resistance of the connected and unconnected pores, and the capacitances of the solid phase and the pore wall-pore solution interface before and after the NSSM test suggested that pore structural changes occur during the test. It was observed based on the interfacial capacitance that the tortuosity of the pore system increases much more than a reduction in porosity; as a result of the NSSM test. The magnitude of changes in the equivalent circuit parameters and their trends were similar for the alkali activated and conventional concretes, establishing the adequacy of accelerated chloride transport tests such as the NSSM test for alkali activated concretes.

References

[1] Duxson, P., Provis, J. L., Lukey, G. C., and van Deventer, J. S. J., "The Role of Inorganic Polymer Technology in the Development of Green Concrete," *Cem. Concr. Res.*, Vol. 37, 2007, pp. 1590–1597.

[2] Roy, D. M., "Alkali-Activated Cements Opportunities and Challenges," *Cem. Concr. Res.*, Vol. 29, 1999, pp. 249–254.

[3] Palomo, A., Grutzeck, M., and Blanco, M., "Alkali-Activated Fly Ashes: A Cement for the Future," *Cem. Concr. Res.*, Vol. 29, 1999, pp. 1323–1329.

[4] Criado, M., Fernández-Jiménez, A., de la Torre, A., Aranda, M. A. G., and Paloma, A., "An XRD Study of the Effect of SiO_2/Na_2O Ratio on the Alkali Activation of Fly Ash," *Cem. Concr. Res.*, Vol. 37, 2007, pp. 671–679.

[5] Fernández-Jiménez, A., Palomo, J. G., and Puertas, F., "Alkali-Activated Slag Mortars: Mechanical Strength Behaviour," *Cem. Concr. Res.*, Vol. 29, 1999, pp. 1313–1321.

[6] Soti, M., van Deventer, J. S. J., Mendis, P. A., and Lukey, G. C., "Engineering Properties of Inorganic Polymer Concretes (IPCs)," *Cem. Concr. Res.*, Vol. 37, 2007, pp. 251–257.

[7] Bernal, S. A., Mejía de Gutiérrez, R., and Provis, J. L., "Engineering and Durability Properties of Concretes Based on Alkali-Activated Granulated Blast Furnace Slag/Metakaolin Blends," *Constr. Build. Mater.*, Vol. 33, 2012, pp. 99–108.

[8] Pacheco-Torgal, F., Abdollahnejad, Z., Camões, A. F., Jamshidi, M., and Ding, Y., "Durability of Alkali-Activated Binders: A Clear Advantage over Portland Cement or an Unproven Issue?," *Constr. Build. Mater.*, Vol. 30, 2012, pp. 400–405.

[9] Ravikumar, D., Peethamparan, S., and Neithalath, N., "Structure and Strength of NaOH Activated Concretes Containing Fly Ash or GGBFS as the Sole Binder," *Cem. Concr. Compos.*, Vol. 32, 2010, pp. 399–410.

[10] Bakharev, T., Sanjayan, J. G., and Cheng, Y. B., "Alkali Activation of Australian Slag Cements," *Cem. Concr. Res.*, Vol. 29, 1999, pp. 113–120.

[11] Shi, C. and Yinyu, L., "Investigation on Some Factors Affecting the Characteristics of Alkali-Phosphorus Slag Cement," *Cem. Concr. Res.*, Vol. 19, 1989, pp. 527–533.

[12] Shi, C., Krivenko, P. V., and Roy, D., *Alkali-Activated Cement and Concretes*, Taylor and Francis, NY, 2006, p. 451.

[13] Ravikumar, D. and Neithalath, N., "Reaction Kinetics in Sodium Silicate Powder and Liquid Activated Slag Binders Evaluated Using Isothermal Calorimetry," accepted for publication in *Thermochem. Acta.*, Vol. 546, 2012, pp. 32–43.

[14] Bernal, S. A., de Gutiérrez, R. M., Pedraza, A. L., Provis, J. L., Rodriguez, E. D., and Delvasto, S., "Effect of Binder Content on the Performance of Alkali-Activated Slag Concretes," *Cem. Concr. Res.*, Vol. 41, 2011, pp. 1–8.

[15] Sakulich, A. R., Anderson, E., Schauer, C., and Barsoum, M. W., "Mechanical and Microstructural Characterization of an Alkali-Activated Slag/Limestone Fine Aggregate Concrete," *Constr. Build. Mater.*, Vol. 23, 2009, pp. 2951–2957.

[16] Altan, E. and Erdoğan, S. T., "Alkali Activation of a Slag at Ambient and Elevated Temperatures," *Cem. Concr. Compos.*, Vol. 34, 2012, pp. 131–139.

[17] Ravikumar, D. and Neithalath, N., "Effects of Activator Characteristics on the Reaction Product Formation in Slag Binders Activated Using Alkali Silicate Powder and NaOH," *Cem. Concr. Compos.*, Vol. 34, 2012, pp. 809–818.

[18] ASTM C989-12a: "Standard Specification for Slag Cement for Use in Concrete and Mortars," *Annual Book of ASTM Standards*, ASTM International, West Conshohocken, PA.

[19] Ravikumar, D., 2012, "Property Development, Microstructure, and Performance of Alkali Activated Fly Ash and Slag Systems," Ph.D. thesis, Clarkson University, p. 217.

[20] ASTM C150-12: "Standard Specification for Portland Cement," *Annual Book of ASTM Standards*, ASTM International, West Conshohocken, PA.

[21] ASTM C618-12: "Standard Specification for Coal Fly Ash and Raw or Calcined Natural Pozzolan for Use in Concrete," *Annual Book of ASTM Standards*, ASTM International, West Conshohocken, PA.

[22] ASTM C1240: "Standard Specification for Silica Fume Used in Cementitious Mixtures," *Annual Book of ASTM Standards*, ASTM International, West Conshohocken, PA.

[23] NT BUILD 492: "Concrete, Mortar and Cement-based Repair Materials: Chloride Migration Coefficient from Non-steady-state Migration Experiments," 1999, Nordtest Method 492.

[24] Neithalath, N. and Jain, J., "Relating Rapid Chloride Transport Parameters of Concretes to Microstructural Features Extracted from Electrical Impedance," *Cem. Concr. Res.*, Vol. 40, 2010, pp. 1041–1051.

[25] Schwarz, N. and Neithalath, N., "Chloride Transport in Glass Powder and Fly Ash Modified Concretes—Influence of Test Methods on Microstructure," *Cem. Concr. Comp.*, Vol. 32, 2010, pp. 148–156.

[26] Feldman, R. F., Chan, G. W., Brousseau, R. J. and Tumidajski, P. J., "Investigation of the Rapid Chloride Permeability Test," *ACI Mat J.*, Vol. 91, 1994, pp. 246–255.

[27] J-Betancourt, G. A. and Hooton, R. D., "Study of the Joule Effect on Rapid Chloride Permeability Values and Evaluation of Related Electrical Properties of Concretes," *Cem. Concr. Res.*, Vol. 43, 2004, pp. 1007–1015.

[28] Neithalath, N., Persun, J., and Hossain, A., "Hydration in High-performance Cementitious Systems Containing Vitreous Calcium Aluminosilicate or Silica Fume," *Cem. Concr. Res.*, Vol. 39, 2009, pp. 473–481.

[29] Neithalath, N. and Ravikumar, D., "Electrically Induced Chloride Ion Transport in Alkali Activated Slag Concretes and the Influence of Microstructure," *Cem. Concr. Res.*, 2012 (in press).

[30] Jain, J. and Neithalath, N., "Electrical Impedance Analysis Based Quantification of Microstructural Changes in Concretes Due to Non-steady State Chloride Migration," *Mater. Chem. Phys.*, Vol. 129, 2011, pp. 569–579.

[31] Neithalath, N., Persun, J., and Manchiryal, R. K., "Electrical Conductivity Based Microstructure and Strength Prediction of Plain and Modified Concretes," *Int. J. Adv. Eng. Sci. Appl. Math.*, 2011.

[32] Siegwart, M., Lyness, J. F., and McFarland, B. J. "Change of Pore Size in Concrete Due to Electrochemical Chloride Extraction and Possible Implications for the Migration of Ions," *Cem. Concr. Res.*, Vol. 33, 2003, pp. 1211–1221.

[33] Sánchez, I., Nóvoa, X. R., de Vera, G., and Climent, M. A., "Microstructural Modifications in Portland Cement Concrete Due to Forced Ionic Migration Tests: Study by Impedance Spectroscopy," *Cem. Concr. Res.*, Vol. 38, 2008, pp. 1015–1025.

[34] Zhang, T. and Gjorv, O. E., "An Electrochemical Method for Accelerated Testing of Chloride Diffusivity in Concrete," *Cem. Concr. Res.*, Vol. 24, 1994, pp. 1534–1548.

[35] Yang, C. C., Cho, S. W., Chi, J. M., and Huang, R., "An Electrochemical Method for Accelerated Chloride Migration Test in Cement-based Materials," *Mat. Chem. Phys.*, Vol. 77, 2002, pp. 461–469.

[36] Castellote, M., Andrade, C., and Alonso, C., "Chloride-binding isotherms in Concrete Submitted to Non-steady-state Migration Experiments," *Cem. Concr. Res.*, Vol. 29, 1999, pp. 1799–1806.

[37] Nielsen, E. P., Herfort, D., and Geiker, M. R., "Binding of Chloride and Alkalis in Portland Cement Systems," *Cem. Concr. Res.*, Vol. 35, 2005, pp. 117–123.

[38] Diaz, B., Nóvoa, X. R., and Perez, M. C., "Study of the Chloride Diffusion in Mortar: A New Method of Determining Diffusion Coefficients Based on Impedance Measurements," *Cem. Concr. Comp.*, Vol. 28, 2006, pp. 237–245.

Geopolymer Binder Systems
STP 1566, 2013
Available online at www.astm.org
DOI:10.1520/STP156620120060

James K. Hicks[1]

Activated Class C Fly Ash Cement

REFERENCE: Hicks, James K., "Activated Class C Fly Ash Cement," *Geopolymer Binder Systems*, STP 1566, Leslie Struble and James Hicks, Eds., pp. 108–118, doi:10.1520/STP156620120060, ASTM International, West Conshohocken, PA 2013.[2]

ABSTRACT: Alkali-activated aluminosilicates, is a relatively new material system that is currently the subject of considerable research and is beginning to see use as a binder in concrete. Of particular interest are newer versions of activated fly ash that are rapidly activated without any need for thermal conditioning or set enhancing additions beyond the basic activator. Set times can be regulated, the materials provide rapid strength development, and resistance to freezing and thawing is excellent due to their low porosity.

KEYWORDS: fly ash, activated, cement, performance

Sustainable Management of Waste Materials

The use of one unit of fly ash reduces approximately one unit of CO_2 emitted by a cement kiln. Fly ash and other CCP's in the cement-making process [1] could also avoid the use of the cement kiln and avoid the high energy requirement associated with the cement kiln and mill operations while significantly reducing the volume of useable material taken to waste management sites [2]. The amount of fly ash beneficially used in the United States is illustrated in Fig. 1.

Recent concerns about the environmental impact of portland cement production have created a renewed interest in these less energy- and less CO_2-intensive binder systems. With energy, resource and infrastructure demands growing in the foreseeable future [3–5], a sustainable concrete that is more durable and costs less to maintain is becoming increasingly desirable [6,7].

Manuscript received June 8, 2012; accepted for publication December 28, 2012; published online May 8, 2013.

[1]Executive Vice President of Engineering and Technology, CeraTech, Inc., Montgomery, TX 77316, United States of America.

[2]ASTM Symposium on *Geopolymer Binder Systems* on June 26–27, 2012 in San Diego, CA.

FIG. 1—*Fly ash utilization in the United States 1966–2009 [8].*

Alkali activated fly ash is a potential substitute for portland cement. Fly ash is mainly composed of glassy alumina (Al_2O_3) and silicate (SiO_2) phases which can be activated (i.e., dissolved) by a concentrated aqueous alkali hydroxide (e.g., NaOH, KOH, alkali silicate, e.g., Na_2SiO_3), or a combination of these solutions. As the concentration of alumina and silicate species approach saturation in the pore fluid, an amorphous to semi-crystalline inorganic polymer is formed which is called by a common name geopolymer [9]. This inorganic geopolymer is mainly composed of an alkali (e.g., Na-alumino-silicate-hydrate gel—in short, NASH) which creates the binding phase; in contrast with calcium-silicate-hydrate (CSH) gel which is the main constituent and binding phase of portland cement concretes [10]. In addition to fly ash (both class F and C); geopolymers can be produced using metakaolin.

The spherical shape of fly ash particles is beneficial for reducing water demand and for maximizing particle packing to reduce porosity. On the other hand, alkali activated Class-F fly ash either requires a highly concentrated alkali solution (highly caustic) for activation or high temperature curing to gain sufficient strength. Also, variability in the composition of fly ash can result in significant variance in the performance of concrete produced unless the ash composition is continuously monitored and changes in mixture proportions are made accordingly. These cements have been engineered for use in fast track concrete repairs and construction, conventional paving, walls and concrete block masonry, new construction and repair projects.

Developments in fly ash based cements offers the user a unique set of mechanical and dimensional properties. In addition, they are now competitive in

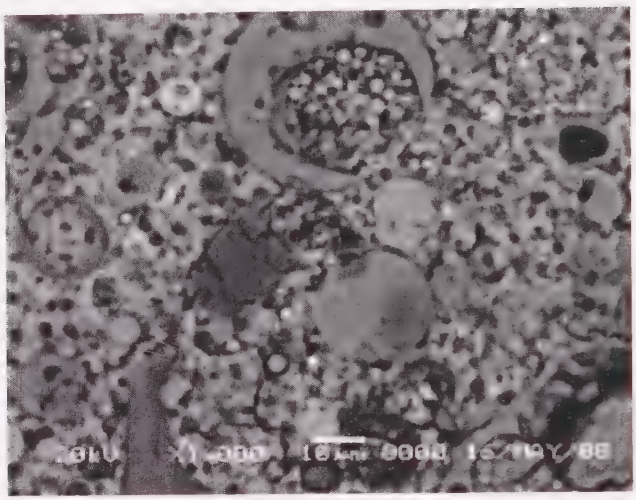

FIG. 2—*Micrograph of CSH formation in activated fly ash cement, sample age is 14 months from addition of water [18].*

cost to current cementitious product offerings. The cements thusly produced develop calcium silicate hydrates (CSH) as shown in Fig. 2 [11].

Below is a recent historical summary of earlier versions of pozzolan based cements:

- Alkali activation of solid, non-portland cement precursors (usually high-calcium slags) was first demonstrated in reasonably modern times by Purdon in 1940, and was developed on a larger scale primarily in Eastern Europe in the succeeding decades [12].

Some geopolymeric cementitious products are in used still today in various parts of the world. Such geopolymers are described and claimed; for example, in U.S. Patents [13]. These geopolymers are primarily composed of silicas and aluminas, mixed and reacted in particular ways to provide the desired structure. While, in general, these geopolymers are perfectly adequate for the purposes intended, as such, they do not always provide the types of strengths sought in a concrete composition. Furthermore, geopolymers typically require post reaction thermal processing for up to 24 h in order to achieve desirable strengths.

Below is a recent historical summary of earlier versions of pozzolan based cements.

- 1970s: Geo-polymers from fly ash, cements high in Al-Si. J. Davidovits makes references to their use in historical construction techniques.
- 1980s: Activated fly ashes blended with cement, e.g., mostly two step mixes unconditionally require addition of the activator at the jobsite.
- 1990s through mid-decade beginning in 2000: development of one step mixes, activator in product package or cement. The cementitious compositions typically consisted of harsh acids and bases such as citric acids

(pH ~ 2.2) and alkali metal activators including alkali hydroxides (pH ~ 12–14) and metal carbonates (pH ~ 11.6). These included patents by Gravitt, Kirkpatrick, Styron, and others. There were some drawbacks to these materials. The prior art required acid-base reactions. These reactions sometimes were difficult to control.

The art has needed and continued to seek a hydraulic cement composition, which provides for utilization in standard situations, while providing both a high early strength and an ultimate, very high strength. In particular, compositions having a minimum strength of 28 MPa (4000 psi) at 4 h, the release strength necessary for prestress work, have been sought [14].

The New Generation of Cement Technology

This new generation of fly ash based cements [15] offers the user a unique set of mechanical and dimensional properties competitive in cost to current cementitious product offerings, providing the user with a value added alternative solution for today's most challenging construction cementitious repair, product and paving applications. The technology is built around a highly flexible chemistry that allows for the inclusion of a wide array of waste materials as part of its binder matrix, establishing it as a truly green sustainable construction material with unique performance and application advantages.

This new green cement technology is of those based upon an all fly ash cement design that requires no portland cement in its matrix [16]. Through a detailed study of various types of chemistry and reactive fly ash-based cement pastes, key aspects of the mineralogy have been identified for determining the usefulness of various fly ash sources as high performance cements, including non acid-alkali activated cements.

Key to green cement development was creating a material matrix that had a very dense crystal structure eliminating the movement of water and other chemicals through the material matrix; water being the catalyst for many of the reactions that occur in the concrete matrix.

This is accomplished through the simultaneous dissolution and retardation of the calcium oxide phase to solubilize both the silicate and aluminate amorphous phases. The minerals recombine to the desired structure providing desired mechanical and dimensional properties. Thusly, pozzolanic materials are modified with chemicals to produce the desired structure. They are characterized by a very dense crystal structure exhibiting the optimum chemical ratio of calcium to silicates to aluminates. The micro pore structure is very small, greatly limiting the movement of liquids within the material matrix. This is evidenced by the low W/Cm (about 0.2–0.22), very high resistance to freezing and thawing and other improved durability factors indicating dense "packing factor."

The crystal structure of portland cement is dominated by tricalcium silicate (C_3S) and dicalcium silicate (C_2S) components producing a crystal structure

that is not as dense leading to relatively a large voids structure within the material matrix [17]. The chemical and mineralogical improvements, coupled with the much higher fineness of pozzolan based cements ground leads to much lower porosity in the concrete. The lower porosity provides for very low water to cementitious ratios and improved durability factors.

Having developed a technique to "fingerprint" raw materials as well as a "road map" of good fly ash sources, the new approach is able to maintain quality assurance on product lines using a broad array of fly ash sources, and blends of sources.

The improved activated hydraulic cement technology is the principal backbone chemistry for a range of product offerings from small area repair packaged goods to new construction concretes. Products from the non acid-alkali activated cements were developed specifically to satisfy user or application performance requirements. Each product is water mixed, single component activated, turnkey concrete, mortar or grout with flexible working times from 15 min to 3 h. The products were engineered to allow for mixing, hauling, placing and finishing using standard industry equipment and practices. The products were designed for applications where speed, strength and durability were desirable performance characteristics. Compressive strengths of more than 17 MPa (2500 psi) in as little as 60 min supported by bond strengths of over 21 MPa (3000 psi) and flexural strengths over 10 MPa (1500 psi) in 7 days frame the technology's mechanical properties. Dimensional stability is highlighted by shrinkage of less than 0.04 % length change in 28 days.

Principle benefits of this new class of products include:

- non-shrink;
- exceptional sustained bond strengths (slant shear and direct tension);
- low coefficient of thermal expansion;
- modulus of elasticity consistent with portland cement concrete;
- low permeability;
- high resistance to freezing and thawing;
- high resistance to scaling. High resistance to sulfate and chemical attack;
- exceptional durability;
- placement temperature tolerant;
- no epoxy resins are contained.

Specific areas of products developed meeting objective criteria fall into several areas:

- rapid repair;
- ready mix including paving;
- volumetric mixer concrete and mortar;
- concrete block/grout/mortar;
- precast;
- high temperature resistant materials such as that being placed in Fig. 3;
- chemically resistant materials.

FIG. 3—*Construction of the base for a heat-treating facility in Houston, TX. Cycling of temperatures caused severe breakdown of conventional concrete [18].*

Some of the more specific examples are:

- Rapid repair products all have cementitious components greater than 90 % coal ash, and contain no portland cement. Based upon the size of the repair, products range in working time from 15 to 45 min, offering return to service ranging from 1 to 4 h (see Fig. 4 and Table 1). As shown in Fig. 4, all products can be mixed with conventional mixing equipment and placed like portland cement products, however without the requirement of bond coats.

FIG. 4—*Marine Corps engineers training for fast track construction and repair prior to deployment [18].*

- Ready-mix truck delivery. For large placements such as roadway slabs, ash-based pozzolanic cements have been adapted to ready-mix batch plant/transit truck mixing and placement. These products are able to be site activated (up to 4 h transit time), and adjusted to placement times from 1 to 3 h. Return to service can be achieved in as little as 6 to 12 h (see Table 1). Slump control can be adjusted to range from roller-compacted concrete (RCC) to a self-consolidating concrete (SCC).

TABLE 1—*Characteristics of an activated pozzolan cement fast return to service ready mixed concrete [18].*

Property	Rapid Set[a]	Standard Set[b]	Test Method
Compressive Strengths, psi (MPa)[4 in. × 8 in. cylinders]			
6 h	3500 (24.1)	NA	ASTM C 39
24 h	3604 (24.9)	2497 (17.2)	ASTM C 39
3 day - 72 h	4502 (31.0)	4193 (29.0)	ASTM C 39
7 days	6487 (44.7)	5998 (41.3)	ASTM C 39
28 days	8511 (58.7)	8502 (58.6)	ASTM C 39
Flexural Strength, psi (MPa)			
7 days	510 (3.5)	485 (3.3)	ASTM C 78
28 days	650 (4.5)	630 (4.3)	ASTM C 78
Splitting Tensile Strength, psi (MPa)			
28 days	720 (5.0)		ASTM C 496
Rapid Freeze Thaw Resistance (Durability Factor - Retained percentage of Dynamic Modulus)			
300 cycles	100 %		ASTM C 666A
Scaling Resistance, lb/ft^2 (kg/m^2)			
50 cycles	0		ASTM C 672
Abrasion Resistance, Depth of wear, millimeters at 28 day	0.14		ASTM C 944 (2005)
Modulus of Elasticity, msi (GPa)			
28 days	5.00 (34.0)		ASTM C 469
Coefficient of Thermal Expansion, in/in/°F			
28 days	4.6		AASHTO TP 60
Length Change, % of total length			
14 days	0.04		ASTM C 157
Creep (365 days) (μ Strain/psi)	1.91		ASTM C 512
Creep Coefficient			

[a]Strength development and working times can be adjusted by varying the cement ratio and by use of various proprietary activator admixtures.

[b]Durability factor results, e.g. freeze-thaw, etc. are similar for both rapid and standard set.

Note: Rapid set test results based on 846 lb of cement per cubic yard mix design and fast set activator. Standard set test results based on 564 lb of cement per cubic yard mix design and fast set activator.

- Volumetric mobile mixer use. The volumetric pozzolanic product utilizes the same backbone chemistry as the rapid repair products. For larger placements that also require fast return to service, the pozzolans have been adapted to work in a volumetric mixer, allowing from 20 to 50 min of placement time, with return to service in as little as 1 h depending upon the user requirements. With DOT and DOD applications, the principal benefit of volumetric placement is the ability to place larger volumes while still taking advantage of the quick return to service. One version of this product can be used as a flowable grout capable of providing up to 3 h of working time, yet providing up to 35 MPa (5000 psi) in compressive strength in 24 h.

This new generation of all ash-based pozzolanic cements also furthers the ability to utilize green building technology for the widest range of end-use markets, including most DOT, DOD, and building construction market applications while meeting International Building Code and ASTM Standards [19].

It is important to note that although the environmental and even economic benefits from using CCP's are apparent, they are still under-utilized. The American Coal Ash Association reported that less than 40 % of CCP [3] is used. The Association only reports affiliated utilities. Larger amounts are currently used and end up in landfills, creating a burden to the environment and the economy of different enterprises [20].

Alkali Activated Slag Cements

An alkali activated slag (AAS) concrete is one in which the binder phase is made of ground granulated blast furnace slag (GGBFS), water, and an alkali activator which triggers the chemical reactions involving dissolution of slag and polymerization of calcium-silicate and aluminum-silicate phases which serve as the binder. These systems contain no portland cement. Although slag is cementitious and can self-activate, the reaction is typically slow and requires external activators to enhance reaction rates and form stronger products. Sufficient alkali content is also necessary for the development of significant strength. Since slag is deficient in alkalis, these have to be supplied externally. These alkali-activated slag systems also appear in the literature with a variety of names such as alkali-activated cements [21] and alkali-slag cements [22].

The most commonly used alkaline activating agents are sodium hydroxide (NaOH) and sodium silicate (Na_2SiO_3), also known as water glass, or combinations of these [23,24]. A variety of industrial by-products containing alkalis and sulfates such as cement kiln dusts are also equally effective in activating slag [25]. Among the activators used, water glass is widely reported to give rise to rapid hardening and high compressive strengths [26]. The main hydration product in AAS systems is calcium silicate hydrate (C-S-H) with a low

Ca/Si ratio regardless of the type of activator used [27]. The morphology of the hydration products changes with the activator and other hydration conditions. Hydrotalcite [magnesium-calcium aluminate hydrate: $(M,C)_4AH_{13}$] and minor amounts of strätlingite (C_2ASH_8) are also found in AAS.

Alkali-activated slag displays very good strength [28], durability [29] and a variety of other potentially valuable characteristics such as fire and waste-water resistance. However, shorter setting time, increased shrinkage, and difficulties with safe handling of the liquid water glass outside the laboratory have limited its use [30]. Sodium silicate with higher modulus (i.e., silica-to-alkali ratio) can often alleviate some of these problems.

Supersulfated slag cement is an example of a cement that has used ettringite in combination with CSH as the main binding phase to a relative degree of success. Supersulfated slag cements consist mostly of granulated blast-furnace slag, gypsum or anhydrite with a small amount of lime or portland cement to catalyse the chemical reaction. Although, they exhibit slow strength development and may undergo deleterious carbonation reactions, they still have significant application potential.

More research is needed to modify the early age properties of the alkali activated slag concrete. The low CO_2 emission rate and the low embodied energy of AAS, as slag being a commercial by-product, compared to traditional portland cement are primarily attributed to the absence of high temperature clinkering processes involving a large amount of fossil fuel-derived energy. While the use of alkaline hydroxide or silicate activating solutions rather than water does reintroduce some greenhouse costs, the overall beneficial effects due to widespread use of alkali activated slag is expected to be highly significant.

References

[1] U.S. Environmental Protection Agency, "Inventory of U.S. Greenhouse Gas Emissions and Sinks: 1990–2006," Report No. 430-R-0805, www.epa.gov/climatechange/emissions/usgginventory.html, 2008.

[2] Floris, V. and Hicks, J. K., "Environmental Benefits of Coal Combustion Products," *Pittsburgh Coal Conference*, Univ. of Pittsburg, PA, 2009.

[3] USGS, "Green Chemistry for Sustainable Cement Production and Use," *Green Chem.*, Vol. 8, 2003, pp. 763–780.

[4] *Minerals Yearbook, Vol. 1*, Metals and Minerals Report, U.S. Geological Survey, U.S. Department of the Interior Bureau of Mines, Reston, VA, February 2012, pp. 1–2.

[5] Phair, J. W., "Green Chemistry for Sustainable Cement Production and Use," *Green Chemistry*, Vol. 8, 2006, pp. 763–780.

[6] Touzo, B. and Espinosa, B., Glasser Symposium, http://www.abdn.ac.uk/chemistry/cement-symposium/abstracts, 2009.

[7] Floris, V., "Challenges and Achievements of Coal-Based Power Generation: Moving Towards a Holistic and Sustainable Approach," *Proceedings of the International Association of Energy Economics*, Santiago, Chile, 2009.

[8] American Coal Ash Association (ACAA), *2009 Fly Ash Survey*, 2010.

[9] Davidovits, J., "Geopolymers: Inorganic Polymeric New Materials," *J. Therm. Anal.*, Vol. 37(8), 1991, pp. 1633–1656.

[10] Fernández-Jiménez, A. and Palomo, A., "Nanostructure/Microstructure of Fly Ash Geopolymers," *Geopolymers: Structure, Processing, Properties, and Industrial Applications*, 2009.

[11] Hicks, J. K., Riley, M., Schumacher, G., Patel, R., and Sampson, P., "Utilization of Recycled Materials for High Quality Cements and Products," *World of Coal Ash Conference*, Lexington, KY, 2009.

[12] Jannie, S. J., van Deventer, S. J., Duxson, P., and Provis, J. L., "The Role of Research in the Commercial Development of Geopolymer Concrete," *International Cement Microscopy Association 2010 Conference*, March 2010.

[13] Davidovits, J., United States Patent Office (USPTO), U.S. Pat. Nos. 4,349,386 (1982) and 4,472,199 www.USPTO.gov (1984).

[14] Juenger, M. C. G., Winnefeld, F., Provis, J. L., and Ideker, J. H., "Advances in Alternative Cementitious Binders," *Cem. Concr. Res.*, Vol. 41, No. 12, 2011, pp. 1232–1243.

[15] Hicks, J., "Durable 'Green' Concrete from Activated Pozzolan Cement," *Proceedings of ASCE Green Streets and Highways Conference*, Denver, CO, 2010.

[16] Hicks, J. K. and Scott, R. M., United States Patent Office (USPTO), U.S Patent 7,288,148 B2, Rapid Hardening Hydraulic Cement from Subbituminous Fly Ash and Products thereof, Oct 23, 2007.

[17] Lea, F. M., *The Chemistry of Cement and Concrete*, Arnold, 1970.

[18] Hicks, J. K., *CCP Beneficial Use versus Production*, American Coal Ash Association, www.acaa-usa.org, 2009.

[19] U.S. Energy Information Administration. www.eia.doe.gov 2007 Schlesinger, Richard. Energybiz, Coal Ash Piles Up, April/March 2009.

[20] U.S. Energy Information Administration, *2010 CO2 Forecast Highlights*, www.eia.doe.gov/international, 2010.

[21] Palomo, A. and López dela Fuente, J. I., "Alkali-Activated Cementitious Materials: Alternative Matrices for the Immobilization of Hazardous Wastes. Part I. Stabilization of Boron," *Cem. Concr. Res.*, Vol. 33, 2003, pp. 285–295.

[22] Roy, D. M., "Alkali-Activated Cements: Opportunities and Challenges," *Cem. Concr. Res.*, Vol. 29, 1999, pp. 249–254.

[23] Shi, C. and Day, R. L., "Some Factors Affecting Early Hydration of Alkali-Slag Cements," *Cem. Concr. Res.*, Vol. 26, 1996, pp. 439–447.

[24] Krizan and D., Zivanovic, B., "Effect of Dosage And Modulus of Water Glass on Early Hydration of Alkali-Slag Cements," *Cem. Concr. Res.*, Vol. 32, 2002, pp. 1181–1188.

[25] Chaunsali, P. and Peethamparan, S., "Evolution of Strength, Microstructure and Mineralogical Composition of a CKD-GGBFS Binder," *Cem. Concr. Res.*, Vol. 41, No. 2, 2011, pp. 197–208.

[26] Oh, J. E., Monteiro, P. J. M., Jun, S. S., Choi, S., and Clark, S.M., "The Evolution of Strength and Crystalline Phases for Alkali Activated Ground Blast Furnace Slag and Fly Ash-Based Geopolymers," *Cem. Concr. Res.*, Vol. 40, 2010, pp.189–196.

[27] Song, S., Sohn, D., Jennings, H. M., and Mason T.O., "Hydration of Alkali-Activated Ground Granulated Blast Furnace Slag," *J. Mater. Sci.*, Vol. 35, 2000, pp. 249–257.

[28] Atis, C. D., Bilim, C., Celik, O., and Karahan, O., "Influence of Activator on the Strength and Drying Shrinkage of Alkali-Activated Slag Mortar," *Constr. Build. Mater.*, Vol. 23, 2000, pp.548–555.

[29] Fernández-Jiménez, A., and Puertas, F., "The Alkali–Silica Reaction in Alkali-Activated Granulated Slag Mortars with Reactive Aggregate," *Cem. Concr. Res.*, Vol. 32, 2000, pp. 1019–1024.

[30] Shi, C., Krivenko, P. V., and Roy, D., *Alkali-Activated Cements and Concretes*, Taylor and Francis, NY, 2006.

Geopolymer Binder Systems
STP 1566, 2013
Available online at www.astm.org
DOI:10.1520/STP156620120080

E. Ivan Diaz-Loya,[1] *Erez N. Allouche,*[2] *and Dexter Cahoy*[3]

Statistical-Based Approach for Predicting the Mechanical Properties of Geopolymer Concretes

REFERENCE: Diaz-Loya, E. Ivan, Allouche, Erez N., and Cahoy, Dexter, "Statistical-Based Approach for Predicting the Mechanical Properties of Geopolymer Concretes," *Geopolymer Binder Systems*, STP 1566, Leslie Struble and James K. Hicks, Eds., pp. 119–143, doi:10.1520/STP156620120080, ASTM International, West Conshohocken, PA 2013.[4]

ABSTRACT: The manuscript presented here is based on the investigation of the mechanical properties of fly-ash-based geopolymer concrete and their link to fly-ash (FA) characteristics. A database of 32 FA samples was created. Each FA sample was analyzed in terms of chemical composition, crystallographic properties, and particle size distribution. The mechanical performance of geopolymer concrete (GPC) made from each FA sample was evaluated in terms of density, setting time, compressive and flexural strengths, static elastic modulus, and Poisson's ratio. The database was randomly divided into two sets; one consisting of 24 FA samples for model building using linear regression, and another consisting of eight FA samples for validation. The results show that the density, elastic modulus, as well as the compressive and flexural strengths of GPC can be predicted with reasonable accuracy by analyzing the chemical, physical, and crystallographic properties of a given FA and following the steps presented in this study.

KEYWORDS: geopolymer, alkali-activated cement, mechanical characterization, fly ash

Manuscript received June 15, 2012; accepted for publication March 5, 2013; published online April 24, 2013.

[1]Ph.D., Research Engineer, CeraTech Inc., Baltimore, MD, United States of America; and Dept. of Civil Engineering, Louisiana Tech Univ., 3501, Brehms Lane Suite D, Baltimore, Maryland 21213, United States of America, e-mail: ivan.diazloya@ceratechinc.com

[2]Ph.D., Associate Professor, Dept. of Civil Engineering, Louisiana Tech Univ., 599 W. Arizona Ave, Ruston, Louisiana 71272, United States of America, e-mail: allouche@latech.edu

[3]Ph.D., Assistant Professor, Dept. of Mathematics and Statistics, Louisiana Tech Univ., 305 Wisteria St., P.O. Box 3178, Ruston, Louisiana 71272, United States of America, e-mail: dcahoy@latech.edu

[4]ASTM Symposium on *Geopolymer Binder Systems* on June 26–27, 2012 in San Diego, CA.

Introduction

According to the most recent survey released by the American Coal Ash Association [1] the United States produced approximately 135×10^6 tons (MT) of coal combustion products (CCPs) in 2009 making it the second largest by-product stream in the United States. The main types of CCPs are fly ash (FA), bottom ash, boiler slag, and flue gas desulfurization material (FGD). FA occupies over 45 % of the total CCP production with approximately 63 MT per year. FA is composed of fine spherical particles that rise with the flue gases during the combustion of coal, which then are captured by pollution-control devices. Although 25 of the 63 MT of FA were used beneficially in 2009, 38 MT were disposed in landfills and storage lagoons at a significant cost, posing a potential risk to the environment.

Whereas FA has been used in ordinary concrete as a supplementary cementitious material for many years to improve its rheology in the fresh mix and durability, permeability, and ultimate strength of the hardened product, it typically used as 10–30 % replacement for ordinary Portland cement (OPC) [2]. However, FA alone is capable of producing a strong cementitious binder when activated under highly alkaline conditions. This binder, often called geopolymer, does not require the presence of ordinary Portland cement (OPC) to harden or gain strength [3,4].

Geopolymers are typically synthesized from materials of geological origin (e.g., metakaolin) or byproducts such as FA that are rich in silica and alumina. Geopolymer binders result from a chemical reaction where silica and alumina molecules contained in FA react under highly alkaline conditions, typically provided by a sodium (or potassium) hydroxide solution and an alkaline silicate (e.g., sodium or potassium silicate). Many researchers agree that the outcome of this reaction is an amorphous three-dimensional (3D) network of silicon and aluminum atoms linked by oxygen atoms in a four-fold coordination similar to the one exhibited by zeolites [5–7]. The cation (Na^+ or K^+) provided by the activator solution serves to balance the negative charge generated by having Al^{3+} atoms in a four-fold coordination [8–10].

One of the main challenges for a widespread use of FA-based geopolymer concrete (GPC) is the significant variability of FA. Its chemical properties depend on the type, size, and composition of its precursor coal. Silica and alumina molecules contained in the FA are the main components of the geopolymer network; thus, the amount and ratio of these influence the resulting mechanical properties of geopolymer. However, even though silica and alumina are the main precursors for the geopolymeric reaction, other factors also play a significant role in the mechanical behavior of geopolymer. Impurities, such as CaO, have a positive impact in geopolymer but cause shorter setting times as they create nucleation sites [11–13]. Another important factor is the fly ash's crystallographic properties, because crystalline phases are

more thermodynamically stable than glassy phases, silicon and aluminum in the latter will leach into solution more readily during the first step of geopolymerization (dissolution of species) [12–14]. The physical properties are mainly a result of the degree of pulverization of the precursor coal, because a significant part of the reaction occurs at the particle-liquid interface; the finer the particles, the greater is the surface area and the more reactive is the FA [12–16]. A second physical factor is the burning efficiency, because a poor burning process yields unburned coal in the FA (quantified as Loss on Ignition, LOI). High content of unburned carbon with high surface area could adversely impact the behavior of the fresh mixture, thereby creating a demand for the addition of activator solution well beyond what is needed to activate the source material, to obtain a workable mixture [12–14].

Significance of Research

This study attempts to gain better understanding of FA as a raw material for GPC by analyzing several FA stockpiles with distinct characteristics and correlating those characteristics with the mechanical properties of GPC. Discerning the relationship between the physical, chemical, and crystallographic characteristics of FA and the mechanical properties of GPC is an important step toward producing large quantities of GPC with reasonably consistent and predictive engineering properties.

Experimental Investigation

Materials and Methods

This study was based on the analysis of 32 FA samples collected from power-generating stations around the United States. The database of FA samples was partitioned into two individual sets: the first consisting of 24 samples for data analysis and model building, and the second consisting of the eight remaining samples for validation purposes. The first set has 14 samples that are classified as type F and 10 as type C according to ASTM C618 [17]. The second set consists of five type F and three type C.

The 32 samples were analyzed via X-ray fluorescence (XRF) and X-ray diffraction (XRD) to obtain their chemical and crystallographic composition. The particle size distribution (PSD) was also obtained to assess the physical characteristics of the samples.

Chemical analysis of the FA stockpiles was performed following ASTM D4326 [18]. Table 1 shows the results of the chemical analysis. PSD analysis was conducted using Microtrac S3500 laser-based equipment with a measuring

TABLE 1—*Chemical composition of fly ash samples.*

FA class	FA Sample	SiO_2	Al_2O_3	SiO_2/Al_2O_3	$SiO_2 + Al_2O_3$	CaO	Fe_2O_3	LOI
C	1	37.77	19.13	1.97	56.90	22.45	7.33	0.17
C	2	32.41	18.40	1.76	57.90	28.07	7.17	0.38
C	3	55.61	19.87	2.80	75.48	12.93	4.52	0.23
F	4	58.52	20.61	2.84	79.13	5.00	9.43	0.05
F	5	61.01	20.06	3.04	81.07	5.48	7.00	0.08
F	6	61.23	19.20	3.19	80.43	5.64	7.27	0.06
F	7	62.12	19.59	3.17	81.71	5.01	6.88	0.10
F	8	59.32	19.72	3.01	79.04	6.90	7.22	0.15
C	9	48.70	16.60	2.93	65.30	18.72	6.93	0.49
F	10	55.07	28.61	1.92	83.68	1.97	6.22	1.82
F	11	56.22	27.15	2.07	83.37	5.43	3.73	2.69
F	12	56.39	27.36	2.06	83.75	4.69	3.34	3.41
F	13	57.11	28.18	2.03	85.29	5.18	4.00	0.44
F	14	57.35	27.78	2.06	85.13	5.57	3.65	0.83
F	15	40.75	22.79	1.79	63.54	4.64	17.76	5.72
F	16	66.5	18.8	3.54	85.30	4.91	1.95	0.26
C	17	39.25	21.09	1.86	60.34	23.53	4.99	0.11
C	18	33.02	19.82	1.67	52.84	26.19	6.75	0.16
F	19	59.25	18.43	3.21	77.68	9.23	5.61	0.04
C	20	56.42	17.63	3.20	74.05	11.66	5.74	0.00
C	21	27.15	17.57	1.55	44.72	33.39	6.08	0.00
C	22	31.26	19.76	1.58	51.02	28.53	6.47	0.00
C	23	30.85	17.07	1.81	47.92	28.47	6.79	0.00
C	24	49.9	19.32	2.58	69.22	15.22	7.63	0.09
C	25	55.15	23.55	2.34	78.70	10.60	4.63	0.31
F	26	52.81	20.83	2.54	73.64	0.98	13.05	0.19
F	27	45.65	20.37	2.24	66.02	6.23	19.43	0.20
F	28	58.04	28.15	2.06	86.19	4.24	3.29	0.07
F	29	51.46	28.04	1.84	79.50	2.96	10.34	0.03
F	30	51.69	21.37	2.42	73.06	3.10	8.28	0.22
C	31	57.55	19.84	2.90	77.39	10.25	5.08	0.07
F	32	52.57	25.22	2.08	77.79	5.10	7.76	0.13
F	Min.	40.75	18.43	1.79	63.54	0.98	1.95	0.03
	Max.	66.50	28.61	3.54	86.19	9.23	19.43	5.72
	Avg.	55.95	23.28	2.48	79.23	4.86	7.70	0.87
C	Min.	27.15	16.60	1.55	44.72	10.25	4.52	0.00
	Max.	57.55	23.55	3.20	78.70	33.39	7.63	0.49
	Avg.	42.70	19.20	2.23	62.44	20.77	6.16	0.15

range between 0.024 μm and 2816 μm. Samples were suspended in isopropyl alcohol and went through the necessary cycles of reading and dispersing using ultrasound to obtain a realistic analysis; a summary of these results is presented in Table 2.

TABLE 2—*Summary of physical properties.*

Sample	Mean Particle Size (μm)	Specific Gravity	Specific Surface Area (m^2/g)
1	11.36	2.50	1.17
2	12.31	2.53	1.02
3	20.87	2.38	0.56
4	27.52	2.32	0.25
5	22.68	2.27	0.55
6	24.93	2.29	0.48
7	28.31	2.27	0.43
8	29.96	2.23	0.50
9	15.17	2.47	0.81
10	22.30	2.17	0.50
11	40.03	1.78	0.28
12	34.57	1.73	0.46
13	36.73	1.82	0.32
14	51.11	1.81	0.13
15	6.62	2.52	1.17
16	92.41	1.47	0.10
17	11.88	2.51	0.98
18	11.32	2.7	0.92
19	30.38	2.18	0.54
20	25.93	2.27	0.25
21	10.38	2.67	1.17
22	6.71	2.55	1.23
23	12.16	2.61	1.07
24	11.95	2.41	0.66
25	30.15	2.05	0.68
26	33.31	2.03	0.26
27	21.00	2.50	0.22
28	20.42	1.88	0.57
29	20.39	2.19	0.72
30	32.64	2.04	0.55
31	25.38	2.11	0.50
32	18.41	2.263	0.79

Note: 1 $m^2/g = 4884.31$ ft^2/lb.

XRD data was obtained using a Bragg-Brentano geometry powder diffractometer using a copper anode at 40 kV. Data was collected between 10° and 65° of two theta angles, with a step size of 0.05° and a count time of 5 s per step. Samples were further analyzed using the Rietveld phase quantification method to determine the amount of crystalline and amorphous components. Table 3 shows a list of the crystalline phases found in the samples with a letter or set of letters assigned to each phase to facilitate calculations presented later in this

TABLE 3—*Nomenclature of crystalline phases.*

Crystalline Phase	Designation
Albite ($NaAlSi_3O_8$)	A
Anhydrite ($CaSO_4$)	C
Anorthite ($CaAl_2Si_2O_8$)	D
Calcite ($CaCO_3$)	E
Calcium catena silicate Ca (SiO_3)	F
Cristoballite (SiO_2)	G
Dicalcium silicate (Ca_2SiO_4)	H
Diopside ($CaMgSi_2O_6$)	I
Dolomite ($CaMg(CO_3)_2$)	J
Gehlenite ($Ca_2Al_2SiO_7$)	K
Grossular ($Ca_3Al_2(SiO_4)_3$)	L
Gypsum ($CaSO_4$ §2(H_2O))	M
Hematite (Fe_2O3)	N
Illmenite ($FeTiO_3$)	P
Jadeite ($NaAlSi_2O_6$)	Q
Lime (CaO)	R
Magnesite ($MgCO_3$)	S
Magnetite (Fe3O4)	T
Merwinite ($Ca_3Mg(SiO_4)_2$)	U
Mullite ($Al_{4.5}Si_{1.5}O_{9.75}$)	V
Olympite (Na_3PO_4)	X
Periclase (MgO)	Y
Perovskite ($CaFe(Ti_2O_6)$)	Z
Pseudobrookite ((Fe^{+++}, Fe^{++})$_2$(Ti, Fe^{++})O_5)	AA
Pyrite (FeS_2)	AB
Spinel ($MgAl_2O_4$)	AC
Quartz (SiO_2)	AF
ZnO	AG
Amorphous	AH

study. The results of the XRD quantitative analysis for each FA stockpile are presented in Table 4.

The mix design for the concrete specimens is presented in Table 5. It was established using the absolute volume method proposed by the Portland Cement Association and based on previous studies [8,12,13]. It is worth mentioning that quantities provided in Table 5 are estimates because there were small variations as the activator solution to FA ratio was adjusted depending on the liquid demand of each FA stockpile to obtain a slump of 10 to 15 cm (4 to 6 in.), i.e., the amount of FA, sand, and gravel in the mixture varied slightly as greater or lesser amounts of activator solution was added to obtain the desired slump value. The activator solution used was composed of a 14 M

TABLE 4—*Crystallographic analysis.*

	A	C	D	E	F	G	H	I	J	K	L	M	N	P	Q	R	S	T	U	V	X	Y	Z	AA	AB	AC	AF	AG	AH
1													0.30			0.30		0.40	9.60			3.20		4.20			23.10		58.90
2		1.70			0.40		3.30				1.20							0.90		1.40		1.80	7.90				5.10		76.20
3	0.10								0.40				0.30					0.60		1.30		0.40					28.30		69.30
4													1.30							6.70			2.10				37.00		52.90
5													1.90					0.50		10.60							14.90		72.10
6													0.20					0.20		5.30							19.20		75.10
7																		0.90		6.20							22.30		70.60
8																		1.00		5.20							20.70		73.10
9				1.60					0.20			1.30					0.90					0.10			0.65		28.10	0.10	67.05
10																				25.27							10.33		64.40
11																2.10				47.90							22.10		27.90
12																1.10				22.70							10.50		65.70
13																1.10				30.10							9.40		59.40
14																0.80		0.10		22.00							7.90		69.20
15		0.90											2.40					3.70								6.10	0.80		86.10
16	2.10	0.30				0.90												0.90		7.60							5.30		82.90
17		0.30																		1.50		0.80	2.50				9.00		85.90
18		1.00								3.20	0.40			5.80				0.40		0.60		2.80	6.00				5.60		74.20
19		0.40																1.10		4.80							20.90		72.80
20		0.30																0.30		2.30							12.20		84.90
21		2.10	1.50							1.80						0.70					1.30	1.20	9.10				3.00		79.30
22		1.40								2.00					0.50	0.50						1.20	5.10				3.50		85.80
23		2.30								3.80					1.20	0.40						2.00	6.30				4.90		78.90
24		0.20											0.50			0.10				2.00		0.20					10.30		86.20
25										0.20						0.20		0.40		7.10							8.00		84.10

TABLE 4—*Continued*

	A	C	D	E	F	G	H	I	J	K	L	M	N	P	Q	R	S	T	U	V	X	Y	Z	AA	AB	AC	AF	AG	AH
26	0.60												1.20							13.70							15.40		69.10
27	0.40	0.80		0.20				2.50					2.40					4.30		5.40		0.40					5.20		78.40
28													0.30			0.80				18.70							7.70		72.50
29																		2.70		29.30							10.00		58.00
30		0.40											0.70			0.40		2.50		13.20		0.40					11.70		70.00
31				2.30												0.70		0.90		10.60							12.40		73.10
32	0.60												1.20							13.70							15.40		69.10

TABLE 5—*Mix proportions for the concrete samples.*[a]

Material	Quantity (kg/m^3)
Fly ash	494
Sand	691
Gravel	858
Activator solution	198–464
Superplasticizer	15

Note: 1 kg/m^3 = 1.685 lb/yd^3.
[a]Values will vary depending on the activator solution demand.

NaOH solution and sodium silicate type "D" from PQ Corporation (45 % by weight and SiO2 to Na2O ratio of 2:1). Tap water was used throughout the experiments in an attempt to mimic field conditions. The two solutions were mixed in a 1:1 ratio by weight. Well-graded sand, meeting ASTM C33 [19], with a bulk density of 1680 kg/m^3 (100 lb/ft^3), a specific gravity of 2.63, and a fineness modulus of 2.4 served as fine aggregate. "Pea gravel" (1 cm or 3/8 in. diameter) with a bulk density of 1934 kg/m^3 (115 lb/ft^3) and specific gravity of 2.70 acted as coarse aggregate. To improve the workability of fresh GPC, a superplasticizer was incorporated 60 s before the end of the mixing cycle. The ingredients were mixed in a vertical mixer with planetary action (beater rotates on its axis in opposite directions as it moves around the bowl). To promote the first phase of geopolymerization, dissolution of silicate and aluminate species, the following mixing procedure was utilized: (1) FA and NaOH solution were mixed for 30 s, (2) sodium silicate was added and mixed for 30 s, (3) sand was added and mixed for 60 s, and, finally, (4) gravel was added and mixed for an extra 120 s (superplasticizer was added 60 s before the end of the mixing cycle). Because of the short setting time of some samples, their mixing times were shortened sufficiently to cast and form the specimens.

The fresh mixture was cast into 15 × 30 cm (6 × 12 in.) cylindrical molds to be tested as per ASTM C39 [20] for compressive strength and ASTM C469 [21] for static elastic modulus and Poisson's ratio. GPC mixture was also cast into 10 × 10 × 40 cm (4 × 4 × 16 in.) rectangular prism molds for flexural strength testing (third-point loading) as per ASTM C78 [22]. Concrete density measurements were taken following ASTM C138 [23]. Setting time measurements were taken on geopolymer paste using a standard Vicat needle. Each data point presented in this study is an average of three measurements with less than 8 % variation or two measurements with less than 6 % variation. All samples were stripped from the mold after 24 h, cured at 60 C (140 F) for 72 h, and then cooled down for 24 h prior to testing. It is worth noting that the significant maximum (90 % to 95 %) mechanical strength of GPC is commonly achieved within 3 to 5 days depending on the curing effort applied [9]. A summary of the fresh mix and mechanical properties of GPC is presented in Table 6.

TABLE 6—*Summary of fresh mix and mechanical properties of GPC samples.*

Fly Ash Type	Sample	w (kg/m^3)	f'_c (MPa)	f_t (MPa)	E_c (MPa)	Poisson's Ratio	Setting Time (min)
C	1	2323	59.50	4.48	33|633	0.12	1.5
C	2	2323	52.28	4.72	34|377	0.12	2
C	3	2291	55.89	4.30	37|108	0.17	25
F	4	2307	40.35	4.14	28|599	0.14	180
F	5	2291	47.55	5.58	29|475	0.16	350
F	6	2307	46.69	5.30	29|358	0.14	320
F	7	2307	46.79	4.61	28|517	0.13	240
F	8	2291	46.11	4.71	26|455	0.12	400
C	9	2339	52.81	5.27	42|878	0.13	17
F	10	2243	47.44	5.12	25|635	0.14	480
F	11	1986	12.20	2.24	7040	0.17	140
F	12	1970	12.82	2.38	6812	0.10	60
F	13	1986	20.68	3.50	7960	0.08	70
F	14	1890	10.34	2.74	7460	0.10	25
F	15	2371	46.56	6.31	28|744	0.15	480
F	16	1810	5.53	1.15	4619	0.12	25
C	17	2307	61.38	6.23	31|447	0.18	8
C	18	2323	39.19	4.19	19|064	0.22	6
F	19	2291	43.38	4.24	25|607	0.13	45
C	20	2371	53.70	4.43	28|910	0.15	285
C	21	2323	36.54	3.58	26|972	0.13	4
C	22	2323	57.18	5.27	29|448	0.19	2
C	23	2339	42.81	5.18	22|567	0.22	3
C	24	2355	64.68	4.90	30|806	0.15	18
C	25	2355	62.19	4.83	29|896	0.14	55
F	26	1938	20.16	2.79	11|273	0.14	16
F	27	2339	52.57	4.17	28|089	0.14	20
F	28	2083	32.45	4.38	22|808	0.13	46
F	29	2195	23.36	2.52	13|176	0.12	75
F	30	2131	22.68	3.94	12|314	0.14	11
C	31	2163	36.24	3.25	21|456	0.14	17
F	32	2243	36.80	4.56	24|725	0.14	47
F	Min.	1810	5.53	1.15	4619	0.08	11
	Max.	2371	52.57	6.31	29|475	0.17	480
	Avg.	2157	32.34	3.91	19|403	0.13	159
C	Min.	2163	36.24	3.25	19|064	0.12	2
	Max.	2371	64.68	6.23	42|878	0.22	285
	Avg.	2318	51.88	4.66	29|889	0.16	34

Note: 1 lb/ft^3 = 16.02 kg/m^3; 145.04 lb/in.^{2} = 1 MPa.

Evaluating the Impact of FA Characteristics on the Resulting GPC

The attributes of GPC that are considerably influenced by FA's chemical, crystallographic, and physical characteristics are the density of the fresh mix, the setting time, and the mechanical properties of the hardened product. As expected, the density of the fresh mix is influenced mainly by the physical characteristics of the FA, i.e., specific gravity, particle size, etc. This can be attributed to the varying interstice systems that can be present in the FA samples [15,16]. The setting time is influenced mainly by the CaO content in FA as proposed in previous work [11,12]. For the mechanical properties, to reduce the number of dependant variables, only compressive strength values were used as a response to perform the evaluation. However, flexural strength and elastic modulus can be obtained using the equations proposed in previous work performed by Diaz-Loya et al. [8], which were developed using a set of 24 FA-based GPC samples. The compressive strength of GPC is dependent on a complex fusion of physical, chemical, and crystallographic factors of FA.

Analytical Investigation

Preparing the Data for Statistical Analysis

Although silica and alumina are the main precursors for the formation of geopolymer networks, and calcium oxide has significant influence in the chemical structure of the binder, these values cannot be taken from the XRF analysis without taking into consideration their crystalline arrangement because they represent absolute totals regardless of their reactivity. Previous studies showed that the crystalline part of FA stays nearly inert, whereas the amorphous component is the reactive one throughout the geopolymerization reaction [12,13]. Therefore, the amount of silica, alumina, and calcium oxide in a crystalline arrangement was not taken into account in the analysis and it was assumed that only the amorphous components participate in the geopolymerization reaction. In addition, given that the total silica, alumina, lime, and LOI are calculated as percentages of the same analysis, potential multicolinearity problems could be avoided by incorporating the crystalline distribution results to the chemical analysis.

Each crystalline phase is composed of one or more elements in the form of oxides (equivalent), e.g., Mullite is composed of 71.79 % Al_2O_3 and 28.21 % SiO_2. Using these values, the crystalline components obtained by XRD were subtracted from the total values obtained by XRF. To illustrate this process, the following example is provided:

Step 1—Crystalline phases in the FA sample containing silica, alumina, or calcium oxide are identified using Table 4. For sample 1, these are lime, merwinite and quartz (R, U, and AF as categorized in Table 3).

Step 2—The chemical composition of the crystalline phases is identified. AF contains 100 % SiO_2, and U contains 36.56 % SiO_2, 51.18 % CaO, and 12.26 % MgO. R contains 100 % CaO.

Step 3—The total content of non-reactive silica, alumina, and calcium oxide (labeled as $NRSiO_2$, $NRAl_2O_3$, and NRCaO) is calculated in the following manner:

$$NRSiO_2 = \frac{AF * 100 + U * 36.56}{100} = \frac{23.10 * 100 + 9.60 * 36.56}{100} = 26.61\%$$

$$NRAl_2O_3 = 0$$

$$NRCaO = \frac{U * 51.18 + R * 100}{100} = \frac{9.60 * 51.18 + 0.30 * 100}{100} = 5.21\%$$

Step 4—The non-reactive silica, alumina, and calcium oxide is subtracted from the total to obtain the reactive components labeled as $RSiO_2$, RAl_2O_3 and RCaO:

$$RSiO_2 = SiO_2 - NRSiO_2 = 37.77 - 26.61 = 11.16\%$$

$$RAl_2O_3 = Al_2O_3 - NRAl_2O_3 = 19.13 - 0 = 19.13\%$$

$$RCaO = CaO - NRCaO = 22.45 - 5.21 = 17.24\%$$

The use of these values instead of the total values obtained from the XRF is expected to increase the accuracy of the model.

Relationship Between FA Characteristics and Compressive Strength of GPC

The values of $RSiO_2$, RAl_2O_3, RCaO, LOI, mean particle size in μm (d50), and specific surface area (SSA) were used as regressors, and the compressive strength values as a response. The statistical software "R" was used in the package LARS to perform simultaneous subset selection and coefficient optimization using the LASSO algorithm [24].

The proposed subsets were evaluated in terms of: (1) adjusted R^2, which is typically preferred over the typical R^2 when comparing various models because of the fact that it penalizes models that have more regressors than they actually need, thus avoiding "over-fitting the model"; (2) variance inflation factor (VIF), a mean to quantify multicolinearity between variables; regressors that exhibit VIF values greater than 5 or 10 are considered to be highly correlated,

and this can cause the model to give misleading results [25]; and (3) Mallow's *Cp*, a parameter that is generally used to assess the fitness of the model; a small *Cp* value is always preferred [25].

The results showed nine steps where regressors were selected and their coefficients were shrunk. The best regressor for a one-variable model was d50. The best regressors for a two-variable model were RAl_2O_3 and d50, while for a three-variable model the best variables were and $RSiO_2$, RAl_2O_3, and d50. The best four-variable model did not include SSA and RCaO, and for the best five-variable model only SSA was dropped.

The subsets proposed in each of the nine steps were evaluated in terms of residual sum of squares and Mallow's *Cp*. The model that exhibited the lowest *Cp* was found in the seventh step:

$$f_c' = -3.62 + 0.59 * RSiO_2 + 3.35 * RAl_2O_3 - 0.48 * RCaO - 0.74 * d50 - 4.39 * LOI(MPa) \quad (1MPa=145.04lb/in.^2) \quad (1)$$

The model had a *Cp* of 5.00 and MSE of 75.18. The R^2 of the model was 0.78. However, the adjusted R^2 was 0.73. Given the number of samples and regressors, the R^2 value has a 95 % confidence interval of $0.66 \geq R^2 \geq 0.90$. VIF values were all below five; hence, it was assumed there were no multicolinearity problems. The adequacy of the model was analyzed through residual analysis. Figure 1 shows the experimental versus fitted values. It can be seen in the graph that observation 8 yielded the largest error, predicting approximately 28 MPa (4060 psi), 19 MPa (2755 psi) less than the actual value of 47 MPa (6815 psi). Three other observations had errors between 10 and 14 MPa (1450 and 2030 psi), while the remaining samples had errors of less than 10 MPa (1450 psi). The average error of the model was approximately 6 MPa (870 psi).

The validation using the second set of FA samples is shown in Fig. 2. It can be observed that observation 6 had the largest error (23 MPa; 3335 psi). Observation 4 had an error of 10 MPa (1450 psi), whereas the remaining observations exhibited errors of less than 4 MPa (580 psi). The validation set had an average error of 6 MPa (870 psi). The residuals versus fitted plot (Fig. 3) appears to exhibit a "double-bow" shape as proposed by Montgomery et al. [25]. This could be an indication that the variance of the errors is not constant, which could present a challenge because OLS works under the assumption of constant variance. The presence of the double-bow shape in the residuals could be attributed to the nature of the collected data set where there are only six responses with values less than 35 MPa (5075 psi) with the rest clustered toward the high end of the range. Hence, the weighted least-squares technique and a transformation of the regressors (or response) are recommended in future work to improve the distribution of the residuals. The normal probability plot

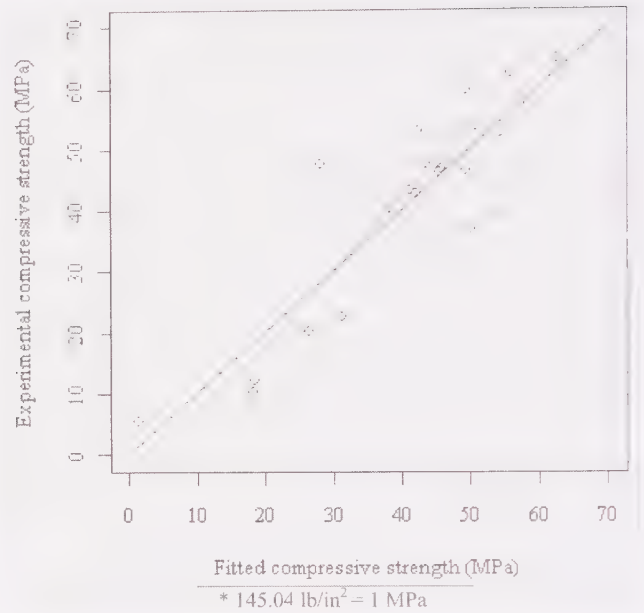

FIG. 1—*Experimental versus fitted compressive strength values.*

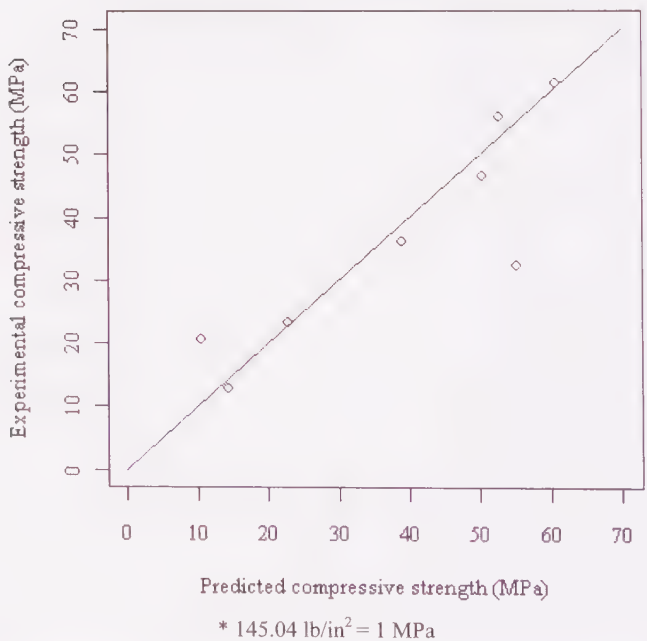

FIG. 2—*Experimental versus predicted compressive strength values (validation dataset).*

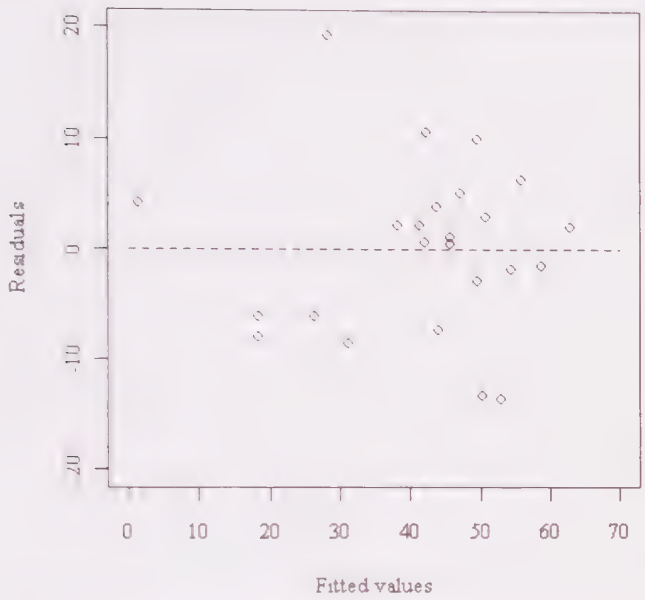

FIG. 3—*Residual versus fitted compressive strength values.*

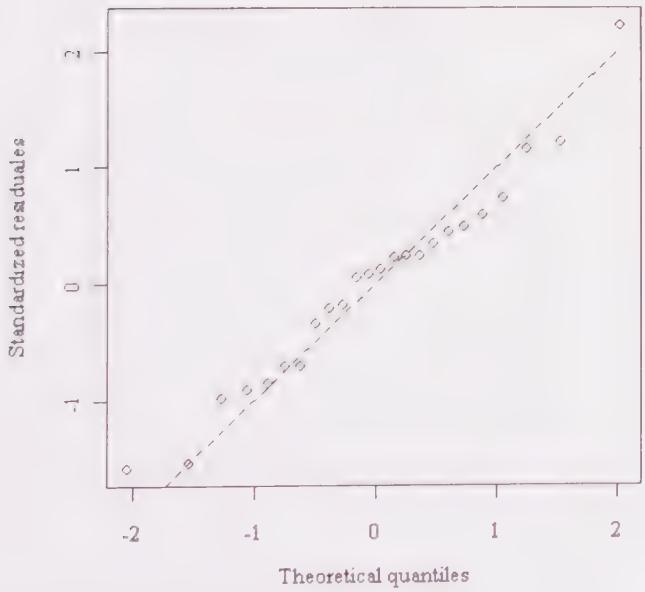

FIG. 4—*Normal probability plot.*

TABLE 7—*ANOVA table of Eq 3.*

Parameter	Degrees of Freedom	Sum of Squares	Mean Square	*F* Value	*P*
$RSiO_2$	1	444.91	444.91	5.9177	0.02564700
RAl_2O_3	1	1567.32	1567.32	20.8467	0.00024000
RCaO	1	0.88	0.88	0.0118	0.91482600
d50	1	2282.85	2282.85	30.3638	3.12×10^{-05}
LOI	1	539.24	539.24	7.1700	0.01534800
Residuals	18	1353.29	75.18		

(Fig. 4) shows that the error distribution is slightly tailed indicating a small departure from normality. However, slight non-normality is typically not expected to affect the model significantly [25].

Experimental Results and Discussion

Discussion of FA Characteristics Versus Compressive Strength

Further analysis of the model showed that d50 had the strongest influence on the compressive strength of GPC followed by RAl_2O_3, LOI, $RSiO_2$, and, finally, RCaO. The analysis of variance (ANOVA) of the model is presented in Table 7 to illustrate how the statistical significance of each regressor was determined. The *P*-value was the parameter used to test the statistical significance of the regressors; the regressor with the lowest *P*-value (d50) is the most significant and the one with the highest value (RCaO) was the least significant. The parameters d50 and SSA both describe physical characteristics of FA, in particular the packing of the particles. However, the d50 result is highly influential, to the point that it may have hindered the impact that SSA exerts in the compressive strength. The parameters $RSiO_2$, RAl_2O_3, and RCaO were expected to have a positive sign in the equation because reactive silica and alumina are the main ingredients for the formation of geopolymer binder and many authors have proposed that calcium also contributes to the compressive strength [11,26–30]. A positive sign indicates that increasing these parameters would result in a direct increase in the compressive strength. However, while RAl_2O_3 and $RSiO_2$ exhibited a positive sign in the model, RCaO presented an unexpected negative sign. This can be attributed to one or more coefficients being calculated over their optimum values forcing RCaO to drop its sign below zero to compensate for it.

The parameter d50 exhibited a negative sign, and had the most significant impact on the compressive strength. This is in good agreement with research previously published by Diaz et al. [12] and Diaz and Allouche [13]. Because the formation of geopolymer binder occurs only at the surface of the FA

particles. FA with larger d50 provide less reaction surface and thus produce GPC with smaller compressive strength values [31].

The parameter LOI had a strong influence on the compressive strength and exhibited a negative sign. LOI is typically a measure of unburned carbon in FA, which has been demonstrated to cause problems in OPC-based concrete [32] as in GPC [12]. Although, the impact of unburned carbon in ordinary concrete is mainly in air entrainment, whereas GPC is in the liquid demand, recent studies performed by Hill and Folliard [33] have shown that LOI may be inaccurate to quantify the impact of carbon in concrete mixtures. The study showed that FA with low LOI in the form of fine carbon may have a greater impact on concrete than FA with high LOI in the form of larger carbon particles and/or perhaps with some of the carbon partially encapsulated in glass, yet this still has to be proven for GPC. This phenomenon was observed during this investigation, as some FA samples, in spite of having high LOI contents, exhibited low liquid demands and average compressive strength.

Relationship between FA Characteristics and Density of GPC

The physical characteristics of FA were compared against the density of GPC to identify any possible correlations. It was found that the specific gravity of FA had the strongest correlation with the resulting concrete density. The regression model obtained from the analysis was:

$$w = 2649 - 1979 * \frac{1}{SG^2} \left(kg/m^3\right)$$
$$\left(1lb/ft^3 = 16.02kg/m^3\right) \quad (2)$$

where w represents the density of GPC as per ASTM C138 [23] and SG is the specific gravity of FA determined following ASTM C188 [34]. Equation 2 had an R^2 value of 0.76 with a 95 % confidence interval of $0.61 < R^2 < 0.91$. A plot of SG versus w that includes a graphical representation of the equation is presented in Fig. 5.

The residuals of Eq 2 were analyzed and no major deficiencies were found. The model converged well with normality and the residuals showed no apparent defects. The largest error was 231 kg/m^3 (14.44 lb/ft^3) over the value of its corresponding observation. Equation 2 predicted an average of 55 kg/m^3 (3.44 lb/ft^3) off target. In general terms, it tended to over-predict at low specific gravity values and under-predict at the higher end of the values. However, the prediction accuracy seems to increase at higher SG values. This could be an indication that another variable was needed to predict GPC density more accurately. As before, the model was built using 24 observations and validated with the remaining eight; the results of the validation of the regression model of FA-specific gravity versus density of GPC are shown in Fig. 6. The average

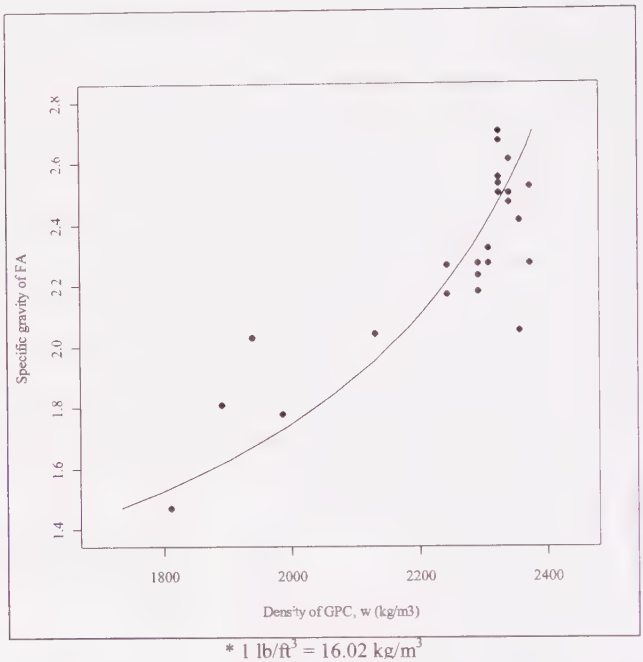

FIG. 5—*Regression model of FA specific gravity versus density of GPC.*

error was approximately 31 kg/m^3 (1.94 lb/ft^3) indicating that the fitted values lay close to their corresponding observation.

It can be presumed that the relationship between the density of GPC and the specific gravity of FA is merely physical. As opposed to OPC concrete, GPC cannot convert water into a solid and reduce the pore volume through the hardening process [16]. Therefore, the packing characteristics of FA have a direct and significant impact in the liquid demand of GPC. FA with low specific gravity values demands more liquid to fill larger voids caused by poor packing resulting in a higher pore volume and thus lowers density in fresh GPC. Ultimately, the pore volume and density of GPC are expected to impact the stiffness of the material.

FA Characteristics Versus Setting Time of GPC

Previous tests [7] showed that setting time of GPC is strongly influenced by the calcium content in FA. This premise remained true throughout this study, as samples were added into the database they followed the same trend. A scatter plot of setting time versus reactive calcium oxide is shown in Fig. 7. It can be seen that the setting time decreases as the RCaO content increases in a manner somewhat similar to an exponential decay curve. This can be attributed to the calcium in the mixture reacting with the silicate and aluminate monomers

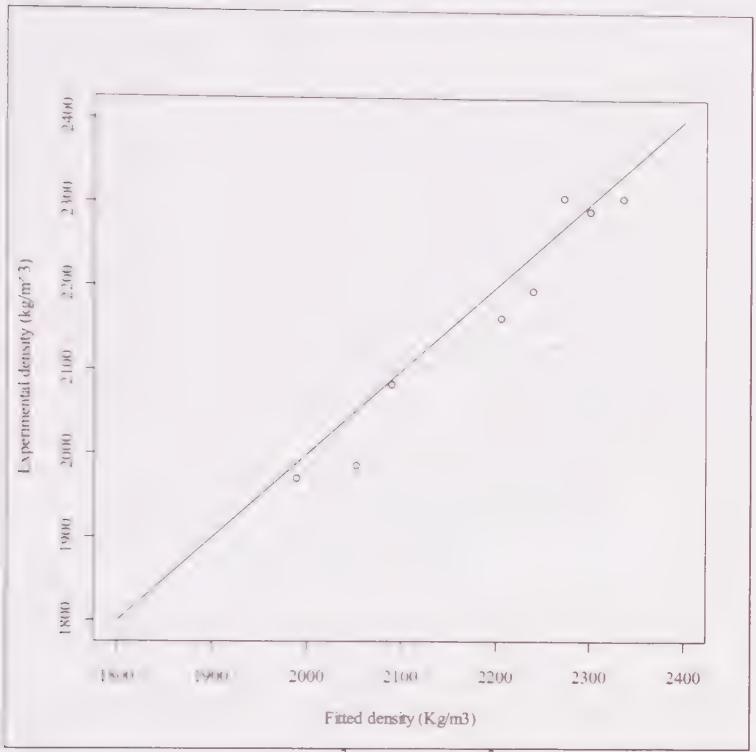

* 1 lb/ft^3 = 16.02 kg/m^3

FIG. 6—*Validation of the regression model of FA specific gravity versus density of GPC.*

dissolved from the source material, forming C-S-H and C-A-S-H [26,28–30]. The hydration of these compounds results in water deficiency and thus raises the alkalinity of the mixture. The increase in alkalinity promotes higher and faster dissolution of silicate and aluminate species from the source material, and consequently an increased rate of polycondensation/geopolymerization. Thus, the presence of calcium contributes to the mechanical strength of geopolymer concrete not only by forming C-S-H and C-A-S-H, but also via the enhancement of the geopolymerization process [11]. However, the "enhanced geopolymerization" and the nucleation sites created by the precipitated C-S-H and C-A-S-H lower the setting time [6].

Despite the evident relationship between RCaO and the setting time of GPC, it was not possible to propose a regression model that captures this interaction because of an excessive dispersion of some points between 0 % and 12 % RCaO. For example, several observations that had approximately 5 % RCaO, yet exhibited setting times ranging from 25 to 480 min. This can be an indication that although RCaO and setting time are inversely related, their

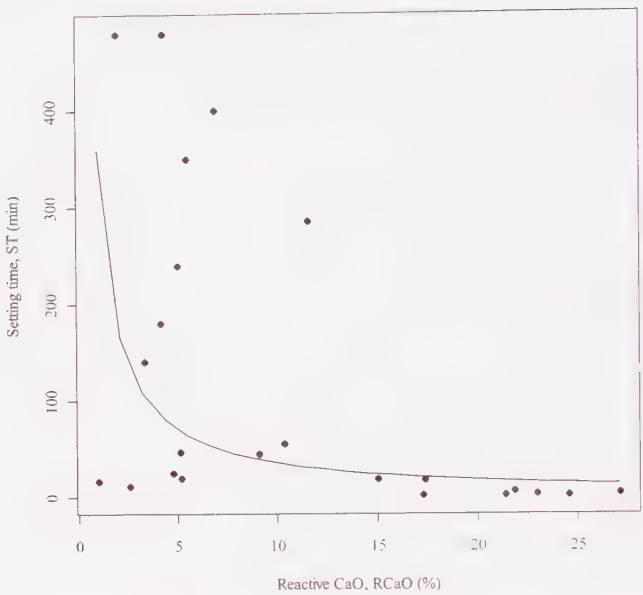

FIG. 7—*Scatter plot of GPC setting time versus reactive CaO content.*

interaction may be more complex and possibly other factors that impact the setting time were not taken into account.

Testing the Models

The accuracy of the overall statistical analysis was further evaluated by using Eq 1 to predict compressive strength and Eq 2 to predict density of GPC, and then using these predicted values to calculate the flexural strength and the elastic modulus using Eqs 1 and 5 as proposed in previous research performed by Diaz et al. [10]. In other words, using the chemical, crystallographic, and physical characteristics of FA, the potential compressive strength, density, flexural strength, and elastic modulus of GPC were predicted using the aforementioned equations. The results are summarized in Table 8. The errors associated with the density and compressive strength are dependant on the accuracy of the models. However, the flexural strength, and elastic modulus values were calculated using the predicted density and compressive strength values, i.e., they are subject to the error related to the prediction of density and compressive strength and the error related to equations used to predict flexural strength and elastic modulus. Yet, the predictions are fairly accurate.

Discussion on the Rationale Behind the Models

The chemical rationale behind the aforementioned model is that silica and alumina are the main precursors for geopolymer binder formation and these are

TABLE 8—*Model testing.*

	w (kg/m3)			f'_c (MPa)			f_r (MPa)			E_c (MPa)		
Sample	O	P	E	O	P	E	O	P	E	O	P	E
3	2291	2300	9	55.89	53.01	2.88	4.3	4.95	0.65	37 108	29 706	7402
6	2307	2272	35	46.69	50.45	3.76	5.3	4.83	0.47	29 358	28 454	904
17	2307	2335	28	61.38	61.01	0.37	6.23	5.31	0.92	31 447	32 605	1158
13	1986	2052	66	20.68	10.46	10.22	3.5	2.2	1.3	7960	11 121	3161
12	1970	1988	18	12.82	14.47	1.65	2.38	2.59	0.21	6812	12 471	5659
28	2083	2089	6	32.45	55.23	22.78	4.38	5.05	0.67	22 808	26 255	3447
31	2163	2204	41	36.24	39.17	2.93	3.25	4.26	1.01	21 456	23 969	2513
29	2195	2238	43	23.36	22.79	0.57	2.52	3.25	0.73	13 176	18 705	5529
Avg E		30.75			5.645			0.745			3722	

Note: O, observed value; E, error; P, predicted value. 1 lb/ft^3 = 16.02 kg/m^3; 145.04 lb/in.^{2} = 1 MPa.

assumed to dissolve from FA in a highly alkaline solution and then recombine using sodium as a charge-balancing agent to form geopolymer gel [35]. Calcium in FA is believed to enhance the mechanical strength not only by forming hydration products in parallel to geopolymer but also by raising the alkalinity as water is consumed by the hydration reactions [11,26–30]. However, not all silica, alumina, and calcium participate in this reaction as some are typically combined in a quasi-inert crystalline arrangement. Therefore, in Eq 1, the molecules that combined in a crystalline form were assumed to be inert and only the reactive components were taken into account for the calculations.

The LOI content and d50 were also found to influence the compressive strength. Their influence can be attributed to physical interactions that affect the reaction kinetics. LOI (typically unburned carbon) was found to have an adverse effect on the mechanical strength of GPC because of its hygroscopic nature that causes a higher liquid demand. However, its effect on GPC may vary depending on its fineness and reactivity. For example, a small amount of highly fine carbon may have a more pronounced effect than a high amount of coarser carbon. The influence of the mean particle size in the compressive strength of GPC can be attributed to the rate of dissolution of silicon, aluminum, and calcium species from the FA. Because it is believed that the geopolymerization reaction occurs only at the particle–liquid interface [14], FA with a smaller mean particle size is expected to provide more surface area that will lead to a higher dissolution rate of the main precursors. Consequently, more chemical species will be available to form geopolymer and thus the compressive strength will be higher.

The density of GPC was found to be strongly influenced by the specific gravity of the FA. The relationship between the two variables can be

considered to be merely physical and attributed to the packing characteristics of FA. Changes in the void content (quantified as SG) will cause variation in the water demand to fill these voids.

The calcium content in FA is not only believed to enhance the mechanical strength but it also has a strong effect on the setting time of GPC. As it was proven by Temuujin et al. [11], calcium forms hydrated calcium products parallel to the formation of geopolymer. The decrease in setting time can be attributed to two mechanisms: (1) the hydrated products act as nucleation sites that accelerate the setting; and (2) the hydration of calcium consumes water that raises the concentration of the activator solution and consequently accelerates the reaction. Although the correlation between calcium and setting time is clear, a regression model with fair accuracy could not be proposed as high variability in the setting time was encountered at low RCaO values. Conversely, at moderate to high RCaO values, the variability in the setting time is reduced and the correlation becomes more evident. This suggests that an additional parameter, which was not taken into account, may play an important role in the setting time of GPC, particularly for FA samples with low calcium content.

Conclusions

This manuscript puts forward a database of XRD analysis, chemical composition, and particle size distribution performed on 32 FA stockpiles collected from different coal-fired power generating stations around the United States. The potential of each FA sample as source material for geopolymer concrete was compared and a statistical analysis was performed to identify and quantify the major causes of variation that impact its mechanical properties, namely; silica, alumina, calcium, and LOI as well as the amorphous content and fineness. As the true reaction mechanism through which geopolymer binders are formed is still debated and not well understood, a set of regression models that attempt to explain the true underlying mechanism are put forward. Equation 1 was found to be the best regression model to predict the compressive strength of GPC, as it uses reactive silica, alumina, and calcium oxide as well as LOI and mean particle size as regressors. It showed to be the best fit by predicting compressive strength with an average accuracy of ± 6 MPa (870 psi), having an adjusted R^2 value of 0.73 and an R^2 of 0.78. Equation 2 was found to be the best fit to predict the density of fresh GPC with an R^2 value of 0.76. It uses the specific gravity of FA as regressor and predicted the density with an average accuracy of ± 31 kg/m^3 (1.94 lb/ft^3). Although an evident relationship between the reactive calcium content and the setting time of GPC was found, it was not possible to propose a regression model to explain this relationship because of a high variability at low calcium contents.

References

[1] American Coal Ash Association, "2009 Coal Combustion Product (CCP) Production and Use Survey," 2010, http://acaa.affiniscape.com/display_common.cfm?an=1&subarticlenbr=3 (Last accessed 5 Jan 2011).

[2] Kosmatka, S., Kerkhoff, B., and Panarese, W., *Design and Control of Concrete Mixes*, 14th ed., Portland Cement Association, Skokie, IL, 2009.

[3] Davidovits, J., "Geopolymers: Inorganic Polymeric New Materials," *J. Therm. Anal.*, Vol. 37, 1991, pp. 1633–1656.

[4] Fernandez-Jimenez, A. and Palomo, A., "Activation of Fly Ashes: A General Overview," *ACI Mater. J.*, Vol. 221, 2004, pp. 351–366.

[5] Fernandez-Jimenez, A. and Palomo, A., "Alkaline Activation of Fly Ashes: Manufacture of Concrete Not Containing Portland Cement," *International RILEM Conference on the Use of Recycled Materials in Building and Structures*, Barcelona, Spain, November 8–11, 2004.

[6] De Silva, P., Sagoe-Crenstil, K., and Sirivivatnanon, V., "Kinetics of Geopolymerization: Role of Al2O3 and SiO2," *Cement Concrete Res.*, Vol. 37, 2007, pp. 512–518.

[7] Provis, J. L. and van Deventer, J. S. J., "Geopolymerization Kinetics: 1. In Situ Energy-Dispersive X-Ray Diffractometry," *Chem. Eng. Sci.*, Vol. 62, 2007, pp. 2309–2317.

[8] Diaz-Loya, E. I., Allouche, E. N., and Vaidya, S., "Mechanical Properties of Fly-Ash-Based Geopolymer Concrete," *ACI Mater. J.*, Vol. 108(3), 2011, pp. 300–306.

[9] Hardjito, D., Wallah, S. E., Sumajouw, D. M. J., and Rangan, B. V., "On the Development of Fly Ash-Based Geopolymer Concrete," *ACI Mater. J.*, Vol. 101(6), 2004, pp. 467–472.

[10] Fernández-Jiménez, A. M., Palomo, A., and López-Hombrados, C., "Engineering Properties of Alkali-Activated Fly Ash Concrete," *ACI Mater. J.*, Vol. 103(2), 2006, pp. 106–112.

[11] Temuujin, J., van Riessen, A., and Williams, R., "Influence of Calcium Compounds on the Mechanical Properties of Fly Ash Geopolymer Pastes," *J. Hazard. Mater.*, Vol. 167, 2009, pp. 82–88.

[12] Diaz, E. I., Allouche, E. N., and Eklund, S., "Factors Affecting the Suitability of Fly Ash as Source Material for Geopolymers," *Fuel*, Vol. 89, 2010, pp. 992–996.

[13] Diaz, E. I. and Allouche, E. N., "Recycling of Fly Ash into Geopolymer Concrete: Creation of a Database," Green Technologies Conference, 2010 IEEE, Grapevine, TX, April 15–16, 2010, pp. 1–7.

[14] Fernandez-Jimenez, A. and Palomo, A., "Characterization of Fly Ashes: Potential Reactivity as Alkaline Cements," *Fuel*, Vol. 82, 2003, pp. 2259–2265.

[15] Martin, M., Renault, M., Jezequel, P.-H., and Garcia, E., "Mixability and Particle Size Distribution Criteria: Study on Model Materials," *Powder Technol.*, Vol. 190(1–2), 2009, pp. 36–40.

[16] Provis, J. L., Duxson, P., and van Deventer, J. S. J., "The Role of Particle Technology in Developing Sustainable Construction Materials," *Adv. Powder Technol.*, Vol. 21(1), 2010, pp. 2–7.

[17] ASTM C618: "Standard Specification for Coal Fly Ash and Raw or Calcined Natural Pozzolan for Use in Concrete," *Annual Book of ASTM Standards*, ASTM International, West Conshohocken, PA.

[18] ASTM D4326: "Standard Test Method for Major and Minor Elements in Coal and Coke Ash By X-Ray Fluorescence," *Annual Book of ASTM Standards*, ASTM International, West Conshohocken, PA.

[19] ASTM C33: "Standard Specification for Concrete Aggregates," *Annual Book of ASTM Standards*, ASTM International, West Conshohocken, PA.

[20] ASTM C39: "Standard Test Method for Compressive Strength of Cylindrical Concrete Specimens," *Annual Book of ASTM Standards*, ASTM International, West Conshohocken, PA.

[21] ASTM C469: "Standard Test Method for Static Modulus of Elasticity and Poisson's Ratio of Concrete in Compression," *Annual Book of ASTM Standards*, ASTM International, West Conshohocken, PA.

[22] ASTM C78: "Standard Test Method for Flexural Strength of Concrete (Using Simple Beam with Third-Point Loading)," *Annual Book of ASTM Standards*, ASTM International, West Conshohocken, PA.

[23] ASTM C138: "Standard Test Method for Density (Unit Weight), Yield, and Air Content (Gravimetric) of Concrete," *Annual Book of ASTM Standards*, ASTM International, West Conshohocken, PA.

[24] Tibshirani, R., "Regression Shrinkage and Selection via the Lasso," *J.R. Stat. Soc.*, Vol. 58(1), 1996, pp. 267–288.

[25] Montgomery, D. C., Peck, E. A., and Vining, G. G., *Introduction to Linear Regression* Analysis, 4th ed., Wiley-Interscience, Hoboken, NJ, 2006, pp. 122–153.

[26] Yip, C. K., Lukey, G. C., Provis, J. L., and van Deventer, J. S. J., "Effect of Calcium Silicate Sources on Geopolymerization," *Cement Concrete Res.*, Vol. 38(4), 2008, pp. 554–564.

[27] Xu, H., Lukey, G. C., and van Deventer, J. S. J., "The Activation of Class C-, Class F-Fly Ash and Blast Furnace Slag Using Geopolymerisation," *ACI Mater. J.*, Vol. 221, 2004, pp. 797–820.

[28] Yip, C. K. and van Deventer, J. S. J., "Microanalysis of Calcium Silicate Hydrate Gel Formed Within a Geopolymeric Binder," *J. Mater. Sci.*, Vol. 38(18), 2003, pp. 3851–3860.

[29] Yip, C. K., Lukey, G. C., and van Deventer, J. S. J., "The Coexistence of Geopolymeric Gel and Calcium Silicate Hydrate at the Early Stage of Alkaline Activation," *Cement Concrete Res.*, Vol. 35(9), 2005, pp. 1688–1697.

[30] Dombrowski, K., Buchwald, A., and Weil, M., "The Influence of Calcium Content on the Structure and Thermal Performance of Fly Ash Based Geopolymers," *J. Mater. Sci.*, Vol. 42(9), 2007, pp. 3033–3043.

[31] van Jaarsveld, J. G. S., van Deventer, J. S. J., and Lukey G. C., "The Effect of Composition and Temperature on the Properties of Fly Ash- and Kaolinite-Based Geopolymers," *Chem. Eng. J.*, Vol. 89, 2002, pp. 63–73.

[32] Gao, Y. M., Shim, H. S., Hurt, R. H., and Suuberg, E. M., "Effects of Carbon on Air Entrainment in Fly Ash Concrete: The Role of Soot and Carbon Black," *Energy Fuels*, Vol. 11(2), 1997, pp. 457–462.

[33] Hill, R. L. and Folliard, K. J., "The Impact of Fly Ash on Air-Entrained Concrete," *Concrete InFocus*, Fall, 2006, pp. 71–72.

[34] ASTM C188: "Standard Test Method for Density of Hydraulic Cement," *Annual Book of ASTM Standards*, ASTM International, West Conshohocken, PA.

[35] Davidovits, J., "Carbon-Dioxide Green-House Warming: What Future for Portland Cement," *Emerging Technologies Symposium on Cement and Concretes in the Global Environment*, Portland Cement Association, Chicago, IL, 1993, p. 21.

Geopolymer Binder Systems
STP 1566, 2013
Available online at www.astm.org
DOI:10.1520/STP156620120095

Kunal Kupwade-Patil,[1] *Erez N. Allouche,*[2] *Courtney Alyssa Watts,*[3] *and Md. Sufian Badar*[4]

Selected Studies of the Durability of Fly-Ash-Based Geopolymer Concretes

REFERENCE: Kupwade-Patil, Kunal, Allouche, Erez N., Watts, Courtney Alyssa, and Badar, Md. Sufian, "Selected Studies of the Durability of Fly-Ash-Based Geopolymer Concretes," *Geopolymer Binder Systems*, STP 1566, Leslie Struble and James K. Hicks, Eds., pp. 144–164, doi:10.1520/STP156620120095, ASTM International, West Conshohocken, PA 2013.[5]

ABSTRACT: The study reported herein investigates the performance of fly-ash-based geopolymer concretes (FA-GPC) when subjected to various durability tests. The durability of FA-GPC was examined for alkali silica reaction (ASR), chloride induced corrosion, carbonation, and sulfate attack. The ASR in FA-GPC was analyzed for three types of reactive aggregates (siliceous limestone, sandstone, and quartz). The effect of the ASR on FA-GPC was found to depend on the calcium contents of the fly ash (FA). FA-GPC made using Class F FA were found to be less vulnerable to ASR as compared with specimens made using Class C FA. Measured values of expansion were below the 0.1 % limit specified by ASTM C1260 [2007, "Standard Test Method for Potential Alkali Reactivity of Aggregates (Mortar-Bar Method)," *Annual Book of ASTM Standards*, ASTM International, West Conshohocken, PA] for all FA-GPC specimens. FA-GPC specimens made from Class F FA exhibited lower corrosion rates and

Manuscript received June 23, 2012; accepted for publication December 26, 2012; published online April 29, 2013.

[1]Research Assistant Professor, Alternative Cementitious Binders Laboratory, Dept. of Civil Engineering, Louisiana Tech Univ., Ruston, LA 71272, United States of America, e-mail: kunalk@latech.edu

[2]Associate Professor of Civil Engineering, Director, Alternative Cementitious Binders Laboratory, Dept. of Civil Engineering, Louisiana Tech Univ., Ruston, LA 71272, United States of America, e-mail: allouche@latech.edu

[3]Research Assistant, Alternative Cementitious Binders Laboratory, Louisiana Tech Univ., Ruston, LA 71272, United States of America, e-mail: caw039@latech.edu

[4]Ph.D. Candidate, Alternative Cementitious Binders Laboratory, Dept. of Civil Engineering, Louisiana Tech Univ., Ruston, LA 71272, United States of America, e-mail: msb042@latech.edu

[5]ASTM Symposium on *Geopolymer Binder Systems* on June 26 -27, 2012 in San Diego, CA.

porosity compared to their Class C FA-GPC and OPC counterparts. Overall, FA-GPC specimens showed limited signs of leaching or corrosion product formation, while OPC specimens exhibited the formation of multiple corrosion products along with significant leaching. Carbonation studies on FA-GPCs prepared with Class C and F FA suggested that carbonation had limited effect on geopolymer binders as rates were well below the threshold for initiation of corrosion. In addition, durability tests were performed on the effect of external sulfate attack on geopolymer concrete using calcium, sodium, and magnesium sulfates. The sulfate ingress treatment was accelerated using applied electro kinetics by applying a constant current density of 1 A/m^2 for 1 week. A decrease in compressive strength was observed due to sodium and magnesium sulfates, while an increase was observed in the case of the calcium sulfates. Geopolymer concrete mortars and pastes perform satisfactorily when exposed to the three sulfate sources, but did not outmatch the performance of OPC Type V cements.

KEYWORDS: durability, geopolymer concrete, corrosion, carbonation, sulfate attack

Introduction

Fly-ash-based geopolymer concrete has the potential to serve as a driver for a paradigm shift in the construction industry toward the development of highly durable, "green," cost-competitive, and low energy-consuming cementitious binder, which features a negligible carbon footprint. Geopolymer concrete is an emerging class of cementitious material, providing 100 % substitute to Portland cement in civil infrastructure applications [1–3]. Seeking to enter niche applications in the $2800 billion per annum cementitious binders global market, geopolymer cements offer an intriguing mixture of superior physical attributes, extensive environmental benefits, and strong prospects for commercial implementation. The field of inorganic polymer cements also presents significant scientific challenges associated with the need for a better understanding of the geopolymerization reaction involved, the relationships between mix design characteristics, the short- and long-term mechanical properties of the resulting cementitious matrix, and the overall durability of the material.

Davidovits first introduced the term "geopolymers" to classify 3D polymeric networks of silico-aluminate binders [1]. The polymerization process involves a rapid reaction of silico-aluminate minerals in the source material with the alkali metal hydroxide/silicate activator solution. The outcome of the polymerization reaction is a 3D polymeric chain/network structure of Si–O–Al/Si–O–Si bonds. The two main ingredients used in preparation of geopolymers are alkaline liquids and source materials that are rich in silica and alumina such as kaolinite, fly ash, and slag [2]. The alkaline liquids typically used are sodium hydroxide (NaOH) or potassium hydroxide (KOH) in combination with sodium silicate. When geopolymers are blended together with aggregates, the resulting mixture can be handled and cast in the same manner as Portland cement-based concrete. Compared to ordinary Portland cement (OPC), geopolymer concrete (FA-GPC) features better overall durability; however, a detailed investigation of durability of FA-GPC and its applicability in the field is required [4].

The utilization of fly ash for the manufacturing of geopolymers represents a significant opportunity for enhanced environmental benefits and cost reduction [5]. Additional benefits can be achieved by using an activator solution prepared from hydroxide and silica-rich industrial waste. Geopolymers are considered eco-friendly construction materials in two distinct ways, i.e., (a) reducing the need for Portland cement and the associated CO_2 emission, and (b) converting currently utilized coal combustion products into beneficial construction materials, thus reducing landfill and disposal facility requirements [6]. Geopolymer concrete technology is particularly attractive because it is not limited to Class C fly ash (for which there is a high demand in the cement industry), but can utilize Class F fly ash (most of which is currently disposed) [7]. Additionally, geopolymers can tolerate higher concentrations of ammonia and other impurities in the raw fly ash compared to current Portland cement applications. This is of particular importance in view of recent air emission regulations imposed on the coal-fired power stations. Measures taken to meet these new standards are expected to adversely affect some traditional utilization of coal-fired by-products because of increased level of impurities. Geopolymer binders' technology offers the potential for supporting sustainable growth of our urban society for decades to come.

Physical Durability of Geopolymers

Durability of concrete has a significant influence on its service behavior, design life, and safety. The deterioration of concrete may occur through a variety of chemical or physical processes, especially when exposed to aggressive environments. The durability performance of concrete is usually examined for sulfate attack, chloride-induced corrosion, resistance to elevated temperatures, atmospheric carbonation, alkali silica reaction (ASR), and freeze-thaw attack.

Micro-structural damage induced by sulfate attack in concrete is a cause of primary concern in building foundations and other structures. Geopolymer mortar specimens showed greater stability when immersed in sodium sulfate solution [8,9]. It was observed that the aggressive nature of the sulfate ion had a minimal negative effect on the evolution of microstructure and on the mechanical strength of the material. The results show that geopolymer concrete mortars and pastes perform satisfactorily when exposed to sulfates. In origin, geopolymer concretes do not contain $Ca(OH)_2$ and monosulphoaluminate, which are being formed from calcium. When geopolymer concrete is exposed to sodium sulfate solutions, there is no growth of gypsum or ettringite, and thus, no cause of expansion.

Alkali silica reaction (ASR) is initiated during the dissolution and condensation-polymerization processes, while the material is still in a gel-like form. The potential for ASR in geopolymer concrete is considered minimal, even with high alkali content. ASR test results indicated that OPC showed a

higher expansion by a factor of six when compared to FA-GPC specimens [10]. In addition, OPC specimens showed signs of severe leaching, minor cracking, and a possible indication of delayed ettringite formation. An XRD analysis of FA-GPC specimens revealed an amorphous layer, which was formed via reaction between the geopolymeric gel and calcium on the surface of the aggregates, resulting in a strong bond at the aggregate/matrix interface.

Limited research has been conducted to date regarding the chloride corrosion resistance of steel reinforcement embedded in FA-GPC matrices. Previous durability related studies suggested that fly-ash-based geopolymers are able to passivate the steel reinforcement, and the stability of the passive layer depends on the concentration of the activator solution [11]. Recent studies conducted showed that the reinforced geopolymer concrete had a greater resistance to chloride penetration because of the dense nature of FA-GPC, and a strong mechanical interlock at the rebar/concrete interface, thus inhibiting the ingress of chloride ions [4]. Reinforced FA-GPC specimens exhibited lower corrosion rates and diffusion coefficients by a factor of 7 when compared to their OPC counterparts, suggesting that FA-GPC concrete might serve as substitute for OPC in reinforced concrete structures located in marine environments or when subjected to prolonged exposure to brackish water. In addition, geopolymer concrete exhibits a higher resistance to acid attack. Studies show that FA-GPC has a high acid resistance as evidenced by reduced mass loss and almost unchanged microstructure prior to and following acid exposure [12].

Experimental Procedures

Method of Preparation

This study examines the durability of geopolymer concretes prepared from both Class C and F fly-ash stockpiles. The chemical composition of fly-ash stockpiles obtained via x-ray fluorescence spectroscopy is shown in Table 1. Class F fly ashes were obtained from Dolet Hills power generation station located at Mansfield, LA and Avon Lake, OH, while the Class C fly ash was obtained from Monticello power generation station located at Mount Pleasant, TX. Sodium hydroxide (14 M NaOH) and sodium silicate obtained from PQ Corporation was used as an activator for preparation of FA-GPC specimens. Sodium silicate composed of 45 % by weight and SiO_2 to Na_2O ratio was 2:1. Sodium silicate to sodium hydroxide ratio was 1:1 and the activator (sodium hydroxide + sodium silicate) to binder ratio was 0.5. After 24 h of batching, the FA-GPC specimens were removed from the molds and cured at a temperature of 80° C for 72 h.

Alkali Silica Reaction

The specimens were batched as per ASTM C490 using reactive aggregates known to initiate ASR reaction [13]. Aggregates used in the testing program

TABLE 1—*Chemical composition of fly-ash stockpiles.*

Raw Material (%)	Fly Ash DH (Class F)	Fly Ash OH (Class F)	Fly Ash MN (Class C)
SiO_2	58.52	55.07	55.61
Al_2O_3	20.61	28.61	19.87
SiO_2/Al_2O_3	2.84	1.94	2.80
CaO	5.00	1.97	12.93
Fe_2O_3	9.43	6.22	4.52
MgO	1.86	1.08	2.49
SO_3	0.49	0.19	0.49
Na_2O	0.52	0.38	0.67
K_2O	–	2.63	0.86
LOI	0.05	1.82	0.22

included quartz, sandstone, and siliceous limestone. These aggregates were selected and prepared as per ASTM C1260 [14]. The specimen dimension was 254 mm in length and 51 mm in breadth and height. Class F fly ashes were obtained from Dolet Hills power generation station (PGS), Mansfield, LA, and Avon Lake PGS, OH, and were abbreviated as "DO" and "OH," respectively. Class C fly ash was obtained from Monticello PGS located at Mount Pleasant, TX, and was designated "MN" as shown in Table 1.

The FA-GPC (Class C and F) specimens were batched using a chemical activator solution (a blend of sodium silicate and 14 M sodium hydroxide), which was mixed with the designated fly ash, fine aggregates, and coarse aggregates. Four specimens were prepared for each combination of binder (i.e., fly-ash stockpile or OPC) and reactive aggregate (i.e., limestone, sandstone, and quartz), for a total of 48 specimens as shown in Table 2. All the specimens were immersed in 1 M NaOH and were placed in an oven at 80 °C. Length change measurements were conducted as per ASTM C490. A SEM analysis was done using a Hitachi S-4800 field emission scanning electron microscope (FE SEM) manufacture by Hitachi, Pleasanton, CA.

Chloride-Induced Corrosion

An experimental investigation was undertaken to evaluate the effect of chloride-induced corrosion on reinforced FA-GPC specimens manufactured from Class F and C fly-ash stockpiles. ASTM G109 specimens were cast using fly-ash-based FA-GPCs and Portland cement Type I [15]. The specimens were 280 mm in length, 114 mm in width, and 150 mm in height. Steel rebars used were 10 mm in diameter and 381 mm in length, as shown in Fig. 1. Plexiglas dams 75 mm wide, 150 mm long, and 75 mm in height were secured using silicone caulk to the top of the cementitious specimens. The specimens were subjected to intermittent wetting and drying cycles of saltwater, with the solution being placed in the Plexiglas dams during the wet cycles. Wet–dry saltwater

TABLE 2—*Summary and designation of binder precursors and aggregates.*

Type of Binder	Source	Fly-Ash Designation	Aggregate	Abbreviation
Fly Ash (Class F)	Dolet Hills Power Generation Station (PGS) Mansfield, LA	Dolet Hills	Quartz	DH-Q
		Dolet Hills	Limestone	DH-LM
		Dolet Hills	Sandstone	DH-S
Fly ash (Class F)	Avon Lake PGS Ohio	Ohio	Quartz	OH-Q
		Ohio	Limestone	OH-LM
		Ohio	Sandstone	OH-SS
Fly ash (Class C)	Monticello PGS Mount Pleasant, TX	Monticello	Quartz	MN-Q
		Monticello	Limestone	MN-LM
		Monticello	Sandstone	MN-SS
Ordinary Portland cement (Type I)	Commercial vendor	OPC	Quartz	OPC-Q
		OPC	Limestone	OPC-LM
		OPC	Sandstone	OPC-SS

cycles consisted of 14 days of 7.5 % NaCl solution exposure (wet cycle), followed by air exposure for 14 days (dry cycle). A high concentration NaCl solution was used to simulate severe conditions and aggravate corrosion. Plastic covers placed on top of the Plexiglas dams were used to minimize atmospheric evaporation. A relative humidity of 50 ± 5 % was maintained during the experiment. Half-cell potential measurements were performed as per Ref [11]. A copper–copper sulfate (CSE) half-cell reference electrode (manufactured by Tinkor and Rasor Inc., San Gabriel, CA) was used to measure the corrosion potential. The half-cell potential was determined by measuring the voltage difference between a reference electrode and the embedded reinforcement using a multimeter. Potentials were recorded using a high-impedance voltmeter with a 1 mV resolution. The corrosion current density of the reinforcement was determined using a linear polarization resistance (LPR) technique. In this study, the LPR experiments were performed using a Solartron potentiostat (model no. 1287, manufactured by Roxboro Group Company, United Kingdom). LPR measurements were taken at a scan rate of 0.1 mV/s from − 20 mV to + 20 mV.

FIG. 1—*ASTM G109 [15] specimens subjected to saltwater exposure.*

TABLE 3—*Interpretation of severity of corrosion rates.*

Corrosion Rate (mpy)	Deterioration (Years)
<0.10	No corrosion damage
0.10 < CR < 0.5	10–15
0.5 < CR < 5	2–10
>5	<2

A plot was developed for the current density and potential variation. The polarization resistance (Rp) is the ratio of change in measured potential to the change in applied current per unit area (Δi) [16].

$$R_p = \frac{\Delta E}{\Delta i} \tag{1}$$

The corrosion current density (I_{corr}) was calculated using the value of R_p and proportionality constant (B). The internal resistance (IR) drop was corrected by using a feedback compensation technique. Guideline for relating I_{corr} with the severity of corrosion is given in Table 3.

$$I_{corr} = \frac{B}{R_p} \tag{2}$$

The resulting value of I_{corr} was used to calculate the corrosion rate (CR), which was derived from Faraday's law as [17]

$$CR = \frac{K_1 \times I_{corr} \times EW}{\rho} \tag{3}$$

where CR is the corrosion rate (mills per year), K_1 is Faraday's constant, EW is the equivalent weight, and ρ is density. The internal resistance (IR) drop was corrected by using feedback compensation technique.

The charge that passed through the reinforced concrete specimens was used to estimate the chloride ion permeability (ASTM C1202) [18]. The total current (I_j) was measured from the voltage (V_j) developed between the anodic and cathodic reinforcement, which were separated by a 100-Ω resistor [15].

$$I_j = \frac{V_j}{100} \tag{4}$$

The charge density (CD) of corrosion in coulombs was calculated by

$$CD_j = CD_{j-1} + \left[(t_j - t_{j-1}) \times \left(\frac{I_j + I_{j-1}}{2} \right) \right] \tag{5}$$

TABLE 4—*Guidelines for chloride ion penetrability based on charge passed [18].*

Charge Passed (Coulombs)	Chloride Ion Penetrability
>4000	High
2000 to 4000	Moderate
1000 to 2000	Low
100 to 1000	Very low
<100	Negligible

Where t = time in seconds, at which the measurement of the macrocell current occurred, and I = macrocell current (amps) at time (t_i). The charge density that was measured was related to chloride ion penetrability using Table 4 as per ASTM C1202 [18]. Porosity was measured using mercury intrusion porosimetry (MIP) with the sample powdered to pass a No. 30 sieve. MIP tests were carried out using Micromeritics Autopore IV 9500. High pressure was applied delivering a peak pressure of 226 MPa.

Sulfate Attack and Carbonation

The experimental setup for evaluating the effect of external sulfate attacks on properties of FA-GPC specimens and OPC controls is shown in Fig. 2. Cylindrical concrete specimens approximately 150 mm (6 in.) in length and 76 mm (3 in.) in diameter were prepared using a mix design in accordance with ACI 211.1 [19]. The OPC and Type V mix was prepared as per ASTM C192 with w/c ratio of 0.5 [20]. Class F fly ashes were obtained from Dolet Hills power

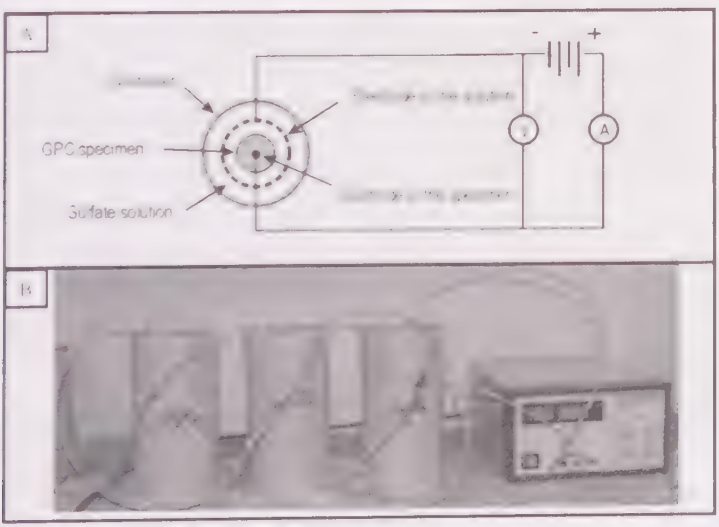

FIG. 2—*Experimental setup of accelerated sulfate ingress in FA-GPC and OPC specimens.*

generation station (PGS), Mansfield, LA, and Avon Lake PGS, OH, and were designated as "DH" and "OH," respectively. Class C fly ash was obtained from Monticello PGS located at Mount Pleasant, TX, and was designated as "MN" (refer to Tables 1 and 2).

Mixed-metal oxide coated titanium wire electrodes (Corrpro, Medina, OH), of 127 mm (5 in.) in length, were placed at the center of each specimen. The specimen was lime-water cured for 7 days at 23 °C. A 35.5 g/l solution of reagent-grade anhydrous sodium sulfate was prepared for specimen immersion. As specified by ASTM C1012, a solution-to-specimen volume ratio of 4:1 was used for specimen immersion at 23°C [21]. The sulfate solution was refreshed weekly, coinciding with length change measurements.

The test specimens were exposed to calcium, sodium, and magnesium sulfate solutions for a period of 30 days. Twelve specimens of each type (FA-GPC, OPC-Type I, and OPC-Type V) were maintained in limewater as control specimens with no sulfate exposure. Following the 30-day period, sulfate ions were extracted from the test specimens for 7 days using the treatment circuit shown in Fig. 2. The negative pole of the power supply was connected to the outer electrode (mixed-metal oxide-coated titanium wire) and the positive pole to the inner wire electrode. The applied current density was 1 A/m^2 as calculated over the outside surface area of the cylinder. The outer electrode was a single loop of the same type of titanium wire that was configured to surround the exterior surface of the specimen. Specimens were subjected to a compressive strength test, which is one of the preferred methods for evaluating the effect of sulfate attack in concrete [22].

An initial study on the effect of carbonation on reinforced geopolymer concrete was conducted. Reinforced cylindrical geopolymer specimens were batched using two Class F and one Class C fly ashes. OPC specimens were also prepared in comparison to FA-GPC samples. The carbonation process was performed in a climatic chamber in which both temperature and relative humidity were controlled. A CO_2 gas tank was used to pass the gas inside the chamber and was tightly sealed to prevent any leakage (see Fig. 3). Long-term data is expected to validate the results of this preliminary test. Corrosion potential and rates were measured to examine the severity of corrosion condition.

Results and Discussion

Alkali Silica Reaction in Geopolymer Concrete

The results of the expansion test, performed as per ASTM C1260 [14], for mortar bar specimens immersed in 1 M NaOH solution at 80°C, are presented in Fig. 4. The FA-GPC specimens made from Dolet Hills, Monticello, and Ohio fly-ash stockpiles showed average expansion of 0.07 %, 0.03 %, and 0.008 %,

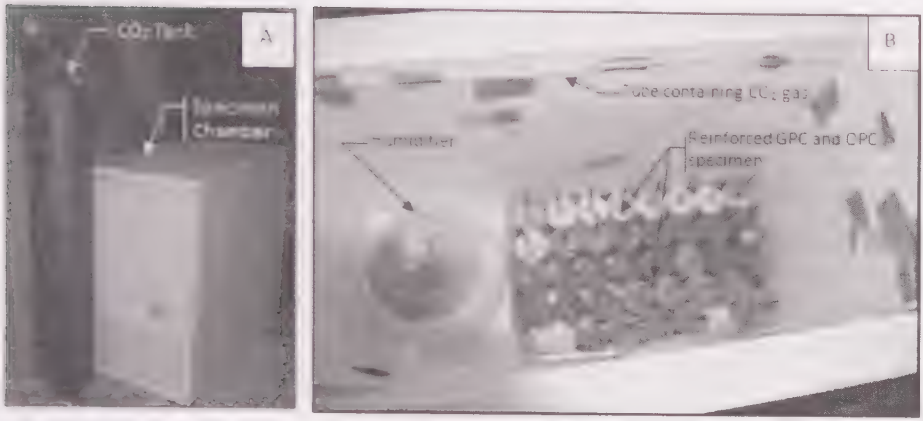

FIG. 3—*Experimental setup for carbonation in geopolymer concrete.*

respectively, following a 14-day immersion treatment. Expansion values following a 34-day exposure to sodium hydroxide solution were 0.024 %, 0.021 %, and 0.031 %. At the end of 90 days of exposure, OH showed 0.06 % while DH and MN exhibited 0.09 %, respectively. An average expansion value

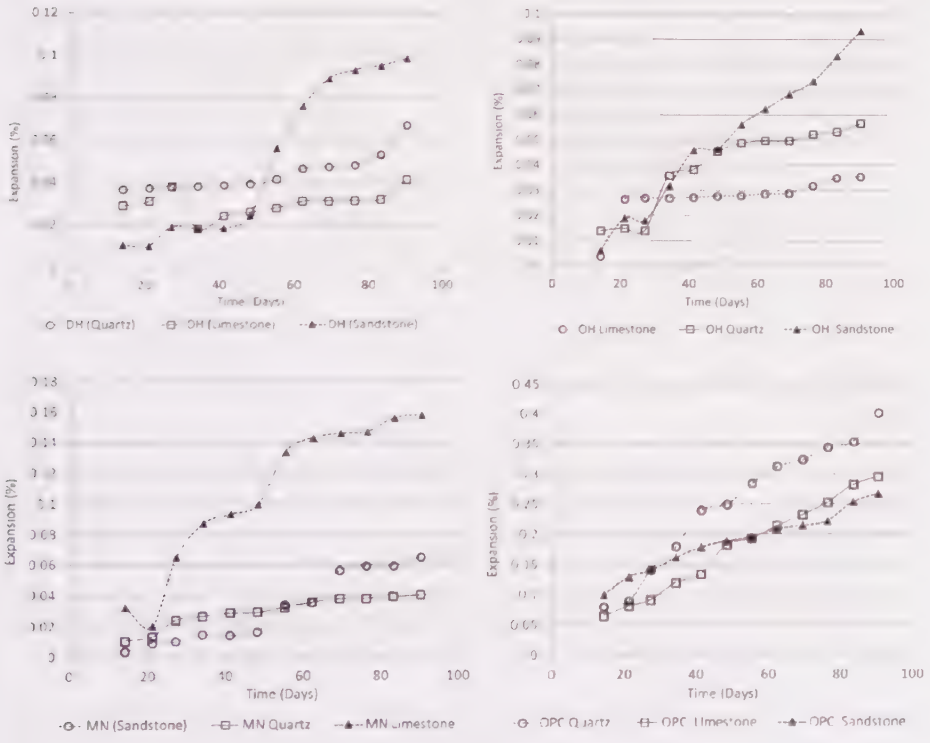

FIG. 4—*ASR Expansion data as per ASTM C1260 [14].*

of 0.32 % was observed for OPC specimens. None of the 36 FA-GPC specimens exceeded the ASTM threshold (0.1 %), and most appeared to be stable. The OPC concrete made from quartz, limestone, and sandstone exhibited an average expansion of 0.1 % after 27 days, exceeding the ASTM threshold (0.1 %). Expansion values for the OPC concrete specimens were found to be ~5 times greater than these of their FA-GPC counterparts following 90 days of exposure to NaOH. Expansion values observed for the OPC specimens proved that the aggregates used in this study were indeed reactive.

SEM micrographs of FA-GPC concrete made with MN and OH are shown in Figs. 5 and 6, respectively. FA-GPC-MN specimens exhibited ASR gel formation at the aggregate/matrix interface (see Fig. 5). An increase in calcium content between a random location in the matrix (Ca = 7 %) and a location at the aggregate–paste interface (Ca = 22 %) was observed. MN fly ash (Class C) contains higher calcium content as compared with the Class F fly ashes (i.e., OH). NaOH exposure resulted in slight dissolution of silica gel, decreasing the

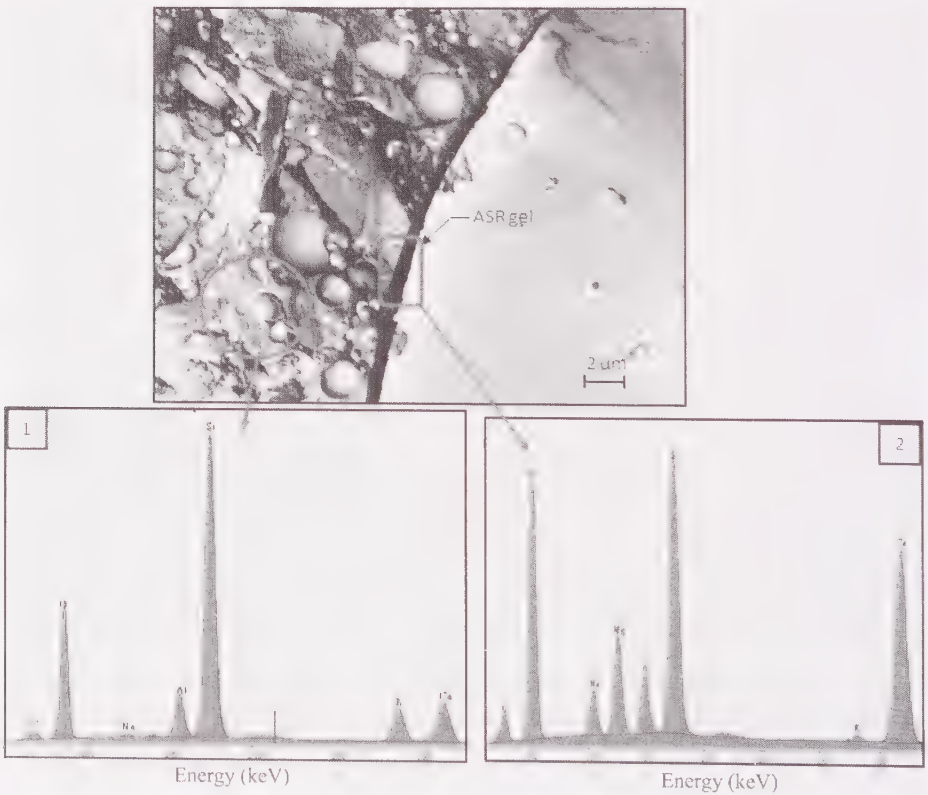

FIG. 5—*SEM image and EDS of FA-GPC using Class C fly ash (MN) exhibiting the ASR gel. Location "1" indicates the matrix while location "2" the aggregate matrix interface (adapted with permission of ASCE [10]).*

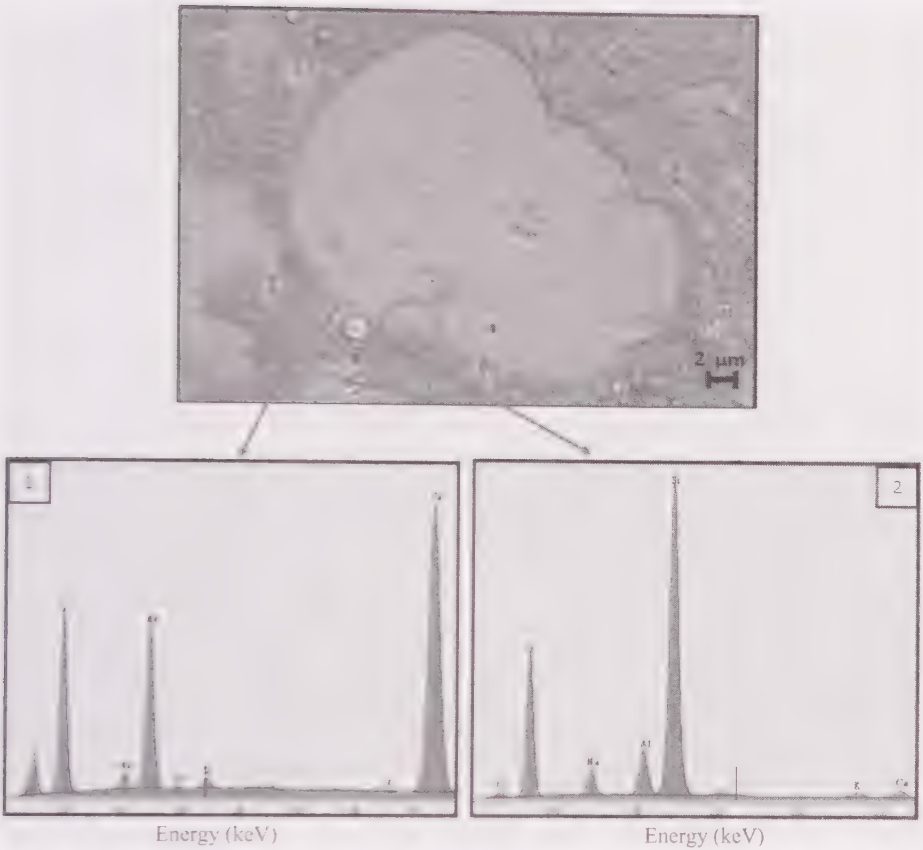

FIG. 6—*SEM image and EDS spectrum of FA-GPC concrete prepared using OH fly ash (Class F). No signs of ASR gel formation were observed at the aggregate–matrix interface (adapted with permission of ASCE [10]).*

silica content from 30 % at location 1 to 23 % at location 2, while increasing calcium content at the ASR reaction product. Increased sodium content in the ASR product was also observed. The ASR expansion could be attributed to the presence of sodium at the product site. Thus, FA-GPC made with high calcium content fly ash could initiate ASR reaction products when used with reactive aggregates.

During the NaOH exposure, hydroxyl ions from the cement paste depolymerized the silica in the aggregate along with alkali-metal ions, generating alkali-silica gel [23,24]. This silica gel caused volumetric expansion, the outcome of which can be seen in Fig. 4. This clearly demonstrates that the aggregates used in the current work were deleterious in nature. The aggregate–cement matrix interface of the FA-GPC samples made with Class F fly ash (Ohio and Dolet Hills) did not exhibit any indication of ASR gel formation as shown in Fig. 6. Expansion values for the FA-GPC samples were well

below the ASTM threshold limit, suggesting that the specimens were innocuous to the reactive aggregate and did not cause reaction product formation. This work supports the notions that fly-ash-based geopolymer concrete is significantly less vulnerable to ASR compared to OPC-based concrete. Utilizing ASR vulnerable aggregates in the production of geopolymer concrete products could contribute to economic advantage in areas where deposits of high-quality aggregates have been depleted.

Chloride-Induced Corrosion in FA-GPC

The average corrosion rates using linear polarization resistance are shown in Fig. 7. Each reading shows the average of three specimens. At the end of the saltwater exposure, corrosion rate values for FA-GPC specimens prepared from Class F fly-ash stockpiles (DH and OH) were 0.04 mpy and 0.085 mpy, respectively, while values of 0.37 and 0.97 mpy were recorded for MN (Class C-GPC) and OPC specimens (see Fig. 7). The corrosion condition of each specimen was estimated based on its corrosion rate value following the guideline given in Table 3. The DH and OH specimens were found to lie in the passive state; the MN specimens were expected to corrode in a period of 10–15 years, while the OPC specimens reside well within the high corrosion severity range, expecting severe degradation within 2 years.

The charge measured in coulombs as per ASTM G109 [15] specimens for the OPC and FA-GPC samples are shown in Fig. 8. Following 154 days of saltwater exposure, DH and OH specimens measured 1600 and 3400 Cs,

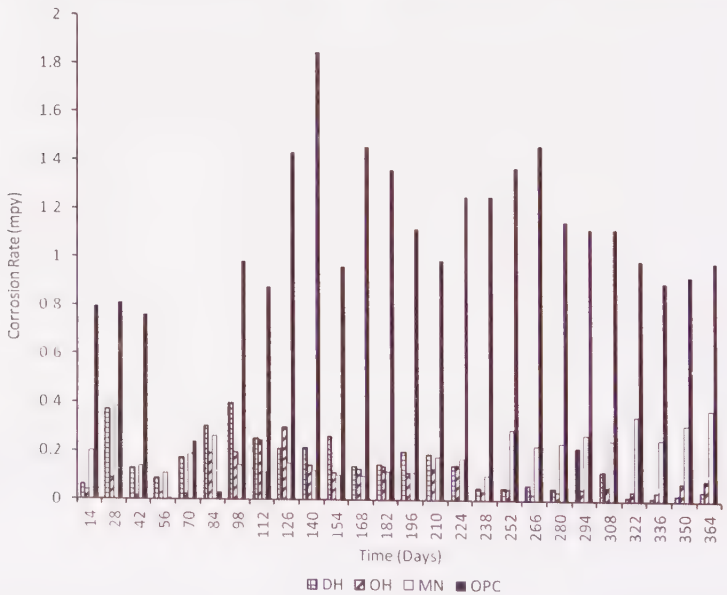

FIG. 7—*Corrosion rates of the top rebar of FA-GPC and OPC concretes.*

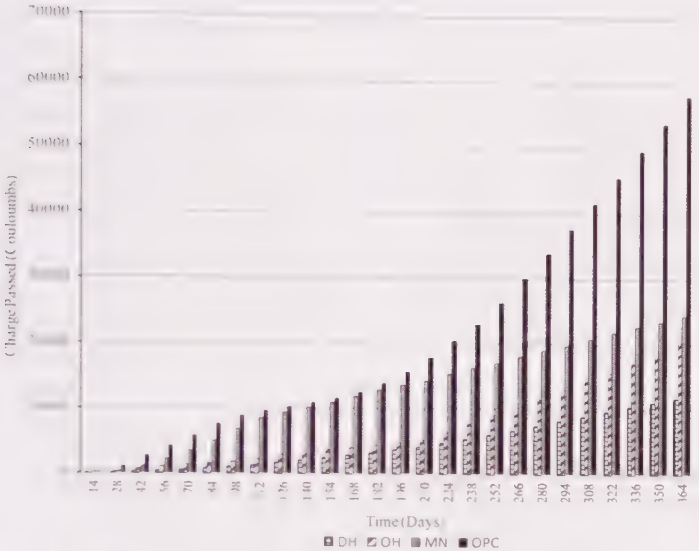

FIG. 8—*Charge measured in coulombs for FA-GPC and OPC.*

respectively, whereas MN and OPC measured 10 200 and 11 000 Cs. Referring to Table 4, FA-GPC specimens made using DH fly ash permitted low chloride ion penetrability; OH specimens exhibited a moderate level of chloride ion penetrability, while MN and OPC specimens exhibited high levels of chloride ion penetrability. At the end of the saltwater exposure, the OPC specimens measured 59 000 Cs, while the FA-GPC Monticello, OH, and Dolet Hills measured 25 000, 20 300, and 12 000 Cs, respectively. FA-GPC specimens made from Class F fly ash exhibited chloride ion penetrability values smaller by a factor of 3 to 5 compared to the OPC specimens.

FA-GPC and OPC specimens after 88 days and 1 year of saltwater exposure are shown in Fig. 9. The OPC specimens exhibited corrosion products along with significant leaching, whereas the FA-GPC specimens exhibited no signs of severe leaching (refer to Fig. 9(*a*) and 9(*b*)). The rebar/cementitious matrix interface of FA-GPC and OPC specimens are shown in Fig. 9(*c*) and 9(*d*). OPC specimens exhibited widespread presence of corrosion products at the rebar/concrete interface, while none of the FA-GPC specimens exhibited visible signs of corrosion products. The compressive strength and porosity measured after 1 year of saltwater exposure is shown in Fig. 10. Class F FA-GPCs, DH and OH, displayed compressive strengths of 66 and 63 MPa, respectively. The corresponding porosity values at the rebar/concrete interface at the termination of the saltwater exposure were 8 % and 11 %. Compressive strengths of 59 and 55 MPa and porosity values of 14 % and 21 % were obtained for the MN and OPC, respectively. FA-GPCs prepared with Class F FA were less vulnerable to chlorides penetration as compared to Class C FA.

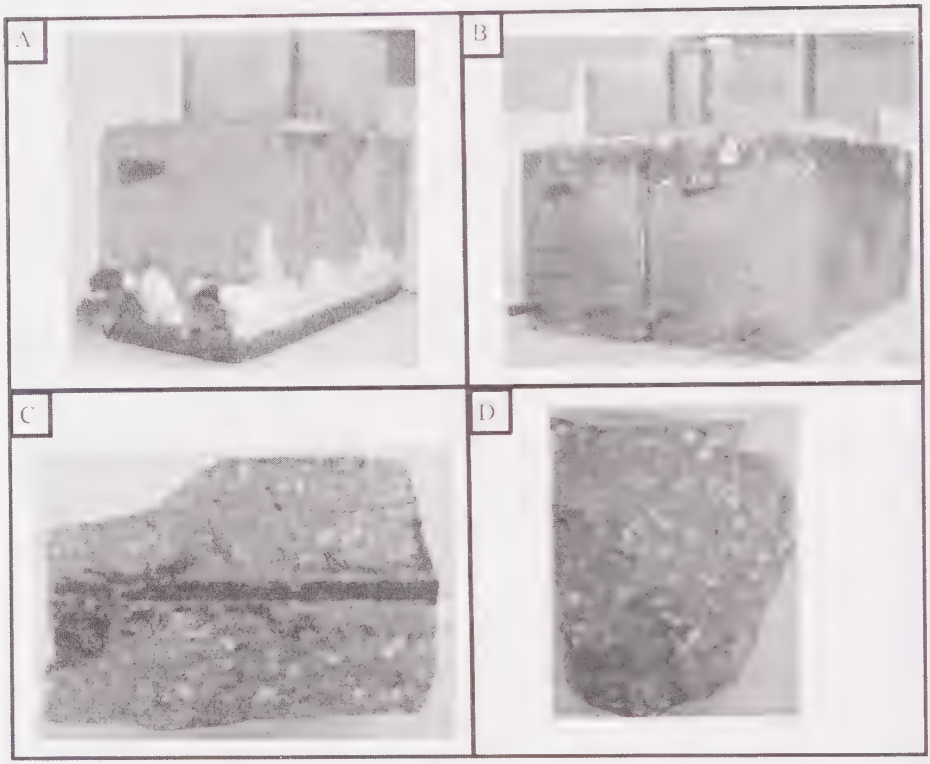

FIG. 9—*(a) Leached OPC, and (b) non-leached FA-GPC after 88 days of saltwater exposure, (c) corroded OPC at the rebar/matrix interface, and (d) non-corroded FA-GPC after 1 year of saltwater exposure.*

Class F FA-GPC samples were found to exhibit lower corrosion rates and porosity as compared to their Class C counterparts. The low chloride ion penetrability observed for the FA-GPC specimens implies a lower chloride ion concentration at the rebar/concrete interface. FA-GPC "DH" provided the highest level of resistance to chloride ingress and corrosion, possibly because of a more complete geopolymerization process, and consequently, a denser matrix, hypothesis supported by the low porosity value (8 %). This implies that the activation of the fly ash and the extent of the subsequent geopolymerization process could play a vital role in the ability of the FA-GPC matrix to resist chloride ingress. Overall, FA-GPC specimens made from Class F fly ash exhibited a significantly higher resistance to chloride induced corrosion compared to OPC specimens as well as FA-GPC specimens made from Class C fly ash.

Sulfate Attack in Geopolymer Concrete

The compressive strength of OPC and FA-GPC specimens subject to 1 year of exposure to $NaSO_4$, $MgSO_4$, and $CaSO_4$ is shown in Fig. 11. Class F fly-ash

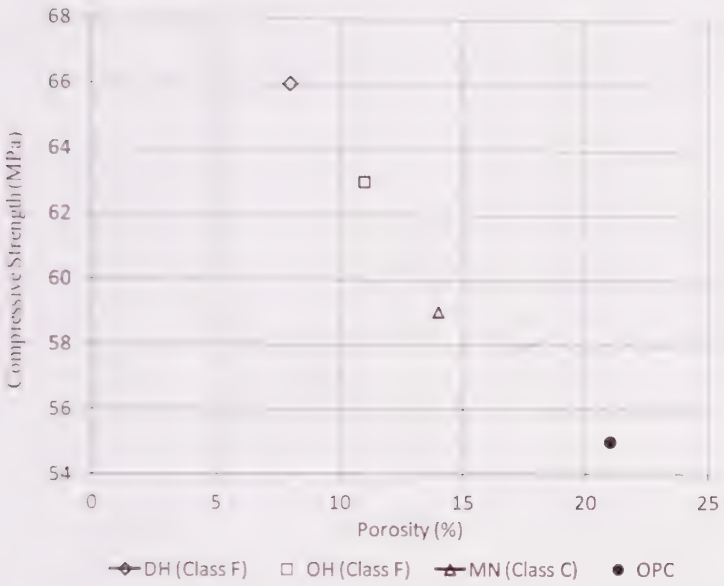

FIG. 10—*Compressive strength versus porosity after 1 year of saltwater exposure.*

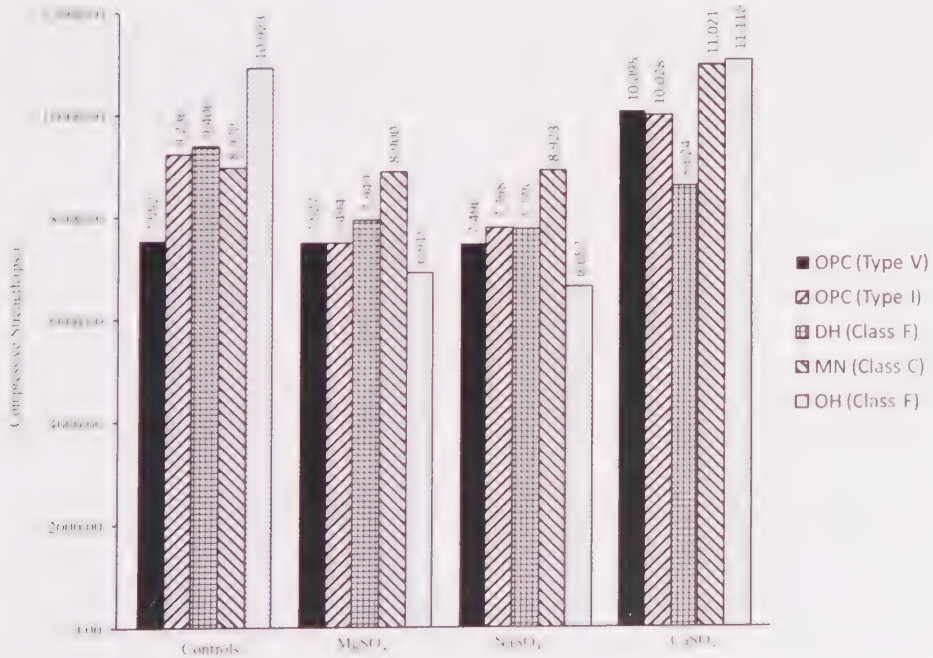

FIG. 11—*Compressive strength of FA-GPC and OPC's subjected to three types of sulfates.*

GPC (DH and OH) exhibited a decrease in compressive strength by 15 % and 36 %, for $MgSO_4$, 16 % and 39 % for $NaSO_4$, respectively. An increase in compressive strength by 2 % was observed for OH, while a decrease by 9 % was observed for DH when subjected to $CaSO_4$. When compared to the controls the Class C, FA-GPC exhibited a decrease in compressive strength ~2 %, for both $MgSO_4$ and $NaSO_4$, while an increase of 18 % was observed for $CaSO_4$. The OPC Type V was not affected by magnesium and sodium sulfates, while it saw an increase in compressive strength by 25 % when compared to the controls. As for OPC Type I, a decreases in compressive strengths of 19 % and 15 % was observed for $MgSO_4$ and $NaSO_4$, while the specimens immersed in $CaSO_4$ saw a slight increase in compressive strength. The increase in compressive strength for OPCs could be related to the formation of additional C-S-H because of the presence of calcium. However, further micro-structural and chemical analyses are required to validate this hypothesis. An increase in compressive strength among FA-GPCs (OH and MN) when subjected to $CaSO_4$ could be related to the formation of hydrated calcium aluminio silicate (C-A-S-H), in addition to the formation of sodium alumino silicate hydrate (N-A-S-H) [25]. Further research is required to investigate the effect of sulfates on the FA-GPC microstructure and the formation of delayed ettringite in the FA-GPC matrix.

Carbonation in FA-GPC

The corrosion potentials and rates of FA-GPC and OPC specimen's subject to 1 year of CO_2 exposure are shown in Figs. 12 and 13, respectively. The FA-GPC specimens prepared with Class F fly ash showed corrosion potentials in the range of (−800 to −900 mV) between day 50 and day 100 days of

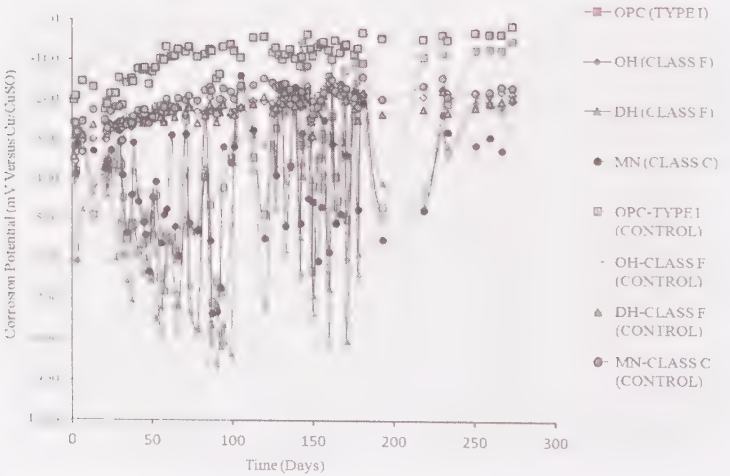

FIG. 12—*Corrosion potential of FA-GPC and OPC samples subjected to 1 year of CO_2 exposure.*

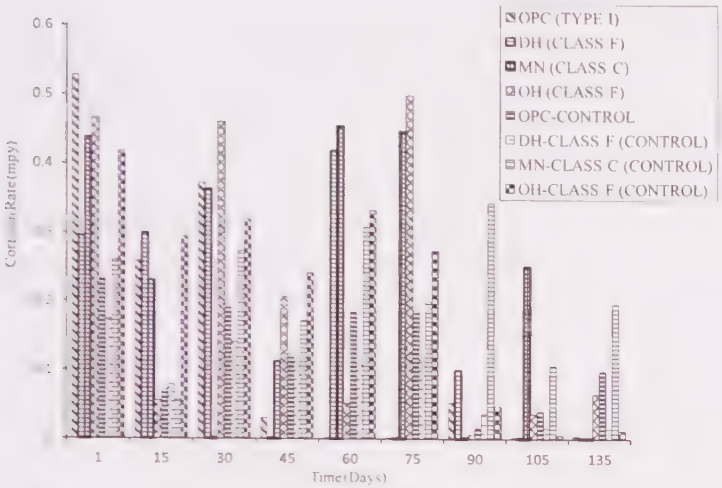

FIG. 13—*Corrosion rates of OPC and FA-GPC specimens subject to CO_2 exposure.*

exposure, while a majority of the Class C fly ash exhibited corrosion potentials in the range of −400 to −550 mV during the same period. The cumulative corrosion potential and rates after 30, 60, and 135 days, is shown in Table 5. The ASTM C786 does not relate the corrosion potentials (E_{corr}) to corrosion current density, which utilized in calculating the corrosion rates [17]. Limited studies have been conducted in relating the negative corrosion potentials to corrosion current densities for corroding structures [26]. FA-GPC specimens prepared with Class F fly ashes (DH and OH) exhibited a corrosion potential of −411 mV and CR of 0.323 mpy. Upon 60 days of wet–dry cycle of CO_2 exposure, the corrosion rate decreased to 0.261 mpy, while the negativity of corrosion potential increased from −411 mV to −504 mV. After 135 days, the corrosion rate dropped further, whereas the negativity of the corrosion potential increased to −515 mV. This phenomenon could be related to the lack of oxygen, which can be indicated by the decrease in corrosion rate causing an increase the negativity of the corrosion potential [26,27]. Similar trend was observed in case of OPC specimens. In the case of FA-GPC specimens prepared with Class C fly ash (MN), the corrosion current increased from 0.222 to

TABLE 5—*Cumulative corrosion potential and rates subject to various time periods.*

Time (days)	30		60		135	
Binder Type	E_{corr} (mV)	CR (mpy)	E_{corr} (mV)	CR (mpy)	E_{corr} (mV)	CR (mpy)
Class F	−411	0.323	−504	0.261	−515	0.184
Class C	−326	0.222	−396	0.247	−406	0.215
OPC	−367	0.386	−463	0.237	−430	0.138

0.247 mpy after 60 days, indicating that the passive film has been destroyed. After 135 days, the corrosion rate dropped from 0.247 to 0.215 mpy, while increasing the corrosion potential from −396 to −406 mV, indicating a decrease in oxygen, which commonly occurs because of carbonation [16]. This data indicates that the FA-GPCs prepared with Class F fly ash might be more durable as compared to the Class C fly ashes, which can be related to the decrease in corrosion rates. Further studies aimed at better understanding of the carbonation mechanism in FA-GPC and for establishing correlations between electrochemical measurement and the microstructure and pore structure of geopolymer concretes are currently underway.

Conclusion

This work supports the notions that fly-ash-based geopolymer concrete is significantly less vulnerable to ASR compared to OPC-based concrete. Utilizing ASR vulnerable aggregates in the production of geopolymer concrete products could provide economic advantage in areas where high-quality deposits of aggregates have been depleted. FA-GPCs prepared with Class F FA were less vulnerable to chlorides penetration as compared with Class C FA. Class F fly-ash GPC samples were found to exhibit lower corrosion rates and porosity as compared to their Class C counterparts. Overall, FA-GPC specimens made from Class F fly ash exhibited a significantly higher resistance to chloride-induced corrosion compared to OPC specimens, as well as FA-GPC specimens made from Class C fly ash. Carbonation studies indicate that the FA-GPCs prepared with Class F fly ash might be more durable as compared to Class C fly ashes, which can be related to the decrease in corrosion rates. In the case of sulfate attack on FA-GPC, specimens suffered strength loss because of sodium and magnesium sulfates, whereas an increase in strength was observed in the presence of calcium sulfates. In comparison to the FA-GPCs, OPC Type V cement exhibited superior resistance to all the threes sulfates ($CaSO_4$, $MgSO_4$, and $NaSO_4$).

References

[1] Davidovits, J., *Geopolymer Chemistry and Applications*, Institut Géopolymère, Saint-Quentin, France, 2011.

[2] Duxson, P., Fernández-Jiménez, A., Provis, J., Lukey, G., Palomo, A., and van Deventer, J. S. J., "Geopolymer Technology: The Current State of the Art," *J. Mater. Sci.*, Vol. 42, No. 9, 2007, pp. 2917–2933.

[3] Provis, J. L. and Van Deventer, J. S. J., *Geopolymers: Structure, Processing, Properties and Industrial Applications*, Woodhead, Cambridge, U.K., 2009.

[4] Kupwade-Patil, K., Allouche, E. N., Vaidya, S., and Diaz, E., "Corrosion Analysis of Reinforced Geopolymer Concretes," *Concrete Solutions*, CRC Press, Boca Raton, FL, 2011.

[5] Duxson, P., Provis, J., Lukey, G., and van Deventer, J. S. J., "The Role of Inorganic Polymer Technology in the Development of 'Green Concrete,'" *Cement Concrete Res.*, 2007, Vol. 7, No. 12, pp. 1590–1597.

[6] Melbourne, R. N., "Build 'Em High, and Make Them Green," *New Sci.*, Vol. 197, No. 2640, 2008, pp. 28–29.

[7] Juenger, M. C. G., et al., "Advances in Alternative Cementitious Binders," *Cement Concrete Res.*, Vol. 41, No. 12, 2011, pp. 1232–1243.

[8] Bakharev, T., "Durability of Geopolymer Materials in Sodium and Magnesium Sulfate Solutions," *Cement Concrete Res.*, Vol. 35, No. 6, 2005, pp. 1233–1246.

[9] Fernandez-Jimenez, A., García-Lodeiro, I., and Palomo, A., "Durability of Alkali-Activated Fly Ash Cementitious Materials," *J. Mater. Sci.*, Vol. 42, No. 9, 2007, pp. 3055–3065.

[10] Kupwade-Patil, K. and Allouche, E. N., "Impact of Alkali Silica Reaction on Fly Ash Based Geopolymer Concrete," *J. Mater. Civil Eng.*, Vol. 25, No. 1, 2013, pp. 131–139.

[11] ASTM C786-09: "Standard Test Method for Corrosion Potentials of Uncoated Reinforcing Steel in Concrete," *Annual Book of ASTM Standards*, ASTM International, West Conshohocken, PA.

[12] Rostami, H. and Brendley, W., "Alkali Ash Material: A Novel Fly Ash-Based Cement," *Environ. Sci. Technol.*, Vol. 37, No. 15, 2003, pp. 3454–3457.

[13] ASTM C490/C490M: "Standard Practice for Use of Apparatus for the Determination of Length Change of Hardened Cement Paste, Mortar, and Concrete," *Annual Book of ASTM Standards*, ASTM International, West Conshohocken, PA.

[14] ASTM C1260: "Standard Test Method for Potential Alkali Reactivity of Aggregates (Mortar-Bar Method)," *Annual Book of ASTM Standards*, ASTM International, West Conshohocken, PA.

[15] ASTM G109: "Standard Test Method for Determining Effects of Chemical Admixtures on Corrosion of Embedded Steel Reinforcement in Concrete Exposed to Chloride Environments," *Annual Book of ASTM Standards*, ASTM International, West Conshohocken, PA.

[16] Broomfield, J. P., *Corrosion of Steel in Concrete: Understanding, Investigation and Repair*, Taylor & Francis, London, 2007.

[17] ASTM G102: "Standard Practice for Calculation of Corrosion Rates and Related Information from Electrochemical Measurements," *Annual Book of ASTM Standards*, ASTM International, West Conshohocken, PA.

[18] ASTM C1202-12: "Standard Test Method for Electrical Indication of Concrete's Ability to Resist Chloride Ion Penetration," *Annual Book of ASTM Standards*, ASTM International, West Conshohocken, PA.

[19] ACI 211.1, 1991, "Standard Practice for Selecting Proportions for Normal, Heavy Weight and Mass Concrete," American Concrete Institute, Farmington Hills, MI.

[20] ASTM C192/C192M: "Standard Practice for Making and Curing Concrete Test Specimens in the Laboratory," *Annual Book of ASTM Standards*, ASTM International, West Conshohocken, PA.

[21] ASTM C1012: "Standard Test Method for Length Change of Hydraulic-Cement Mortars Exposed to a Sulfate Solution," *Annual Book of ASTM Standards*, ASTM International, West Conshohocken, PA.

[22] Boyd, A. J. and Mindess, S., "The Use of Tension Testing to Investigate the Effect of W/C Ratio and Cement Type on the Resistance of Concrete to Sulfate Attack," *Cement Concrete Res.*, Vol. 34, No. 3, 2004, pp. 373–377.

[23] Diamond, S., "A Review of Alkali-Silica Reaction and Expansion Mechanisms. 1: Alkalies in Cements and in Concrete Pore Solutions," *Cement Concrete Res.*, Vol. 5, No. 4, 1975, pp. 329–345.

[24] Diamond, S., "A Review of Alkali-Silica Reaction and Expansion Mechanisms. 2: Reactive Aggregates," *Cement Concrete Res.*, Vol. 6, No. 4, 1976, pp. 549–560.

[25] Shi, C., Jiménez, A. F., and Palomo, A., "New Cements for the 21st Century: The Pursuit of an Alternative to Portland Cement," *Cement Concrete Res.*, Vol. 41, No. 7, 2011, pp. 750–763.

[26] Poursaee, A. and Hansson, C. M., "Potential Pitfalls in Assessing Chloride-Induced Corrosion of Steel in Concrete," *Cement Concrete Res.*, Vol. 39, No. 5, 2009, pp. 391–400.

[27] Soleymani, H. R. and Ismail, M. E., "Comparing Corrosion Measurement Methods to Assess the Corrosion Activity of Laboratory OPC and HPC Concrete Specimens," *Cement Concrete Res.*, Vol. 34, No. 11, 2004, pp. 2037–2044.

Geopolymer Binder Systems
STP 1566, 2013
Available online at www.astm.org
DOI:10.1520/STP156620120061

Rodney W. Zubrod[1]

Performance-Based Specification for Geopolymer Cement Binders and Supporting Laboratory Data

REFERENCE: Zubrod, Rodney W., "Performance-Based Specification for Geopolymer Cement Binders and Supporting Laboratory Data," *Geopolymer Binder Systems*, STP 1566, Leslie Struble and James K. Hicks, Eds., pp. 165–184, doi:10.1520/STP156620120061, ASTM International, West Conshohocken, PA 2013.[2]

ABSTRACT: This paper documents laboratory testing and results showing that a new performance-based ASTM standard specification is appropriate for geopolymer concrete. The paper will provide recommended guidelines for the specification and limit the analysis to alkali-activated pozzolan cements, with no Portland cement. Specific performance-based specifications and supporting test data will be presented that characterize the minimum requirements for geopolymer concrete proposed for use in any construction application, without the need for the application of external heat. These performance specifications will include shrinkage, set-time, compressive strength, freeze and thaw resistance, chloride ion penetration resistance, sulfuric and hydrochloric acid attack resistance, elastic modulus, and Poisson's ratio. The specification does not include specific constituent detail, but is performance-based.

Introduction

Portland cement production increases global greenhouse gas emissions through the development of clinker in hydrocarbon-heated furnaces. If the calcination of various ingredients to produce cement can be removed, this would be a positive contribution to the construction industry if normally expected quality characteristics can be maintained or exceeded. Although various Portland cement production greenhouse gas emission reports are published and are dependent

Manuscript received June 8, 2012; accepted for publication April 11, 2013; published online May 8, 2013.

[1]SRMZ Technical, Inc., Farmington, New Mexico 87401, United States of America.

[2]ASTM Symposium on *Geopolymer Binder Systems* on June 26–27, 2012, in San Diego, CA.

upon the constituent materials and the kiln combustion fuel, calculations based on the International Energy Authority [1] and generally accepted Portland production industry values (1 ton of Portland production emits 1 ton of carbon dioxide) suggest that the production of Portland cement contributes approximately 7 % of global greenhouse gas emissions.

Geopolymer cements consist of alkalis and/or alkali silicates combined with naturally occurring or man-made pozzolans. For the purpose intended herein, the analysis will be limited to sodium alkalis and sodium alkali silicates. Geopolymer cements are more resistant to sulfate attack, acid attack, chloride ion penetration, and freeze and thaw degradation. Geopolymer cements achieve these quality characteristics through the development of calcium silicate hydrate (CSH), a high aluminosilicate content, and a low water and gas permeability feature. For the purpose intended herein, CSH is defined as the by-product of the combination of any added or ancillary (contained in other products) calcium hydroxide or free lime, with sodium silicate.

Although naturally occurring pozzolans will satisfy the quality and durability necessities for geopolymer concrete (alkali-activated fly ash concrete), its traditional and environmentally positive attribute is that it typically utilizes fly ash as its base and majority ingredient. Huge volumes of fly ash are currently being generated around the world through coal power generation. Most of the fly ash is not used and a large part is disposed of in landfills. As the need for power increases, the volume of fly ash will increase. Although sustainable and "green" power generation methods are being developed such as wind and solar, these methods will not replace coal power generation any time soon. Disposal of fly ash and other coal combustion by-products is becoming more difficult with new and ever-changing regulations. Existing stockpiles of fly ash and bottom ash will sustain the production of alkali-activated fly ash concrete for centuries to come, with or without continued coal power generation.

The U.S. Department of Transportation Federal Highway Administration (FHWA) published a brief in March of 2010 [2]. This brief noted "User-friendly geopolymer cements that can be used under conditions similar to those suitable for Portland Cement are the current focus of extensive world-wide research efforts. These cements must be capable of being mixed with relatively low-alkali activating solutions and must cure in a reasonable time under ambient conditions (Davidovits 2008). Until such cements are developed, geopolymer applications in transportation infrastructure will be limited. The production of versatile, cost-effective geopolymer cements that can be mixed and hardened essentially like Portland Cement would represent a 'game changing' advancement, revolutionizing the construction of transportation infrastructure."

Although for obvious reasons the publication of successful "game-changing" mixture recipes that satisfy the intent of the above-referenced FHWA brief have not occurred, this document indicates that successful

processes and mixtures have been developed, but does not disclose the specific constituents or processes.

In the presence of less harmfully caustic (nearer to Portland *p*H) but high-quality geopolymer production approaches, a specification is necessary that allows for the production of these mixtures, without disclosing the specific processes or materials therein. Despite the dynamic and improved modulus properties of geopolymer concretes, current structural design assumptions and requirements should not be altered, including those presented in the American Concrete Institute *Manual of Concrete Practice* [3]. A revision of these structural design documents allowing for equivalent or better cementitious materials in lieu of traditional Portland cements is proposed.

Current researchers and developers utilize calcined and hydrous materials/minerals, fly ash (ranging from high to low calcium oxide contents), various chlorides, various sulfates, and various forms of sodium, potassium, magnesium, and other hydroxides combined with silicates of various elements and ion concentrations to produce geopolymer cements/concrete with low to no shrinkage, high strength, low permeability (air and water), variable modulus properties, and high resistance to chloride, sulfate, and low *p*H material penetration/attack. The mixtures produced with these specific constituents can be utilized in various applications including self-consolidating, self-leveling, conventional, permeable, cellular, and shotcrete mixtures, to name a few. The geopolymer mixtures utilize dry and liquid forms of hydroxides, silicates, and other proprietary materials.

Because various combinations of assorted minerals, hydroxides, silicates, and other materials will achieve similar but higher-quality properties, limiting the specification to specific concentrations of explicit materials will constrain researchers and developers unnecessarily. However, production must be controlled for quality purposes using specifications that incorporate controls and measures. This document describes controls that allow the technical architectural, structural, and materials design communities to utilize any number of high-quality geopolymer concrete mixtures.

Significance

Coal power generation is a current necessary evil, so to speak. The derogatory nature of coal power generation consists of the waste materials produced during coal burning. The waste consists of various materials including bottom ash, fly ash, flue-gas desulfurization materials (most typically calcium sulfite or calcium sulfate), and various flue-gas materials including carbon dioxide, carbon monoxide, nitrous dioxide, mercury, and sulfur dioxide to name a few of the primaries. The production of Portland cement requires the production of clinker in rotary kilns using coal, natural gas, and other combustible hydrocarbons for heat. The production of similar and many times exacting waste

materials occurs with the production of Portland cement, and, therefore, any measures possible to reduce greenhouse gas emissions through a reduction of Portland cement usage is a positive step, providing safety and quality can be maintained. Alkali-activated fly ash (geopolymer) concrete reduces greenhouse gas emissions by removing Portland cement, and utilizes waste materials from the production of electrical power and steel. Therefore, measures taken to accommodate the use of geopolymers are environmentally positive on a global scale.

Laboratory Program

The data presented herein consists of selected data from laboratory studies performed over the last several years. The materials and proportions presented are provided in a generalized form to avoid any implied commercialization and to maintain confidentiality of proprietary recipes.

Our program was begun as a result of Portland cement scarceness in our region that led to requests to design concrete mixtures with a substantial reduction or complete removal of Portland cement. At the time, early available information in 2006 on geopolymer and alkali-activated fly ash concretes indicated that heat treatment at 140°F to 180°F (60°C to 82.2°C), with and without humidity control, for 6 to 12 h was necessary to avoid undesirable and substantial low strength and drying shrinkage. In construction applications other than controlled pre-cast concrete production, such heat treatment efforts would be prohibitive, and a key objective of our work is to find a way to produce such concrete without heat treatment.

Although our home base region includes the presence of two commercial coal burning power generation facilities and an associated plentiful supply of coal combustion waste products for use in geopolymers, our laboratory has been engaged in various concrete material design projects that originated in Sweden, China, Canada, the United Arab Emirates, Germany, and the United States. Accordingly, various sources of aggregate, mineral, pozzolan, chemical, and waste products from coal power generation and steel production were available for our mixture analysis in geopolymers.

The projects described above performed for projects in and outside the United States were primarily oriented toward development of self-leveling, self-consolidating, cellular, conventional, and pneumatically placed concretes. These design processes were applied using geopolymers of which conventional mixture analysis is presented herein.

Using low calcium Class F fly ash (maximum 4 % CaO) and conventional liquid or dry sodium silicates, initial set time was quite long, exceeding 24 h unless heat or electrical treatment was applied. Adding calcium hydroxide or calcium oxide in variable concentrations (from 0.001 to 0.010 mol/m^3 in the

added water) remedied this issue. But then the mixtures quickly began to lose cohesion. The addition of sodium citrate dihydrate, glucose derivatives, and other proprietary products including waste synthetic polymer materials (including but not limited to polyethylene, silicon, cellulose, and neoprene) provided for set-time control (from 5 min to 6 h for initial set).

Mixture heat development was seen from perhaps 5 F with calcium hydroxide to about 30 F with additions of calcium oxide (2.8 C to 16.7 C, respectively).

Waste synthetic polymer materials were limited to those with small particle size, those that degraded partially or wholly in high *p*H environments, and those that were typically disposed of in landfills. Although some carbonation was observed, synthetic waste polymers and other proprietary materials mitigated it effectively.

When utilizing high calcium Class C fly ash or granulated ground blast furnace slag (GGBFS), inherent free lime contents were sufficient to increase strength substantially. Initial set-time was very rapid, often within 5 min, but set-time was controlled using similar additions as described above. Also, some conventional Portland cement chemical set-time retarders were found to be effective when using high calcium fly ash or GGBS.

When using sodium metasilicate (dry silicate), heat development occurred similar to the heat developed when using calcium oxide. This characteristic was reduced by using sodium metasilicate pentahydrate, which produced a temperature rise of only about 3 F (1.7 C). However, the pentahydrate failed to completely integrate into the mixture without first reducing its particle size or combining it with metasilicate (a minimum of 5 % metasilicate and a maximum of 95 % pentahydrate).

Drying shrinkage measured on specimens treated with from 140 F to 180 F (60 C to 82.2 C) heat in laboratory ovens (no humidity control), or electrical treatment (described below) produced negligible or no shrinkage over extended periods (including 2.7 years).

Drying shrinkage of laboratory-cured specimens (cured in laboratory conditions with a 7-day initial water submersion) was in excess of 0.5 % and specimens degraded considerably as evidenced by surface and full-depth cracking (in 75 mm by 75 mm by 250 mm specimens). Shrinkage was controlled initially by adding expansive materials; for example, magnesium and calcium sulfate combined with calcium hydroxide and other proprietary materials. But this approach was abandoned because of carbonation in mixtures containing expansive ettringite (by-product of the combination of some sulfates and oxides). Drying shrinkage was ultimately controlled using proprietary materials, primarily minerals, and adjusting the size and proportion of these materials using a standard 0.45 power-grading chart. The size distribution analysis of particles was performed

using a spreadsheet developed internally. The proportions were adjusted to an approximate maximum density (grading was near the maximum density/zero air voids line). Because of the fact that extremely small silica particles degraded in the initial high *p*H environment produced with sodium silicates and hydroxides, many times the lower portion of the composite grading was kept above the maximum density line to create a dense mortar portion even in the presence of degrading materials. Each individual mineral material size was reported by the supplier with percentages of sizes within approximately three to four ranges. Individual mineral material sizes varied from about 0.5 μm to about 50 μm. Through trial and error processes, adjustments were made to the distribution of particles and corresponding shrinkage tests performed until shrinkage was moderated. Degrading silica materials created a sticky texture to the mixture, which was mitigated with proprietary materials and calcium hydroxide.

The heat treatment was performed in standard laboratory ovens at 170°F (76.7°C) temperature. Typical heat curing lasted for 7 h, with no rest period prior to entering the oven. Relative humidity during this treatment was approximately 15 % to 30 % and not controlled. Compressive strength test results varied with treatment time.

Electrical curing was also used. Initially, 3-in. diameter and 6-in. tall cylindrical specimens were fabricated. They were treated only after initial set; otherwise, electrical treatment caused excessive heat and damaged the specimens. Our initial attempts at electrical treatment utilized the rapid chloride permeability (RCP) testing apparatus, which induced a 60-volt dc (DC) electrical charge through the specimen, which produced a temperature in excess of 190°F within 15 s as measured with a standard infrared laboratory thermometer. By reducing the time of the current to 2 s, pulsed every 5 s for a total of 120 s, we were able to achieve similar strength and drying shrinkage characteristics as with heat treatment without damaging the specimens or producing excessive heat. Final electrical treatment processes utilized a standard rheostat voltage control device and was performed on slightly larger specimens, 4-in. diameter by 8-in. tall specimens, with 5 to 60 V DC or 10 to 120 V AC for variable times and pulse sequences. It was determined that electrical treatment on geopolymer mixtures reduced necessary curing times to a minimum of approximately 5 min using higher voltage currents (DC or AC), and approximately 30 min using lower voltage currents, as compared to approximately 7 h using heat treatment, or days and weeks using conventional ambient or water curing environments.

For the test results presented herein and representing typical normal production batch operations, no liquid materials were used with the exception of mixing water. More specifically, the geopolymer mixtures included all dry composite materials that were added to aggregate composites, then mixing

water was added. The 3-cubic foot mixtures were then mixed for 15 min in a standard laboratory revolving mixer.

For the purpose intended herein, it is assumed that strength gain with geopolymer concrete is an issue that while measured, is not a primary analysis task because of the ease in which strength is achieved with heat and electrical treatment, and without. Therefore, our program concentrated on various durability characteristics including shrinkage, resistance to freeze and thaw cycle degradation, resistance to chloride penetration using the rapid chloride permeability procedure, resistance to acid exposure degradation, and elastic modulus/Poisson's ratio determinations.

Test Results

As noted in the commentary above, specific mixture details are not provided. However, a generalized description of the mixtures presented herein is provided below.

Drying shrinkage (length change) was measured in general accordance with the ASTM C157 [4] test procedure, except the samples were maintained in the laboratory environment after the 7-day water soaking period. Length change was measured and calculated on a percentage basis from the initial

TABLE 1—*General mixture composites of constituents exceeding 10 % of total volume.*

	Limestone Size #57	Limestone Sand	Quartzite Size #67	Quartzite Sand	Silicate (%)	Low Calcium Fly Ash (F)	High Calcium Fly Ash (C)
Sample series A	Yes	Yes	No	No	15	Yes	No
Sample series B	Yes	Yes	No	No	25	Yes	No
Sample series C	Yes	Yes	No	No	35	Yes	No
Sample series D	No	No	Yes	Yes	15	Yes	No
Sample series E	No	No	Yes	Yes	25	Yes	No
Sample series F	No	No	Yes	Yes	35	Yes	No
Sample series G	Yes	Yes	No	No	15	No	Yes
Sample series H	Yes	Yes	No	No	25	No	Yes
Sample series I	Yes	Yes	No	No	35	No	Yes
Sample series J	No	No	Yes	Yes	15	No	Yes
Sample series K	No	No	Yes	Yes	25	No	Yes
Sample series L	No	No	Yes	Yes	35	No	Yes

Notes: All samples contained a non-reported amount and type of zeolites, kaolin clay (hydrous or calcined), GGBS, and other non-reported materials. All coarse aggregate contents were maintained at a 57-43 coarse aggregate-to-sand ratio. All fly ash contents were maintained at 500 pounds per cubic yard. The silicate % is the percentage of sodium silicate, sodium metasilicate, or sodium metasilicate pentahydrate as a percentage of all hydroxides, zeolites, fly ash, clays, and other cementing ingredients. Other non-reported materials were a maximum of 10 % of the fly ash and silicates. All batches performed were a minimum of 3-cubic-foot laboratory trials. The laboratory trials were composited based upon a 27 cubic foot per cubic yard design. Slump consistencies on all trials were maintained between 5 and 6 inches. Water contents on all trials were maintained between 200 and 225 pounds per cubic yard.

TABLE 2—*Chemical composition of select binders.*

	Granulated Ground Blast Slag, U.A.E.	Granulated Ground Blast Slag, Canada	Granulated Ground Blast Slag, U.S.	Class C Fly Ash, U.A.E.	Class F Fly Ash, U.S.	Class F Fly Ash, Sweden	Hydrous Kaolin Clay, U.S.	Calcined Kaolin Clay, Canada	Chabazite Zeolite, U.S.	Clinoptilolite Zeolite, U.S.
SiO_2	39.6	36.8	36.5	41.1	62.1	51.1	59.9	61.8	68.1	70
Al_2O_3	11.1	11.9	10.2	17.9	25.8	18.2	32.8	31.8	18.6	12.1
Fe_2O_3	0.9	1.5	1	5.3	4.42	16.6	0.9	1.1	2.84	1.6
CaO	38.8	40.5	42.1	22.1	1.9	3.9	0.8	0.4	0.27	3.4
MgO	2.5	7.2	5.4	5.5	1.24	0.9	0.1	0.3	0.75	1.5
SO_3	0.7	0.4	0.2	1.1	0.2	1.1	0.1	0.03	0.1	0.1

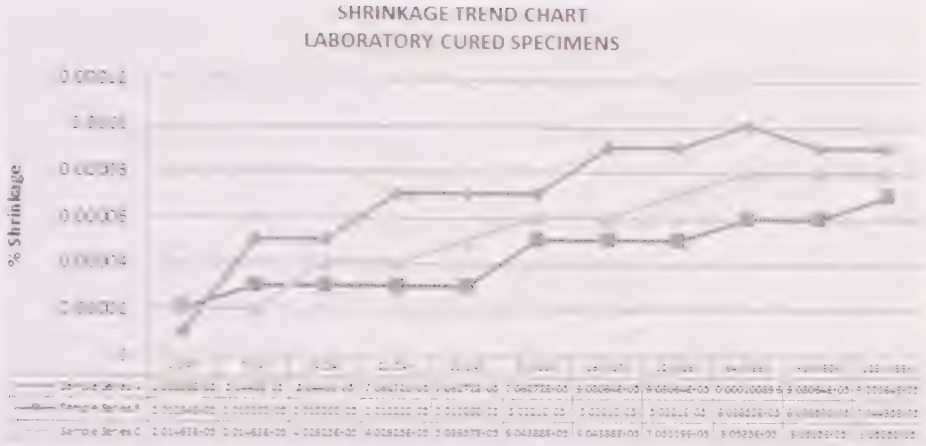

FIG. 1—*Shrinkage trend and results for sample series A, B, and C.*

measurement obtained after de-molding. Because length change of heated or electrically cured specimens was negligible or zero, only laboratory-cured specimen results are provided below.

In the absence of balancing constituent materials and adding proprietary minerals and chemicals, the shrinkage of specimens exceeded 0.5 % in all trials. The reduced shrinkage presented above was achieved partially by densely grading the fine and coarse material proportions. Through trial and error processes, proprietary minerals and chemicals were utilized to reduce mixture volume change consistently to below that generally expected with conventional Portland mixtures. Increasing proprietary minerals and chemicals induced some manageable swell in the specimens.

Resistance to freeze and thaw cycle degradation was performed in general, but altered conformance with the ASTM C666 [5] test procedure. Test

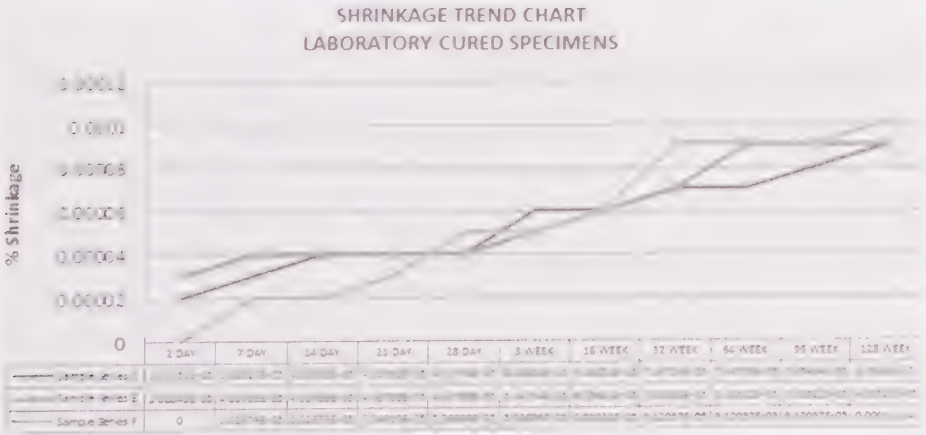

FIG. 2—*Shrinkage trend and results for sample series D, E, and F.*

FIG. 3—*Shrinkage trend and results for sample series G, H, and I.*

specimens consisted of 4-in. diameter by 12-in. long cylindrical samples molded in accordance with the ASTM C192 [6] test procedure. The dynamic modulus procedure described in the referenced ASTM C666 [5] test procedure was not used, but the ASTM C469 [7] test procedure was performed to determine the reduction of elastic modulus and strength during cycling.

Oven-treated specimens were used in our laboratory process using limestone aggregates only because the combined water absorption of the limestone aggregates was higher than that of the quartzite aggregates. Higher aggregate water absorptions generally have an increased expansion and contraction effect during freeze and thaw cycling, thereby using a worst-case scenario with the aggregates utilized. The oven-treated specimens provided a reasonable range of compressive strength and elastic modulus and further, limited space was available in our cycling chamber for more tests.

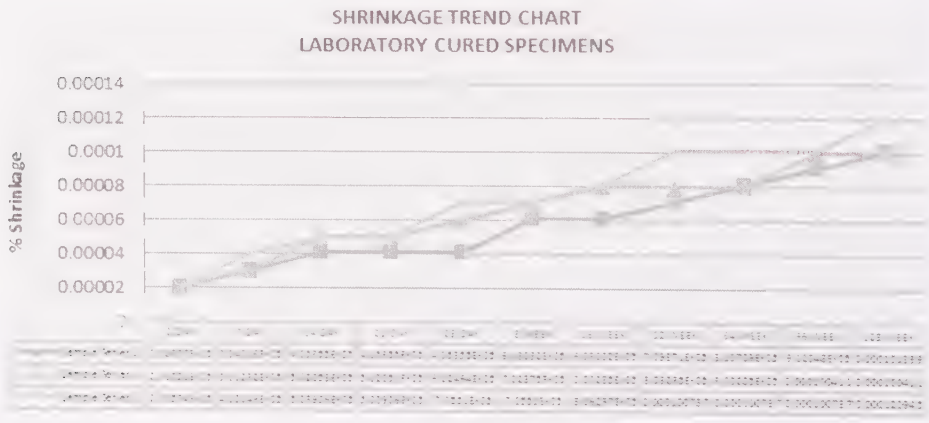

FIG. 4—*Shrinkage trend and results for sample series J, K, and L.*

TABLE 3—*Freeze and thaw durability test results all series heat-treated specimens.*

	Heat-Treated Specimens in a 170°F (77°C) Oven (7 hr)			Freeze and Thaw Durability (120 Cycles, Begin Day 2)	
	24-hr Strength (psi)	24-hr Young's (psi × 10^6)	24-hr Poisson's	Strength (psi)	Young's (psi × 10^6)
Sample series A	4250	3.9989	0.23	3890	3.6675
Sample series B	6870	5.6237	0.21	6630	5.4212
Sample series C	9310	7.5151	0.2	9400	7.6328
Sample series D	4080	4.1185	0.23	Not measured	Not measured
Sample series E	6280	5.3887	0.21	Not measured	Not measured
Sample series F	8830	7.4482	0.2	Not measured	Not measured
Sample series G	6110	6.5251	0.2	5190	5.7784
Sample series H	9040	8.1164	0.19	8470	7.9964
Sample series I	12010	10.2228	0.16	12250	10.2119
Sample series J	6190	6.5947	0.2	Not measured	Not measured
Sample series K	8910	7.6634	0.2	Not measured	Not measured
Sample series L	12240	10.0351	0.17	Not measured	Not measured

Note: All test results are the average of three specimens.

Using sample series A through C (low calcium fly ash), the retained elastic modulus is calculated at 91.7 % and 96.4 % for series A and B, respectively, and no loss for sample series C, which contained the highest silicate content. Using sample series G through I, the retained elastic modulus is calculated at 88.6 %, 98.5 %, and 99.9 %, respectively.

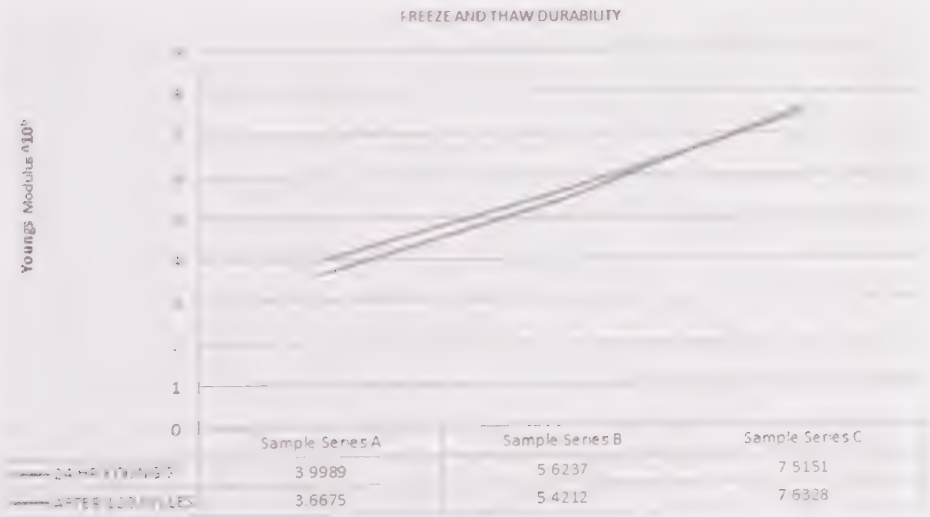

FIG. 5—*Freeze and thaw durability trend for sample series A, B, and C.*

	Sample Series G	Sample Series H	Sample Series I
24 HR YOUNG'S	6.5251	8.1164	10.2228
AFTER 120 CYCLES	5.7784	7.9964	10.2119

FIG. 6—*Freeze and thaw durability trend for sample series G, H, and I.*

ASTM C666 (dynamic modulus method) requires the specimens to be subjected to 300 cycles, or until the dynamic modulus reaches 60 % of the initial dynamic modulus. Time limitations prohibited the specimens presented herein to be cycled for 300 cycles. Although the dynamic modulus is expected to reduce on a somewhat exponential basis when approaching 300 cycles because of continued specimen degradation, the results suggest that geopolymer concrete is substantially resistant to freeze and thaw cycling when comparing results to typical air-entrained, and non-entrained Portland cement concrete test results. This is particularly evident when considering higher silicate concentrations (sample series C and I).

The revised ASTM C94 Specification presented herein requires a retained modulus of 70 %, which is more stringent than the ASTM C666 requirement.

Chloride ion penetration resistance was measured in accordance with the ASTM C1202 [8] test procedure. Samples cured with heat, and samples cured in the referenced laboratory environment were used.

The test equipment utilized for the rapid chloride permeability (ASTM C1202 [8]) was approximately 1-year old when the tests presented herein were performed. Although the test procedures are not overly complex and the equipment was relatively new, the test results prompted an investigation because of the inability to pass an electrical current through the geopolymer specimens. Based upon tests performed in varying cells using Portland cement concrete specimens side by side with geopolymer specimens, the equipment was shown to be operating correctly.

Exposure to acid resistance was measured by fully submerging 4-in. diameter by 8-in. long cylindrical specimens, in 15 % solutions of reagent grade hydrochloric or sulfuric acid. 1-day heat-treated specimens (cured for 7 h in a 170°F [77°C] oven) were utilized. Mass loss was measured after 7 days, 28 days, and 16 weeks of submersion.

TABLE 4—*Rapid chloride permeability results for heat-treated and laboratory-cured specimens*

4–in. Diameter × 2–in. Thick Cylindrical Specimens (Rapid Chloride Permeability)			
	Heat-Treated Specimens in a 170°F (77°C) Oven (7 hr)		
	Time of Test	Coulombs Passed	C1202 [8]
Sample series A	360 min	0	Negligible
Sample series B	360 min	0	Negligible
Sample series C	360 min	0	Negligible
Sample series D	360 min	0	Negligible
Sample series E	360 min	0	Negligible
Sample series F	360 min	0	Negligible
Sample series G	360 min	0	Negligible
Sample series H	360 min	0	Negligible
Sample series I	360 min	0	Negligible
Sample series J	360 min	0	Negligible
Sample series K	360 min	0	Negligible
Sample series L	360 min	0	Negligible
4-in. Diameter × 2-in. Thick Cylindrical Specimens (Rapid Chloride Permeability)			
	28-Day Laboratory-Cured Specimens		
	Time of Test	Coulombs Passed	C1202
Sample series A	360 min	0	Negligible
Sample series B	360 min	0	Negligible
Sample series C	360 min	0	Negligible
Sample series D	360 min	0	Negligible
Sample series E	360 min	0	Negligible
Sample series F	360 min	0	Negligible
Sample series G	360 min	0	Negligible
Sample series H	360 min	0	Negligible
Sample series I	360 min	0	Negligible
Sample series J	360 min	0	Negligible
Sample series K	360 min	0	Negligible
Sample series L	360 min	0	Negligible

Notes: All test results are the average of three specimens. Coulombs passed are corrected for diameter.

The test results and graphical presentation suggest that the geopolymer mixtures tested herein have an elevated resistance to very low *p*H material attack. In previous studies, Portland cement mixtures were tested in side-by-side comparison approaches. The 15 % solutions degraded air-entrained and non-entrained conventional Portland mixtures producing as much as 87.8 % mass loss during a 16-week test for limestone aggregate mixtures and 31.1 % mass loss for quartzite aggregate mixtures.

Elastic modulus, Poisson's ratio, and strength were measured in general accordance with the ASTM C469 [7] test procedure, except that vertical and transverse extensometers measured vertical and transverse strain during compression to the nearest 0.00001 in., rather than the 0.000005 in. specified in the procedure.

Geopolymer concrete mixtures can be produced with strength and elastic characteristics highly similar to conventional concrete. As demonstrated above, these characteristics were realized in a conventional 1 -, 7 -, and 28-day curing

TABLE 5—*Test results for heat-treated specimens in sulfuric and hydrochloric acid (all series).*

4-in. × 8-in. Cylindrical Specimens in 15 % Sulfuric Acid Solution			
	Heat-Treated Specimens in a 170 °F (77°C) Oven (7 hr)		
	7-Day Mass Loss (%)	28-Day Mass Loss (%)	16-Week Mass Loss (%)
Sample series A	0.21	1.12	5.08
Sample series B	0.12	0.99	4.12
Sample series C	0.03	0.08	1.55
Sample series D	0.06	0.88	2.44
Sample series E	0.00	0.08	0.86
Sample series F	0.00	0.02	0.11
Sample series G	0.44	2.85	7.32
Sample series H	0.13	1.62	5.99
Sample series I	0.06	1.11	4.81
Sample series J	0.10	0.99	1.59
Sample series K	0.08	0.65	1.32
Sample series L	0.05	0.22	1.11
4-in. × 8-in. Cylindrical Specimens in 15 % Hydrochloric Acid Solution			
	Heat-Treated Specimens in a 170 °F (77°C) Oven (7 hr)		
	7-Day Mass Loss (%)	28-Day Mass Loss (%)	16-Week Mass Loss (%)
Sample series A	0.32	2.70	5.08
Sample series B	0.22	1.51	4.12
Sample series C	0.06	0.11	1.55
Sample series D	0.15	1.20	2.44
Sample series E	0.00	0.11	0.86
Sample series F	0.00	0.05	0.11
Sample series G	0.55	4.22	7.32
Sample series H	0.28	3.10	5.99
Sample series I	0.13	1.90	4.81
Sample series J	0.22	1.84	2.66
Sample series K	0.93	1.40	2.04
Sample series L	0.14	0.83	1.77

Note: All test results are the average of three specimens.

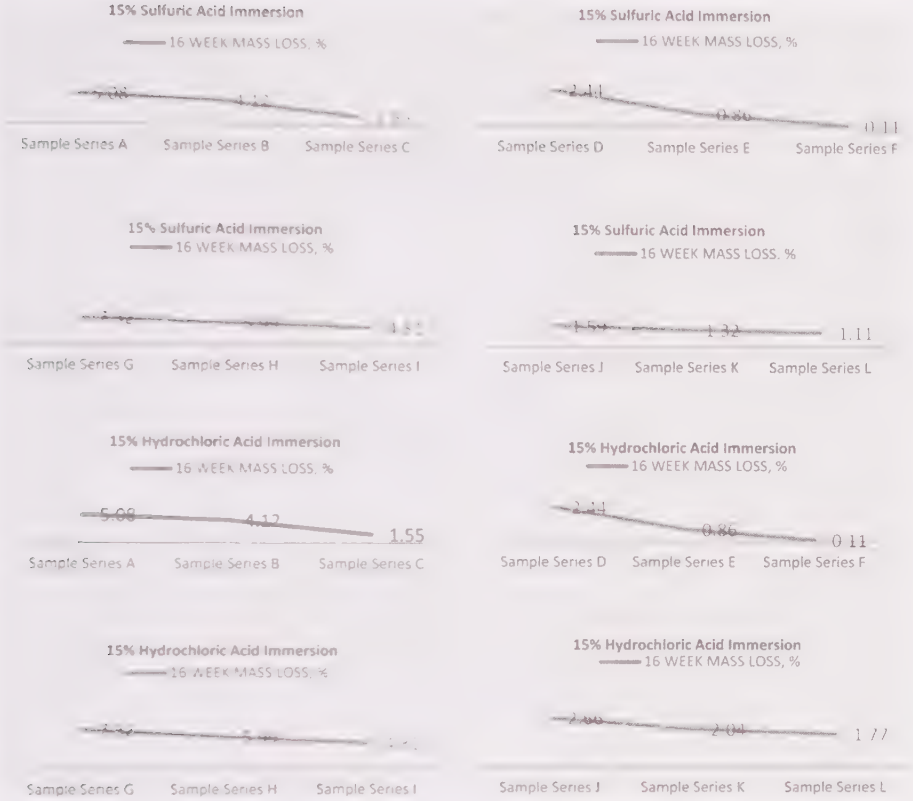

FIG. 7—*Comparison trend of mass loss in sulfuric and hydrochloric acid solutions.*

scenario, but more dynamically in a matter of hours and/or minutes with variable curing treatments. The proposed specification allows designers to select strength and elastic properties thereby meeting existing design and building code requirements, and achieving these properties in conventional or expedited methodologies.

Proposed Specification

Scope

1. This specification relates to alkali-activated fly ash concrete (geopolymer) manufactured and delivered to a purchaser in a freshly mixed and unhardened state as hereinafter specified. Requirements for quality of concrete shall be either as hereinafter specified or as specified by the purchaser. In any case where the requirements of the purchaser differ from these in this specification, the purchaser's specification shall govern. This specification does not cover the

TABLE 6—*Strength, modulus, and poisson's ratio results for heat-treated and electrically treated specimens (all series).*

	Heat-Treated Specimens in a 170°F (77°C) Oven (7 hr)		
	24-hr Strength (psi)	24-hr Young's (psi × 10^6)	24-hr Poisson's
Sample series A	4250	3.9989	0.23
Sample series B	6870	5.6237	0.21
Sample series C	9310	7.5151	0.2
Sample series D	4080	4.1185	0.23
Sample series E	6280	5.3887	0.21
Sample series F	8830	7.4482	0.2
Sample series G	6110	6.5251	0.2
Sample series H	9040	8.1164	0.19
Sample series I	12l010	10.2228	0.16
Sample series J	6190	6.5947	0.2
Sample series K	8910	7.6634	0.2
Sample series L	12l240	10.0351	0.17
	Electrically Treated Specimens (Pulsed 120 s, Tested at 24 hr)		
	24-hr Strength (psi)	24-hr Young's (psi × 10^6)	24-hr Poisson's
Sample series A	3560	3.2645	0.25
Sample series B	4710	4.6989	0.22
Sample series C	6320	5.1886	0.21
Sample series D	3770	3.3345	0.24
Sample series E	4890	4.5911	0.22
Sample series F	7150	6.1530	0.20
Sample series G	4100	3.7887	0.24
Sample series H	5260	4.6221	0.21
Sample series I	6990	5.0040	0.20
Sample series J	4290	3.6672	0.23
Sample series K	5160	5.0188	0.21
Sample series L	6950	5.3357	0.20

Note: All test results are the average of three specimens.

placement, consolidation, curing, or protection of the concrete after delivery to the purchaser, and these requirements will be provided by the supplier.

2. Geopolymer concrete is herein defined as any cementitious mixture that contains no Portland cement and relies upon heat, electricity, or ambient temperatures to react with sources of silicon (Si) and aluminum (Al), which are deposited in high, moderate, or low alkaline environments to produce a cementitious material complying with the specifications presented herein.

3. This standard does not purport to address all the safety concerns, if any, associated with its use. It is the responsibility of the user of this standard to establish appropriate safety and health practices and determine the applicability

TABLE 7—*Strength, modulus, Poisson's ratio, and set-time for laboratory-cured specimens.*

Laboratory-Cured Specimens (De-molded 24-hr After Fabrication)						
1-Day Strength (psi)	7-Day Strength (psi)	28-Day Strength (psi)	28-Day Young's (psi × 10^6)	28-Day Poisson's Ratio	Initial Time of Set (hr)	Loss of Cohesion (hr)
(A) 870	3670	4450	4.0131	0.23	3.21	1.99
(B) 1370	5540	7120	7.0922	0.20	2.25	1.46
(C) 2450	6810	9550	8.2192	0.19	2.06	1.44
(D) 960	3670	4820	4.2378	0.22	3.32	2.22
(E) 1340	5400	6920	7.1115	0.19	2.45	1.33
(F) 2390	6770	8870	7.8832	0.19	1.84	1.21
(G) 1410	4490	6930	6.5482	0.20	2.88	1.83
(H) 2550	7860	9540	8.5317	0.19	2.01	1.25
(I) 3120	9040	13880	11.1291	0.17	1.32	0.75
(J) 1400	4890	7350	7.4586	0.20	2.48	1.77
(K) 2250	7550	9220	8.2241	0.20	1.84	1.08
(L) 2970	10020	14790	11.0398	0.16	1.26	0.92

Notes: Loss of cohesion is the amount of hours when the sample was observed to lose significant slump loss. All test results are the average of three specimens. The laboratory curing environment consisted of an ambient temperature ranging from 70 °F to 74 °F (23.3 °C to 23.1 °C), and a relative humidity ranging from 15 % to 30 %.

of regulatory limitations prior to use. (Warning: fresh alkali-activated fly ash mixtures may be caustic and may cause chemical burns to skin and tissue upon prolonged use.

4. The ASTM C94/C94M-12 [9] standard specification for ready-mixed concrete is incorporated herein by reference, but with the following changes:

4a. All references to ASTM C150 [10], ASTM C595 [11], ASTM C1157 [12], or other Portland products are removed. Geopolymer mixtures will contain no Portland or blended hydraulic cements.

4b. All references to ASTM C173 [13] and ASTM C231 [14] and other air-entraining procedures and specifications are removed. All references to ACI documents are incorporated herein by reference, except ACI 211.1 [15] and 211.2 [16], 305R [17], 306R [18], and any reference to Portland cement or associated products in ACI 318 [19].

4c. Mixture design methodologies will be performed in accordance with geopolymer suppliers instructions.

4d. In 5: Materials 5.2.1 is removed. Geopolymer mixtures will utilize materials that comply with this specification, design stipulations, and local, industry, State, and Federal environmental and health requirements.

4e. In 5.2.2: supplementary cementitious materials —coal fly ash or natural pozzolans shall conform to the following:

Chemical requirements (Table 1):

Silicon dioxide (SiO_2) plus aluminum oxide (Al_2O_3); plus or minus 10 % of target.

Sulfur trioxide (SO_3), max, % 5.0.

Physical requirements (Table 2):

Fineness:

Amount retained when wet-sieved on 45 μm (No. 325) sieve.

Plus or minus 10 % of target.

Uniformity requirements:

Density, maximum variation from average, % 10.

4f. Table 1 recommended total air content for air-entrained concrete is removed.

Concrete shall have a retained dynamic modulus of a minimum of 70 % of initial modulus values when tested in accordance with the ASTM C666 [5] test method.

4g. In 6.3 Option A: References to ACI 211.1 [15] and ACI 211.2 [16] are removed. Mixture design methodologies will achieve specification performance requirements.

4h. In 6.4 Option B: 6.5 Option C is removed. The manufacturer will assume all responsibility for the selection of proprietary proportions.

4i. In 8: Air-entrained concrete is removed.

4j. In 9: Measuring materials—all references to "hydraulic cement" are replaced with geopolymer cementitious materials.

4k. In 12: Mixing and delivery—the minimum mixing time shall be specified by the manufacturer of the geopolymer materials.

4l. Minimum and maximum concrete temperatures identified in 12.8 are removed. The geopolymer material supplier will specify minimum and maximum temperatures.

4m. 14.2.2, 14.2.3, 14.2.4, 14.2.5, and 14.2.6 are removed.

5. The geopolymer mixture shall result in no greater than 0.04 % shrinkage when measured in accordance with the ASTM C157 [4] test procedure. The C157 [4] procedure will be modified to include an air bath curing after the 7-day soaking period, in accordance with ACI requirements.

6 The geopolymer mixture shall result in no greater than 1000 coulombs passed when tested in accordance with the ASTM C1202 [8] test procedure.

7. The geopolymer mixture shall result in no greater than 1 % mass loss when subjected to soaking in a 5 % sulfuric or hydrochloric acid solution. Specimens shall consist of standard 4 in. $\times$ 8 in. cylindrical samples. 28-day specimens will be utilized and soaked for 12 weeks at a temperature of 73°F $\pm$ 3 (22.8°C $\pm$ 1.7).

8. The geopolymer mixture shall result in specified elastic modulus and Poisson's ratio values.

Closure

This paper does not presume to suggest it presents every material characteristic analysis approach toward presenting a foundation for utilizing the specification. However, worldwide researchers are and have been studying this material extensively. The studies include structural failure models, contact and behavior with reinforcing steel, thermal expansion and contraction, and creep to name a few. We are aware of no studies documenting poor performance in properly designed mixtures and, as such, taken as an industry aggregate summation of study there appears to be no reason not to use this environmentally palatable and cost-effective material.

The specification presented herein is a basic approach to geopolymer concrete production, which provides the generally categorized means to produce the material. Should mixtures be produced and placed that are compliant to this specification, they will be durable features withstanding de-icing chemical attack, low *p*H material attack, freeze and thaw cycling, and construction placement issues including shrinkage. Left to their own creative approach, material developers have successfully addressed issues such as pump-ability, time of set, caustic behaviors, finish-ability, rheology, and innovative curing methodologies.

Viable mixture recipes exist, which will increase the quality of construction while reducing greenhouse gas emissions. These mixtures are user-friendly approaches to geopolymer concrete construction that will reduce climate, time, and chemical-oriented infrastructure deterioration worldwide. These mixtures will utilize waste materials humans have accumulated during our electric power production on this earth, while reducing the ongoing production of the same waste materials. If performance needs are defined, mixtures can be produced and used.

References

[1] International Energy Agency, 9 rue de la Federation, 75739 Paris Cedex 15, France.

[2] "Concrete Pavement Technology Program," *TechBrief FHWA-HIF-10-014*, U.S. Department of Transportation, Federal Highway Administration, Washington, D.C., 2010.

[3] *American Concrete Institute Manual of Concrete Practice*, American Concrete Institute, Farmington Hills, MI, 2011.

[4] ASTM C157/C157M-03, 2008, "Standard Test Method for Length Change of Hardened Hydraulic Cement, Mortar, and Concrete," *Annual Book of ASTM Standards*, ASTM International, West Conshohocken, PA.

[5] ASTM C666/C666M-03, 2008, "Standard Test Method for Resistance of Concrete to Rapid Freezing and Thawing," *Annual Book of ASTM Standards*, ASTM International, West Conshohocken, PA.

[6] ASTM C192/192M-07, 2012, "Standard Practice for Making and Curing Concrete Test Specimens in the Laboratory," *Annual Book of ASTM Standards*, ASTM International, West Conshohocken, PA.

[7] ASTM C469-02, 2010, "Standard Test Method for Static Modulus of Elasticity and Poisson's Ratio of Concrete in Compression," *Annual Book of ASTM Standards*, ASTM International, West Conshohocken, PA.

[8] ASTM C1202-07, 2012, "Standard Test Method for Electrical Indication of Concrete's Ability to Resist Chloride Ion Penetration," *Annual Book of ASTM Standards*, ASTM International, West Conshohocken, PA.

[9] ASTM C94/94M-12, 2013, "Standard Specification for Ready-Mixed Concrete," *Annual Book of ASTM Standards*, ASTM International, West Conshohocken, PA.

[10] ASTM C150/150M-11, 2012, "Standard Specification for Portland Cement," *Annual Book of ASTM Standards*, ASTM International, West Conshohocken, PA.

[11] ASTM C595/595M-11, 2012, "Standard Specification for Blended Hydraulic Cements," *Annual Book of ASTM Standards*, ASTM International, West Conshohocken, PA.

[12] ASTM C1157/C1157M-11, 2011, "Standard Performance Specification for Hydraulic Cement," *Annual Book of ASTM Standards*, ASTM International, West Conshohocken, PA.

[13] ASTM C173/173M-10b, "Standard Test Method for Air Content of Freshly Mixed Concrete by the Volumetric Method," *Annual Book of ASTM Standards*, ASTM International, West Conshohocken, PA.

[14] ASTM C231/C231M-10, "Standard Test Method for Air Content of Freshly Mixed Concrete by the Pressure Method," *Annual Book of ASTM Standards*, ASTM International, West Conshohocken, PA.

[15] ACI 211.1, 2011, "Standard Practice for Selecting Proportions for Normal, Heavyweight, and Mass Concrete," *Manual of Concrete Practice*, American Concrete Institute, Farmington Hills, MI.

[16] ACI 211.2, 2011, "Standard Practice for Selecting Proportions for Structural Lightweight Concrete," *Manual of Concrete Practice*, American Concrete Institute, Farmington Hills, MI.

[17] ACI 305R, 2011, "Guide to Hot Weather Concreting," *Manual of Concrete Practice*, American Concrete Institute, Farmington Hills, MI.

[18] ACI 306R, 2011 "Guide to Cold Weather Concreting," *Manual of Concrete Practice*, American Concrete Institute, Farmington Hills, MI.

[19] ACI 318/318M, "Building Code Requirements for Structural Concrete and Commentary," American Concrete Institute, Farmington Hills, MI.

Geopolymer Binder Systems
STP 1566, 2013
Available online at www.astm.org
DOI:10.1520/STP156620120078

John L. Provis[1]

Alkali-activated Binders and Concretes: The Path to Standardization

REFERENCE: Provis, John L., "Alkali-activated Binders and Concretes: The Path to Standardization," *Geopolymer Binder Systems*, STP 1566, Leslie Struble and James K. Hicks, Eds., pp. 185–195, doi:10.1520/STP156620120078, ASTM International, West Conshohocken, PA 2013.[2]

ABSTRACT: A key obstacle in the pathway to the widespread utilization of any novel binder technology is the issue of compliance with existing regulatory standards, which are almost always written considering the specific physicochemical properties of portland-cement-based materials. Prescriptive standards that specify allowable binder compositions are in force in many jurisdictions and are a significant obstacle to the deployment of alkali-activated binders in large-scale concrete applications. Alkali-activated concretes are ideally suited to regulation through a performance-based approach, as embodied in ASTM C1157, and this approach to standardization clearly provides more avenues for future developments in non-traditional binder systems. This paper presents an analysis of the standards environment currently facing the worldwide alkali-activation community and provides a summary of the progress that has been made in recent years (including through the work of a RILEM Technical Committee, TC 224-AAM, working in the area). The international standards environment is showing increasing acceptance of alkali-activation technology in principle, and also in some instances in practice, showing that the need for sustainable binders is driving regulatory developments in this area and thus enabling the uptake and utilization of these materials. Standards incorporating key aspects that incorporate the scope for production and accurate durability testing of alkali-activated binders are now available in some jurisdictions, and the advancement of scientific knowledge to underpin these developments has proven essential in this process.

KEYWORDS: alkali-activated binders, geopolymers, standardization, performance-based specifications

Manuscript received June 15, 2012; accepted for publication August 10, 2012; published online April 26, 2013.

[1]Dept. of Chemical & Biomolecular Engineering, Univ. of Melbourne, Victoria 3010, Australia, e-mail: j.provis@sheffield.ac.uk (Currently at Dept. of Materials Science and Engineering, Univ. of Sheffield, Sheffield, UK S1 3JD).

[2]ASTM Symposium on *Geopolymer Binder Systems* on June 26–27, 2012 in San Diego, CA.

Introduction

The push to move from the historical prescriptive standards frameworks toward a performance-based approach to the specification of cements and concretes is gaining increasing traction worldwide at present [1–6]. This is particularly relevant to the implementation of novel construction materials, technologies, and systems based on non-portland cements [7–10], as these materials do not in general comply with the composition-based requirements set out in prescriptive cement and concrete standards. However, it is entirely possible that non-portland cement concretes will be fit for purpose in specific applications and will also enable environmental savings through the use of lower-CO_2 binders. This has been demonstrated in numerous full-scale applications in the Americas, Europe, Asia, and Australia for the specific case of alkali-activated (including "geopolymer") concretes (abbreviated as AAMs, for alkali-activated materials) [8,11–17]. Despite this demonstration of good performance, this technology has not yet been widely adopted. There are various reasons for this, with some related to commercial and supply-chain factors, as discussed in another paper in this volume [18], and others related to standardization and the need to implement a performance-based approach to the specification of non-traditional concretes, which are explored in more detail in this paper.

The concepts and discussion presented here have been developed based on the work of RILEM Technical Committee TC 224-AAM (2007–2012) [19], and the input of all of the members of that committee is gratefully acknowledged. This paper presents a very brief set of remarks aimed at stimulating and guiding discussion in this area. More questions than answers are presented; this provides a relatively accurate picture of the state of the discussion at present, as many questions remain to be answered, particularly with regard to the validity of certain test methods as applied to AAMs, but it also shows a clear way forward toward future standards development in this area.

Designing a Performance-based Approach to AAM Standards

The first question that must be asked when implementing a performance-based approach is the very fundamental issue of how to actually define "performance." Is this simply specified in terms of mechanical (usually compressive) strength, water content, and binder content (with the term "binder" defined in some way), with a host of other engineering and durability properties assumed to follow from the use of a material with defined solids and water content that develops a particular strength after a certain number of days of curing (usually 28 days, although there is an increasing push to develop relationships based on earlier-age strength) under certain conditions? Although this approach has generally been shown to be valid (to a first approximation, at least) for the case of portland cement and concretes in which it is the sole (or

overwhelmingly dominant) binder, the relationships between 28-day compressive strength and other mechanical (flexural, tensile, elastic, creep) and transport (i.e., durability) parameters will differ as a function of binder chemistry. This has been demonstrated for AAMs with regard to flexural strength and elastic modulus [20–22], which show different dependence on the 28-day compressive strength than the well-known (and standardized) relationships that hold for normal-strength portland cement concretes (noting that even high-strength portland cement concretes require different correlations to describe their properties). If this approach is to be implemented more broadly for new binder types, it appears that it will be necessary to develop and validate the empirical correlations between 28-day compressive strength and other mechanical properties for each specific binder class or subclass, noting that, for example, alkali-activated slag and alkali-activated fly ash, both being subsets of the general class of AAMs, show very different strength development rates under the same curing conditions up to 28 days of age and microstructural differences that would be expected to lead to differences in flexural and elastic properties. The volume of work involved in developing such correlations across all the potential binder types (and including differences in mix designs, aggregate types, admixtures, and so on) is likely to prove a major impediment in implementing such a "prescriptive" approach to the specification of non-traditional concretes. An example of this is shown in Fig. 1, displaying the flexural–compressive strength correlation for a range of AAM concretes compared to the provisions of Eqs 9 and 10 of ACI 318-11 for 28-day cured normal-strength, normal-weight portland cement concretes; there are clear differences in the performance of the different types of materials plotted in this graphic.

A secondary, but no less important, question relates to the issue of sample preparation and curing prior to testing. It has been identified for the case of portland cement concretes containing moderate to high volumes of supplementary cementitious materials (SCMs) that testing at 56 days provides results that better predict long-term performance under field conditions than those obtained from tests conducted after 28 days [29], and the same is likely to be true for AAM concretes, in which the solid component of the binder is derived 100 % from materials classifiable as SCMs. The fact that the microstructural and mechanical evolution of AAM concretes might in many cases be more gradual than that of modern portland cement concretes (with high C_3S content tailored for rapid initial strength gain) makes this an important point to consider when formulating specifications based on a given definition of "performance."

The same is true for the curing conditions applied to the sample prior to testing. Curing is well known as a critical factor in enabling satisfactory strength and microstructural development in AAMs, and curing and sample conditioning protocols are specified in almost all existing standards. However, the curing conditions that are ideally suited to standardized testing of strength

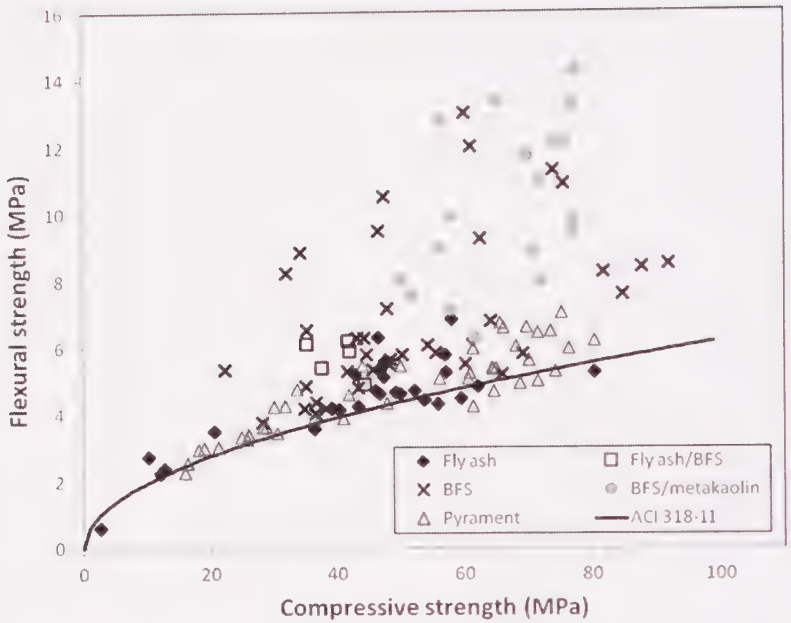

FIG. 1—*Relationship between flexural and compressive strength of alkali-activated concretes synthesised from various precursors as marked, at ages between 4 h and 1 year, with the relationship for ordinary portland cement (OPC) concretes as specified in ACI 318-02 shown for comparison. Data for AAM concretes are taken from Refs 13 and 20–28. BFS is blast furnace slag.*

development in portland-cement-based materials (particularly immersion in saturated lime water from an early age) do not give equivalently good results for AAMs; early-age immersion can lead to leaching of the alkali metal component of the activator from the pore network of the material, hindering or halting strength and microstructural development upon immersion. Sealed curing, or curing in a humidity chamber at close to saturation, has been repeatedly demonstrated to give better outcomes in terms of AAM strength and microstructural development. Although it might not be feasible in field applications to cure a concrete for extended periods under sealed conditions, this will effectively be the condition applied to the centre of a large block or member, and so it is relevant to the discussion of long-term field performance.

Different AAM mixes also require different thermal conditions for optimal curing; NaOH-activated fly ashes are very amenable to steam curing [30,31], whereas the curing of alkali-activated slag at elevated temperatures has been shown to lead in some cases to a poor-quality hardened paste product [32] or a loss of later strength [33]. In the context of the standardization of these materials, it has been suggested [19] that one possible approach is to enable the

manufacturer to specify the desired curing conditions (and possibly also the age at testing) for each particular product and report these along with the test outcomes in the presentation of the results of the tests conducted to show compliance with performance-based standards. This is an extremely open-ended pathway to standardization, and it does present challenges in terms of the comparability of products from different manufacturers who choose to specify different curing regimes in the application of the test methods, but it also opens the door for the utilization of the broadest possible range of binders without restricting applicability to only those binders that are able to develop properties optimally under a single set of arbitrarily defined conditions.

The other key question—and a very important one—related to performance-based standardization is related to finding a pathway toward resolving the myriad open questions surrounding durability testing. In order to implement a performance-based framework, both the testing methods and the qualification criteria (i.e., "pass/fail marks") must be validated in terms of correlation with real-world performance under corresponding (for some definition of this word) service conditions. There are a number of tests that are generally (and variously rightly or wrongly) assumed to give useful indications of the durability of portland cement concretes under different types of aggressive service conditions. These are analyzed in detail for each specific category of durability test in Ref 19, and a full summary of that document is beyond the scope of the current paper, aside from a few brief comments on specific testing methods and modes of degradation.

- Sulfate resistance testing of AAMs can probably follow the procedures laid down for OPC-based materials relatively closely, although the effect of the cation accompanying the sulfate ions (most commonly Na^+ or Mg^{2+}) will almost certainly differ. The same caveats regarding the selection of testing conditions (particularly concentration and temperature) for OPC [34] are likely to apply. Expansive reactions in AAMs are unlikely to involve ettringite formation, although the precipitation of gypsum is sometimes observed.
- Alkali–aggregate reactions are an area in which there is enormous variance in outcomes among different testing methods, but the in-service performance of AAMs has not demonstrated significant alkali–aggregate reactivity. Laboratory tests based on the measurement of expansion are complicated by the early-age shrinkage of some AAM mixes, and the extent to which the acceleration of alkali–aggregate reactivity can be achieved through the elevation of temperature and alkalinity is likely to differ from the case of OPC. The high Al content of many AAMs appears advantageous in reducing alkali–aggregate reaction damage [35–37].
- The analysis of the porosity and permeability of AAMs is complex, as it is for all heterogeneous materials with pore radii spanning many orders

of magnitude. Direct air and water permeability tests are very prone to cracking and/or drying effects induced during the (often overly damaging) sample conditioning processes, and differences in moisture states (which are not yet well understood for AAMs) can have a very strong influence on the results obtained by these tests. The water and air permeability values measured for AAM concretes (obtained via standard methods that test aggressively dried, and thus damaged, samples under high applied pressure) are often rather high, but the capillary sorptivity of the materials has been measured in some cases as very low, and it is likely that this difference is related to effects in the tortuosity of the pore network.

- The ASTM C1202 [38] rapid chloride penetration test does not appear to give an appropriate measure of the permeability of AAMs, as the measurement of charge passed under an applied current is dominated by effects related to the pore solution chemistry rather than the binder structure [21].
- The electrochemical interactions among AAM binders, pore solutions, and embedded steel reinforcing bars are complex and not well understood. It appears from the available data that the AAM binder is able under many circumstances to give a good degree of electrochemical protection from rebar corrosion.
- The analysis of the carbonation of alkali-activated binders under accelerated test conditions is known to be problematic [39,40] because of the strong influence of humidity and CO_2 partial pressure on the test results, and it is the subject of a good deal of ongoing research. It appears that accelerated test methods generally provide an excessively aggressive environment for AAM concretes, and so the performance of these materials in service is likely to be better than would be predicted from the test outcomes.
- Drying shrinkage of AAM concretes is likely to be a very important issue that requires further analysis, but the fact that some autogenous dimensional changes can happen earlier than the usual start of measurement in many standardized tests complicates the measurement of this property. Shrinkage and cracking are likely to be interrelated and are beginning to be better understood in the academic literature [41–46]. The control of these properties is essential in achieving long-term durability.
- The creep of AAM concretes appears to follow a different time dependence than the creep of portland cement concretes, but data available in the open literature are scarce. This is a key area requiring further work.
- The freeze-thaw resistance of AAMs can also be measured as either very good or rather poor depending on the test method applied. Again, curing and conditioning of the samples prior to the test is critical.

Concluding Remarks

From this basis, it is evident that major developments in understanding and measuring the durability of AAM concretes must form an integral part of the development of a performance-based testing regime specific to these materials. In the interim, it is likely that most of the tests that are currently applied to portland-cement-based concretes in performance-based standardization regimes are relatively close to applicable to AAM concretes, and so the design of AAM concretes to comply with standards such as ASTM C1157 [3] will probably lead to the production of a good, reliable concrete. As scientific understanding is further developed in the various areas of binder and concrete materials science that are relevant to durability testing, it might be that the acceptance criteria and/or the test methods that are recommended for application to AAMs will be adjusted to differ from those applied to portland-cement-based concretes, either because the existing protocols are found to be rather conservative (which will most likely, in the opinion of the author, be the case with respect to carbonation, permeability/porosity, and alkali–aggregate reaction tests) or because differences in the real-world performance of AAMs start to show the need for stricter controls of less well-understood phenomena (for example, potentially in the area of creep). There is thus a clear route forward to standards compliance for these alkali-activated concretes: comply as far as possible with the existing performance-based standards (while encouraging their wider acceptance among the end-user community) while continuing to work to adjust and optimize test methods and acceptance criteria to ensure that the tests encoded in the standards are as closely applicable as possible to description of the real-world performance of alkali-activated concretes.

Acknowledgments

This work has been funded by the Australian Research Council (ARC), including some co-funding from Zeobond Pty Ltd (a producer of alkali-activated concretes) through the ARC Linkage Projects scheme, as well as by support through the Particulate Fluids Processing Centre (a Special Research Centre of the ARC) and through a DORA fellowship awarded to the author. Valuable discussions with all members of RILEM TC 224-AAM over the past 5 years are also gratefully acknowledged.

References

[1] ACI Innovation Task Group 8, "Report on Performance-Based Requirements for Concrete," *ACI ITG-8R-10*, American Concrete Institute, Farmington Hills, MI, 2010.

[2] Dhir, R. K. and Paine, K. A., *Performance Related Approach to Use of Recycled Aggregates*, Waste Resources Action Program, Banbury, UK, 2007.

[3] ASTM C1157/C1157M: "Standard Performance Specification for Hydraulic Cement," *Annual Book of ASTM Standards*, ASTM International, West Conshohocken, PA.

[4] CEN/TC 51, "Cement-performance Testing for Sulfate Resistance," *Technical Report CEN/TR 15697*, CEN, Brussels, Belgium, 2008.

[5] Kropp, J. and Hilsdorf, H. K. (Eds.), "Performance Criteria for Concrete Durability," *RILEM Report REP12*, E & FN Spon, London, 1995.

[6] AS3972-2010, 2010, "General Purpose and Blended Cements," Standards Australia, Sydney.

[7] Juenger, M. C. G., Winnefeld, F., Provis, J. L., and Ideker, J., "Advances in Alternative Cementitious Binders," *Cem. Concr. Res.*, Bol. 41, 2011, pp. 1232–1243.

[8] van Deventer, J. S. J., Provis, J. L., and Duxson, P., "Technical and Commercial Progress in the Adoption of Geopolymer Cement," *Minerals Eng.*, Vol. 29, 2012, pp. 89–104.

[9] Gartner, E., "Industrially Interesting Approaches to 'Low-CO_2' Cements," *Cem. Concr. Res.*, Vol. 34, 2004, pp. 1489–1498.

[10] Gartner, E. M. and Macphee, D. E., "A Physico-chemical Basis for Novel Cementitious Binders," *Cem. Concr. Res.*, Vol. 41, 2011, pp. 736–749.

[11] Davidovits, J., *Geopolymer Chemistry and Applications*, Institut Géopolymère, Saint-Quentin, France, 2008.

[12] Shi, C., Krivenko, P. V., and Roy, D. M., *Alkali-Activated Cements and Concretes*, Taylor & Francis, Abingdon, UK, 2006.

[13] Husbands, T. B., Malone, P. G., and Wakeley, L. D., *Performance of Concretes Proportioned With Pyrament Blended Cement*, U.S. Army Corps of Engineers Construction Productivity Advancement Research Program, Vicksburg, MS, 1994.

[14] van Deventer, J. S. J., Provis, J. L., Duxson, P., and Brice, D. G., "Chemical Research and Climate Change as Drivers in the Commercial Adoption of Alkali Activated Materials," *Waste Biomass Valoriz.*, Vol. 1, 2010, pp. 145–155.

[15] Krivenko, P. V., "Alkaline Cements," *Proceedings of the First International Conference on Alkaline Cements and Concretes*, Kiev, Ukraine, October 11–14, 1994, VIPOL Stock Company, Kiev, Ukraine, pp. 11–129.

[16] Krivenko, P. V., "Alkaline Cements: From Research to Application," *Geopolymers 2002 Turn Potential into Profit* (CD-ROM), Siloxo Pty Ltd, Melbourne, Australia, 2002.

[17] Xu, H., Provis, J. L., van Deventer, J. S. J., and Krivenko, P. V., "Characterization of Aged Slag Concretes," *ACI Mater. J.*, Vol. 105, 2008, pp. 131–139.

[18] Van Deventer, J. S. J., Brice, D. G., Bernal, S. A., and Provis, J. L., "Development, Standardization and Applications of Alkali-activated Concretes," *ASTM STP 1566*, West Conshohocken, PA, 2013.

[19] Provis, J. L. (Ed.), *State of the Art Report of RILEM TC 224-AAM* (to be published).

[20] Diaz-Loya, E. I., Allouche, E. N., and Vaidya, S., "Mechanical Properties of Fly-ash-based Geopolymer Concrete," *ACI Mater. J.*, Vol. 108, 2011, pp. 300–306.

[21] Bernal, S. A., Mejía de Gutiérrez, R., and Provis, J. L., "Engineering and Durability Properties of Concretes Based on Alkali-activated Granulated Blast Furnace Slag/Metakaolin Blends," *Constr. Build. Mater.*, Vol. 33, 2012, pp. 99–108.

[22] Soti, M., van Deventer, J. S. J., Mendis, P. A., and Lukey, G. C., "Engineering Properties of Inorganic Polymer Concretes (IPCs)," *Cem. Concr. Res.*, Vol. 37, 2007, pp. 251–257.

[23] Häkkinen, T., "The Influence of Slag Content on the Microstructure, Permeability and Mechanical Properties of Concrete: Part 2. Technical Properties and Theoretical Examinations," *Cem. Concr. Res.*, Vol. 23, 1993, pp. 518–530.

[24] Fernández-Jiménez, A. M., Palomo, A., and López-Hombrados, C., "Engineering Properties of Alkali-activated Fly Ash Concrete," *ACI Mater. J.*, Vol. 103, 2006, pp. 106–112.

[25] Bernal, S., de Gutierrez, R., Delvasto, S., and Rodriguez, E., "Performance of an Alkali-activated Slag Concrete Reinforced With Steel Fibers," *Constr. Build. Mater.*, Vol. 24, 2010, pp. 208–214.

[26] Collins, F. G. and Sanjayan, J. G., "Workability and Mechanical Properties of Alkali Activated Slag Concrete," *Cem. Concr. Res.*, Vol. 29, 1999, pp. 455–458.

[27] Douglas, E., Bilodeau, A., Brandstetr, J., and Malhotra, V. M., "Alkali Activated Ground Granulated Blast-furnace Slag Concrete: Preliminary Investigation," *Cem. Concr. Res.*, Vol. 21, 1991, pp. 101–108.

[28] Wu, Y., Cai, L., and Fu, Y., "Durability of Green High Performance Alkali-activated Slag Pavement Concrete," *Appl. Mech. Mater.*, Vol. 99–100, 2011, pp. 158–161.

[29] Lawler, J. S., Connolly, J. D., Krauss, P. D., Tracy, S. L., and Ankenmann, B. E., "Guidelines for Concrete Mixtures Containing Supplementary Cementitious Materials to Enhance Durability of Bridge Decks," *NCHRP Report No. 566*, Transportation Research Board, Washington, D.C., 2007.

[30] Kovalchuk, G., Fernández-Jiménez, A., and Palomo, A., "Alkali-activated Fly Ash: Effect of Thermal Curing Conditions on Mechanical and Microstructural Development—Part I," *Fuel*, Vol. 86, 2007, pp. 315–322.

[31] Criado, M., Fernández-Jiménez, A., and Palomo, A., "Alkali Activation of Fly Ash. Part III: Effect of Curing Conditions on Reaction and Its Graphical Description," *Fuel*, Vol. 89, 2010, pp. 3185–3192.

[32] Guerrieri, M. and Sanjayan, J., "Investigation of the Cause of Disintegration of Alkali Activated Slag at Temperature Exposure of 50°C," *J. Mater. Civ. Eng.*, Vol. 23, 2011, pp. 1589–1595.

[33] Bakharev, T., Sanjayan, J. G., and Cheng, Y. B., "Effect of Elevated Temperature Curing on Properties of Alkali-activated Slag Concrete," *Cem. Concr. Res.*, Vol. 29, 1999, pp. 1619–1625.

[34] Glasser, F. P., "The Thermodynamics of Attack on Portland Cement With Special Reference to Sulfate," *RILEM TC 211-PAE Final Conference, Concrete in Aggressive Aqueous Environments*, Toulouse, France, June 3–5, 2009, RILEM, Paris, France, pp. 3–17.

[35] Fernández-Jiménez, A. and Puertas, F., "The Alkali-Silica Reaction in Alkali-activated Granulated Slag Mortars With Reactive Aggregate," *Cem. Concr. Res.*, Vol. 32, 2002, pp. 1019–1024.

[36] Krivenko, P. V., Petropavlovsky, O., Gelevera, A., and Kavalerova, E., "Alkali-Aggregate Reaction in the Alkali-activated Cement Concretes," *Proceedings of the 4th International Conference on Non-Traditional Cement & Concrete*, Brno, Czech Republic, June 27–30, 2011, Brno University of Technology and ZPSV a.s., Brno, Czech Republic.

[37] Thomas, M., "The Effect of Supplementary Cementing Materials on Alkali-Silica Reaction: A Review," *Cem. Concr. Res.*, Vol. 41, 2011, pp. 1224–1231.

[38] ASTM C1202-12: "Standard Test Method for Electrical Indication of Concrete's Ability to Resist Chloride Ion Penetration," *Annual Book of ASTM Standards*, ASTM International, West Conshohocken, PA.

[39] Bernal, S. A., Provis, J. L., Brice, D. G., Kilcullen, A., Duxson, P., and van Deventer, J. S. J., "Accelerated Carbonation Testing of Alkali-activated Binders Significantly Underestimates Service Life: The Role of Pore Solution Chemistry," *Cem. Concr. Res.*, Vol. 42, 2012, pp. 1317–1326.

[40] Bernal, S. A., Provis, J. L., Mejía de Gutiérrez, R., and van Deventer, J. S. J., "Accelerated Carbonation Testing of Alkali-activated Slag/Metakaolin Blended Concretes: Effect of Exposure Conditions," *Cem. Concr. Res.* (submitted).

[41] Collins, F. and Sanjayan, J. G., "Numerical Modeling of Alkali-activated Slag Concrete Beams Subjected to Restrained Shrinkage," *ACI Mater. J.*, Vol. 97, 2000, pp. 594–602.

[42] Collins, F. and Sanjayan, J. G., "Cracking Tendency of Alkali-activated Slag Concrete Subjected to Restrained Shrinkage," *Cem. Concr. Res.*, Vol. 30, 2000, pp. 791–798.

[43] Kukko, H. and Mannonen, R., "Chemical and Mechanical Properties of Alkali-activated Blast Furnace Slag (F-Concrete)," *Nordic Concrete Research*, Vol. 1, 1982, pp. 16.11–16.16.

[44] Byfors, K., Klingstedt, G., Lehtonen, H. P., and Romben, L., "Durability of Concrete Made With Alkali-activated Slag," *Proceedings of the 3rd International Conference on Fly Ash, Silica Fume, Slag and Natural Pozzolans in Concrete*, ACI SP114, Trondheim, Norway, May 1987, American Concrete Institute, Detroit, MI, pp. 1429–1444.

[45] Shen, W., Wang, Y., Zhang, T., Zhou, M., Li, J., and Cui, X., "Magnesia Modification of Alkali-activated Slag Fly Ash Cement," *Journal of Wuhan University of Technology—Materials Science Edition*, Vol. 26, 2011, pp. 121–125.

[46] Bernal, S. A., Mejía de Gutierrez, R., Pedraza, A. L., Provis, J. L., Rodríguez, E. D., and Delvasto, S., "Effect of Binder Content on the Performance of Alkali-activated Slag Concretes," *Cem. Concr. Res.*, Vol. 41, 2011, pp. 1–8.

Geopolymer Binder Systems
STP 1566, 2013
Available online at www.astm.org
DOI:10.1520/STP156620120083

Jannie S. J. van Deventer,[1] *David G. Brice,*[2,3]
Susan A. Bernal,[3,4] *and John L. Provis*[3,4]

Development, Standardization, and Applications of Alkali-activated Concretes

REFERENCE: van Deventer, Jannie S. J., Brice, David G., Bernal, Susan A., and Provis, John L., "Development, Standardization, and Applications of Alkali-activated Concretes," *Geopolymer Binder Systems*, STP 1566, Leslie Struble and James K. Hicks, Eds., pp. 196–212, doi:10.1520/STP156620120083, ASTM International, West Conshohocken, PA 2013.[5]

ABSTRACT: Alkali-activated "geopolymer" concrete has been commercialized in Australia, and it is meeting with strong demand from the end-user community and approval from regulatory authorities. Interest in the application of this technology throughout the Asia-Pacific region is growing, as end-users, engineers, and architects increase their environmental awareness and as some jurisdictions introduce a carbon tax or carbon pricing policy. VicRoads, the roads authority of the state of Victoria in Australia, is a signature specifier that has already changed its specification for non-structural concrete to accommodate geopolymer concrete. In addition, progress has been made in a RILEM Technical Committee to establish a framework for a performance standard for alkali-activated concrete. The commercialization of geopolymer technology is linked closely with scientific developments in this area, in particular through the use of innovative methods to analyze and predict durability and in understanding and controlling reaction mechanisms. The importance of leading-edge scientific research in enhancing the performance and utility of geopolymer concretes is also highlighted, with the identification of some of the remaining technical and non-technical hurdles that

Manuscript received June 16, 2012; accepted for publication September 7, 2012; published online April 25, 2013.

[1]Zeobond Pty Ltd, P.O. Box 210, Somerton, VIC 3062, Australia; and Dept. of Chemical & Biomolecular Engineering, Univ. of Melbourne, VIC 3010, Australia, e-mail: jannie@zeobond.com

[2]Zeobond Pty Ltd, P.O. Box 210, Somerton, VIC 3062, Australia.

[3]Dept. of Chemical & Biomolecular Engineering, Univ. of Melbourne, VIC 3010, Australia.

[4]Dept. of Materials Science and Engineering, Univ. of Sheffield, Sir Robert Hadfield Building, Mappin St., Sheffield S1 3JD, United Kingdom.

[5]ASTM Symposium on *Geopolymer Binder Systems* on June 26–27, 2012 in San Diego, CA.

must be overcome. This paper outlines the process of commercializing an alternative binder system at the production scale, including obtaining regulatory approval for groundbreaking applications in civil infrastructure. There has been much discussion of the potential of alkali-activation technology over the past decades, but until now, large-scale application has been limited. Some of the reasons for this slow progress, as well as the methods by which obstacles have been overcome, are discussed.

KEYWORDS: Alkali-activated, Geopolymer, Standards, Durability, Commercialization

Introduction

There is general international agreement that the global average temperature increase must be kept below 2 C in order to avoid irreversible damage to the water supply, agricultural productivity, the sea level, human habitability, and global security. This paper does not intend to contribute to the debate on whether climate change is caused by human activity. Instead, it is assumed here that there is economic and social benefit both in reducing carbon emissions and in utilizing waste materials such as fly ash and metallurgical slag at the same time. Cement production currently contributes 5 % to 8 % of global anthropogenic carbon emissions [1], and the rapid establishment of civil infrastructure in China, India, and the developing world is expected to increase the demand for cement even further. Concrete made using ordinary Portland cement (OPC) (including its blends with mineral admixtures) is second only to water as the commodity most used by mankind today.

The decarbonation of the limestone used in cement clinker production releases roughly 0.53 tonnes of CO_2 per tonne of clinker [2]. In 2005, cement production (total cementitious sales including OPC and OPC blends) had an average emission intensity of 0.89 with a range of 0.65 to 0.92 tonnes of CO_2 per tonne of cement binder [3]. Therefore, the decarbonation of limestone contributes about 60 % of the carbon emissions of OPC, with the remaining 40 % attributed to energy consumption, most of which is related to clinker kiln operations. Based on a binder-to-binder comparison, it is possible to reduce carbon emissions by 80 % using alkali-activation, whereas the comparison on a concrete-to-concrete basis gives a 60 % reduction, as the energy cost of aggregate production and transport is identical for the two binders [4].

Consequently, an alternative binder chemistry needs to be adopted if such carbon emissions from cement manufacturing are to be reduced significantly. Juenger et al. [5] recently presented a review of potential alternatives to OPC technology, including calcium sulfoaluminate cements, magnesium cements, the magnesium phosphate system, and alkali-activated materials or geopolymers. However, many of these alternative binders require a new supply chain for raw materials, the development of new chemical admixtures, regulatory approval, new durability testing protocols, and an in-service track record before they can be adopted widely by the industry.

Alkali-activated binders or "geopolymers" face the same obstacles, but they have a longer track record of application [4,6,7], supported by an expanding body of research relating gel chemistry and nanostructure to durability. The benefits of alkali activation in comparison with OPC technology are largely based on the ability to convert high-volume industrial waste streams into concrete, with a highly significant reduction in carbon emissions [8]. Fly ash and slag appear at present to be the most promising source materials for large-scale industrial production of alkali-activated binder because of their more favorable rheological properties and lower water demand relative to mixes based on calcined clays [9]. The history, chemical principles, reaction phenomena, and engineering properties of geopolymer concrete have been reviewed extensively [10–16].

This paper summarizes recent research linking microstructure, durability testing, and regulatory approval for alkali-activated concrete and identifies gaps in our knowledge. By using selected case studies, the paper aims to explain how technical, commercial, and regulatory barriers to industrial adoption have been overcome during the commercialization of alkali-activated concrete in Australia.

Developments in Alkali-activation Chemistry

The industrial uptake of alkali-activated concrete benefits from research on the characterization of aluminosilicate source materials, the microstructure of geopolymer binders, the control of setting time through the manipulation of binder and aqueous-phase chemistry, surface chemical interactions affecting workability, and the prediction of durability as a function of microstructure. There are increasing numbers of papers on the properties of alkali-activated materials on the laboratory scale. Unfortunately, much of this information has limited direct value in commercial adoption, in view of the more challenging conditions faced in industrial practice. An overview of selected chemical advances conducive to commercial adoption is presented here.

Duxson and Provis [17] proposed an ideal composition range for glassy aluminosilicate precursors containing network-modifying cations (calcium, magnesium, sodium, and potassium) in order to give sufficient solubility to supply the necessary aluminum into the growing geopolymer gel. The need for a separate alkali source can be greatly reduced or even eliminated if the correct glass can be selectively synthesised. This can be achieved via the addition of components into pulverised coal prior to combustion or the manufacture of a highly reactive raw material [18] that can be blended with less-reactive raw material. It is essential that a workable one-part ("just add water") mix be developed if alkali-activated binders are to achieve widespread market penetration, as this would largely simplify the logistics of material supply and distribution.

Yip et al. [19,20] suggested that both geopolymeric (alkali aluminosilicate) gel and calcium aluminosilicate hydrate (C-A-S-H) gel can co-exist at low alkalinities, whereas geopolymeric gel is the dominant product at high

alkalinities. Buchwald et al. [21] and others showed the coexistence of the two types of gel at relatively high alkalinity. Various studies by the authors and others have shown that these gels behave differently toward an aggressive environment and thus affect the durability of the concrete along different chemical pathways. Although the role of calcium is pivotal in determining the engineering properties and durability of alkali-activated concrete, the precise chemical mechanisms remain poorly defined. Iron does not appear to migrate much from its original position within fly ash particles during alkali activation [22,23]. However, the effect of iron on the lability of precursor glassy phases and the role that iron might play during geopolymer reactions remain largely undescribed.

With the introduction of nanoparticles, there has been renewed interest in nucleation in cementitious gels. Rees et al. [24] showed that the induction period could be eliminated when nanoparticle seeds were added during the alkali activation of fly ash, as the nanoparticles immediately catalyzed the formation of nuclei. Subsequent work by Hajimohammadi et al. [25–27] using spatially resolved synchrotron radiation Fourier transform infrared microscopy showed that the release rates of both Si and Al are critical in determining strength development and microstructural evolution in growing geopolymer gels.

Linking Microstructure and Durability in Alkali-activated Concrete

The durability of reinforced concrete is generally understood as requiring the maintenance of a dense, impermeable gel that stabilizes a highly alkaline environment, with appropriate chemical and redox conditions to protect the embedded steel in a passive state. A brief overview of the link between microstructure and durability in alkali-activated concrete is presented here.

Studies such as that by Bernal et al. [28] commenting on the trends in microcracking intensity in alkali-activated concretes as a function of paste content and curing regime highlight the value of understanding interactions between the binder and aggregate and effects related to heat generation and heat and moisture transport during curing in mitigating the effects of microcracking on concrete performance and durability. The main interactions are thought to take place in the interfacial transition zone (ITZ), and the microstructure of the ITZ of any concrete is critical in terms of both strength and durability performance. Alkali-activated binders are believed to have a denser ITZ than OPC, with concomitantly better flexural performance. This higher density also reduces the possibility of the ITZ serving as a percolated porous pathway for mass transport through the binder, thus enhancing durability [29–33].

Water and air permeability measurements of alkali-activated binders have shown a range of performance, depending mainly on the mix designs tested. Well-cured alkali-activated binders with low water/binder ratios perform

acceptably in these tests [34–36] but generally do not display outstanding performance in terms of permeability coefficients, probably as a result of the low levels of space-filling bound water associated with these gels. Electrically accelerated chloride permeability testing of alkali-activated mortars and concretes has shown generally very good but variable performance, depending significantly on the testing methodology used. The outcome of this test is strongly dependent on the pore solution chemistry. Methodologies that provide a more direct measurement of the progress of chloride migration into the binder—for example, ponding tests or the NordTest Build 492 accelerated test—will be more likely to provide a valid comparison that is relatively independent of the pore solution chemistry of the binder, and work in this area is ongoing.

Microtomography [37] and drying tests [38] have shown that the C-A-S-H phase does bind some water, but to a lesser extent than the OPC hydrate products. As the gel evolves and its porosity decreases over time, the tortuosity of the pore network also increases. Thermal curing is often required in order for poorly designed alkali-activated mixes to achieve adequate strength, but this is not the case for a well-designed mix with sufficiently well-controlled activation conditions. Nevertheless, the tomography results demonstrate that regardless of the rate of early strength development, an extended period of curing will provide marked advantages in microstructure, service life, and durability performance.

Evidently, it is important to understand and control the porosity, permeability, and microstructural development of alkali-activated binders. The sodium aluminosilicate (geopolymer) and C-A-S-H type gels that dominate these binders have an intrinsically higher porosity than the calcium silicate hydrate gels formed during OPC hydration. Based on laboratory tests, it thus seems possible that the alkali-activated gels might compare poorly to OPC gels in terms of durability. However, evidence from the in-service performance of geopolymer and other alkali-activated binders [6,7,39] shows that the observed performance is significantly better than would be expected based on raw permeability or carbonation rate data [6,28,32,40,41]. The carbonation of alkali-activated binders is an open and active area of research, and much remains to be explained in this area, particularly with regard to the relationship between carbonation and steel degradation, which might or might not be similar to the corresponding relationship in OPC concretes. Therefore, additional effects might compound or mitigate the direct influence of porosity on permeability (particularly ionic permeability, which also relates to gel chemistry-specific effects and interactions) and durability.

How Reliable is Durability Testing?

The discrepancy between unsatisfactory results obtained in some accelerated durability tests and the satisfactory performance of alkali-activated concrete in

field applications raises questions about the reliability of durability tests and the service life prediction of this new class of concrete. Alkali-activated concrete, which has been subjected to detailed investigation only recently, cannot possibly have the support of decades of in-service testing and durability data to prove its long-term stability, as OPC does. The question of whether alkali-activated concrete is durable remains a major obstacle to recognition in standards for structural concrete, in the minds of users, and thus to its commercial adoption. When faced with a decision about the choice of concrete within tight timelines, a specifier (usually an architect) will tend to choose OPC, with its associated guarantees and track record, instead of selecting a new, less proven concrete with a higher risk profile. The exception to this will be a specifier whose key performance indicators include parameters related to the uptake of low emissions materials and innovative technology. It is indeed such a push toward low emissions and innovation that has provided the main driver for the adoption of alkali-activated concrete in Australia. In countries like China and India, the utilization of industrial waste such as fly ash and metallurgical slag might also provide a necessary driver for the adoption of alkali-activated concrete, in addition to the reduction of carbon emissions, but this is unlikely to be as much of a driver in most of the developed world, where these materials are already in many cases considered by-products rather than wastes.

The testing of concrete durability usually involves exposing small samples to extreme conditions such as harsh drying, wetting-drying cycling, freeze-thaw cycling, and highly concentrated acid or salt solutions, with or without the application of electrical field gradients, for short periods of time. The data obtained from these tests are then used to predict how the concrete will perform under natural environmental conditions over periods of 100 to 300 years. In some of these predictive models, engineering concepts including mass transport through porous media, reaction kinetics, and particle packing are used, although usually in a simplified and semi-empirical form to enable utilization of the derived equations by non-specialists in the field. However, the key shortcoming of this approach to "proving" durability is that it can provide only indications of the expected performance, rather than definitive proof. Therefore, there has been a very slow process of adoption of new materials, as it is considered necessary to wait up to 20 to 30 years for "real world" verification. The adoption of supplementary cementitious materials (SCMs), including fly ash and slag, in OPC concrete serves as an example: the use of these SCMs was resisted for decades in many markets. It is the authors' experience that asset owners and their insurance companies are willing to use alkali-activated concrete in low-risk applications based on accelerated durability testing. Higher-risk applications such as high-rise buildings, which constitute a smaller fraction of the total concrete market, will follow only when the market is comfortable with the real-world track record of the material in low-risk applications. Therefore, a staged approach toward the development of

standards and commercial adoption needs to be followed, as outlined by Van Deventer et al. [4].

Overcoming Regulatory and Specification Barriers

The regulatory framework governing the use of concrete in various applications relies on a typical cascade of standards, with application standards referring to concrete standards, and concrete standards referring to standards covering cement and other raw materials. Thus, when considering the regulatory framework for a concrete binder system such as alkali-activated cement or concrete, most of the attention to regulatory aspects should be focused on the cement standards, although some aspects of concrete standards also need to be considered. In general, all of the world's concrete application, concrete, and cement standards are based on two "super" standards, EN 197 [42] and ASTM C150, C595, and C1157 [43–45]. For instance, Chinese cement and concrete standards are based largely on European Union standards, whereas Australian standards are based mainly on the U.S. standards.

In most countries there are prescriptive standards for what is considered an "acceptable" concrete mix design for a particular application. Such standards have been developed over many years with input from cement and concrete manufacturing companies, specifiers, and the like, with the chemistry and behavior of OPC-based concretes either specifically or intrinsically in mind. Despite this, standards containing constraints such as "minimum cement content" are beginning to be viewed as overly prohibitive, even for OPC-based systems, because prescribing a high OPC content essentially encourages mix designs that use poor quality aggregates and high water content when high strength is not required.

The Appendix to Australian Standard AS3972 states, "For many years cement standards all over the world have been to a large degree prescriptive. Prescription-based specifications are convenient: the tests needed to police prescriptions are usually simple and quick to carry out. However this convenience is achieved at the expense of innovation and being able to easily incorporate new or advanced knowledge. With prescriptive specifications only a narrow range of solutions to any one problem is acceptable even though many other solutions may be available which would give equal or better performance" [46]. This approach and attitude are very relevant to the utilization of alkali-activated materials, and they provide an environment that is, to at least some extent, conducive to innovation in construction materials technologies.

Products such as alkali-activated concrete, or other non-OPC and even high-performance cementitious-based systems, might not simply be an evolution of existing OPC technology; instead they might require an entirely different chemical paradigm in order for their behavior to be understood, and they might perform entirely acceptably but without conforming exactly to the

established regulatory standards, particularly with regard to rheology and chemical composition. It therefore becomes critical, for the adoption of alkali-activated concrete, to extend the performance-based standard concept to explicitly include systems without any OPC that meet all relevant performance criteria, and to generate new and more relevant criteria.

It is important to address the development of specifications and standards both locally in the short term and globally long term. As outlined by Provis [47], the RILEM (International Union of Laboratories and Experts in Construction, Materials, Systems and Structures) Technical Committee on Alkali-Activated Materials (TC 224-AAM) has developed a global framework for performance-based standards for alkali-activated cement and concrete that will hopefully serve as a reference for the long-term setting of standards in different jurisdictions.

Regulatory Progress in Australia

Key domestic standards organizations and industry representative bodies may present short-term barriers to the industrial adoption of alkali-activated binders. However, the process of building strong working and collaborative relationships with local water and road authorities, including VicRoads and Queensland Main Roads, has provided a pathway for alkali-activated concrete (Zeobond's E-Crete) to achieve specification in a range of structural concrete applications in Australia.

VicRoads is a Victorian Government Corporation that is responsible for managing the Victorian road network. VicRoads is the key specifying agency for roads and associated infrastructure built in Melbourne and surrounding areas. VicRoads has many prescriptive standards for concrete specification; however, through open discussion and the demonstration of E-Crete, VicRoads is now actively involved in developing durability standards for E-Crete to be used in VicRoads' own specifications, including structural applications.

VicRoads [48] has approved E-Crete grades 20, 25, and 32 MPa for general concrete paving and non-structural use in footpaths, curb, and guttering (contained in Section 703 of their standard specifications). It is currently assessing 32 MPa, 40 MPa, and 55 MPa E-Crete for approval in the structural specification (Section 610).

VicRoads has also recently commissioned a number of significant E-Crete pours:

- 55 MPa pre-cast panels for the Salmon St. pedestrian bridge in Port Melbourne,
- 40 MPa retaining walls at Swan St. bridge, an iconic location in Melbourne,
- 32 MPa concrete pavement works on the Kings Rd. overpass on the Calder Freeway, Melbourne, and
- 25 MPa footpath for the Westgate Freeway upgrade, Melbourne.

VicRoads has used the Australian National Association of Testing Authorities (NATA) accredited standard industry testing techniques to determine the suitability of its concretes for a number of different uses. These tests provide firm results for short-term performance and an indicator of long-term performance. Concretes made using Zeobond's alkali-activated cements have performed within specifications for these tests, which include (a) compressive strength testing, (b) slump and slump spread, (c) drying shrinkage, (d) soluble salts, and (e) alkali aggregate reactivity.

In addition, VicRoads is undertaking independent long-term assessment across a broad spectrum of standard concrete tests including compressive strength, volume of permeable voids, and protection of embedded steel. These tests will assess the situ performance of E-Crete relative to existing OPC-based concretes and provide ongoing validation of short-term test results.

Building Industry Knowledge and Confidence

Stakeholders and Drivers for Uptake

The experience in Australia is that customers are looking for innovative solutions, particularly if they can generate high reductions in carbon emissions in construction projects. This is particularly true in large infrastructure projects and private projects for which "greenness" has a premium from both political and image perspectives. In the longer term, as Zeobond's E-Crete and other low-emission concretes become more widely adopted, these drivers will necessarily become reduced as it is increasingly demonstrated that the materials are competitive both in performance and in economic terms, but in the near future this environmental benefit does provide a significant driver for uptake.

Consulting engineering firms play an influential role in driving the adoption of low-emission cement. If a supplier of alkali-activated concrete is not able to get these firms to use a new material such as E-Crete, then it is immaterial whether or not the customer or architect specifies E-Crete, as the engineer must sign off on the design structurally. However, this hierarchy also provides an opportunity in two ways. Firstly, in the current environment, ecological factors play an important role in the design and construction of buildings. Secondly, it also plays an important role in the tendering process for design firms. Although the customer is not in a position to require a company to utilize certain materials, it is in a position to drive demand for innovation. Indeed, this is the situation that has evolved in Australia, with consulting engineers now looking for an environmental edge in the market to provide a point of difference from their competitors, or simply to maintain equal footing and not lose market share. Architects are, in terms of attitudes, quite similar to consulting engineers, but without the aspect of professional indemnity in terms of structural

elements. Therefore, these stakeholders are also looking for new and innovative environmental aspects to incorporate in designs to make them relevant in terms of general innovation in architecture, as well as for market gains.

The demonstration of a new construction material like E-Crete in projects of a sufficiently large scale to have strategic and symbolic significance is essential in order to establish confidence and build knowledge of the product amongst industry stakeholders. Market demand for E-Crete in Australia has been stimulated through close collaboration with and education of key specifying agencies, local councils, government authorities, corporations, project developers, engineers, and architects, including the following parties:

- *Property and infrastructure developers*: GroCon, VicUrban, Stockland Group, MIB, Symonds Homes, Winslow Construction, Lend Lease (Delfin), VicRoads, WestGate Freeway Alliance, Monash Freeway Alliance, and Reinforced Concrete Pipe Australia;
- *Local government city councils*: Banyule, Brimbank, Cardinia, Dandenong, Darebin, Hume, Manningham, Maribyrnong, Maroondah, Melton Shire, Moonee Valley, Nillumbik, Whitehorse, and Whittlesea; and
- *Precast and premix concrete manufacturers*: build understanding and confidence in manufacturing, placing, and handling E-Crete with concrete placement tradesmen.

Pathways to Commercialization and the Role of Research and Development

The fundamental properties of OPC-based products have been developed, refined, and improved over decades. This demonstration of functionality, flexibility, and reproducibility provides the construction industry with a high degree of confidence that the product will be fit for purpose. In contrast, alkali-activated concrete, as a new product that is designed to compete with OPC, must ultimately demonstrate that it can perform equivalently in terms of cost, form, and function while still delivering significant reductions in carbon emissions. The conceptual diagram in Fig. 1 depicts the interdependence of research and development (R&D) with the various steps of commercial adoption of alkali-activated concrete in an established market.

In Fig. 1, R&D is shown to identify methods and processes to improve and test alkali-activated concrete, and it includes many benchmark tests comparing the new material to OPC-based products. Through the ongoing demonstration of product performance combined with improved understanding of fundamental properties, confidence in the capabilities of the product is improved and key technical risks are addressed.

Application development as depicted in Fig. 1 involves building a detailed understanding of the customers' requirements for the existing OPC-based products and translating these requirements into an equivalent outcome

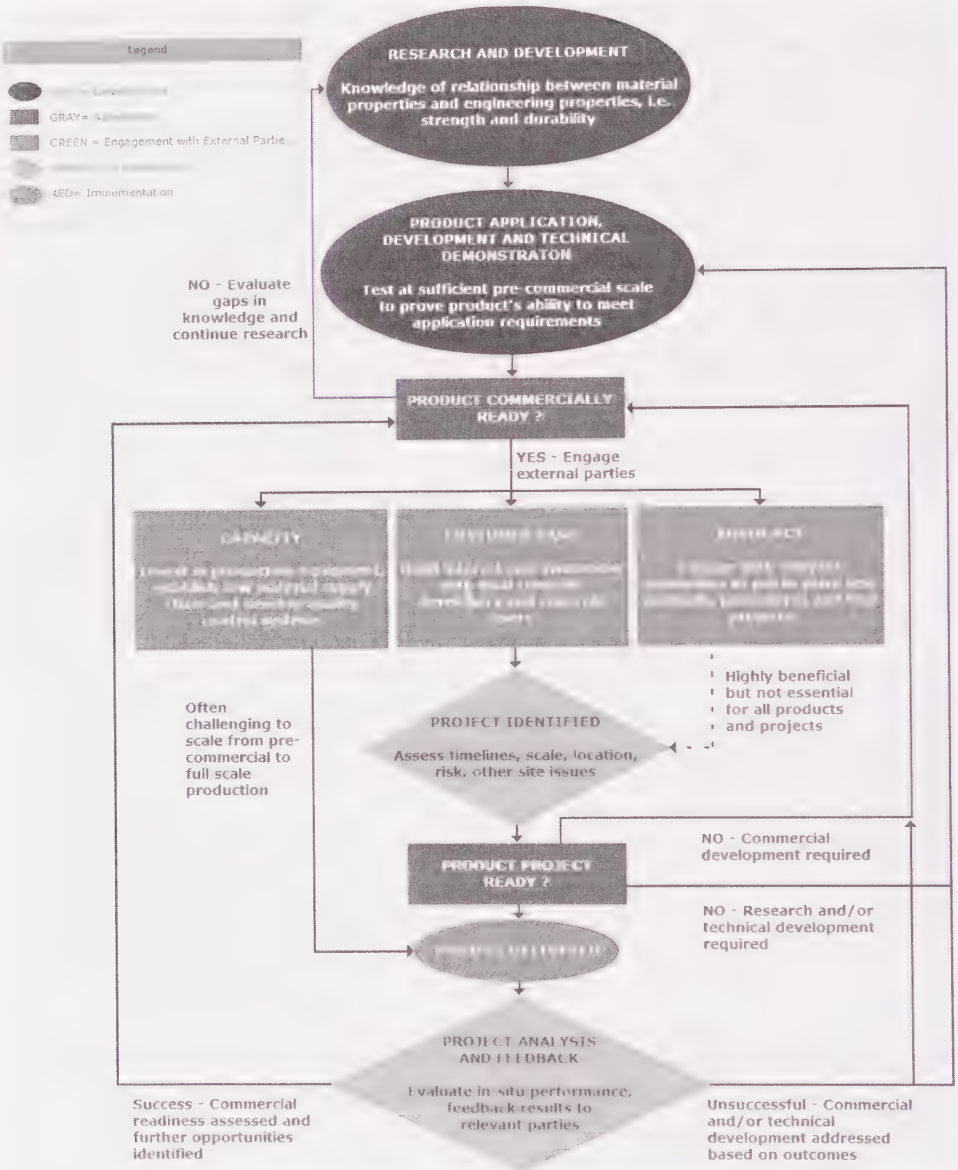

FIG. 1—*Conceptual diagram demonstrating the interdependence of R&D and commercial adoption.*

using alkali-activated materials. Each application requires knowledge of the specific characteristics that are required of the material and the ability to match these with knowledge gained from R&D. Following an initial assessment of product requirements, alkali-activated concrete is tested in a

prototype system at a laboratory or pilot scale. Subsequent to successful pilot-scale trials, multiple production trials are typically conducted using manufacturing-scale equipment.

Products are observed at the pre-commercial scale for their compatibility with existing market practices, process and handling requirements, and overall performance relative to the OPC benchmark system. Standard, independent, NATA-accredited OPC-based performance tests are used to ensure that the product meets basic specifications for the application targeted. For non-structural, low-risk applications, the test methods are basic, including density, air content, slump, set time, compressive strength (early and ultimate), and shrinkage. In addition, for structural, higher risk applications, the following tests may also be included: flexural and tensile strength, acid, chemical and fire resistance, water permeability, carbonation, sorptivity, creep, and steel protection. Knowledge gained from product development is continuously fed back into the product improvement cycle and stimulates further R&D, including fundamental research.

Experience shows that most customers and end users are more readily open to initially tackling projects of lowest risk, such as footpaths, driveways, kerb and channel, and low-strength pits. The risk is low with such projects because their timelines are often more flexible (reduced time risk), the consequences associated with not meeting performance requirements are low (compressive strength, shrinkage), and the cost of replacement is low (accessible, non-structural, easily replaced). As technical risk increases for an application, testing requirements and the demonstration of technical capability increase. It is highly advantageous, therefore, to engage with regulatory authorities to put in place key testing and trial projects in order to drive acceptance in higher risk applications. Demonstration and independent evaluation by a regulatory authority provide confidence to the market and enable progress. E-Crete, for instance, has been used by VicRoads in products with high technical and performance risk but low in situ risk and cost, such as small 55 MPa precast panels on the Salmon St. bridge in Port Melbourne, to demonstrate the performance properties of the material for the longer term.

Besides demonstrating that a new concrete performs technically, it is equally important to demonstrate to customers and the wider market that a product like E-Crete can be delivered on time, in appropriate quantities, with security of a supply chain and the financial support to fund the operation in place. Whereas OPC-based products are available anywhere in the world, the limited scale and locality of production of a new product like E-Crete restrict the scope of applications that could be considered during the early stages, especially for larger premixed concrete projects.

Although existing OPC concrete batching equipment could be modified to use the leverage of existing infrastructure, it often limits the expansion of production of alkali-activated concrete when inadequate space is available for the

installation of storage silos and material-handling equipment. Also, dependence on a supply chain controlled by OPC interests could involve challenges in the quality control of source materials, as alkali-activated binders might have different requirements in terms of fly ash and slag properties than the materials that are optimal for use as SCMs in OPC concretes.

Final Observations

Significant progress has been made in understanding the reaction mechanisms governing the alkali-activation of calcium aluminosilicates. Nevertheless, the role of calcium in geopolymer phase formation remains poorly understood. The relationship between the gel microstructure and the long-term durability of alkali-activated concrete requires further research. Although alkali-activated concrete has performed well in accelerated durability tests, the results have been variable, and the applicability of some durability tests to the chemistry of alkali-activation remains in question. In the absence of a long in-service track record, research is essential in order to validate durability testing methodology and improve alkali-activated cement technology.

Demand pull by a carbon conscious market continues to be the main driver for the short-term uptake of alkali-activated concrete in Australia. The scale-up from the laboratory to the real world is technically challenging, but the core challenge is the scale-up of industry participation and acceptance of alkali-activated cement. High-profile application projects in Australia have demonstrated the vast regulatory, asset management, liability, and industry stakeholder engagement processes required in order to commercialize alkali-activated cement. It is important for commercial producers of alkali-activated binders and concretes to work closely with research partners to develop testing methods for accelerated durability, especially as longer term in-service testing data become available. Substantial progress has been made in Australia, where the local road authority has recognized geopolymer concrete for non-structural applications.

Most premixed and precast concrete standards are based on the assumption of the use of OPC, which remains a hurdle to the industrial adoption of alkali-activated concrete. Even when asset owners and specifiers such as government, architects, and engineers accept the results of durability testing of alkali-activated concrete, a key barrier to entry of these materials into an established market is access to a suitable supply of source materials including fly ash, granulated blast furnace slag, and alkaline activators. The development of a new supply chain requires substantial capital investment, political support, and the will to overcome competitive pressure from incumbents. This crucial aspect of commercialization is seldom appreciated by the research community, governments, or the ultimate users of concrete.

Acknowledgments

This work has been funded by Zeobond Pty. Ltd. and the Australian Research Council (ARC) through an ARC Linkage Project grant awarded jointly with JLP. J.S.J.v.D. and D.G.B. hold financial interests in Zeobond Pty. Ltd., a producer of alkali-activated cements and concretes.

References

[1] WWF-Lafarge Conservation Partnership, 2008, "A Blueprint for a Climate Friendly Cement Industry: How to Turn Around the Trend of Cement Related Emissions," http://assets.panda.org/downloads/cement_blueprint_-climate_fullenglrep_lr.pdf (Last accessed 15 June 2012).

[2] Damtoft, J. S., Lukasik, J., Herfort, D., Sorrentino, D., and Gartner, E., "Sustainable Development and Climate Change Initiatives," *Cem. Concr. Res.*, Vol. 38, No. 2, 2008, pp. 115–127.

[3] International Energy Agency, 2007, "Tracking Industrial Energy Efficiency and CO_2 Emissions—Executive Summary," http://www.iea.org/Textbase/npsum/tracking2007SUM.pdf (Last accessed 15 June 2012).

[4] van Deventer, J. S. J., Provis, J. L., and Duxson, P., "Technical and Commercial Progress in the Adoption of Geopolymer Cement," *Minerals Eng.*, Vol. 29, 2012, pp. 89–104.

[5] Juenger, M. C. G., Winnefeld, F., Provis, J. L., and Ideker, J., "Advances in Alternative Cementitious Binders," *Cem. Concr. Res.*, Vol. 41, No. 12, 2011, pp. 1232–1243.

[6] Shi, C., Krivenko, P. V., and Roy, D. M., *Alkali-Activated Cements and Concretes*, Taylor & Francis, Abingdon, UK, 2006, p. 376.

[7] Xu, H., Provis, J. L., van Deventer, J. S. J., and Krivenko, P. V., "Characterization of Aged Slag Concretes," *ACI Mater. J.*, Vol. 105, No. 2, 2008, pp. 131–139.

[8] Duxson, P., Provis, J. L., Lukey, G. C., and van Deventer, J. S. J., "The Role of Inorganic Polymer Technology in the Development of 'Green Concrete,'" *Cem. Concr. Res.*, Vol. 37, No. 12, 2007, pp. 1590–1597.

[9] Provis, J. L., Duxson, P., and van Deventer, J. S. J., "The Role of Particle Technology in Developing Sustainable Construction Materials," *Adv. Powder Technol.*, Vol. 21, No. 1, 2010, pp. 2–7.

[10] Davidovits, J., *Geopolymer Chemistry & Applications*, 2nd ed., Institut Géopolymère, Saint-Quentin, France, 2009, p. 590.

[11] Duxson, P., Fernández-Jiménez, A., Provis, J. L., Lukey, G. C., Palomo, A., and van Deventer, J. S. J., "Geopolymer Technology: The Current State of the Art," *J. Mater. Sci.*, Vol. 42, No. 9, 2007, pp. 2917–2933.

[12] Komnitsas, K. and Zaharaki, D., "Geopolymerisation: A Review and Prospects for the Minerals Industry," *Minerals Eng.*, Vol. 20, No. 14, 2007, pp. 1261–1277.

[13] Pacheco-Torgal, F., Castro-Gomes, J., and Jalali, S., "Alkali-Activated Binders: A Review. Part 1. Historical Background, Terminology, Reaction Mechanisms and Hydration Products," *Constr. Build. Mater.*, Vol. 22, No. 7, 2008, pp. 1305–1314.

[14] Pacheco-Torgal, F., Castro-Gomes, J., and Jalali, S., "Alkali-Activated Binders: A Review. Part 2. About Materials and Binders Manufacture," *Constr. Build. Mater.*, Vol. 22, No. 7, 2008, pp. 1315–1322.

[15] *Geopolymers: Structures, Processing, Properties and Industrial Applications*, Provis, J. L. and van Deventer, J. S. J., Eds., Woodhead Publishing/CRC Press, Cambridge, UK, 2009, p. 454.

[16] Shi, C., Fernández-Jiménez, A., and Palomo, A., "New Cements for the 21st Century: The Pursuit of an Alternative to Portland Cement," *Cem. Concr. Res.*, Vol. 41, No. 7, 2011, pp. 750–763.

[17] Duxson, P. and Provis, J. L., "Designing Precursors for Geopolymer Cements," *J. Am. Ceram. Soc.*, Vol. 91, No. 12, 2008, pp. 3864–3869.

[18] van Deventer, J. S. J., Feng, D., and Duxson, P., "Dry Mix Cement Composition, Methods and Systems Involving Same," U.S. Patent No. 7,691,198 B2 (2010).

[19] Yip, C. K., Lukey, G. C., and van Deventer, J. S. J., "The Coexistence of Geopolymeric Gel and Calcium Silicate Hydrate at the Early Stage of Alkaline Activation," *Cem. Concr. Res.*, Vol. 35, No. 9, 2005, pp. 1688–1697.

[20] Yip, C. K., Lukey, G. C., Provis, J. L., and van Deventer, J. S. J., "Effect of Calcium Silicate Sources on Geopolymerisation," *Cem. Concr. Res.*, Vol. 38, No. 4, 2008, pp. 554–564.

[21] Buchwald, A., Hilbig, H., and Kaps, C., "Alkali-Activated Metakaolin-Slag Blends—Performance and Structure in Dependence on Their Composition," *J. Mater. Sci.*, Vol. 42, No. 9, 2007, pp. 3024–3032.

[22] Lloyd, R. R., Provis, J. L., and van Deventer, J. S. J., "Microscopy and Microanalysis of Inorganic Polymer Cements. 2: The Gel Binder," *J. Mater. Sci.*, Vol. 44, No. 2, 2009, pp. 620–631.

[23] Provis, J. L., Rose, V., Bernal, S. A., and van Deventer, J. S. J., "High Resolution Nanoprobe X-ray Fluorescence Characterization of Heterogeneous Calcium and Heavy Metal Distributions in Alkali Activated Fly Ash," *Langmuir*, Vol. 25, No. 19, 2009, pp. 11897–11904.

[24] Rees, C. A., Provis, J. L., Lukey, G. C., and van Deventer, J. S. J., "The Mechanism of Geopolymer Gel Formation Investigated through Seeded Nucleation," *Colloids Surf., A*, Vol. 318, Nos. 1–3, 2008, pp. 97–105.

[25] Hajimohammadi, A., Provis, J. L., and van Deventer, J. S. J., "The Effect of Alumina Release Rate on the Mechanism of Geopolymer Gel Formation," *Chem. Mater.*, Vol. 22, No. 18, 2010, pp. 5199–5208.

[26] Hajimohammadi, A., Provis, J. L., and van Deventer, J. S. J., "The Effect of Silica Availability on the Mechanism of Geopolymerisation," *Cem. Concr. Res.*, Vol. 41, No. 3, 2011, pp. 210–216.

[27] Hajimohammadi, A., Provis, J. L., and van Deventer, J. S. J., "Time-Resolved and Spatially-Resolved Infrared Spectroscopic Observation of Seeded Nucleation Controlling Geopolymer Gel Formation," *J. Colloid Interface Sci.*, Vol. 357, No. 2, 2011, pp. 384–392.

[28] Bernal, S. A., Mejía de Gutierrez, R., Pedraza, A. L., Provis, J. L., Rodríguez, E. D., and Delvasto, S., "Effect of Binder Content on the Performance of Alkali-Activated Slag Concretes," *Cem. Concr. Res.*, Vol. 41, No. 1, 2011, pp. 1–8.

[29] Shi, C. and Xie, P., "Interface between Cement Paste and Quartz Sand in Alkali-Activated Slag Mortars," *Cem. Concr. Res.*, Vol. 28, No. 6, 1998, pp. 887–896.

[30] Lee, W. K. W. and van Deventer, J. S. J., "The Interface between Natural Siliceous Aggregates and Geopolymers," *Cem. Concr. Res.*, Vol. 34, No. 2, 2004, pp. 195–206.

[31] Lee, W. K. W. and van Deventer, J. S. J., "Chemical Interactions between Siliceous Aggregates and Low-Ca Alkali-Activated Cements," *Cem. Concr. Res.*, Vol. 37, No. 6, 2007, pp. 844–855.

[32] Provis, J. L., Muntingh, Y., Lloyd, R. R., Xu, H., Keyte, L. M., Lorenzen, L., Krivenko, P. V., and van Deventer, J. S. J., "Will Geopolymers Stand the Test of Time?" *Ceram. Eng. Sci. Proc.*, Vol. 28, No. 9, 2007, pp. 235–248.

[33] Zhang, J. X., Sun, H. H., Wan, J. H., and Yi, Z. L., "Study on Microstructure and Mechanical Property of Interfacial Transition Zone between Limestone Aggregate and Sialite Paste," *Constr. Build. Mater.*, Vol. 23, No. 11, 2009, pp. 3393–3397.

[34] Shi, C., "Strength, Pore Structure and Permeability of Alkali-Activated Slag Mortars," *Cem. Concr. Res.*, Vol. 26, No. 12, 1996, pp. 1789–1799.

[35] Olivia, M., Nikraz, H., and Sarker, P., "Improvements in the Strength and Water Penetrability of Low Calcium Fly Ash Based Geopolymer Concrete," *3rd ACF International Conference—ACF/VCA*, T. Uomoto and T. V. Nga, Eds., Ho Chi Minh City, Vietnam, November 11–13th, 2008, Vietnam Institute for Building Materials, Hanoi, Vietnam, pp. 384–391.

[36] Sagoe-Crentsil, K., Brown, T., and Yan, S., "Medium to Long Term Engineering Properties and Performance of High-Strength Geopolymers for Structural Applications," *Adv. Sci. Technol.*, Vol. 69, 2010, pp. 135–142.

[37] Provis, J. L., Myers, R. J., White, C. E., Rose, V., and van Deventer, J. S. J., "X-ray Microtomography Shows Pore Structure and Tortuosity in

Alkali-Activated Binders," *Cem. Concr. Res.*, Vol. 42, No. 6, 2012, pp. 855–864.

[38] Ismail, I., Provis, J. L., van Deventer, J. S. J., and Hamdan, S., "The Effect of Water Content on Compressive Strength of Geopolymer Mortars," *Proceedings of 7th AES-ATEMA 2011 International Conference on Advances and Trends in Engineering Materials and Their Applications*, Milan, Italy, July 4–8, AES Technical Reviews International Journal Series, McGill University, Montreal, Canada, 2011.

[39] Deja, J., "Carbonation Aspects of Alkali Activated Slag Mortars and Concretes," *Silic. Ind.*, Vol. 67, No. 1, 2002, pp. 37–42.

[40] Rodríguez, E., Bernal, S., Mejía de Gutiérrez, R., and Puertas, F., "Alternative Concrete Based on Alkali-Activated Slag," *Mater. Constr.*, Vol. 58, No. 291, 2008, pp. 53–67.

[41] Adam, A. A., 2009, "Strength and Durability Properties of Alkali Activated Slag and Fly Ash-Based Geopolymer Concrete," Ph.D. thesis, RMIT University, Melbourne, Australia.

[42] EN 197: "Cement- Part 1: Composition, Specifications and Conformity Criteria for Common Cements," European Committee for Standardization, Brussels, Belgium, 2011.

[43] ASTM C150: "Standard Specification for Portland Cement," *Annual Book of ASTM Standards*, ASTM International, West Conshohocken, PA.

[44] ASTM C595: "Specification for Blended Hydraulic Cements," *Annual Book of ASTM Standards*, ASTM International, West Conshohocken, PA.

[45] ASTM C1157: "Performance Specification for Hydraulic Cements," *Annual Book of ASTM Standards*, ASTM International, West Conshohocken, PA.

[46] AS3972: "General Purpose and Blended Cements," Standards Australia, Sydney, Australia, 2010.

[47] Provis, J. L., "Alkali-Activated Binders and Concretes: The Path to Standardization," *ASTM Symposium on Geopolymer Binder Systems*, San Diego, CA, June 26–27, 2012, ASTM International, West Conshohocken, PA.

[48] VicRoads, 2010, "Standard Documents," http://www.vicroads.vic.gov.au/Home/Moreinfoandservices/TendersAndSuppliers/StandardDocuments.htm (Last accessed 17 June 2012).

Summary of Panel Discussion

A panel discussion on standardization for geopolymers and related alkali-activated aluminosilicate binder systems was held at the end of the symposium. Panelists were James Hicks, Susan Bernal, John Provis, Robin Gibson, Erez Allouche, and Rodney Zubrod (all of whom were speakers at the symposium). The panel was moderated by Leslie Struble.

The key issue discussed by the panel was whether existing performance standards for hydraulic cement are suitable for geopolymer materials. Most companies that manufacture geopolymer materials for use as a binder in concrete cite conformance with ASTM C1157, Standard Performance Specification for Hydraulic Cement, and a few cite ASTM C1600, Standard Specification for Rapid Hardening Hydraulic Cement. However, it was noted that these performance standards were not developed for material systems that are fundamentally different from portland cement, and there are some concerns and problems when using the standards for geopolymer materials.

For example, the relevant ASTM standards generally take zero time as the time when water and cement are first mixed, but for geopolymers this time would more reasonably be when activator solution (alkali hydroxide and water and perhaps alkali silicate) and precursor (aluminosilicate powder) are mixed, perhaps the time and point of manufacture. Another example is the curing condition used in the ASTM standards, immersion in a saturated lime solution, because many geopolymer mixtures do not benefit at all (or are even badly damaged) by such curing. A third example is that standards for alkali-silica reaction call for comparing expansion of the test mixture with expansion of a similar mixture containing no pozzolan, a problem with geopolymers because pozzolans (metakaolin, fly ash, or slag) are usually the main ingredient.

A broader, important, and more difficult issue is whether the tests specified in these standards are *sufficient* to assure that an alkali-activated binder will behave appropriately in service. This has been discussed in RILEM Technical Committees DTA, Durability Testing of Alkali-Activated Materials, and 224-AAM, Alkali-Activated Materials.

So a key question is whether ASTM C01 should develop a new standard explicitly for geopolymers and related materials for use in concrete (perhaps through C01.13 on Special Cements). Our recommendation is that such a new standard is needed. If a new standard is not developed, or before it can be developed, the existing ASTM performance specifications (C1157 and C1600) should be revised so as to be more suitable for geopolymers and other alkali-activated materials. These materials are being manufactured and sold, and the existing standards should be clarified.

Leslie Struble and James Hicks


RECEIVED
LIBRARY

www.astm.org

ISBN: 978-0-8031-7554-9
Stock #: STP1566